SYNTHESIS AND CHARACTERIZATION OF POLYMER-SUPPORTED CYCLODEXTRIN NANOSCAFFOLDS FOR USE IN FUTURE ENVIRONMENTAL STUDIES

By

James Adrian McKee

RECOMMENDED:

Dr. Brian Rasley

Dr. William Simpson

Dr. Thomas Trainor

Dr. Thomas Green
Advisory Committee Chair

Dr. Thomas Green, Chair
Department of Chemistry

APPROVED:

Dr. Paul Layer
Dean, College of Natural Science and Mathematics

Dr. John Eichelberger
Dean of the Graduate School

18 August 2016
Date

SYNTHESIS AND CHARACTERIZATION OF POLYMER-SUPPORTED CYCLODEXTRIN NANOSCAFFOLDS FOR USE IN FUTURE ENVIRONMENTAL STUDIES

A

THESIS

Presented to the Faculty

of the University of Alaska Fairbanks

in Partial Fulfillment of the Requirements

for the Degree of

DOCTOR OF PHILOSOPHY

By

James Adrian McKee, B.S., M.S.

Fairbanks, AK

August 2016

Abstract

The toxicity of transitional and post-transitional metals in natural water systems is well known. Coordination of these metals by selected ligands is a common means of environmental remediation. Macrocyclic coordination complexes impart thermodynamic and kinetic stability beyond their corresponding chelation analogues due to the pre-organized physical constraints of the coordinating ligands. Cyclodextrins are biologically produced and well-studied cyclic glucose macrocycles that possess chemically distinct hydroxyls. Amphiphilic cyclodextrins used as polymer-supported macrocyclic nanoscaffolds that are capable of scavenging trace metal pollutants could offer exciting new avenues of remediation research. Amphiphilic sodium hexakis (2,3-O-dibenzyl-6-O-sulfobutyl) cyclomaltohexaose (DBSBA) and sodium heptakis (2,3-O-dibenzyl-6-O-sulfobutyl) cyclomaltoheptaose (DBSBB) were synthesized in four steps. Aggregation colloids that possess an aromatic pseudophase in an aqueous system could provide new avenues of research for emulsion polymerization studies. The strong π-π interactions between the benzyls on the secondary rim and the polystyrene should anchor cyclodextrin nanoscaffolds to the nanoparticle surface. The aggregation of DBSBA and DBSBB was investigated using diffusion ordered NMR spectroscopy (DOSY), conductivity, and pyrene fluorescence techniques. These amphiphiles were found to possess near spherical symmetry at critical micelle concentrations of approximately 0.1 mM in all techniques used to study the phenomenon. These surfactants contain a high percentage of aromatic moieties in their structures, which affected the thermodynamics of aggregation by decreasing the CMC with increased temperature. Highly charged monodisperse polystyrene latex nanoparticles were produced using DBSBB as a surfactant in emulsion polymerization. The choice of surfactant was selected to examine its effect on polystyrene latex surface properties; amphiphilically modified

cyclodextrins have not been used in emulsion polymerization recipes to date. Surface charge densities, up to 27 $\mu S/cm^2$, scaled with increasing amounts of added surfactant with a concomitant decrease in particle size. The addition of increasing amounts of DBSBB into emulsion polymerization recipes resulted in larger percentage coverage of latex particles. ^1H NMR studies found that the primary sulfobutyl substituents possessed fast molecular motions and therefore projected into solution and away from the latex surface. The strong physical adsorption of DBSBB and the presence of solvated primary rim substituents suggests that cyclodextrins can be used as future nanoscaffolds for the alteration of latex surface properties through non-covalent surface modification.

Dedication

To my wonderful and supportive parents,

Jim and Trudy

Two great chemists that showed me the path and gave me more than I can ever repay.

Table of Contents

Page

Page

Page

Page

Page

Page

List of Figures

Page

Chapter 1.

Page

Chapter 2.

Page

Page

Page

Page

Page

List of Tables

Page

Chapter 1

Chapter 3.

Page

Page

List of Appendices

Page

Acknowledgements

This dissertation could not have been completed without the great amount of support that I have received over the years. I would like to thank the following people for their contributions to my research, my education, and my growth as a scientist.

To my research advisor, Thomas (Tom) Green, thank you for your time, patience, insights, and criticism. Thank you for giving me the space to venture out and ask questions of my own, to allow me to solve my own problems, and become a better chemist for doing so. You are a gentleman and a scholar. I can only hope to follow your example.

To the members of the Green Laboratory Group, past and present, for your help, insight, tutelage, and friendship. The assistance and guidance of Dan Kirschner, Michael Jaramillo, Zhipeng Dai, Terilyn Stephen, among others, will always be part of my graduate school experience.

To my graduate advisory committee, Dr. Brian Rasley, Dr. William (Bill) Simpson, and Dr. Thomas (Tom) Trainor, thank you for your suggestions, your criticism, and for your support. You were all tough but fair, and that is all a graduate student can hope for.

To the faculty of the Department of Chemistry and Biochemistry, thank you for your support and suggestions, your open doors and minds, and use of your laboratory equipment when the need arose. To the departmental staff, specifically Emily Reiter, Jacy Pietsch, and Mist D'June-Gussak, thank you for everything you did to make a student feel welcome and appreciated. You simply made my life easier at a time when I thought I would never finish.

To my friends and family, thank you for your love and support.

Chapter 1. Overview and Research Aims

1.1 Trace Metals in the Environment

The composition of natural waters is the sum of many sources, natural and anthropogenic, that contribute to its chemistry.[1] Trace elements, environmental species that naturally occur in small amounts, are present in sufficient bioavailable concentrations to be toxic to living organisms.[2] These elements, encompassing transition and post-transitional metals, are often associated with pollution and toxicity. The effects of these trace metals in environmental waters have been well studied.[3] These metals (*e.g.* Cu, Cd, Ni, Pb, Zn) can excessively enter into natural waters from a variety of natural and man-made sources[3,4] These metals enter the environments through transport and industrial emissions, and some geological events. Heavy metals concentrate in soil and soil surface (deposition) and can mobilize/transport via surface run-off into natural waters. The main anthropomorphic point sources include acid mine drainage, industrial electroplating, and power generation. [5,6]

The availability of potable water is a daily need for every American. Water is a potent polar solvent that solubilizes a wide spectrum of metal ions, organic and inorganic compounds thereby influencing water quality. The Clean Water Act and the Safe Water Drinking Act mandates that natural waters must be processed in order to remove or reduce the bioavailability of toxic metal compounds that can affect the health of users of municipal water systems. An increase in population growth and future anticipated water shortages under non-drought conditions in many states demand investigation into inexpensive and recyclable water remediation technologies.[7] Current technologies perform this function but at high cost and/or with low selectivity for specific toxic metal ions. Different areas of the country are confronted with unique combinations

of metal pollution in their municipal water systems and natural waters. Speciation of metals in natural waters is controlled by pH and reduction potential of the system. Most waters (lakes, rivers) that can be categorized as an open system *(i.e.* equilibrated with the atmosphere) have sufficient dissolved oxygen and carbon dioxide to be considered slightly acidic and oxidizing.[1] The inner sphere complexes of metal cations under these conditions are found as aquo complexes, which all ligands are water molecules, or complexes with ligands in sufficient concentration (*i.e.* carboxy). The speciation of trace metals determines its toxicity in the environment and affects its properties of adsorption and binding.

1.2 Remediation of Trace Metals

Conventional methods of removal of metal ions and their complexes include ion exchange systems, reduction/oxidation chemistry, chelation, reverse osmosis, filtration, adsorption, precipitation, and biosorption technologies.[3] Ion exchange systems possess the advantages of the effective removal of metals/inorganics from the water supply, the ability to regenerate the matrix and the initial low cost at the beginning of water detoxification. Disadvantages of these systems include the ineffective removal of particles from solution, high operating costs over long term due to maintenance, and poor selectivity with respect to the removal of an ion of interest.[8] Water distillation and reverse osmosis processes can remove a broad range of contaminants but uses large amounts of water and energy in the process of elimination. Filtration technologies can remove all size particles/microorganisms greater than pore size, bind dissolved organics, require minimal maintenance and are regenerable. Disadvantages to filtration include its cost of operation and may not remove dissolved inorganics. Biosorbents, much like anionic exchange resins, possess chemically active anionic functional groups, that can interact with and sequester metal cations.[9] Unlike exchange resins, however, biosorbents also possess geometries and

multiple interactions which can preferentially selected cations. Heavy metals (*e.g.* Pb^{2+}, Cd^{2+}, Cu^{2+}, Ni^{2+}, Zn^{2+}) interact strongly with amino acid residues (*e.g.* cysteine) to disrupt enzymatic active sites from their natural process.[10]

Chitosan, alginate, pectins, amino acids,(cysteine threonine, lysine arginine, aspagine, glutamate, tyrosine, phenylalanine) and polypeptides (glutathione, metallothionien) all contain functional groups that chelate toxic metal species without the aid of metabolism.[11-13] The adsorption of metals by biological matter (biosorption) possesses the advantage of low cost and availability, but the damage due to inorganic/ organic complexation limits re-use.[4]

Beneficial aspects of metal remediation based upon reduction/oxidation chemistry can remove iron/reducible species but is often offset by high equipment maintenance costs and is ineffective against non-reducible species at natural conditions.[8] The use of organic molecules to chelate metals and decrease their bioavailability has been successful due to effective complexation with inorganics. Chelators/multidentate ligands and their metal coordination complexes cannot be recovered from natural waters, are persistent in the environment, and are non-selective with respect to the metal of interest.[14]

1.3 Coordination

Toxic metal cations in natural aqueous systems are considered to be under dilute conditions. Low concentration of these species does not limit their insidious presence. On the contrary, the danger of metals in the environment comes from bioaccumulation.[15] These metals are not in isolation in an aqueous system but solvated by water; metals form coordination complexes. All coordination complexes consist of an electron deficient central atom (electron acceptor or Lewis acid) that is characterized by its coordination number and one or more ligands that act as electron donors

(Lewis base). There are two kinds of complexes; inner-sphere and outer-sphere.[16] Inner sphere complexes are formed from the production of a new molecular orbital; the orbital of the electron donating ligand overlaps with the empty bonding orbital of the metal cation. The coordination number is defined as the number of ligands that a metal ion can accommodate. The most common, in natural waters, are four and six. Complexes that have coordination numbers of 4 have two main structural configurations, square planar and tetrahedral. The bonding orbitals in square planar complexes are hybrids; they are p^2d^2 or sp^2d^4.[17] Metal ions with coordination numbers of 6 form octahedral complexes; 4 square planar ligands and 2 orthogonal ligands (one above and one below the plane). These bonding orbital are hybrids (sp^3d^2). Complexes that incorporate transition metals with eight electrons in their d orbitals (d^8) form square planar complexes.[18]

The rates of complexation reactions span orders of magnitude. Water exchange rates for the coordination sphere approximately scale with z/d^3, where z is the charge of the cation and d is the ½ the sum of the radii between the oxygen and metal atoms. The arrangement of ligands around a metal ion varies with the coordination number and orbitals available for bonding. Second row metals have s and p orbitals and can form 4 molecular orbitals (from one s and three p orbitals) while third row metals possess s, p, and five d orbitals, thereby having the capability to form nine molecular orbitals.[17]

The interaction between aqueous metal cations and ligands of interest form coordination complexes of defined geometries. Cu^{2+}, Cd^{2+}, Ni^{2+}, and Pb^{2+} complexes adhere to octahedral geometries while Zn^{2+}complexes have square planar geometry. Ligand displacement of the coordination complexes are defined by kinetic and thermodynamic factors; the sum of all complexes are defined by mass balance equations. A metal cation with a coordination number of

six can therefore complex with six water molecules to form a hexacoordinate inner sphere complex. The most common ligand is water; metals do not exist in solution as free species but as aquo complexes with four to eight water molecules as ligands, depending on coordination number.[16] Equation 1 illustrates formation of an aquo complex with octahedral geometry.

$$M^{2+} + 6\,H_2O \rightleftharpoons M(H_2O)_6^{2+} \qquad (1)$$

Complexation increases the acidity of water molecules bound to the metal via proton-cation electrostatic repulsions.[16] Hydrolysis of waters adjacent to the solvent shell is a result of increased acidity and can thereby lower the pH of the system.

$$M(H_2O)_6^{2+} \rightleftharpoons M(H_2O)_5^{+} + H^{+} \qquad (2)$$

Metal complexation is a complex process. The simplest case of binding between a metal and a ligand is if only one site for binding (n = 1, where n is the number of available binding sites) and one ligand exists. This interaction can be expressed as:

$$A + B \rightleftharpoons A - B \qquad (3)$$

where ligand A binds to metal B to form complex A-B. A binding constant is used as the criteria for the evaluation of the host-guest complexation process. The equilibrium binding constant of this monodentate complexation expressed as:

$$K = \frac{[A-B]}{[A][B]} \qquad (4)$$

where [A] is the molar concentration of free (unbound) ligand, [B] is the molar concentration of the free metal cation, and [A-B] is the molar concentration of the complex. Knowledge of these respective concentrations allows the equilibrium constant to be calculated. The determination of

the equilibrium constants of subsequent binding of ligands to the cationic metal ion becomes progressively more complex; examination of multiple binding equilibria is warranted. For ae concentration of the bound ligand can be generally expressed as:

$$[B - A_i] = [B - A] + 2[B - 2A] + 3[B - 3A] + \cdots i[B - iA] = \sum_{i=0}^{n}[B - A_i] \qquad (5)$$

The coefficients in this summation of i liganded complexes would indicate that each mole of [B-Ai] has i moles of ligand complexed with it. The total amount of metal, complexed and uncomplexed, can be expressed as:

$$[B] + [B - A] + 2[B - 2A] + \ldots = \sum_{i=0}^{n}[B - A_i] \qquad (6)$$

The extent of complexation can be illustrated by:

$$\beta_i = \frac{[AB_i]}{[A][B]^i} \qquad (7)$$

where β_i is the mixed equilibrium constant for all of the complexation species under consideration.

Metals across the periodic table possess different interaction characteristics with respect to ligands due to nuclear shielding, atomic radius, and charge. The characteristics of metal cations can be grouped into ACD (Ahrland-Chatt-Davies) or hard and soft acid base (HSAB) classifications, which assists in guiding future research pathways.[19,20] These systems overlap to a large degree as they are both based on polarizability and the ability for the metals and ligands to form either weaker electrostatic or stronger covalent bonds. The strength of inner complex formation is a function of the properties of the metal anion and the ligand. The “hard-soft” designation describes the ability of the electron shell around the metal to deform or polarize during a metal-ligand interaction. Transition and post-transition metals tend to be soft or

polarizable, while IA, IIA and IIIA metals tend to be 'harder' or less polarizable. The "acid-base" designation refers to Lewis acids (species that accept electron pairs during interaction) and Lewis bases (electron donors).[21]

A metal-ligand interaction is a Lewis acid/base reaction. Lone pairs on the oxygen of the water molecule act as an electron donor where the d orbitals on the metal cation act as an electron acceptor. Ligands that have lone a pair/non-bonding electrons can interact with metal cations in a similar Lewis acid/base reaction. Natural waters contain many anions that have non-bonding pairs (*i.e.* OH^-, Cl^-, CO_3^{2-}, NO_3^{2-}, SO_4^{2-}, SO_3^{2-}) and numerous organic molecules with functional groups (*i.e.* carboxyls, alcohols, amides, amines, thiols) that satisfy these criteria.

Release of water ligands from an ordered complex produces a large increase in entropy. Positive entropy in the system contributes to a release of free energy (ΔG) that explains the formation of chelation complexes. The magnitude of entropy increases when a non-water ligand replaces a water ligand in an aquo complex is a function of the magnitude of the interaction between water and the metal. A small release in entropy corresponds to a weakly bound water ligand. The effect of the entropic component on spontaneous ligand exchange decreases with subsequent ligand substitutions. The magnitude of the free energy release is illustrated by the numerical value of the equilibrium constant K. These values contribute to the understanding and prediction of distribution of metal-ligand species in natural waters.

Taking Cu^{2+} ions as an illustrative example, the cupric ion undergoes many different reactions of formation with anionic ligands in a natural water system. The intermediate polarizability (on Pearson hardness scale) allows for complexation with a wide variety of ligands. The equilibrium constants, K, in Table 1 are with respect to the following equation:

$$Cu(H_2O)_6^{2+} + X^- \rightleftharpoons Cu(H_2O)_5X^+ \quad (8)$$

Table 1: Selected Equilibrium Constants for Cu^{2+}cations in Natural Waters[16]

OH^-	Log K	CO_3^{2-}	Log K	SO_4^{2-}	Log K	NH_3	Log K
CuOH	6.3	$CuCO_3$	6.7	$CuSO_4$	2.4	$CuNH_3$	4.0
$Cu(OH)_2$	11.8	$Cu(CO_3)_2$	10.2			$Cu(NH_3)_2$	7.5
$Cu(OH)_4$	16.4					$Cu(NH_3)_3$	10.3
$Cu_2(OH)_2$	17.7					$Cu(NH_3)_4$	11.8

An examination of Table 1 reveals that complexation with the nitrogen of a single ammonia molecule, or the oxygen of single hydroxide, has reasonably small equilibrium constants for complete complexation in a natural water setting. The intermediate polarizability of the copper (II) ion has good compatibility with the intermediate/hard ammonia species. The pH range of natural waters (pH 6-8) would yield the ammonia species, as opposed to the ammonium ion (pKa = 10) and therefore has good potential for strong complexation of multiple amine based ligands.

Outer sphere complexes form electrostatic bonds with intact hydrated metal ions; the metal ion does not lose waters of hydration. These ligands do not form orbital overlap with bonding orbitals of metal ions. These complexes are also known as "ion pair" complexes. The strength of the outer sphere bonding interactions (K_{os}) can be estimated by considering the Fuoss equation, an extension of electrostatic theory that connects the formation constants of ion pairs with the ionic strength of the solution.[22]

$$K = \left(\frac{4}{3}\right)\left(\pi N_A a^3 e^{-b}\right)\times 10^{-3} M^{-1} \quad (9)$$

$$b = \frac{Z_M Z_L e_0^2}{aDkT} \qquad (10)$$

where N_A is Avagadro's number, a is the distance between metal and ligand centers, e_0 is the electronic charge, D is the dielectric constant, k is Boltzmann's constant, and T is temperature in Kelvin (K = ~0.1 for uncharged ligand, ~1 for monoanion, and ~200 for dianion). Outer sphere complexes are weak with respect to inner complexes and are not expected to contribute to complexations in dilute conditions.

1.4 Chelation

Complexation reactions between metals and ligands are actually substitution reactions. Ligands are diverse, but have a few common attributes. They include an electronegative atom that has at least one pair of available electrons to form bonds with the central metal atom. They are classified by the number of binding sites they contain (*i.e.* monodentate, bidentate, etc.…) The binding strength of the chelating agent scales with the number of binding sites; an increase in the number of binding sites increases the number of filled bonding orbitals on the central metal cations. The release of water molecules from the coordination complex into bulk water increases the system entropy thereby making the process favorable.[1,16] The most commonly used chelation species is EDTA (ethylene diamine tetraacetic acid; pKa = 1.8), often represented by the symbol Y. EDTA is a single molecule that completely coordinates with the cupric ion, although non-selectively, because it possesses intramolecular ligands for multidentation. Chelation renders the toxic aqueous metal cation chemically inert; administration of EDTA for this result is a common practice. Chelation agents and their metal coordination complexes cannot be recovered, however, and are therefore persistent in the environment.[16]

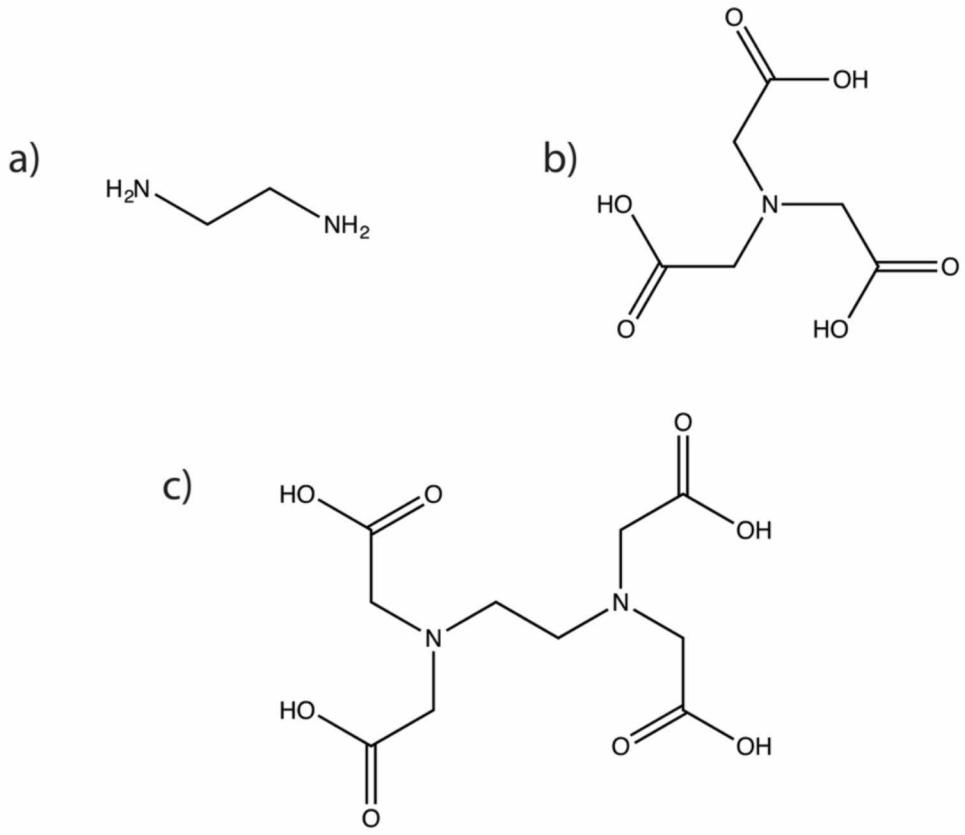

Figure 1. Chelating agents with different number of binding sites. a) Ethylene diamine (EDA) b) nitrilotriacetic acid (NTA) and c) Ethylene diamine tetraacetic acid (EDTA).

An illustration of the effect of the number of dentation sites on a chelating agent is observed in Table 2 and Figure 1. As the denticity get progressively larger for EDA (2), NTA (4), and EDTA (6), the equilibrium binding constant for copper (II) becomes progressively larger.

Table 2. Equilibrium binding constants (K) between selected chelating agents and Cu^{2+}cations. [16]

EDA	log K	NTA	log K	EDTA	log K
CuL	10.5	CuL	14.2	CuL	20.5
CuL_2	19.6	CuL_2	18.1		

The selectivity of open-chain chelating agents for different metal species depends on the nature of the ligand atom and the chemical composition of the waters in which it resides. In waters where the total calcium ion concentration (Ca_T) dominates over the trace concentration of aqueous copper (*i.e.* $Ca_T >> Y_T >> Cu_T$) and the complexation of copper is dictated by the equilibrium reaction:

$$CaY^{2-} + Cu^{2+} = CuY^{2-} + Ca^{2+} \quad (11)$$

$$K = \frac{K_{Cu}}{K_{Ca}} \quad (12)$$

The intrinsic equilibrium constant of EDTA for Ca^{2+} is smaller than that of Cu^{2+}, but the much larger concentration will drive Equation 11 toward reactants, and the calcium-EDTA complex will dominate.[16,22] Effective remediation of natural water systems requires a stronger complexation of trace metal species that are present in waters where calcium and sodium ions concentrations dominate.

1.5 Macrocycles

The chelate effect is the observation that coordination complexes with multidentate ligands have greater stability than those complexes with an equivalent number of monodentate ligands. Coordination of aqueous metal ions to macrocycles possess enhanced thermodynamic and kinetic stability, beyond that of the chelate effect. This enhancement is known as the macrocyclic effect; complexes with macrocyclic ligands have greater stability than those complexes with equivalent open chain ligands.[23]

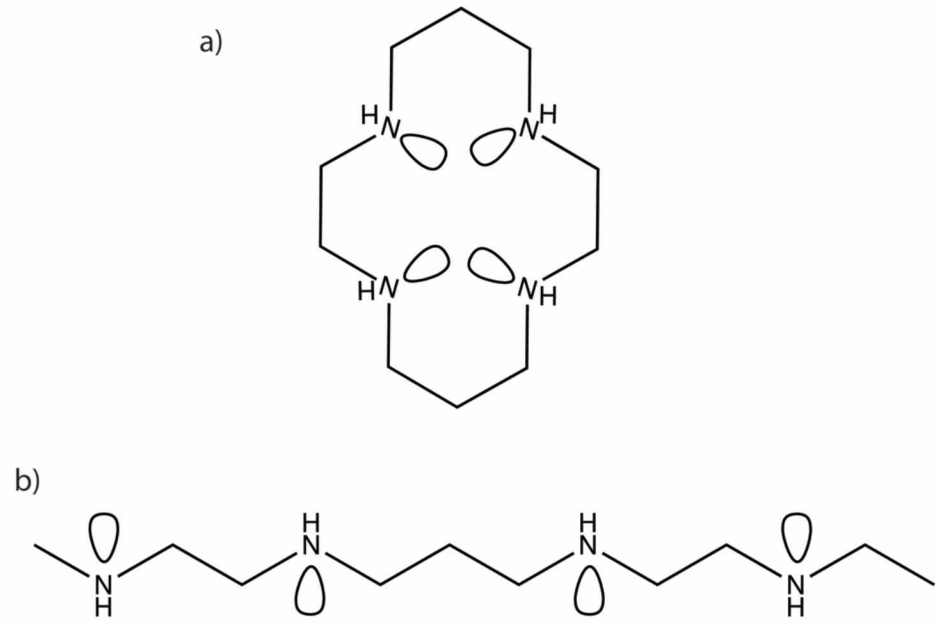

Figure 2. Comparison between cyclam (1,4,8,11-tetraazatetracyclodecane) and N^1-(2-(ethylamino)ethyl)-N^3-(2-(methylamino)ethyl)propane-1,3-diamine structures. The structure of the cyclam macrocycle (a) forces the nitrogen lone pairs into proximity to each other. The open chain analogue (b) allows maximum distance between the nitrogen lone pairs and thereby minimizes the energy of the structure.

The macrocyclic effect is an extension of the chelate effect. Macrocycles, covalently linked molecular ring compounds, are of potential interest in metal coordination and capture because they are often derivatizable and have less rotational and translational freedom than open chain ligand. There will be a less dramatic ordering effect upon coordination to the macrocycle to a metal than with open chain ligands. The macrocycle is pre-organized for coordination.[24]

The strength of the chelation effect is based in entropic consideration; binding affinity of macrocyclic compounds is a function of enthalpy and entropy. Uncomplexed open-chain dentates adopt an elongated conformation to minimize enthalpically unfavorable interactions

between lone pairs. Complexation of these analogues to the metal center involves conformation rearrangement and an enthalpic penalty. Cyclic ligands, as illustrated in Figure 2, are "pre-organized" for binding, with proximal lone pairs that encourage stronger complexation despite having binding sites that are intrinsically unfavorable due to repulsions; cyclic ligands have, in a sense, already paid this enthalpic penalty during their synthesis. The pre-arranged conformation of the are macrocycle, as seen in Table 3, are enthalpically and entropically more favored than its open-chain counterpart. Therefore, the preorganization of ligand, desolvation of donor atoms, intrinsic basicity effects, and enforced repulsion all contribute to enhanced binding capabilities of macrocycles, *i.e.* the macrocyclic effect.

Table 3. Thermodynamic comparison between macrocyclic and open-chain ligand complexation with Cu^{2+} cations.[25]

Ligand	Log K	ΔH (kJ/mol)	TΔS (kJ/mol)
2a	27.2	-155.2	135.6
2b	20.9	-115.3	83.7

Numerous macrocycles have been associated with complexation of metals, including crown ethers, cyclophanes, calixarenes, cucurbiturils, rotaxanes, catenanes, and cyclodextrins. Cyclodextrins are of interest from an energetic point of view because of their enzymatic production; the energy required to place the hydroxyls in close proximity has been added biochemically. Subsequent addition of energy to place substituents proximal to each other (*i.e.* energy required to overcome repulsion of lone pairs) is the remaining energy penalty to be paid during synthesis because the macrocyclic nanoscaffold had been "pre-made" by the glucosyl

transferase enzyme located in several microorganisms (*e.g. Bacillus macerans*).[26] All other macrocycles that are similar to cyclodextrins in shape and chemistry are produced synthetically and therefore require a greater energy input by the synthetic chemist.

1.5.1 Cyclodextrins

Cyclodextrins are of interest in the present context due to the large number of publications that address derivitization, chirality, and nanoparticles. Polysaccharides (alginates, lignin, chitosan) contain functional groups on substituted hydroxyls and have been shown to sequester toxic metal species.[27-29] If the linear glucose chains are linked such that a macrocycle forms, the results are cyclodextrins. The hydroxyls of cyclodextrins have been known to coordinate metal cations.[30] Cyclodextrins (CDs) comprise a family of cyclic oligosaccharides. CDs are enzymatically manufactured from starch and derive their system of nomenclature from the number of glucose residues in their structure. Figure 3 demonstrates that the naming convention of these crystalline compounds differ based upon of the number of D- (+) glucopyranose units attached by α- (1,4) glucosidic bonds.[26] The most commonly used cyclodextrins are α–, β–, and γ–cyclodextrins that contain 6, 7, and 8 units respectively. Table 4 illustrates that each of these commonly used cyclodextrins have a different cavity diameter, molecular weight, and solubility.[31] The water solubility of the β-cyclodextrin is the lowest of the three due to internal structural hydrogen bonding rather than neighboring water molecules. All of the cyclic oligosaccharides are less soluble than acyclic saccharides of comparable molecular weight.[31] The primary and secondary hydroxyls are situated on opposite ends of the cyclodextrin cavity, the primary hydroxyls being on the smaller end of the cavity.

Table 4: Physical properties of natural cyclodextrins

Cyclodextrin	Mass g/mol	Cavity diameter (nm) Inner rim	Outer rim	Solubility g/kg H_2O
Alpha (α)	972	0.45	0.53	129.5
Beta (β)	1134	0.60	0.65	18.4
Gamma (γ)	1296	0.75	0.85	249.2

Each glucose unit contributes one primary and two secondary hydroxyls and therefore α– ,β– , and γ–cyclodextrins have 18, 21, and 24 hydroxyls respectively.[26] β-CD has 21 hydroxyl groups capable of derivatization that can be used to increase its solubility, attach catalytic groups for biomimetic/enzyme model chemistry, and allow cyclodextrin polymerization.[32] The complexity of these substitutions can be demonstrated by considering β-CD. For this compound, the 21 hydroxyl functional groups allow 2^{21} possible combinations for substitutions. These hydroxyls are arranged on the outside of the cyclodextrin ring, which, in conjunction with the internal electron density, promotes a hydrophobic cavity. Hydrogen atoms and glycosidic oxygens, whose non-bonding electron pairs are focused on the inside of cavity, line the inner cavity of the cyclodextrin ring.[26] The electrostatic interactions between the ligand and the inner cavity of the cyclodextrin, coupled with hydrophobic interactions of the solvent, allow complexation. Cyclodextrins also allow enantiomeric separation of racemic molecules through the formation of diastereomeric complexes; they consist of optically active glucose residues.

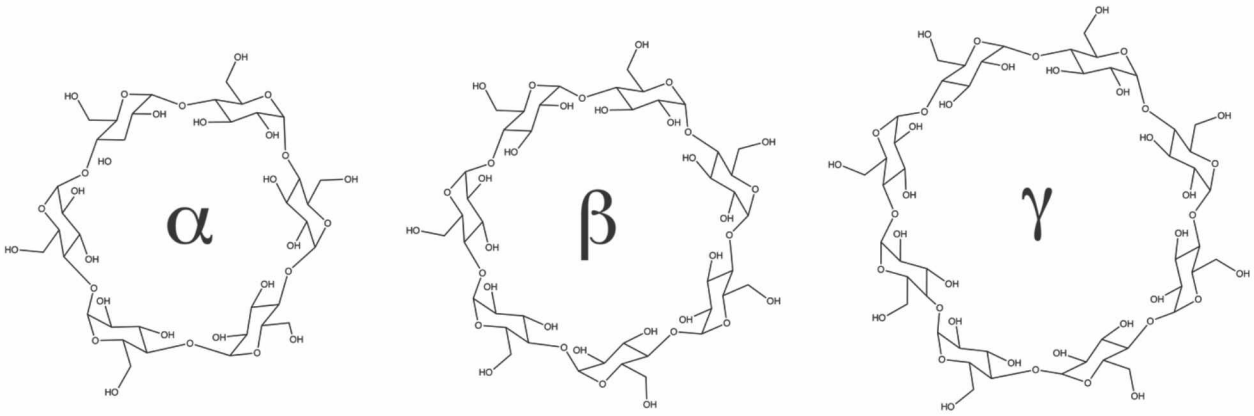

Figure 3: Chemical structure of cyclodextrins. Alpha (α) cyclodextrin has 6 glucose subunits, beta (β) cyclodextrin has 7 subunits, and gamma (γ) cyclodextrin has 8 subunits.

Metal ions can interact with native (underivatized) cyclodextrins where either the cation coordinates with one (or more) of the rim hydroxyls, coordinates with an encapsulated organic ligand, or the metal is chemically bound as an organometallic compound situated in an inclusion complex.[33] The direct metal-ligand interaction of cyclodextrins via the hydroxyl is an outer sphere complex. Inner sphere complex interactions are more prevalent if the hydroxyls are deprotonated. Unfortunately, the pKa's of the cyclodextrin are ~ 12 which require conditions too basic for natural waters.

Macrocyclic complexes are usually thermodynamically and kinetically more stable than complexes with related noncyclic ligands. As with chelation, the stability of macrocyclic complexes are greater than the equivalent free ligands; complexation strength increases as more donors are incorporated into the polydentate macrocycle.[24] For example, the stability of Cu^{2+} complexes containing four nitrogen donors is much greater as a cyclam macrocycle (*i.e* tetraazamacrocycles) than 4 ammonia molecules in solution.

The most easily determined parameter for selection of potentially strong metal-macrocyclic complexes is the radius of the cavity which can then be matched directly with known metal radii (Pauling radii but some advocate van der Waals radii) The best way to to obtain an estimate of hole size for a macrocycle is to draw a best fit circle through the donors of the ligand in hypothetical conformation in which they are endocyclic and planar. Determination of macrocyclic hole size, and cavity radius,r , is calculated as the distance d between two diametrically opposed donors. Subtraction of the radius of the donor atom (r(D)) obtains the hole size, r(H). Exocyclic lone pairs of donors are oriented away from cavity while endocyclic lone pairs are oriented into the cavity. The flexibility of the ligand allows the nitrogen donors to move to allow optimal metal-donor distances.

Cyclodextrins have been used in the environmental remediation of hazardous compounds. They are naturally produced biodegradable remediation agents for the removal of nonaqueous phase organic liquids (NAPLs), toxic aqueous metal species, and possess catalytic properties. Cyclodextrins are chemically modifiable water soluble compounds that are capable of encapsulating hydrophobic molecules such as NAPLs. The aqueous solubility of NAPLs are often very low and require large volumes of water to remove from a contaminated site.[34] Cyclodextrin remediation technologies include reduction/oxidation chemistry and catalytic degradation of organic compounds. Natural β-cyclodextrins enhance the ability of TiO_2 nanoparticles to photooxidize organics via the hydroxyl radical. The cyclodextrin acts as an encapsulation agent as well as a means to enhance oxidation.[35] The supramolecular properties of cyclodextrins have been well documented[36]. Molecules are bound by cyclodextrins in the hydrophobic interior of the molecule where subsequent chemistry can be performed. Hydrophilic cations, however, have demonstrated poor complexation with native cyclodextrins.

Modification of cyclodextrin hydroxyls can increase the solubility, extend the apolar cavity, and improve complexation with metal aqueous species. Common substitutions include methylation (CRYSMEB, RAMEB), hydroxypropylation (HPBCD), carboxymethylation (CMCD), and sulfobutylation (SBE).[35] Hydroxypropyl β cyclodextrin has hydroxypropyl substituents with an average degree of substitution of 4-6. The degree of substitution is the number of substituted hydroxyls out of the 18 free hydroxyls or 21 free hydroxyls when using alpha and beta cyclodextrin, respectively.[26,37]

Cyclodextrins are well known for their ability to encapsulate small molecules [30,36] Their well-defined structure, The chemically distinct sets of hydroxyls on the opposite sides of the macrocycle, and the large amount of literature with respect to derivatization of hydroxyls suggests they can also be used as nanoscaffolds the attachment for metal-binding ligands. [38-40] The affinity of metal ions to selected ligands depends on the local environment of the ligand and the polarizability of the metal.[41] Substitution of the remaining cyclodextrin hydroxyls with auxiliary ligands can alter the binding properties of the ligands to the metals ions, thus allowing for tuning of the metal-binding properties of the ligands.

Synthetic chemists have been interesting in CDs because of they are chemically stable, possess hydroxyls that can be modified regioselectively, and they are cyclic polymers of glucose that are of finite and known length.[39] The well-characterized structure of cyclodextrins has a rigid scaffold upon which functional groups can be attached. It has a predictable array, where the relationship of every molecule to another is known.[31] The X-ray crystal structure of an unsubstituted alpha CD is shown in Figure 4. This feature allows for increased structure specificity with respect to grafting functional groups for the binding of ionic species. Synthetically, knowledge of the precise structure gives greater selectivity over the metal ion in

question. Unless the crosslinked polymer has a regular array, the exact distribution of groups is not known, only a statistical distribution. An amorphous structure built solely from crosslinking reagents possesses only estimated distance relationships between intrastructural functional groups.

The structures of cyclodextrins have been well studied and the stereochemical arrangements of atoms with respect to position have been quantified.[42] Chemical modification of cyclodextrin hydroxyls are most commonly the result of electrophilic attack on the nucleophilic hydroxyl oxygen by alkyl halides, epoxides, sulfones, sulfonic acid chlorides, phosphoric acid chlorides, phosphonic acid chlorides.[43] The synthesis of persubstituted cyclodextrin derivatives requires reagents that are regioselective, optimization of reaction conditions, separable products, and a means of estimation of purity. Bulky reagents preferentially react with primary hydroxyls due to steric issues, while the two secondary hydroxyls differ in acidity (pKa of OH(2) is 12.2) while the OH(3) hydroxyl is the least reactive. [43,44] Typically, substitution of OH(3) occurs only have OH(2) and the primary alcohol has been rendered unavailable for substitution by protecting groups. [45] The choice of solvent contributes as well due to solubility and polarity considerations (*e.g.* polar solvents facilitate SN_2 nucleophilic substitutions).[46]

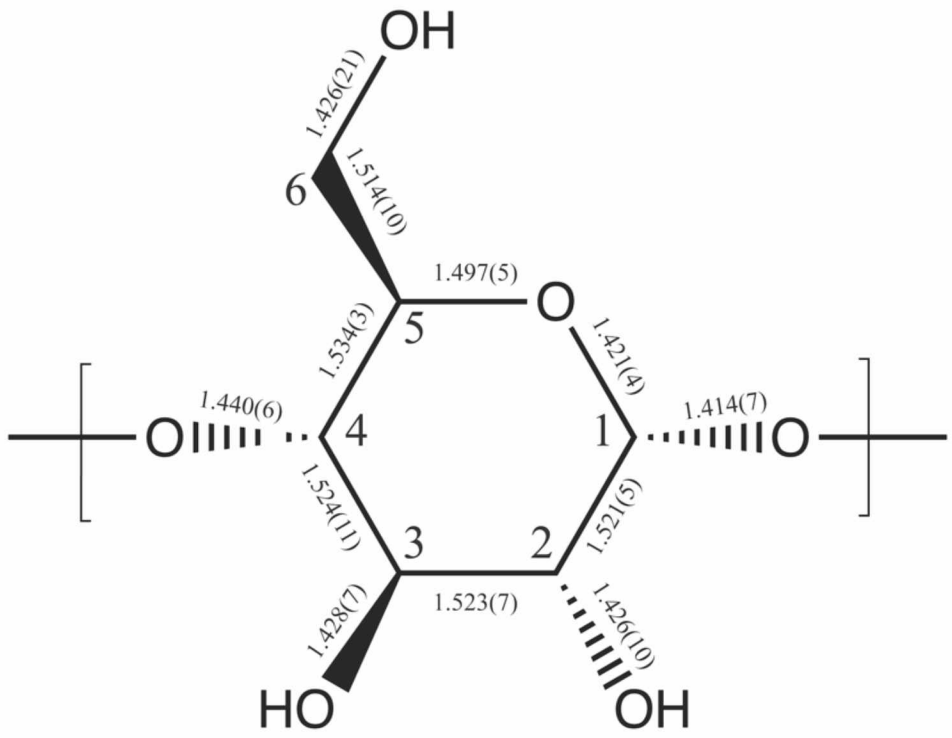

Figure 4. Bond distances between carbon and oxygen atoms in alpha cyclodextrin in units of nm. The numbers in parentheses are standard deviations.

1.5.2 Amphiphilic Cyclodextrins

Substituted cyclodextrins can be classified by which end of the torus (primary or secondary) has been modified. Medusa-like cyclodextrins have hydrophobic moieties on their primary face, Skirt-like cyclodextrins on their secondary, and bouquet-like cyclodextrins possess either hydrophilic or hydrophobic anchors on both primary and secondary rims.[30] Amphiphilic cyclodextrins, because they possess both hydrophilic (ionic or non-ionic) and hydrophobic substituents, have demonstrated the ability to form aggregation colloids.[47-51] There is caution in making generalizations about amphiphilic molecules; not all amphiphilic molecules possess the intrinsic capability to form aggregates.[52] Micelles have the capability to solubilize hydrophobic molecules in aqueous solution due to an internal hydrophobic core. Surfactants have a

characteristic behavior of demonstrating sharp changes in physical properties when their concentration in solution reaches a critical value. This value, the critical micelle concentration (cmc), is an important parameter in the solution behavior of the surfactant and occurs at a sharp discontinuity on a concentration versus "physical property" curve.[53] A facile method to determine the intrinsic solubilization ability of an amphiphilic molecule is the pyrene fluorescence method. This method determines how the polarity of local molecular environment around the pyrene molecule changes with increasing amphiphile concentration.[54] The changes in the fluorescent spectrum of pyrene depends on the polarity of the solvent. This effect is quantified by the ratio of the two intensities (I_1/I_3) in the fine structure of pyrene. A reduction in the ratio signifies a more hydrophobic environment. The I_1/I_3 ratio for pyrene in water is between 1.8 and 1.9.[55] Native cyclodextrins can interact with pyrene molecules ($K = 190\ M^{-1}$) but examination of Figure 5 finds that this interaction has little effect on the change in the polarity of the immediate environment surrounding pyrene.[56]

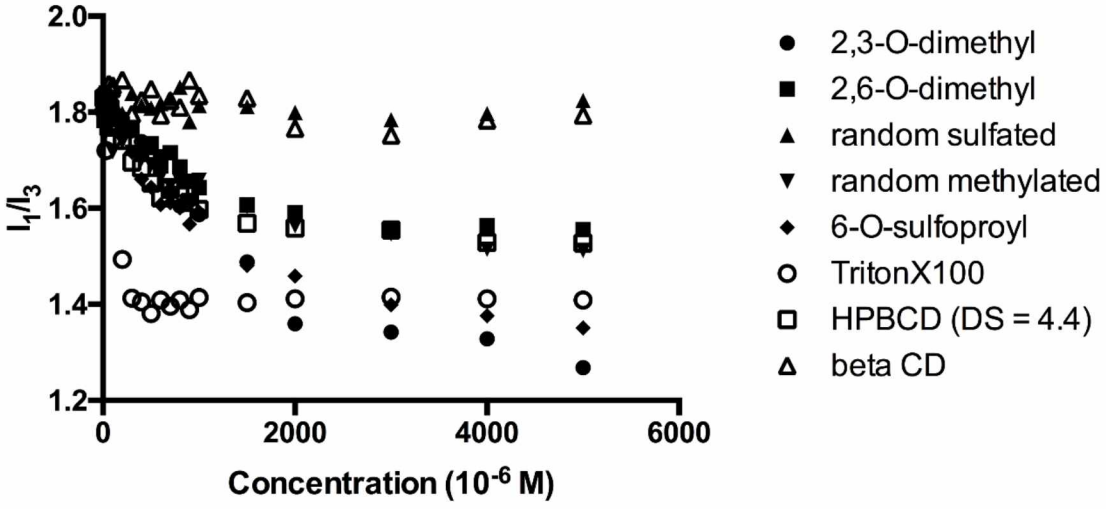

Figure 5. Pyrene fluorescent data of modified cyclodextrins and Triton X-100. Triton X-100 has a CMC of 110 μM which occurs at the point of discontinuity.

Figure 5 is the result of preliminary studies in the ability of many common cyclodextrins to solubilize pyrene.[1] Of the cyclodextrins studied using pyrene fluorescence, those CDs with no substituents or polar ones (randomly sulfated) demonstrated no increase in hydrophobicity index. Addition of small hydrophobic substituents (2,6 and random methyls); addition of sulfopropyl increases hydrophobicity index. 2,3-O-dimethyl-β-CD shows a large hydrophobicity change, probably due to amphiphilic directionality of structure. Triton X-100 was included for comparison of the CDs to a known surfactant with a well-defined point of discontinuity that defines the critical micelle concentration of 110 μM.[57]

Solubilization in aqueous media has useful attributes because it can potentially replace the use of organic solvents (or co-solvents) to dissolve reagents that are insoluble in water, are used as detergents (removal of grease, hydrophobic materials), a fixture for emulsion polymerization (an important factor in initiation step) and can separate materials for commercial or analytical purposes. They are also useful in oil recovery (solubilization produces reduced interfacial tensions required for oil mobilization), and in biological drugs/pharmaceutical solubilization.

1.5.3 New Amphiphilic Cyclodextrins for Nanoparticle Synthesis.

The pyrene fluorescence studies of cyclodextrin with various substituents and degrees of substitution in Figure 5 demonstrates that the microenvironment surrounds the pyrene molecular probe becomes more hydrophobic with addition of hydrophobic substituents (*i.e.* I_1/I_3 ratio < 1.8). However, none of the cyclodextrins under consideration approximate the behavior of a known surfactant, Triton X-100, where there is a well-defined point of inflection from which the hydrophobic microenvironment becomes invariant with increasing concentration. The location of

[1] Unpublished work

the substituents seems to have more an effect on the physical behavior of these cyclodextrins than the degree of substitution; 6-O-sulfopropyl and 2,3-O-dimethyl-β-CDs exhibit the most hydrophobic environments of the cyclodextrins in this study. The placement of these moieties gives the molecule a polar orientation that is necessary for surfactant behavior, but not sufficient. These cyclodextrins do not demonstrate the same solution behavior as Triton X-100; many polar molecules meet the requirements of a surfactant (*i.e.* polar headgroup and non-polar hydrophobic tail) but lack the right combination of these attributes to demonstrate aggregation behavior (*e.g.* octanol).[53] The regioselectivity of cyclodextrin chemistry easily allows the place of hydrophobic and hydrophilic groups on opposite sides of the torus. Sulfobutyl groups on the primary rim of the cyclodextrin with twice as many hydrophobic groups on the corresponding secondary rim hydroxyls should provide a headgroup polar enough for solubilization and electrostatic stabilization of micelles yet allow sufficient hydrophobicity for micelle formation. The choice of benzyl groups as hydrophobic moieties was seen as appropriate due their hydrophobic nature and the strong π-π interactions with other aromatic surfaces and/or moieties.

Synthesis of hexakis (2,3-O-dibenzyl-6-O-sulfobutyl) cyclomaltohexaose (DBSBA) and heptakis (2,3-O-dibenzyl-6-O-sulfobutyl) cyclomaltoheptaose (DBSBB) should provide a simple means to place sulfonate groups (or chelating groups of interest) on the polystyrene surface using the strong π-π interactions between benzyls and polystyrene chains. Emulsion polymerization of styrene, using amphiphilic cyclodextrins as an emulsifier, could be a convenient means to synthesize functionalized surface bound nanoparticles in a single step.

Polystyrene surfaces have been modified with sulfonate groups in a variety of ways, including the *in situ* formation of styrene sulfonate, the addition of sulfonated monomer in the emulsion polymerization recipe, use of a sulfonating agent (*e.g.* sulfuric acid), or introducing a sulfonated

surface active monomer. [58-61] These methods of sulfonation use chemical means to add sulfonate groups (and surface charge) to the polystyrene surface. The particle surface chemistry of emulsifier-free systems is dictated by the initiator, *e.g.* persulfate initiators produce sulfate stabilized latexes. [62,63] Sulfonation of the polystyrene surface using physisorption is problematic due to the investment of cleanup cost and time. Emulsion polymerization in the absence of surfactant was developed because a surface active agent is difficult to remove from latex once they have sorbed to the particle surface. The ability of an emulsifier to stabilize an emulsion arises from its electrostatic and/or steric repulsion capability and the intrinsic sorption of the molecule to the polystyrene surface.[63] Nanoparticles with freely available moieties extending from the solid polystyrene phase into the liquid aqueous phase have been previously synthesized using physical and chemical grafting techniques, most commonly using a diblock copolymer free radical mechanism or use of surface active monomers (surfmers). These techniques use multiple steps and require tightly controlled procedures. [64-67] The ability to synthesize the polystyrene nanoparticles requires an understanding of the emulsion polymerization; a review of emulsion polymerization theory is therefore warranted and appropriate.

1.6. Emulsion Polymerization

Emulsion polymerization is a unique modification of radical chain polymerization in which the loci of polymer synthesis occurs in a colloidal dispersion (emulsion). An emulsion is a discontinuous liquid phase that is dispersed in an immiscible liquid phase. The colloidal nature of emulsion polymerization is its main advantage over other methods of polymerization (suspension, dispersion) because of its measure of control. The physical forces that dictate the nature of the colloidal dispersion allow control over the dimensions, surface chemistry, polymerization rate, and molecular weight of the latex (aqueous polymer dispersion). Moreover,

the solvent used in emulsion polymerization, water, is a natural heat sink that retards autoacceleration reactions. The major function of the surfactant is stabilizing (electrostatically or sterically) particle nuclei produced during stage I of emulsion polymerization; growing polymer particles are supplied with surfactant from either the continuous aqueous phase or the monomer droplet. Emulsions, however, are kinetically stable as they remain unchanged over long periods of time. The differences between solubilization and emulsification warrant elucidation. Solubilization is thermodynamically stable and the solubilized molecules are in the same phase as the solubilizing agent (micelles). Emulsification is the dispersion of one liquid phase in another, which is thermodynamically unstable and will separate given sufficient time.

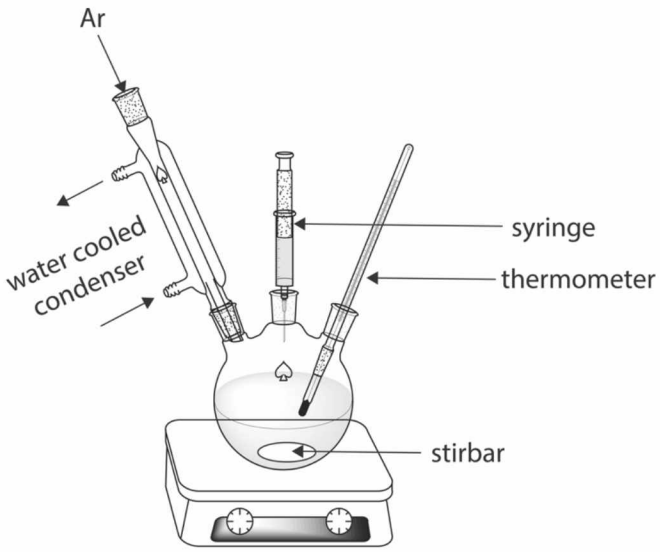

Figure 6. Batch emulsion polymerization reactor. All emulsion polymerization procedures were performed as a single "one-pot" synthesis with no further synthetic modifications.

Monodisperse polystyrene latexes that are produced from emulsion polymerization are strong candidates to model colloid studies because they are known to form nearly monodisperse spheres under certain conditions.[68,69] An ideal model colloid possesses the characteristics of

monodispersity, spherical shape, in which the number of functional groups on its surface are calculated empirically.[69,70] Polystyrene is an extensively used aromatic polymer that is thermally stable, biocompatible, and has been used as solid phase support for biosensors, photonic crystals, catalysts, protein absorption, and density reducing agent.[71] Emulsion polymerization is a well-studied means of synthesizing monodisperse, high molecular weight nanoparticles that form spontaneously in solution. It is an environmentally benign method; organic solvents are replaced with water as a reaction medium. Emulsion polymerization uses well-defined recipes in order to control the characteristics of the particles produced. The components of the recipes are varied with respect to need, but all recipes require an emulsifier (or stabilization agent), reaction medium (typically water), monomer, and water soluble initiator. Modifications of emulsion polymerization recipes can include a crosslinker and/or a buffering agent.

The emulsion polymerization process has several advantages over solution bulk polymerization. The colloidal nature/emulsion allows more control over the process. The main components of emulsion polymerization are monomer(s), dispersing medium, emulsifier, and water soluble initiator. The dispersing medium is typically water, which reduces the environmental burden of the process. The recipe of the components and their ratios dictate the physical properties of the system. Knowing this, we were interested in the possibility of performing a "one-pot" synthesis (Figure 6) of self-assembling polystyrene nanoparticles in which benzyl moieties of DBSBB should strongly interact /swell with styrene monomers during the first stage of EP and strongly physisorb to the polystyrene surface through strong interactions between the secondary rim benzyls and the polystyrene. Initiation, illustrated in Figure 7, begins the process of polymerization process. Emulsion polymerization uses water-soluble free radical initiators that

decompose in the aqueous phase. The most common, potassium persulfate, decomposes thermally at 50 °C.[72] The decomposition proceeds as:

$$S_2O_8^{2-} \rightarrow 2\ {}^{\cdot}OSO_3^- \qquad (13)$$

$$^{\cdot}SO_4^- + H_2O \rightarrow HSO_4^- + {}^{\cdot}OH \qquad (14)$$

$$2\ {}^{\cdot}OH \rightarrow H_2O + \frac{1}{2}O_2 \qquad (15)$$

Therefore, each initiator molecule produces two primary radicals that either remain as sulfate radicals or progress to hydroxyl radicals under acidic conditions. The presence of oxidants can severely diminish the polymer molecular weight as well as promote the formation of surface hydroxyl and/or carboxyl groups.[73]

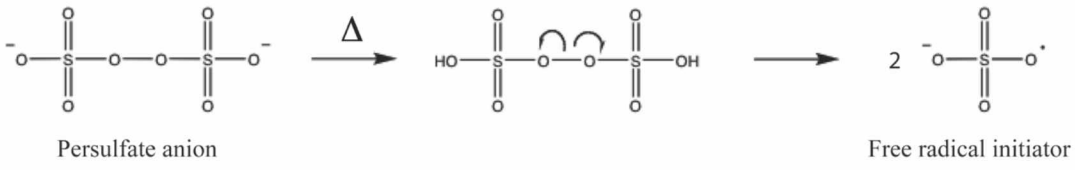

Persulfate anion Free radical initiator

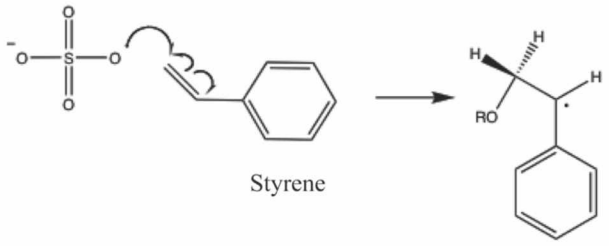

Styrene

Figure 7. Initiation of polymerization of styrene using persulfate initiator. Homolytic cleavage via thermal decomposition of persulfate begins the polymerization process.

Vanderhoff found that adjustment of pH to circumneutral or slightly basic conditions (pH 7-8) eliminated the production of hydroxyl free radicals; persulfate anions decomposed into only

sulfate radicals.[69] A buffering agent (*e.g.* $NaHCO_3$) is often employed as an additive for this reason. The Harkins-Smith-Ewart model (Figure 8) provides a good overview of the mechanism that controls the emulsion polymerization of styrene. This model is useful for batch emulsion polymerization (Figure 6) of a sparingly soluble monomer (*e.g.* styrene) in a system where the surfactant concentration is sufficiently large to form micelles. It is composed of three stages or intervals (I, II and III). Conversion of monomer into polymer begins and accelerates in Interval I. The hydrophobic environment of the micelles serves as polymerization loci. The monomer reservoir exists in large (with respect to micelles) droplets. Monomer migrates from the droplet reservoir through the aqueous phases to the micelles due to the surface area advantage possessed by micelles. Due to the aqueous solubility of the initiator and sparingly soluble nature of the monomer, the most likely loci of initiation occurs in the aqueous phase.[74]

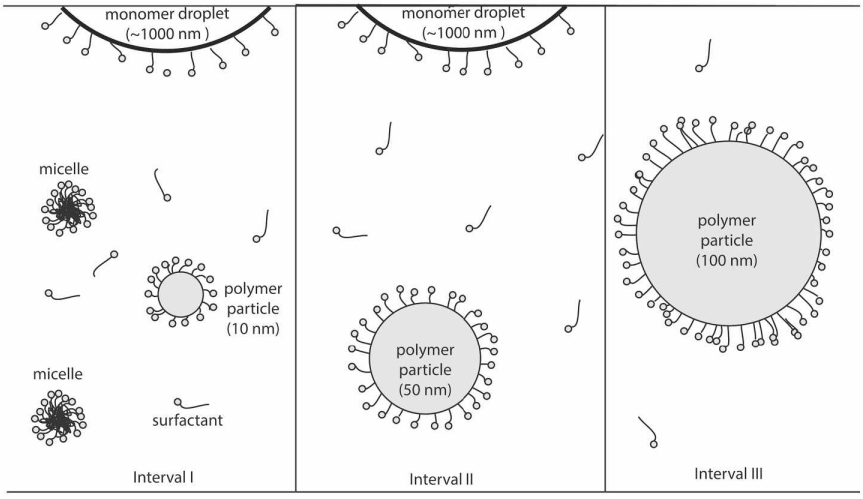

Figure 8. Overview of Intervals I, II, III of emulsion polymerization. Interval I is characterized by presence of monomer droplet, micelles, and beginning of polymerization. Interval II has no micelles present and continuation of polymerization. Interval III occurs when no monomer droplet is present and all remaining monomer is located in particles awaiting conversion to polymer.

Propagation (Figure 9) continues until the aqueous solubility of the amphiphile is exceeded upon which the oligomeric radical is incorporated into the micelle while the polar moiety remains on the surface. Polymerization proceeds rapidly once the micelle has been "stung". The average number of radicals per particle is 0.5; polymerization loci either have zero (termination) or one radical (propagation). Micellar compartmentalization of radicals is one of the strengths of emulsion polymerization. Polymer particles grow at the expense of micelle stability; the engorging particle adsorbs increasingly larger amounts of surfactant monomer to stabilize its expanding interfacial area. All micelles and 10-15% of monomer have been consumed at the end of Interval I.[74,75]

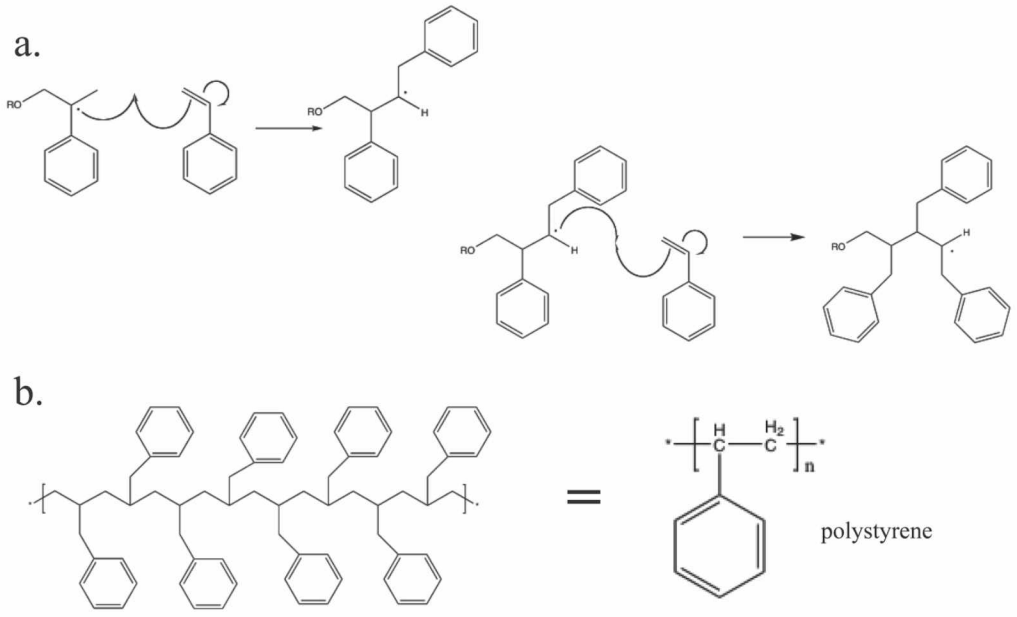

Figure 9. Propagation of styrene polymerization. Each step of polymerization produces a new radical species that attacks another molecule of styrene. Large molecular weight polymers of polystyrene are produced. Propagation ceases with termination step.

Interval II commences when the rate of polymerization is constant (i.e. no acceleration) and continues until the monomer droplet is consumed. The number of particles in now fixed. The number of latex particles (N) can be calculated if the radical capture efficiency of the micelle (K), the rate of initiation (ρ), the volumetric growth rate of latex particles (μ), the surface area of the surfactant head group (a_s), and the surfactant concentration (S) are known. [76,77]

$$N = K\left(\frac{\rho}{\mu}\right)^{2/5}(a_s S)^{3/5} \quad (16)$$

The values for K can range from 0.37 to 0.70; Smith and Ewart used a value of 0.53.[76,78] The rate of initiation scales with the concentration of the initiator in the recipe, therefore during an ideal Interval II polymerization, the reaction rate and the subsequent number of particles are proportional to $[I]^{2/5}$ and $[S]^{3/5}$. 30-40% of monomer has been converted to polymer at the completion of this stage. The rate of polymerization begins to decrease at the beginning of Interval III; the interval concludes when the monomer supply is exhausted. Conversion percentages are often in excess of 99%.

The chemical grafting of functional groups onto polystyrene surfaces requires additional steps, further rounds of polymerization, and often harsh conditions.[79] Physical grafting, however, could be a viable alternative to chemical grafting if the interactions between the core and the shell are strong enough to limit and/or eliminate desorption. Aromatically modified dextrans (linear glucose polysaccharide composed of a 1,6 linkages) have been shown to adhere strongly to polystyrene beads with the aromatic rings as points of contact with the particle surface. These aromatic dextrans produced a hydrophilic shell sufficiently strong enough to anchor a subsequent layer of bovine serum albumin (BSA).[80] This core-shell structural motif has been quite common.[81-84]

1.6.1 Characterization of Nanoparticles

Natural colloids are a dominant feature in environmental chemistry; they are exist in large concentrations, present a large surface area for interfacial interactions, and are found in variety of natural waters, including ground, surface, ocean, sediment and interstitial.[1] The impact of colloids lies in their large surface area to volume ratio and accumulation at the solid-water interface. Colloids are surrounded by an interface that separate aqueous and solid phases and are characterized by their stability and particle size distribution. Electrostatically stabilized colloids are defined by the transition zone between these phases (*i.e.* electrical double layer). The amount of surface charge per unit area (surface charge density) is an intensive function of surface bound ionic functional groups and the pH of the system.

$$\sigma_P = \sigma_0 + \sigma_H + \sigma_{IS} + \sigma_{OS} \qquad (17)$$

where σ_P is the total net surface charge, σ_0 is the permanent surface charge, σ_H is the net proton charge, σ_{IS} is the inner-sphere complex charge, and σ_{OS} is the outer-sphere complex charge. The sum of $\sigma_{IS} + \sigma_{OS}$ is the Stern layer while the $\sigma_0 + \sigma_H$ is the intrinsic surface charge density. The relationship of these parameters as a function of distance from the particle surface describes the electrical diffuse layer (Figure 10) IHP, the inner Helmholtz plane, which has an electric potential Ψ^{IS} that corresponds to a charge density, σ^{IS}, and is located at a distance from the surface where specifically adsorbed ions (i.e. inner-sphere complex) are located. OHP, the outer Helmholtz layer, has a corresponding potential Ψ^{OS}, the diffuse layer, and is the locus of non-specific ion complexation. The IHP and the OHP comprise the Stern layer. The electrokinetic surface charge, σ^{ek}, corresponds to the zeta (ζ) potential, at the distance of the slipping plane (*i.e.* boundary between the hydrodynamically mobile particle and the immobile (bulk) fluid. The zeta

potential is characteristic of the surface charge of a particle as it moves through an electric field. At low ionic strength, the zeta potential is approximately equal to the electric potential of the diffuse layer (Ψ^d). The electrostatic stability of a colloid can be measured by the zeta potential as it is reflective of the intrinsic surface charge. Zeta potentials that are equal to, or in excess of, +/- 30 kV are considered electrostatically stable.[53,85] The corresponding surface charge associated with the zeta potential will, of course, be lower than the intrinsic surface charge due to shielding considerations.

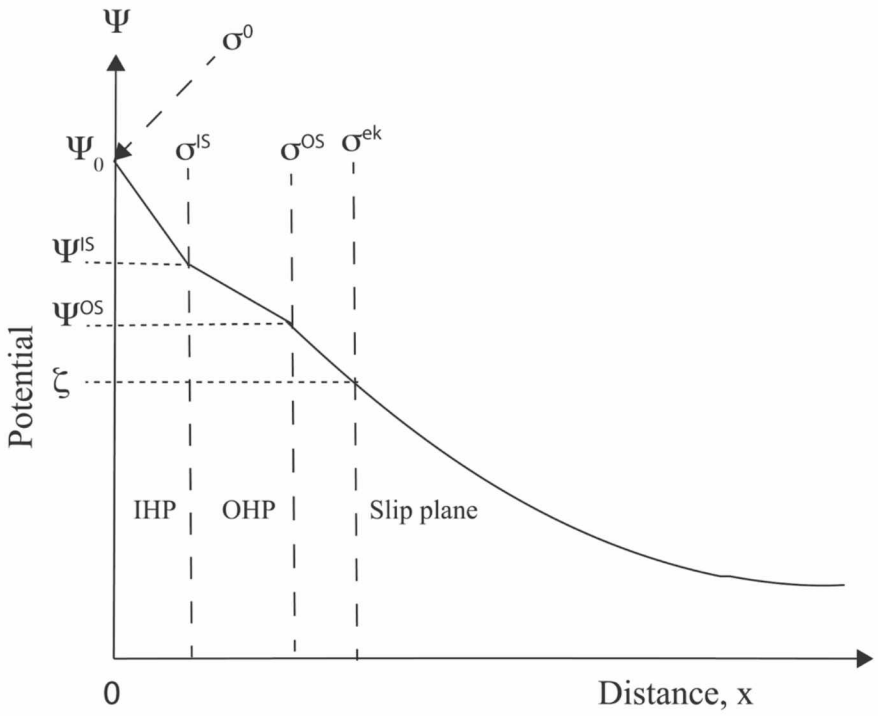

Figure 10. Representation of charges (σ), potentials (Ψ), and their relationship to distance (x) from a charged interface. Electric potential drops with increasing distance due to shielding from counterions.

The surface charge of a colloidal particle is shielded by a diffuse layer of solvated counterions. The electrostatic surface potential (zeta) is highly dependent on immediate environment. The fixed surface charge and diffuse layers equals the "double layer". The surfaces of electrostatically stabilized colloids can be characterized by conductivity and zeta potential measurements.[86] These values can grant insights into the surface chemistry of colloids, the likelihood of their stability, or any trends in relation to surface chemistry if multiple samples are examined. The pH must be tightly controlled due to the sensitivity of many functional groups to the hydrogen ion concentration. The Gouy-Chapman theory relates the surface charge density (σ_P) to the surface potential (ψ_0):

$$\sigma_P=(8RT\varepsilon\varepsilon_0 c \times 10^3)^{1/2} \sinh\left(\frac{Z\psi_0 F}{2}RT\right) \quad (18)$$

where surface potential is in units of volts, R is the molar gas constant, T is the absolute temperature, F is Faraday's constant (96490 C mol^{-1}), ε is the relative dielectric constant (ε_{H2O} = 78.5, T = 273 K), ε_0 is the permittivity of free space, and c is the molar electrolyte concentration in moles per liter. Many colloidal particles do not carry a constant surface potential (depends of on electrolyte concentration) but do have a constant surface charge density (σ). Surface charge density should be a more characteristic quantity than zeta potential; electrokinetic mobility can be rewritten as a function of σ and κa (μ = μ (σ,κa). The Smoluchowski equation is a well-known relationship between electrophoretic mobility (μ) of spherical colloidal particle of radius a and its zeta potential (ζ).

$$\mu = \frac{\varepsilon_r \varepsilon_0}{\eta}\xi \quad (19)$$

where ε_r and η are the relative permittivity and viscosity of the electrolyte solution. Dispersion is a generic term (from the Latin to remove or redistribute) for systems with regard to state of matter forming the dispersed and continuous phases. Water is an important liquid that is the continuous phase in natural and industrial dispersions.

Colloidal stabilization is a function of balance between repulsive (electrostatic) and attractive (van der Waals) forces between all of the interacting particles. Van der Waals interactions, always attractive, are a function of surface area. The large surface area to volume ratio of colloids advocates for aggregation if there are no forces that oppose attractive interactions. Coagulation/sedimentation occurs if attractive forces dominate over repulsive forces. The relationship between interparticle distance and these attractive and repulsive forces is summarized by DVLO theory, named after two groups of researchers (Derjaguin/Landau and Verwey/Overbeek), that quantitatively determines the interaction energy between particles as a balance between attractive van der Waals attractions and repulsive double layer effects. This interaction energy is considered as a function of interparticle distance.[87] Colloids are thermodynamically unstable with respect to the bulk solution but kinetically nonlabile. The energy of attraction between the centers of two particles *i* and *j*, separated by a distance R_{ij}, varies with their separation as $1/R^6_{ij}$. The sum of these interactions decreases only approximately $1/R_2$; this arises from the fact that at small distances only a few molecules interact but at large distances many individual molecules are about the same distance from one another and contribute equally to the sum, so the total interaction does not fall off as fast as the single molecule-molecule interactions.

Calculation of particle size is derived from the calculation of diffusion coefficient and the assumption of spherical particles.[52] The ability to correlate the distance a particle has travelled

over a given time interval allows the calculation of particle size. Dynamic light scattering (DLS), diffusion ordered nuclear magnetic resonance (NMR) spectroscopy, and other particle sizing methods use this correlation between distance and time to calculate particle size.[88-90] Accurate prediction of the outcome of single molecules is unlikely, but it is possible to statistically determine the probability of its displacement. The mean rate of translational diffusion is described by the diffusion coefficient, D.[91] Unrestricted particles move at a velocity dictated by their kinetic energy. Solvated particles are restricted in their motion by the other surrounding molecules due to friction.

$$F_f = -fv = -6\pi\eta r v \qquad (20)$$

where *r* is the particle radius, *v* is the velocity of the particle, η is the viscosity of the medium, and *f* is the frictional coefficient. Therefore, the relationship between the kinetic energy of a single molecule and the friction generated from its solvent cage is dictated by the Stokes-Einstein equation.[92]

$$D = \frac{k_B T}{f} = \frac{k_B T}{6\pi\eta r} \qquad (21)$$

This relationship between particle size (solvated) and its velocity is succinctly summarized by its diffusion coefficient, D (m^2/seconds). The probability of a particle displaced over a given distance, Z, in a given time, t, is described by the Gaussian distribution function:

$$\mathrm{P(Z)} = \frac{1}{\sqrt{4\pi \mathrm{Dt}}} \exp\left(-\frac{\mathrm{Z}^2}{4\mathrm{Dt}}\right) \qquad (22)$$

Examination of equation 22 finds that diffusion coefficients and the probable distance travelled over a given time are inversely proportional; particles with smaller diffusion coefficients move

faster.[88] Diffusion coefficients can be used to estimate the molecular weight of a compound as D scales with the inverse cube root of molecular mass. More importantly for supramolecular studies, changes in diffusion coefficient correspond to changes in molecular mass (*i.e.* aggregation). These changes can be determined from the comparison between an experimentally measured diffusion coefficient and one calculated from the dimensional parameters of a single molecule.[93]

1.7 Research Aims

The focus of my research is the synthesis of derivatized cyclodextrin polystyrene bound nanoparticles and the investigation of their colloidal properties. These goals were accomplished in three stages or aims.

Aim 1. Synthesis of Amphiphilic Cyclodextrins (DBSBA and DBSBB)

The synthesis of single isomer amphiphilic cyclodextrins was crucial to the elucidation of the chemical and physical properties of both the molecular and colloidal level. A lack of macrocyclic symmetry means that observables are a function of both the intrinsic system properties of the molecule and the degree of substitution. Any principles that can be extracted from an averaged system with a large variance will be less insightful than the data that arises from system properties dictated by a single isomer. Chapter 2 illustrates that hexakis (2,3-O-dibenzyl, 6-O-sulfobutyl) cyclomaltohexaose and heptakis (2,3-O-dibenzyl, 6-O-sulfobutyl) cyclomaltoheptaose (Figure 11) were synthesized using the development of new techniques that substantially improved yield while reducing the need for chromatographic purification. Isolation of the persubstituted 2,3-O-benzylated isomer once required numerous chromatographic columns while the sulfobutylation procedure, while successful, utilized several steps of ion exchange

chromatography and extraction to remove the 18-crown-6 additive once necessary for complete sulfobutylation. These sulfonic acid salts were used to promote colloidal electrostatic stabilization due to complete ionization of the moiety under observed conditions (pKa ~1.2) and synthetic considerations.[9,94]

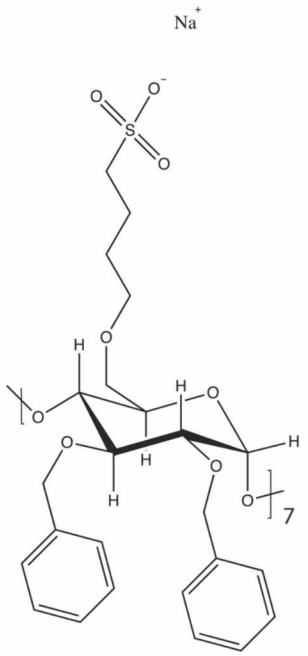

Figure 11. Structure of heptakis (2,3-dibenzyl, 6-O-sulfobutyl) cyclomaltoheptaose sodium salt (DBSBB).

Aim 2. Characterization and analysis of DBSBA and DBSBB aggregation

Any analysis of a surfactant begins with how system properties change with increasing concentration. Using established techniques, Chapter 3 demonstrates the characterization and analysis of the single isomer amphiphilic colloidal properties in solution were performed using established techniques. The changes in given observable properties with concentration of the synthesized cyclodextrin amphiphile was recorded and analyzed. The critical micelle

concentration, an abrupt change in physical property that is both observable and reflective of aggregation state, is an important characteristic of the colloidal system that begins the search for insights into the intrinsic system properties of the molecule. The changes in observed diameter, conductivity profile, and the immediate change in local dipole moment (pyrene fluorescence) with concentration were performed. Analysis of thermodynamic data can elucidate the nature of interactions with water, a solvent with interesting thermodynamic properties in its own right. Finally, previous micelle systems have demonstrated the ability to solubilize hydrophobic molecules. Solubilization is the spontaneous dissolving of a substance by reversible interaction with micelles to form a thermodynamically stable isotropic solution with reduced thermodynamic activity of the solubilized material, or solubilzate.[95] Since the hydrophobic anchors of these single isomers are aromatic, our choice of solubilizate, hexafluorobenzene, is well known to strongly interact with aromatic groups and should provide insights into the colloidal system.

Aim 3. Characterization of Polystyrene-Supported Cyclodextrin Nanoparticles.

The formation of polystyrene nanoparticles using a single isomer amphiphilic cyclodextrin (heptakis(2,3-O-dibenzyl, 6-O-sulfobutyl) cyclomaltoheptaose) was documented in Chapter 4. Benzyl groups and polystyrene interact strongly via π-π interactions. The regioselective synthesis of benzyl groups on the secondary rim of the cyclodextrin provided loci where the proposed nanoscaffold can anchor onto the polystyrene surface. Emulsion polymerization was a facile method of nanoparticle production where benzylated amphiphilic cyclodextrins, styrene monomer, and other additives of established recipes, self-assembled into nanoparticles upon which future remediation studies can occur. Characterization of polystyrene used well known methods; calculation of the particle diameter, surface charge density, zeta potential, and NMR

investigation of free sulfobutyl chain were performed using particle sizing, electrokinetic, conductivity and NMR spectrometry.

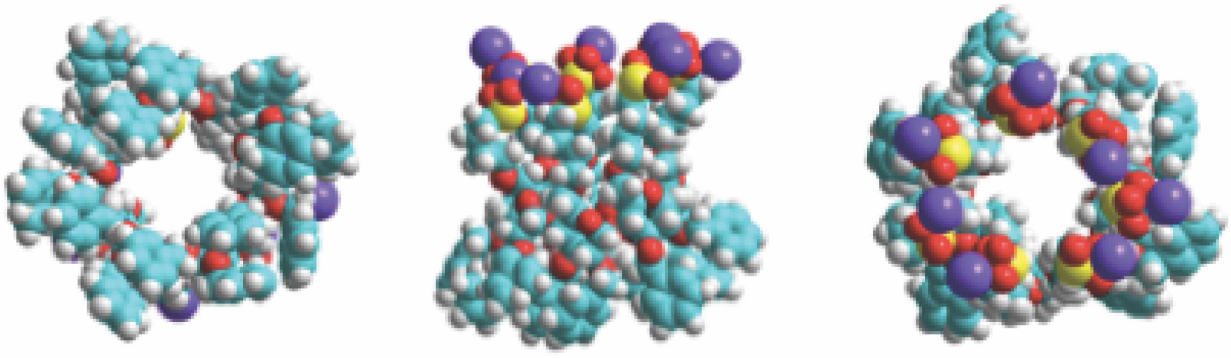

Figure 12: Space filling model representation of DBSBB.

The large surface area of nanoparticles is critical to effective sequestration of aqueous toxic metal species. Nanoparticles with modified cyclodextrins on the surface (at the solid/liquid interface) were efficiently produced in a single step using emulsion polymerization of styrene to form polystyrene beads. Amphiphilic cyclodextrins, using benzyl groups to promote self-assembly and strong interactions with polystyrene surfaces and sulfobutyl groups for electrostatically stability) were synthesized to form micelles that promote formation of uniform polystyrene beads and possess intrinsic solubilization of VOCs. Figure 12 shows a model of the proposed structure (*vide supra)* of heptakis (2,3-dibenzyl, 6-O-sulfobutyl) cyclomaltoheptaose and was constructed using the HyperChem 8.01 molecular modeling program.[96]

1.8 Conclusions

Cyclodextrins have been used in remediation of organic molecules and toxic metal aqueous species. [35,97-99] They have been adapted to membranes, activated carbon, resins, and polymers. [100-103] The derivatization capabilities of cyclodextrin, their well-known structure, and the large volume of literature dedicated to cyclodextrin chemistry and cyclodextrin-remediation technologies provides a suitable foundation for the adaption of tunable ligands to be grafted to cyclodextrins. The tunable aspect of this approach allows for combinations and relative amounts of cyclodextrin derivatives that reflect the remediation needs of the community under consideration. Filters composed of these tunable cyclodextrin derivatives could be synthesized to meet or exceed water quality standards of a variety of locations including rural, urban, and suburban.

1.9 References

(1) Stumm, W.; Morgan, J. J. *Aquatic Chemistry*, 3rd ed.; John Wiley & Sons, Inc, 1996.

(2) Adriano, D. C. *Trace Elements in Terrestrial Environments*, 2nd ed.; Springer New York: New York, NY, 2001.

(3) Strandesen, M.; Birkved, M.; Holm, P. E.; Hauschild, M. Z. Fate and Distribution Modelling of Metals in Life Cycle Impact Assessment. *Ecological Modelling* 2007, *203* (3-4), 327–338.

(4) Schnoor, J. L. *Environmental Modeling: Fate and Transport of Pollutants in Water, Air, and Soil.*; John Wiley and Sons, 1996.

(5) Lynes, M. A.; Kang, Y. J.; Sensi, S. L.; Perdrizet, G. A.; Hightower, L. E. Heavy Metal Ions in Normal Physiology, Toxic Stress, and Cytoprotection. *Annals of the New York Academy of Sciences* 2007, *1113*, 159–172.

(6) Krauskopf, K. B. Environmental Geochemistry. *Encyclopedia of Physical Science and Technology*; New York, 1992; Vol. 6, pp 185–214.

(7) Fiscal Year 2014-2018 EPA Strategic Plan, 2014.

(8) Langmuir, D. *Aqueous Environmental Geochemistry*, 1st ed.; Prentice Hall, 1997.

(9) Vandenbossche, M.; Jimenez, M.; Casetta, M.; Traisnel, M. Remediation of Heavy Metals by Biomolecules: a Review. *Critical Reviews in Environmental Science and Technology* 2015, *45*, 1644–1704.

(10) Volesky, B.; Holan, Z. R. Biosorption of Heavy Metals. *Biotechnology Progress* 1995, *11*, 235–250.

(11) Volesky, B. Biosorption and Me. *Water Research* 2007, *41*, 4017–4029.

(12) Plazinski, W. Binding of Heavy Metals by Algal Biosorbents. Theoretical Models of Kinetics, Equilibria and Thermodynamics. *Advances in Colloid and Interface Sci*ence 2013, *197*, 58–67.

(13) Fourest, E.; Volesky, B. Contribution of Sulfonate Groups and Alginate to Heavy Metal Biosorption by the Dry Biomass of Sargassum Fluitans. *Environmental Science & Technology* 1995, *30*, 277–282.

(14) Nowack, B. Chelating Agents and the Environment. *Environmental Pollution* 2008, *153*, 1–2.

(15) Newman, M. C. *Fundamentals of Ecotoxicology*; CRC Press, 2010.

(16) Morel, F.; Herring, J. *Principles and Applications of Aquatic Chemistry*; John Wiley & Sons: New York, 1993.

(17) Housecraft, C.; Sharpe, A. *Inorganic Chemistry*, 3rd ed.; Prentice Hall: New York.

(18) Bhattacharya, P. *Metal Ions in Biochemistry*; Alpha Science International Ltd, 2005.

(19) Parr, R. G.; Pearson, R. G. Absolute Hardness: Companion Parameter to Absolute Electronegativity. *Journal of the American Chemical Society* 1983, *105*, 7512–7516.

(20) Pearson, R. G. Hard and Soft Acids and Bases, HSAB, Part II: Underlying Theories. *Journal of Chemical Education.* 1968, 45, 643-648

(21) Brezonik, P.; Arnold, W. *Water Chemistry*; Oxford University Press: New York, NY, 2011.

(22) Hancock, R. D.; Martell, A. E. *Metal Complexes in Aqueous Solutions*, 2nd ed.; Fackler, J., Ed.; Springer Science+ Business Media LLC, 1996.

(23) Cabbiness, D. K.; Margerum, D. W. Macrocyclic Effect on the Stability of Copper (II) Tetramine Complexes. *Journal of the American Chemical Society* 1969, *91*, 6540–6541.

(24) Davis, F.; Higson, S. *Macrocycles*; John Wiley & Sons, Ltd.: West Sussex, UK, 2011.

(25) Constable, E. *Coordination Chemistry of Macrocyclic Compounds*; Oxford University Press: New York, 1999.

(26) Szejtli, J. Introduction and General Overview of Cyclodextrin Chemistry. *Chemical Reviews* 1998, *98*, 1743–1754.

(27) Guo, X.; Zhang, S.; Shan, X.-Q. Adsorption of Metal Ions on Lignin. *Journal of Hazardous Materials* 2008, *151*, 134–142.

(28) Abdel-Halim, E. S.; Al-Deyab, S. S. Removal of Heavy Metals From Their Aqueous Solutions Through Adsorption Onto Natural Polymers. *Carbohydrate Polymers* 2011, *84*, 454–458.

(29) Merrifield, J. D.; Davids, W. G.; MacRae, J. D.; Amirbahman, A. Uptake of Mercury by Thiol-Grafted Chitosan Gel Beads. *Water Research* 2004, *38*, 3132–3138.

(30) *Cyclodextrins and Their Complexes*, 1st ed.; Dodziuk, H., Ed.; WILEY-VCH Verlag GmbH & Co.: Heidelberg, Germany, 2006.

(31) Szejtli, J. Past, Present, and Future of Cyclodextrin Research. *Pure and Applied Chemistry* 2004, *76*, 1825–1845.

(32) Del Valle, E. M. M. Cyclodextrins and Their Uses: a Review. *Process Biochemistry* 2004, *39*, 1033–1046.

(33) Szejtli, J. Utilization of Cyclodextrins in Industrial Products and Processes. *Journal of Material Chemistry* 1997, *7*, 575–587.

(34) Wang, X.; Brusseau, M. L. Solubilization of Some Low-Polarity Organic Compounds by Hydroxypropyl-. Beta.-Cyclodextrin. *Environmental Science & Technology* 1993, *27*, 2821–2825.

(35) Landy, D.; Mallard, I.; Ponchel, A.; Monflier, E.; Fourmentin, S. Remediation Technologies Using Cyclodextrins: an Overview. *Environmental Chemistry Letters* 2012, *10*, 225–237.

(36) Breslow, R.; Dong, S. D. Biomimetic Reactions Catalyzed by Cyclodextrins and Their Derivatives. *Chemical Reviews* 1998.

(37) Ko, S.-O.; Schlautman, M. A. Partitioning of Hydrophobic Organic Compounds to Hydroxypropyl-B-Cyclodextrin: Experimental Studies and Model Predictions for Surfactant-Enhanced Remediation. *Environmental Science & Technology* 1999, *33*, 2765–2770.

(38) Dong, Z.; Luo, Q.; Liu, J. Artificial Enzymes Based on Supramolecular Scaffolds. *Chemical Society Reviews* 2012, *41*, 7890–19.

(39) Wenz, G. Cyclodextrins as Building Blocks for Supramolecular Structures and Functional Units. *Angewandte Chemie International Edition in English* 1994, *33*, 803–822.

(40) Han, B.-H.; Antonietti, M. One-Step Synthesis of Copper Nanoparticles Containing Mesoporous Silica by Nanocasting of Binuclear Copper (II) Complexes with Cyclodextrins. *Journal of Materials Chemistry* 2003, *13*, 1793–1796.

(41) Alexandratos, S. D.; Zhu, X. Polyols as Scaffolds in the Development of Ion-Selective Polymer-Supported Reagents: the Effect of Auxiliary Groups on the Mechanism of Metal Ion Complexation. *Inorganic Chemistry* 2008, *47*, 2831–2836.

(42) Szente, L.; Szejtli, J. Highly Soluble Cyclodextrin Derivatives: Chemistry, Properties, and Trends in Development. *Advanced Drug Delivery Reviews* 1999, *36*, 17–28.

(43) Khan, A. R.; Forgo, P.; Stine, K. J.; D'Souza, V. T. Methods for Selective Modifications of Cyclodextrins. *Chemical Reviews* 1998, *98*, 1977–1996.

(44) Gelb, R. I.; Schwartz, L. M.; Bradshaw, J. J.; Laufer, D. A. Acid Dissociation of Cyclohexaamylose and Cycloheptaamylose. *Bioorganic Chemistry* 1980, *9*, 299–304.

(45) Takeo, K. I.; Ueraura, K.; Mitoh, H. Derivatives of α-Cyclodextrin and the Synthesis of 6-O-α-D-Glucopyranosyl-α-Cyclodextrin. *Journal of Carbohydrate Chemistry* 1988, *7*, 293–308.

(46) Reichardt, C. *Solvents and Solvent Effects in Organic Chemistry*, Third. Wiley-VCH Verlag GmbH & Co.: Weinheim, 2003.

(47) Roux, M.; Perly, B.; Djedaïni-Pilard, F. Self-Assemblies of Amphiphilic Cyclodextrins. *European Biophysical Journal* 2007, *36*, 861–867.

(48) Lombardo, D.; Longo, A.; Darcy, R.; Mazzaglia, A. Structural Properties of Nonionic Cyclodextrin Colloids in Water. *Langmuir* 2004, *20*, 1057–1064.

(49) Sallas, F.; Darcy, R. Amphiphilic Cyclodextrins – Advances in Synthesis and Supramolecular Chemistry. *European Journal of Organic Chemistry. 2008,* 6, 957–969.

(50) Geze, A.; Aous, S.; Baussanne, I.; Putaux, J.; Defaye, J.; Wouessidjewe, D. Influence of Chemical Structure of Amphiphilic Beta-Cyclodextrins on Their Ability to Form Stable Nanoparticles. *International Journal of Pharmaceutics* 2002, *242*, 301–305.

(51) Degobert, G.; Dubes, A.; Parrot-Lopez, H.; Fessi, H. Sulfated and Non-Sulfated Amphiphilic-β-Cyclodextrins: Impact of Their Structural Properties on the Physicochemical Properties of Nanoparticles. *International Journal of Pharmaceutics* 2008, *351*, 289–295.

(52) Wennerstrom, H.; Evans, D. F. *The Colloidal Domain: Where Physics, Chemistry, and Biology Meet*, 1st ed.; Wiley-VCH.

(53) Hiemenz, P.; Rajagopalan, R. *Principles of Colloid and Surface Chemistry*, 3rd ed.; CRC Press, 1997.

(54) Kalyanasundaram, K.; Thomas, J. K. Environmental Effects on Vibronic Band Intensities in Pyrene Monomer Fluorescence and Their Application in Studies of Micellar Systems. *Journal of the American Chemical Society* 1977, *99*, 2039–2044.

(55) Dong, D. C.; Winnik, M. A. The Py Scale of Solvent Polarities. *Canadian Journal of Chemistry* 1984, *62*, 2560–2565.

(56) Nakajima, A. A Study of the System of Pyrene and β-Cyclodextrin in Aqueous Solution Utilizing the Intensity Enhancement Phenomenon. *Spectrochimica Acta Part A: Molecular Spectroscopy* 1983, *39* (10), 913–915.

(57) Mukerjee, P.; Mysels, K. J. *Critical Micelle Concentrations of Aqueous Surfactant Systems.* NSRDS-NBS-36. National Standard Reference Data System. 1971.

(58) Karaman, M. E.; Meagher, L.; Pashley, R. M. Surface Chemistry of Emulsion Polymerization. *Langmuir* 1993, *9* (5), 1220–1227.

(59) Brijmohan, S. B.; Swier, S.; Weiss, R. A. Synthesis and Characterization of Cross-Linked Sulfonated Polystyrene Nanoparticles. *Industrial & Engineering Chemistry* 2005, *44*, 8039–8045.

(60) Gibson, H. W.; Bailey, F. C. Chemical Modification of Polymers. 13. Sulfonation of Polystyrene Surfaces. *Macromolecules* 1980, *13* (1), 34–41.

(61) Xu, X. J.; Goh, H. L.; Siow, K. S.; Gan, L. M. Synthesis of Polymerizable Anionic Surfactants and Their Emulsion Copolymerization with Styrene. *Langmuir* 2001, *17* (20), 6077–6085.

(62) Zou, D.; Derlich, V.; Gandhi, K.; Park, M.; Sun, L.; Kriz, D.; Lee, Y. D.; Kim, G.; Aklonis, J. J.; Salovey, R. Model Filled Polymers. I. Synthesis of Crosslinked Monodisperse Polystyrene Beads. *Journal of Polymer Science Part A: Polymer Chemistry* 1990, *28* (7), 1909–1921.

(63) Capek, I. Sterically and Electrosterically Stabilized Emulsion Polymerization. Kinetics and Preparation. *Advances in Colloid and Interface Science* 2002, *99*, 77–162.

(64) Prescott, S. W.; Ballard, M. J.; Rizzardo, E.; Gilbert, R. G. RAFT in Emulsion Polymerization: What Makes It Different? *Aust. J. Chem.* 2002, *55*, 415–424.

(65) Apostolovic, B.; Quattrini, F.; Butté, A.; Storti, G.; Morbidelli, M. *Ab Initio* Emulsion Polymerization by RAFT (Reversible Addition–Fragmentation Chain Transfer) Through the Addition of Cyclodextrins. *Helvetica Chimica Acta* 2006, *89*, 1641–1659.

(66) Summers, M.; Eastoe, J. Applications of Polymerizable Surfactants. *Advances in Colloid and Interface Science* 2003, *100-102*, 137–152.

(67) Wang, X.; Sudol, E. D.; El-Aasser, M. S. Emulsion Polymerization of Styrene Using a Reactive Surfactant and Its Polymeric Counterpart: Kinetic Studies. *Macromolecules* 2001, *34* , 7715–7723.

(68) Stone-Masui, J.; Watillon, A. Characterization of Surface Charge on Polystyrene Latices. *Journal of Colloid and Interface Science* 1975, *52* , 479–503.

(69) Vanderhoff, J. W. Well-Characterized Monodisperse Polystyrene Latexes as Model Colloids. *Pure and Applied Chemistry* 1980, *52*, 1263–1273.

(70) Deželić, N.; Petres, M.; Deželić, G. Preparation of Monodisperse Polystyrene Latices. *Kolloid-Zeitschrift und Zeitschrift für Polymere* 1970, 242 (1), 1142-1150

(71) Wang, X.; Zhang, Y.; Lv, F.; Shen, B.; Zhang, R.; Zhou, F.; Chu, P. K. Cross-Linked Polystyrene Microspheres as Density-Reducing Agent in Drilling Fluid. *Journal of Petroleum Science and Engineering* 2011, *78* (2), 529–533.

(72) Kolthoff, I. M.; Miller, I. K. The Chemistry of Persulfate. I. the Kinetics and Mechanism of the Decomposition of the Persulfate Ion in Aqueous Medium 1. *Journal of the American Chemical Society* 1951, *73* (7), 3055–3059.

(73) Ebewele, R. O. *Polymer Science and Technology*. 1st ed. CRC Press: New York, 2000.

(74) Rudin, A. *The Elements of Polymer Science and Engineering*, 2nd ed.; Academic Press: San Diego, 1999.

(75) Odian, G. *Principles of Polymerization*, 4th ed.; John Wiley & Sons, Inc.: Hoboken, 2004.

(76) Smith, W. V.; Ewart, R. H. Kinetics of Emulsion Polymerization. *Journal of Chemical Physics.* 1948, *16*, 592-598.

(77) Roe, C. P. Surface Chemistry Aspects of Emulsion Polymerization. *Industrial & Engineering Chemistry* 1968, *60*, 20–33.

(78) Thickett, S. C.; Gilbert, R. G. Emulsion Polymerization: State of the Art in Kinetics and Mechanisms. *Polymer* 2007, *48*, 6965–6991.

(79) Bhattacharya, A.; Misra, B. Grafting: a Versatile Means to Modify Polymers Techniques, Factors and Applications. *Progress in Polymer Science* 2004, *29*, 767–814.

(80) Fournier, C.; Leonard, M.; Le Coq-Leonard, I. Coating Polystyrene Particles by Adsorption of Hydrophobically Modified Dextran. *Langmuir* 1995, *11*, 2344–2347.

(81) Giacomelli, C.; Schmidt, V.; Putaux, J.-L.; Narumi, A.; Kakuchi, T.; Borsali, R. Aqueous Self-Assembly of Polystyrene Chains End-Functionalized with β-Cyclodextrin. *Biomacromolecules* 2009, *10*, 449–453.

(82) Larpent, C.; Geniès, C.; De Sousa Delgado, A. P.; Caminade, A.-M.; Majoral, J.-P.; Sassi, J.-F.; Leising, F. Giant Dendrimer-Like Particles From Nanolatexes. *Chemical Communications* 2004, 16, 1816–1817.

(83) Ghosh Chaudhuri, R.; Paria, S. Core/Shell Nanoparticles: Classes, Properties, Synthesis Mechanisms, Characterization, and Applications. *Chemical Reviews* 2012, *112*, 2373–2433.

(84) Gawande, M. B.; Goswami, A.; Asefa, T.; Guo, H.; Biradar, A. V.; Peng, D.-L.; Zboril, R.; Varma, R. S. Core-Shell Nanoparticles: Synthesis and Applications in Catalysis and Electrocatalysis. *Chemical Society Reviews* 2015, *44*, 7540–7590.

(85) Hunter, R. *Zeta Potential in Colloid Science*, 3rd ed.; Academic Press, New York, 1988.

(86) Zhu, S.; Panne, U.; Rurack, K. A Rapid Method for the Assessment of the Surface Group Density of Carboxylic Acid -Functionalized Polystyrene Microparticles. *Analyst* 2013, *138*, 2924–2930.

(87) Evans, D. F.; Ninham, B. W. Molecular Forces in the Self-Organization of Amphiphiles. *Journal of Physical Chemistry* 1986, *90*, 226–234.

(88) Price, W. S. *NMR Studies of Translational Motion: Principles and Applications*; Cambridge University Press, New York, 2009.

(89) Tscharnuter, W. *Photon Correlation Spectroscopy in Particle Sizing*; John Wiley & Sons, Ltd: Chichester, UK, 2000.

(90) Hunter, R. *Foundations of Colloid Science*, 2nd ed.; Oxford University Press, New York, 2001.

(91) Cohen, Y.; Avram, L.; Frish, L. Diffusion NMR Spectroscopy in Supramolecular and Combinatorial Chemistry: an Old Parameter? New Insights. *Angewandte Chemie International Edition in English* 2005, *44*, 520–554.

(92) Price, W. S. Pulsed-Field Gradient Nuclear Magnetic Resonance as a Tool for Studying Translational Diffusion: Part 1. Basic Theory. *Concepts in Magnetic. Resonance*. 1997, *9*, 299–336.

(93) Pochapsky, T.; Pochapsky, S. *NMR for Physical and Biological Scientists*, 1st ed.; Rogers, R., Scholl, S., Eds.; Garland Science. Taylor and Francis Group LLC: New York, 2007.

(94) Kirschner, D.; Green, T. K. Nonaqueous Synthesis of a Selectively Modified, Highly Anionic Sulfopropyl Ether Derivative of Cyclomaltoheptaose (β-Cyclodextrin) in the Presence of 18-Crown-6. *Carbohydrate Research* 2005, *340*, 1773–1779.

(95) Rosen, M. J.; Kunjappu, J. T. Surfactants and Interfacial Phenomena. 1st ed; John Wiley & Sons: New York, 2012.

(96) Hypercube, Inc. HyperChem(TM) Professional 8.01. 8 ed. Hypercube, Inc., 1115 NW 4th Street, Gainesville, Florida 32601, USA: Gainesville, FL.

(97) Boving, T. B.; McCray, J. E. Cyclodextrin-Enhanced Remediation of Organic and Metal Contaminants in Porous Media and Groundwater. *Remediation Journal* 2000, *10*, 59–83.

(98) Skold, M. E.; Thyne, G. D.; Drexler, J. W.; McCray, J. E. Solubility Enhancement of Seven Metal Contaminants Using Carboxymethyl-β-Cyclodextrin (CMCD). *Journal of Contaminant Hydrology* 2009, *107*, 108–113.

(99) Blach, P.; Fourmentin, S.; Landy, D.; Cazier, F.; Surpateanu, G. Cyclodextrins: a New Efficient Absorbent to Treat Waste Gas Streams. *Chemosphere* 2008, *70*, 374–380.

(100) Morin-Crini, N.; Crini, G. Article in Press. *Progress in Polymer Science* 2012, 1–25.

(101) Mallard Favier, I.; Baudelet, D.; Fourmentin, S. VOC Trapping by New Crosslinked Cyclodextrin Polymers. *Journal of Inclusion Phenomenon and Macrocyclic Chemistry* 2010, *69*, 433–437.

(102) Celebioglu, A.; Demirci, S.; Uyar, T. Cyclodextrin-Grafted Electrospun Cellulose Acetate Nanofibers via "Click" Reaction for Removal of Phenanthrene. *Applied Surface Science* 2014, *305*, 581–588.

(103) Araki, M.; Kawasaki, N.; Nakamura, T. Removal of Bisphenol A in Soil by Cyclodextrin Derivatives. *Toxicological and Environmental Chemistry* 2001, *79*, 23–29.

Chapter 2. Synthesis of 2,3-*O*-dibenzyl-6-*O*-sulfobutyl-α and β cyclodextrins: New Chiral Surfactants for Capillary Electrophoresis.[1]

2.1 Introduction

Cyclodextrins (CDs) are chiral oligosaccharide macrocycles composed of 6, 7, and 8 α-1, 4-D-glucopyranose units classified as α-, β-, and γ-cyclodextrin, respectively. CDs command great interest not only because of complexation ability of the native macrocycle, but due to possession of two secondary hydroxyls and one primary hydroxyl per glucopyranose unit. Each face of the pocket opening can be tailored with different moieties. Synthetic modification strategies are varied and have been well documented.[1-3] Undersubstitution of these CD hydroxyls is common due to the harsh conditions typically required for full substitution and the extensive purification necessary for isolation of single cyclodextrin isomers.[4] Selectively modified cyclodextrins that are undersubstituted are characterized by an average degree of substitution.

CDs and modified CDs have been used extensively as chiral selectors in capillary zone electrophoresis. In micellar electrokinetic chromatography, the buffer contains a micelle-forming surfactant as a pseudo-stationary phase.[5] The analytes differentially partition into the micelle and are separated. For chiral separation, a micelle-forming surfactant such as sodium dodecyl sulfate is typically used with the chiral cyclodextrin added to establish a secondary equilibrium with the micelle. Sometimes, a single chiral surfactant such as a bile salt is employed.[6]

Our interest has been in developing micelle-forming amphiphilic cyclodextrins that can be used as chiral surfactants in capillary electrophoresis. A number of amphiphilic CDs have been

---

[1] McKee, J. A.; Green, T. K. Synthesis of 2,3-*O*-dibenzyl-6-*O*-sulfobutyl-α and β cyclodextrins: New Chiral Surfactants for Capillary Electrophoresis. *Tetrahedron Lett.* 2015, *56*, 4451–4454

previously synthesized, including both ionic and nonionic CDs.[7-15] As far as we are aware, amphiphilic CDs which form micelles have not been used in capillary electrophoresis studies. The intention of this work was to synthesize sodium hexakis (2,3-*O*-dibenzyl-6-*O*-sulfobutyl) cyclomaltohexaose (5a, Scheme 1) and sodium heptakis (2,3-*O*-dibenzyl-6-*O*-sulfobutyl) cyclomaltoheptaose (5b, Scheme 1) for this purpose. These cyclodextrin derivatives present 12 and 14 aromatic moieties, respectively, on one side of the cyclodextrin while 6 and 7 anionic sulfobutylethers, respectively, protrude from the other side of the molecule. The synthesis is described here and, as shown below, both CD derivatives form micelles with critical micelle concentrations (CMCs) of ~ 90 μM.

The ability of 5b to act as a chiral selector in capillary electrophoresis is demonstrated with a fluorescent derivative of D/L-serine. D/L-serine was a chosen as a test analyte because of the biological significance of D-serine as a neuromodulator[16] and the challenge it presents in chiral separation among CBI-D/L-amino acids.[17] Specifically, the D/L-serine is derivatized with naphthalene-2,3-dicarboxaldehyde and cyanide under basic conditions[18] to form a fluorescent cyanobenz[f]isoindole -D/L-serine (CBI-D/L-serine) derivative. We demonstrate that chiral resolution is achieved with 50-200 μM of 5b in the background electrolyte.

2.2 Results and Discussion

Sodium hexakis (2,3-*O*-dibenzyl-6-*O*-sulfobutyl) cyclomaltohexaose (5a) and sodium heptakis (2,3-*O*-dibenzyl-6-*O*-sulfobutyl) cyclomaltoheptaose (5b) were synthesized according to Scheme 1. The primary hydroxyl groups were readily protected using standard procedures.[2] *tert*-Butylammonium iodide (TBAI) in catalytic amounts has been used to quantitatively benzylate sterically hindered hydroxyls on a glucose derivatives at room temperature in the presence of

excess sodium hydride in tetrahydrofuran (THF).[19] This concept was adapted to perbenzylate the secondary hydroxyls of cyclodextrins by using 0.01 equivalents of TBAI, two equivalents of benzyl bromide, excess sodium hydride in THF and heating the reaction to reflux for two days. Larger amounts of benzyl bromide were required for complete benzylation if the reaction was performed at room temperature. The addition of TBAI was found to be critical for the synthesis of both 3a and 3b; benzylation in its absence, regardless of amount of benzyl bromide or time allotted, was found to produce only undersubstituted benzyl derivatives as determined by NMR spectroscopy. We hypothesize that the requirement of TBAI is the catalytic *in situ* formation of benzyl iodide, with its better leaving group. Ammonium fluoride was chosen over the more traditional tetrabutylammonium fluoride as a deprotection agent due to ease of workup; 4a and 4b are soluble in chloroform whereas ammonium fluoride is not, thus eliminating the need for column chromatography of 4a and 4b.

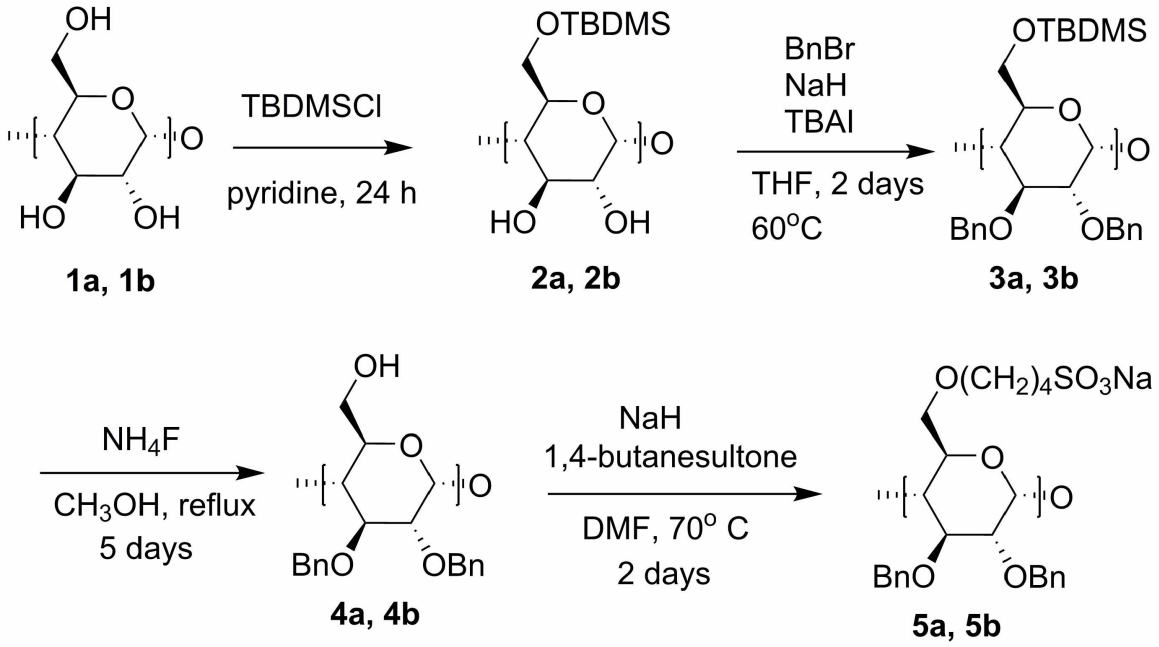

Scheme 1: Synthesis of amphiphilic cyclodextrin derivatives (n = 6,7)

Complete sulfoalkylation of primary hydroxyls in tetrahydrofuran (THF) has been shown previously to be problematic.[20] Kirschner and Green were able to synthesize single isomer 2,3-dialkyl-6-sulfoalkylated cyclodextrin derivatives using a 3-fold molar excess of 18-crown-6 ether in addition to alkanesultone and potassium hydride in THF.[20] 18-crown-6 ether, by complexing with potassium counterion, helps to solubilize the increasing anionic CD. This procedure, while successful, requires addition of large amounts of 18-crown-6 ether, followed by ion-exchange chromatography and numerous extractions for its removal. We find that addition of 1,4 butanesultone (3 eq per hydroxyl), and excess sodium hydride in dry DMF, with mild heating, allows for complete sulfobutylation to 5a and 5b. The products were conveniently purified by ultrafiltration. The products were fully characterized by ^{1}H, ^{13}C, COSY, and HMQC NMR spectroscopy as well as ESI-MS.

Pyrene fluorescence has been used to determine CMCs of calixarene-based surfactants.[21] We used a modified procedure from Lopez-Diaz *et al.*[22] to determine the CMCs of 5a and 5b. Pyrene solution in methanol (1.25 μL of 2 mM) was pipetted into vials and blown dry with nitrogen. Aqueous solutions of 5a or 5b (2.5 mL) ranging from 5 μM to 5 mL were subsequently added and stirred resulting in a pyrene concentration of 1 μM. The emission spectrum of pyrene was obtained using an excitation wavelength of 320 nm. The emission range was set between 350 and 450 nm. Emission intensities were recorded at 373 nm for 1st vibration peak (I_1) and 384 nm for 3rd vibrational peak (I_3).[22]

The ratio of I_1/I_3 in the emission spectrum of pyrene changes in response to the solvent polarity; the I_1/I_3 ratio is a reflection of the local structure in the vicinity of the probe. A change in local dipole moment indicates the equilibrium partitioning from an aqueous environment to a more hydrophobic one.[23] Hydrophobic molecules (*e.g.* pyrene) have a greater affinity for the

hydrophobic micellar core than the hydrophilic bulk solution. A plot of the (I_1/I_3) ratio against the log of surfactant concentration produces a sigmoidal shaped curve. The CMCs of the amphiphilic cyclodextrin derivatives were determined from the sharp changes in the slopes as pyrene transitions from an increasing less polar to a micelle hydrophobic environment.[24] The values of the I_1/I_3 ratio were used to estimate the hydrophobicity of the aggregate microenvironment using an empirical scale of the relative band intensities of pyrene in different solvents.[25] Initial I_1/I_3 values at the CMC in Figure 1 indicate a methanol/methylene chloride-like environment inside the aggregates but with the local polarity approaching benzyl alcohol as the concentration of amphiphile increases.[25] This apparent change in the hydrophobicity of the interior with concentration past the CMC may be due to activity effects and/or greater exclusion of water from the interior as concentration of monomer increases. The CMCs of both 5a and 5b are determined to be approximately 90 μM.

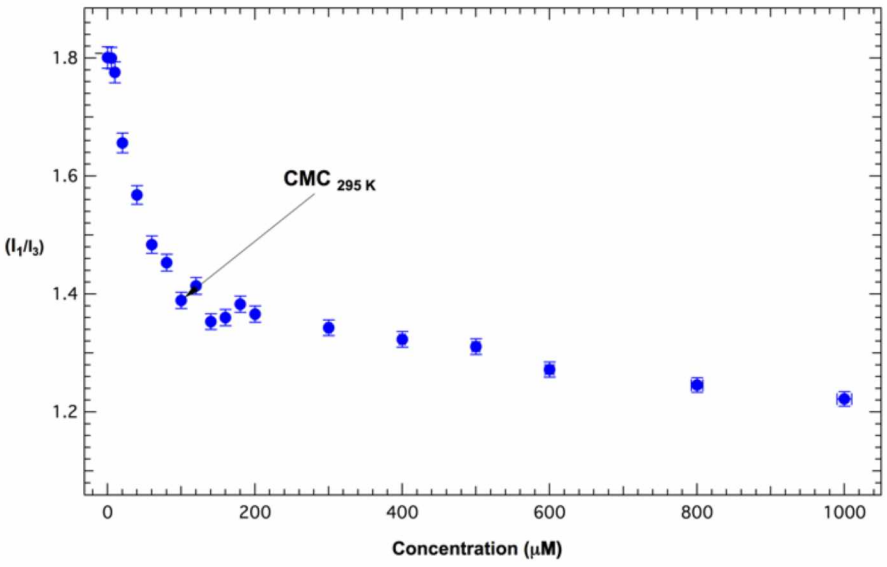

Figure 1. Determination of CMC of 5a using pyrene fluorescent molecular probe. CMC = 90 ± 2 μM.

We found that 5b was effective as a chiral selector in capillary electrophoresis studies of fluorescent CBI-derivatives of D,L amino acids. Electrophoresis was performed in reverse polarity mode (anode on detector side) at -25 kV with low pH (2.00) phosphate buffer. Under this condition, electroosmotic flow is minimized and highly charged anionic 5b migrates toward the detector. CBI-amino acids may interact through their hydrophobic naphthalene group to form inclusion complexes in the CD cavity and/or through interaction with the benzyl groups of the secondary rim of the CD. CBI-amino acids can also interact through H-bonding with the CD. Strong complex formation should result in sweeping of the CBI-amino acids toward the detector.

Average migration times of fluorescent CBI-D/L-serine pair were observed to decrease with increasing concentration of 5b. This result is expected since, as concentration of 5b increases, the equilibrium shifts toward complex and, given that the complex is negatively charged (-7), the CBI-D-serine is driven toward the detector more rapidly. Apparent electrophoretic mobilities (average of CBI-D/L-serine pair), μ_i, were calculated from the migration times according to the equation[26]

$$\mu_i = \frac{v_i}{E} = \frac{L_d/t_m}{V/L_t} \qquad (1)$$

where $\boldsymbol{v_i}$ is electrophoretic velocity (cm/s), E is field strength (V/cm), $\boldsymbol{L_d}$ is length of capillary to the detector, $\boldsymbol{L_t}$ is the total length, $\boldsymbol{t_m}$ is the migration time, and V is the applied voltage (V). Mobility depends on charge/size ratio. To obtain actual mobilities, apparent mobilities should be corrected for both (1) electroosmotic flow and (2) viscosity changes in the background electrolyte due to increasing concentration of 5b. At pH 2.00, however, electroosmotic flow is virtually abolished and is too small to measure. Also, we find that viscosity changes are

negligible over the concentration range of 5b (0-1 mM). Thus the apparent mobilities are the actual mobilities in this study.

Actual mobilities as a function of [5b] are shown in Figure 2. Mobility of the analyte increases with [5b] as the equilibrium concentration of charged complex increases (higher charge/size ratio). Maximum mobility is reached at ~800 - 1000 µM of 5b, which indicates nearly complete complexation of the CBI-serine pair in this concentration range.

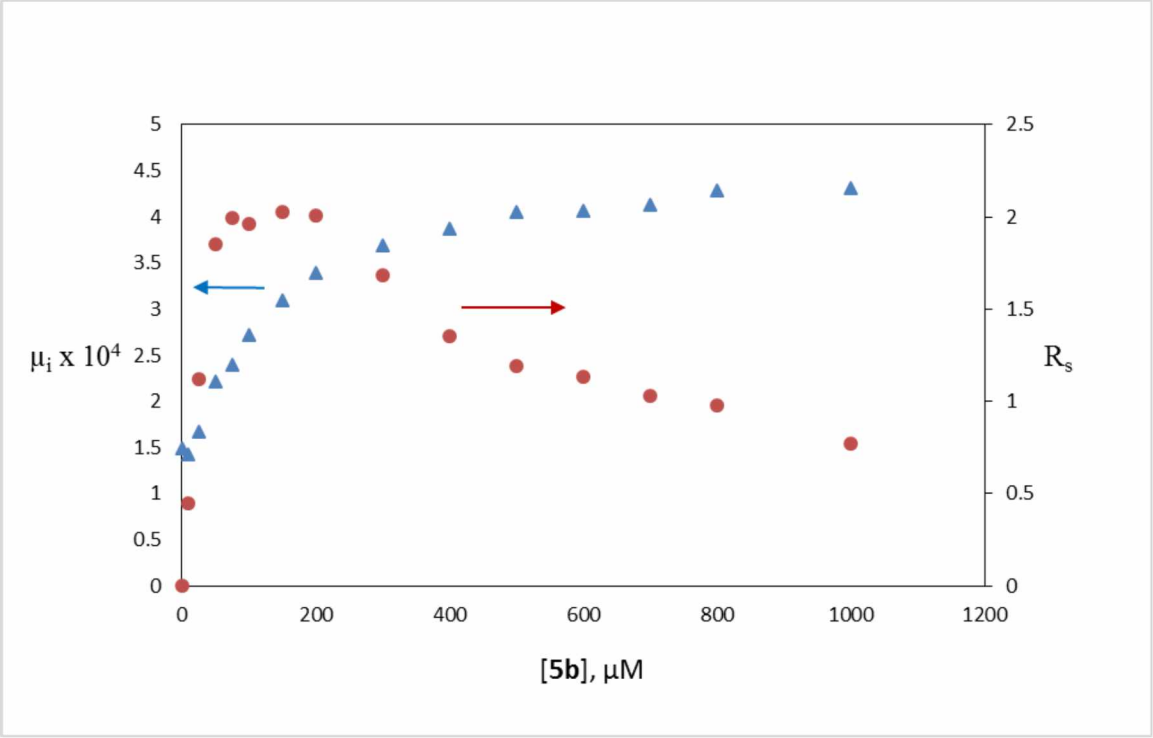

Figure 2. Electrophoretic mobilities, μ_i (cm^2 V^{-1} s^{-1}) and chiral resolution (R_s) of CBI-D/L-serine pairs versus concentration of 5b. Capillary electrophoresis: 50 µm id, 68 cm total, 48 cm to detector, -25 kV, 25 mM phosphate, pH 2.0, 410 nm LIF detection.

Chiral resolution (R_s) reaches a maximum of ~2 (baseline resolution is 1.50) at concentrations of 50-200 µM of 5b with a migration times of 6-9 min. An electropherogram using 100 µM of 5b

is illustrated in Figure 3. A number of other chiral CBI-amino acids were baseline-resolved at equally low concentrations.

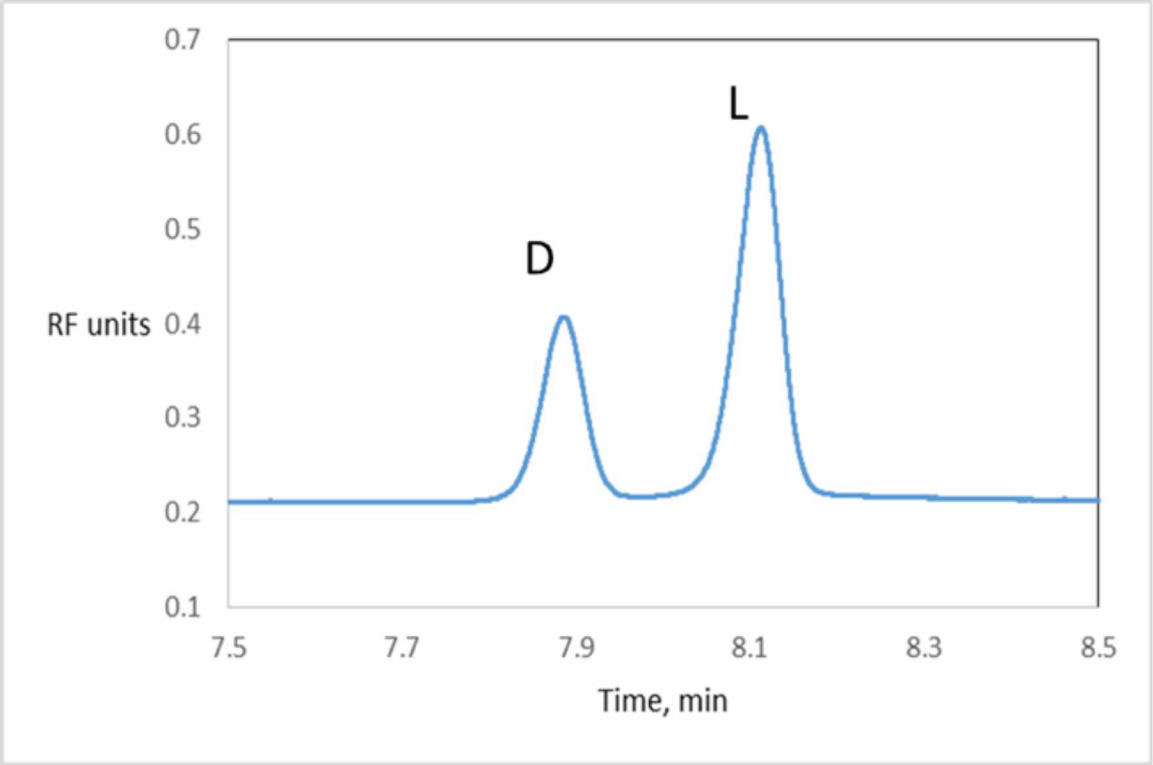

Figure 3. Resolution of CBI-D/L-serine using 100 μM of 5b. See Figure 2 for CE conditions.

Most chiral separations of fluorescently-tagged amino acids employ a CD or modified CD in combination with a micelle-forming surfactant such as sodium dodecyl sulfate.[16] Typically, the CD is neutral and the surfactant is negatively charged. The analyte distributes between the CD, the micelle and the aqueous phase to provide separation. In most circumstances, the CD and surfactant are in used concentrations greater than 1 mM. For example, CBI-D/L-serine enantiomers have been separated using 30 mM β-CD/60 mM chiral sodium taurocholate[27] and 10 mM γ-CD/50 mM sodium dodecylsulfate.[28] Other CBI/-DL-amino acids have been separated

with hydroxypropyl-β-CD/50 mM sodium dodecylsulfate, but this mixture failed to resolve the serine enantiomers.[29]

In some cases, the use of a surfactant is not required. Quan *et al.* employed combination of chiral selectors in 20 mM hydroxypropyl-γ-CD/15% (w/v) D-(+)-glucose to provide resolution of the serine enantiomers.[30] We have optimized resolution using 10 mM commercially-available randomly sulfated β-CD in reverse polarity mode at low pH.[17] All of these examples to point to the usual requirement of high concentrations of cyclodextrin (mM range) in the background electrolyte, either with or without surfactant.

In contrast, we obtain baseline chiral resolution of CBI-D/L-serine with 50 μM of 5b in the background electrolyte. The ability of 5b to resolve CBI-D/L-serine enantiomers at such low concentrations must be considered in the context of intermolecular interactions. First, it is clear that the 5b has unusually high binding to the serine derivatives. This is evident from Figure 2, where the average mobility reaches a plateau at or near 800 μM of 5b, indicative of nearly complete complexation with CBI-D/L-serine at this concentration. The binding constant, K, assuming 1:1 interaction between 5b and analyte, was determined by nonlinear curve fitting of the following equation[31]

$$\mu_i = \frac{\mu_f + \mu_c K[CD]}{1 + K[CD]} \qquad (2)$$

where $\boldsymbol{\mu_i}$ is the calculated mobility, $\boldsymbol{\mu_c}$ is the saturated mobility, $\boldsymbol{\mu_f}$ is the mobility with no CD. Both K and $\boldsymbol{\mu_c}$ are treated as adjustable parameters in the fit.

The treatment yields a K of 5510 ± 560 M^{-1} and μ_c of 4.89 ± 0.11 x 10^{-4} cm^2 V^{-1} s^{-1}. In contrast, a similar treatment of the mobility curve of randomly sulfated β-CD (average degree of sulfation of 9) yields a K of 81 ± 3 M^{-1} and μ_c of 3.91 ± 0.05 x 10^{-4} cm^2 V^{-1} s^{-1} (see Supplementary Data). The much stronger binding of 5b to serine is most probably due to its well-defined and extended hydrophobic cavity, with its sulfobutyl groups on the primary face and the benzyl groups on the secondary face. The randomly sulfated β-CD has sulfate groups on both faces of the CD and lacks the extended hydrophobic cavity.

Wren and Rowe developed a model relating enantiomer mobility to the concentration of CD chiral selector.[32] Penn *et al.* extended the treatment[33] and showed that maximum mobility difference (related to resolution) occurs when the CD concentration equals the inverse of the average binding constant, K. For 5b, this corresponds to 180 μM, consistent with the maximum in R_s achieved at 50-200 μM observed in Figure 2. For randomly sulfated β-CD, maximum mobility difference is calculated to be 12 mM, consistent with that optimized experimentally.[17]

2.3 Conclusion

In summary, we have synthesized, for the first time, amphiphilic 2,3-*O*-dibenzyl-6-*O*-sulfobutyl-α and β-cyclodextrins, sodium salts (5a and 5b). Both molecules form micelles and exhibit CMCs of about 90 μM. 5b is shown to bind strongly to fluorescent CBI-D/L-serine derivatives while providing chiral resolution at low concentrations. These new CDs have potential as chiral surfactants in capillary electrophoresis studies that employ fluorescence detection.

2.4 References

1. Boger, J.; Corcoran, R. J.; Lehn, J. M. Cyclodextrin Chemistry. Selective modification of all primary hydroxyl groups of α- and β- cyclodextrins. *Helvetica Chimica Acta* 1978, *61*, 2190-2218.

2. Takeo, K.; Mitoh, H.; Uemura, K. Selective chemical modification of cyclomalto-oligosaccharides via tert-butyldimethylsilyation. *Carbohyrate Research.* 1989, *187*, 203–221.

3. Szejtli, J. Introduction and General Overview of Cyclodextrin Chemistry. *Chemical Reviews* 1998, *98*, 1743–1754.

4. Kraus, T.; Buděšínský, M.; Závada, J. General Approach to the Synthesis and Persubstituted Hydrophilic and Amphiphilic β-Cyclodextrin Derivatives. *Journal of Organic Chemistry* 2001, *66*, 4595–4600.

5. Terabe, S. Twenty-five years of micellar electrokinetic chromatography. *Procedia Chemistry* 2010, *2*, 2-8.

6. Terabe, S.; Shibata, M.; Miyashita Y. Chiral separation by electrokinetic chromatography while bile salt micelles. *Journal of Chromatography. A* 1989, *480*, 403-411.

7. For reviews of amphiphilic CDs see (a) Roux, M.; Perly, B.; Djedaïni-Pilard Self-assemblies of amphiphilic cyclodextrins. *European Biophysical Journal* 2007, *36*, 861-867 and (b) Sallas, F.; Darcy, R. Amphiphilic cyclodextrins-advances in synthesis and supramolecular chemistry. *European Journal of Organic Chemistry* 2008, *6*, 957-969.

8. Badi, N.; Jarroux, N.; Guégan, P. Synthesis of per-2, 3-di-O-heptyl-β-and γ-cyclodextrins: a new kind of amphiphilic molecules bearing hydrophobic parts. *Tetrahedron Letters* 2006, *47*, 8925-8927

9. Dubes, A.; Bouchu, D.; Lamartine, R.; Parrot-Lopez, H. An efficient regio-specific synthetic route to multiply substituted acyl-sulphated β-cyclodextrins. *Tetrahedron Letters* 2001, *42*, 9147-9151.

10. Dubes, A.; Degobert, G.; Fessi, H.; Parrot-Lopez, H. Synthesis and characterization of sulfated amphiphilic α-, β-, and γ- cyclodextrins: application to the complexation of acyclovir. *Carbohydrate Research.* 2003, *338*, 2185-2193.

11. Falvey, P. *et al.* Bilayer Vesicles of Amphiphilic Cyclodextrins: Host Membranes That Recognize Guest Molecules. *Chemistry European Journal* 2005, *11*, 1171-1180.

12. Nolan, D.; Darcy, R.; Ravoo, B. J. Preparation of vesicles and nanoparticles of amphiphilic cyclodextrins containing labile disulfide bonds. *Langmuir* 2003, *19*, 4469-4472.

13. Silva, O. F.; Fernándex, M. A.; Pennie, S. L.; Gil, R. R.; de Rossi, R. H. Synthesis and characterization of an amphiphilic cyclodextrin, a micelle with two recognition sites. *Langmuir* 2008, *24*, 3718-3726.

14. Wazynska, M.; Temeriusz, A.; Chmurski, K.; Bilewicz, R.; Jurczak, J. Synthesis and monolayer behavior of amphiphilic per (2,3-di-O-alkyl)-α- and β-cyclodextrins and hexakis (6-deoxy-6-thio-2,3-di-O-pentyl)-α-cyclodextrin at an air–water interface. *Tetrahedron Letters* 2000, *41*, 9119-9123.

15. Gallois-Montbrun, D.; Thiebault, N.; Moreau, V.; Le Bas, G.; Archambault, J-C.; Lesieur, S.; Djedaïni-Pilard, F. Direct synthesis of novel amphiphilic cyclodextrin. *Journal of Inclusion Phenomenon and Macrocyclic Chemistry* 2007, *57*, 131-135.

16. Kirschner, D. K.; Green, T. K. Separation and sensitive detection of D-amino acids in biological matrices. *Journal of Separation Sci*ence 2009, *32*, 2305-2318.

17. Kirschner, D. L.; Jaramillo, M.; Green, T. K. Enantioseparation and Stacking of Cyanobenz[*f*]isoindole-Amino Acids by Reverse Polarity Capillary Electrophoresis and Sulfated β-Cyclodextrin. *Analytical Chemistry* 2007, *79*, 736-743

18. De Montigny, P. *et al.* Naphthalene-2,3-dicarboxyaldehyde/cyanide ion: a rationally designed fluorogenic reagent for primary amines *Analytical Chem*istry 1987, *59*, 1096-1101.

19. Czernecki, S.; Georgoulis, C.; Provelenghiou, C. Nouvelle methode de benzylation d'hydroxyles glucidiques encombres. *Tetrahedron Letters* 1976, *17*, 3535–3536.

20. Kirschner, D.; Green, T. K. Nonaqueous synthesis of a selectively modified, highly anionic sulfopropyl ether derivative of cyclomaltoheptaose (β-cyclodextrin) in the presence of 18-crown-6 *Carbohydrate Research* 2005, *340*, 1773–1779.

21. Basilio, N.; García-Río, L.; Martín-Pastor, M. NMR Evidence of Slow Monomer-Micelle Exchange in a Calixarene-Based Surfactant. *Journal of Physical Chemistry B* 2010, *114*, 4816–4820.

22. Lopez-Diaz, D.; Velázquez, M. M. Variation of the Critical Micelle Concentration with Surfactant Structure: A Simple Method To Analyze the Role of Attractive–Repulsive Forces on Micellar Association. *Chemical Educator* 2007, *12*, 327–330.

23. Kalyanasundaram, K.; Thomas, J. K. Environmental effects on vibronic band intensities in pyrene monomer fluorescence and their application in studies of micellar systems. *Journal American Chemical Society.* 1977, *99*, 2039–2044.

24. Evans, D. F.; Wennerstrom, H. *The Colloidal Domain: where physics, chemistry, and biology meet*; 2nd ed.; Wiley-VCH., New York, 1999.

25. Dong, D. C.; Winnik, M. A. The Py scale of solvent polarities. *Canadian Journal of Chemistry* 1984, *62*, 2560–2565.

26. Weinberger, R. *Practical Capillary Electrophoresis* 2nd ed., Academic Press, San Diego, 2000.

27. Zhao, S.; Song, Y.; Liu, Y. M. A novel capillary electrophoresis method for the determination of d-serine in neural samples *Talanta* 2005, *67,* 212-216.

28. Ueda, T. *et al.* Chiral separation of naphthalene-2,3-dicarboxaldehyde-labeled amino acid enantiomers by cyclodextrin-modified micellar electrokinetic chromatography with laser-induced fluorescence detection *Analytical Chemistry* 1991, 63, 2979-2981.

29. DeSilva, K.; Kuwana, T. Separation of Chiral Amino Acids by Micellular Electrokinetic Chromatography with Derivatized Cyclodextrins. *Biomedical Chroma*tography 1997, *11*, 230-235.

30. Quan, Z.; Songa, Y.; Fenge, Y.; LeBlanc, M.; Liua, Y. Detection of D-serine in neural samples by saccharide enhanced chiral capillary electrophoresis *Analytica Chimica Acta* 2005, *528*, 101-106.

31. Rundlett, K. L.; Armstrong, D. W. Methods for the determination of binding constants by capillary electrophoresis *Electrophoresis* 2001, *22*, 1419-1427.

32. Wren, S. A. C.; Rowe, R. C. Theoretical aspects of chiral separation in capillary electrophoresis: I. Initial evaluation of a model *Journal of Chromatography A* 1992, *603*, 235-241.

33. Penn, S. G.; Bergstöm, E. T.; Goodall, D. M; Loran, J. S. Capillary Electrophoresis with Chiral Selectors: Optimization of Separation and Determination of Thermodynamic Parameters for Binding of Tioconazole Enantiomers to Cyclodextrins. *Analytical Chemistry* 1994, 66, 2866-2873.

Appendix

A.1 General Methods

Chemicals were purchased from Oakwood Products Inc. (West Columbia, SC), Sigma Aldrich (St. Louis, MO), TCI America (Portland, OR), and Alfa Aesar (Ward Hill, MA). All chemicals, with the exception of sodium hydride, tetrahydrofuran and N, N-dimethylformamide, were used as purchased. Tetrahydrofuran and N, N-dimethylformamide were freshly distilled over 4 Å sieves. Sodium hydride was washed with hexanes and blown dry with nitrogen gas before use. All glassware and materials were dried in oven under reduced pressure prior to use. Randomly sulfated cyclodextrin was purchased from Fluka (St. Louis, MO).

Caution: NaH (water reactive), Hexanes (flammable), DMF (flammable, toxicity, reproductive hazard), and 1,4 butane sultone (toxicity, suspected carcinogen) were used in the synthesis of sodium hexakis (2,3-*O*-dibenzyl-6-*O*-sulfobutyl) cyclomaltohexaose and sodium heptakis (2,3-*O*-dibenzyl-6-*O*-sulfobutyl) cyclomaltoheptaose.

A.2 Pyrene Fluorescence

The critical micelle concentration was determined from the change in pyrene fluorescence with solvent hydrophobicity. A series of twenty aqueous nominal concentrations ranging from 5 μM to 5 mM of sodium hexakis (2,3-*O*-dibenzyl-6-*O*-sulfobutyl) cyclomaltohexaose and sodium heptakis (2,3-*O*-dibenzyl-6-*O*-sulfobutyl) cyclomaltoheptaose were prepared in 3 mL aliquots. 1.25 μL of 2 mM pyrene solution in methanol was pipette into vials and blown dry with nitrogen. 2.5 mL aliquots of each surfactant concentration were subsequently added and stirred resulting in a pyrene concentration of 1 μM. The emission spectrum of pyrene was obtained using an excitation wavelength of 320 nm and a bandwidth of 2.5 nm. The emission range was set

between 350 and 450 nm. Fluorescence spectra were recorded on a Perkin Elmer Luminescence Spectrometer LS50B. Emission intensities were recorded at 373 nm for 1st vibration peak (I) and 384 nm for 3rd vibrational peak (III). The pyrene concentration remained constant in each solution concentration. Excitation and emission slit widths were set to 2.5 nm with a scan rate of 100 nm/sec.

A.3 Electrospray Ionization Time-of-Flight Mass Spectrometry

Sodium hexakis (2,3-*O*-dibenzyl-6-*O*-sulfobutyl) cyclomaltohexaose and sodium heptakis (2,3-*O*-dibenzyl-6-*O*-sulfobutyl) cyclomaltoheptaose were dissolved in 80% methanol/20% water solution. Mass spectra of surfactants were recorded on a MaXisQTOF using LS-ESI as an ion source. LS-ESI capillary was set to -2200 V and flow rate of 4.0 l/min.

A.4 NMR

All NMR experiments were performed on a Bruker Advance 600 MHz BBO NMR spectrometer using Topspin 3.2 software. Samples for structure characterization were prepared with d_6-DMSO (99%). ^{1}H, ^{13}C, ^{1}H-^{1}H COSY, ^{1}H-^{13}C HMQC spectra of the intermediate and final products are included in supporting information.

A.5 CE-LIF

All capillary electrophoresis experiments using laser induced fluorescence were performed on an Agilent 7100 CE equipped with Picometrics ZetaLif fluorescence detector using a 410 nm laser. Reversed polarity (anode on detector side) was used on all experiments with a voltage of -25 kV. Temperature was 25 °C. CBI-D/L-serine derivatives were synthesized by mixing equal volume of 1 mM naphthalene-2,3-dicarboxaldehyde in methanol, 1 mM D/L-serine in water, and 1 mM

sodium cyanide in 60 mM borate, pH 9.3. After reacting for 15 min, the resulting solution was diluted to yield a concentration of 10 μM CBI-D/L-serine. Capillaries were preconditioned with 0.1 N NaOH and Milli-Q water before each run.

A.5.1 Electrophoretic Mobilities and Binding Constants, K, of 5b

The capillary used possessed a 50 μM internal diameter, 68 cm total length, 48 cm to the detector for 5b. The background electrolyte (BGE) used was a 25 mM phosphate buffer titrated to pH of 2.00. Injection was by pressure (50 mbar, 1 sec). Resolution values were calculated using Peakfit™ V4 software by fitting peaks to a Gaussian lineshape.

Apparent electrophoretic mobilities, μ_i, were calculated according to the equation

$$\mu_i = \frac{v_i}{E} = \frac{L_D/t_m}{V/L_T} \qquad (1)$$

where v_i is the electrophoretic velocity, E is the electric field strength (V/cm), L_D is the length to the detector, L_T is the total length, and t_m is the migration time in seconds. The apparent mobilities are not corrected for electroosmotic flow (EOF). However, EOF is minimized at pH 2.00 in this study. Attempts were made to measure EOF by UV detection using short-end injection (8 cm to detector by UV detection) of an EOF marker of DMSO. No peak was detected at 3 hours using conditions above. We calculate the effect of EOF on the mobilities at 2% or less. Over the concentration range studied (0-1 mM), no measureable change in viscosity in the background electrolyte was detected using a standard Cannon glass capillary viscometer.

Binding constants were determined by two-parameter nonlinear curve fitting of the following equation using Lab Fit™ software (Silva, W.P. and Silva, C.M.D.P.S., LAB Fit Curve Fitting Software, V7.2.48)

$$\mu_i = \frac{\mu_f + \mu_c K[CD]}{1 + K[CD]} \qquad (2)$$

where $\boldsymbol{\mu_i}$ is the calculated mobility, $\boldsymbol{\mu_c}$ is the saturated mobility, $\boldsymbol{\mu_f}$ is the mobility with no CD. Both K and $\boldsymbol{\mu_c}$ are treated as adjustable parameters in the fit.

Synthesis and Characterization of 5a and 5b.

Compounds 2a and 2b were synthesized according to the literature.[2] 3a and 3b were synthesized using a modified procedure in which 0.01 equivalents of TBAI, two equivalents of benzyl bromide, excess sodium hydride in THF were used, followed by heating the reaction to reflux for two days [6] 4a and 4b were synthesized using a modified procedure of Takeo in which ammonium fluoride was used as a deprotecting agent.[2] Intermediates were characterized by ^{1}H, ^{13}C, ^{1}H-^{1}H COSY, and ^{1}H-^{13}C HMQC.

Sodium hexakis (2,3-*O*-dibenzyl-6-*O*-sulfobutyl) cyclomaltohexaose (5a). Compound 4a (10.7 g, 5.21 mmol) was added to 500 mL of anhydrous N, N-dimethylformamide under nitrogen. Sodium hydride (3.00 g, 0.125 mol, 4 eq. per hydroxyl) was added, and the reaction was allowed to stir for 3 hours. Dry sodium iodide (0.47 g, 3.1 mmol, 0.1 eq. per hydroxyl) was added to the reaction, then 1,4 butanesultone (9.6 mL, 93.8 mmol, 3 eq per hydroxyl) dissolved in DMF was added dropwise via syringe/septum using a modification of a procedure developed by Kirschner and Green.[7] The reaction was heated to 70 °C and allowed to stir for 2 days. Excess sodium hydride was decomposed by slowly adding methanol. The solvent was removed using rotary evaporation under reduced pressure; the resulting brown solid was dried in a vacuum oven. Compound 5a was purified by ultrafiltration through an Amicon ultrafiltration cell with a 1000 MWCO RC membrane to yield a brown solid after concentration and drying in vacuum oven.

Dry acetone was added to the solid, and via successive washes, yielded an off-white solid upon drying with N_2 gas (10.3 g, 71%). ^{1}H NMR (600 MHz, d_6-DMSO): 6.9-7.3 (10H, H-Ar), 5.08 (s, 1H, H-1), 5.02 (d, 1H,-CH_2-Ar), 4.68 (d, 1H,-C*H*$_2$-Ar), 4.57 (d, 1H,-CH_2-Ar), 4.45 (d, 1H, CH_2-Ar), 3.95 (m, 3H, H-3, H-5, H-6a), 3.80 (t, 1H, H-4), 3.2 -3.5 (m, 4H, H-2, H-6b, -O-C*H*$_2$-$(CH_2)_3$-SO_3^-), 2.52 (m, 2H,-O-$(CH_2)_3$-C*H*$_2$-SO_3^-), 1.64 (2H,-O-$(CH_2)_2$-C*H*$_2$-CH_2-SO_3^-), 1.55 (m, 2H,-O-CH_2-C*H*$_2$-$(CH_2)_2$-SO_3^-). ^{13}C NMR (150 MHz, d_6-DMSO)), 139.2, 138.6 (=C-), 128.1, 127.9, 127.8, 127.4, 127.1, 126.9 (=CH), d 97.6 (C-1), 80.5 (C-3), 79.0 (C-2), 78.8 (C-4), 75.0 (-*C*H_2-Ar), 71.9 (-*C*H_2-Ar), , 70.6 (C-5, -O-*C*H_2-$(CH_2)_3$-SO_3^-), 69.3 (C-6), 51.2 (-O-$(CH_2)_3$-*C*H_2-SO_3^-), 28.7 (-O-CH_2-*C*H_2-$(CH_2)_2$-SO_3^-), 21.9 (-O-$(CH_2)_2$-*C*H_2-CH_2-SO_3^-). ESI-TOF (negative mode), calcd for C_{144} $H_{174}O_{48}S_6^{6-}$, m/z 477.2, found m/z 477.3; calcd for $C_{144}H_{174}O_{48}S_6Na^{5-}$, m/z 577.2, found m/z 577.6.

Sodium heptakis (2,3-*O*-dibenzyl-6-*O*-sulfobutyl) cyclomaltoheptaose, 5b. The synthesis of 5b used a similar procedure to 5a and achieved similar results (4.0 g, 65%). ^{1}H NMR (600 MHz, d_6-DMSO): 6.9-7.3 (10H, H-Ar), 5.17 (s, 1H, H-1), 4.97 (d, 1H,-CH_2-Ar), 4.62 (d, 1H,-C*H*$_2$-Ar), 4.56 (d, 1H,-CH_2-Ar), 4.49 (d, 1H, CH_2-Ar), 3.75 – 4.00 (m, 4H, H-3, H-4, H-5, H-6a), 3.2 -3.5 (m, 4H, H-2, H-6b, -O-C*H*$_2$-$(CH_2)_3$-SO_3^-), 2.51 (m, 2H,-O-$(CH_2)_3$-C*H*$_2$-SO_3^-), 1.64 (2H,-O-$(CH_2)_2$-C*H*$_2$-CH_2-SO_3^-), 1.55 (m, 2H,-O-CH_2-C*H*$_2$-$(CH_2)_2$-SO_3^-). ^{13}C NMR (150 MHz, d_6-DMSO)), 139.1, 138.6 (=C-), 127.9, 127.5, 127.2, 127.0 (=CH), d 97.3 (C-1), 80.6 (C-3), 78.9 (C-2), 77.7 (C-4), 74.7 (-*C*H_2-Ar), 71.9 (-*C*H_2-Ar), 70.9 (C-5), 70.5 (-O-*C*H_2-$(CH_2)_2$-CH_2-SO_3^-), 69.0 (C-6), 51.1 (-O-$(CH_2)_3$-*C*H_2-SO_3^-), 28.7 (-O-CH_2-*C*H_2-$(CH_2)_2$-SO_3^-), 21.8 (-O-$(CH_2)_2$-*C*H_2-CH_2-SO_3^-). ESI-TOF (negative mode), calcd for C_{168} $H_{203}O_{56}S_7^{7-}$, m/z 477.2, found m/z 477.3; calcd for $C_{168}H_{203}O_{56}S_7Na^{6-}$, m/z 560.5, found m/z 560.8.

A 1.5.2 Electrophoretic Mobilities and Binding Constants, K, using Randomly Sulfated Beta Cyclodextrin.

All conditions for electrophoresis were the same as 5b except that the capillary was 68 cm total length and 48 cm to the detector. The mobilities were corrected for viscosity effects over the range of 0 – 20 mM. Kinematic viscosities, η, ranged from 0.700 mm^2/s with no sulfated CD to 0.781 mm^2/s at 20 mM sulfated CD. The mobilities were corrected by multiplying by a factor η/η_0, where η was the viscosity for the solution with corresponding CD concentration at 25 °C and η_0 was the viscosity with no CD.

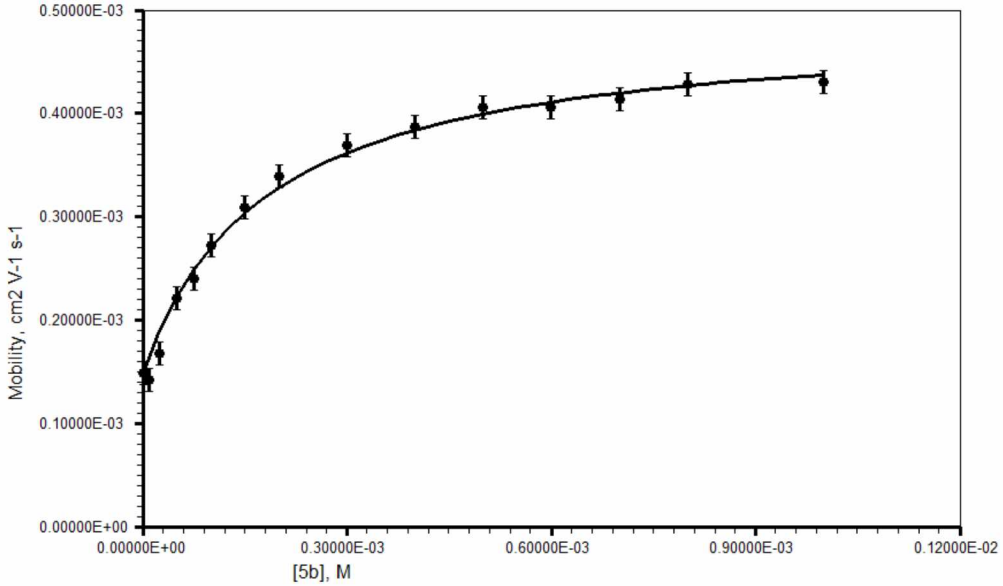

Figure A1. Two-parameter nonlinear curve fitting of mobility data for 5b and CBI-D/L-serine using Equation 2. See experimental for capillary electrophoresis conditions. K = 5510 ± 560 M^{-1} and $\boldsymbol{\mu_c}$ = 4.89 ± 0.11 x 10^{-4} cm^2 V^{-1} s^{-1}.

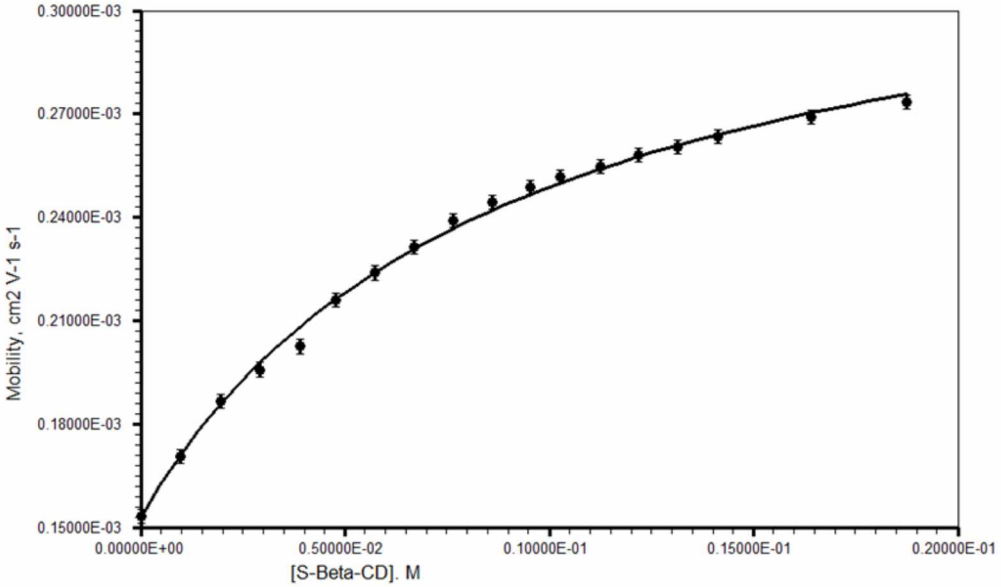

Figure A2. Two-parameter nonlinear curve fitting of mobility data for randomly sulfated beta cyclodextrin and CBI-D/L-serine using Equation 2. See experimental for capillary electrophoresis conditions. $K = 81 \pm 3\ M^{-1}$ and $\boldsymbol{\mu_c} = 3.91 \pm 0.05 \times 10^{-4}\ cm^2\ V^{-1}\ s^{-1}$.

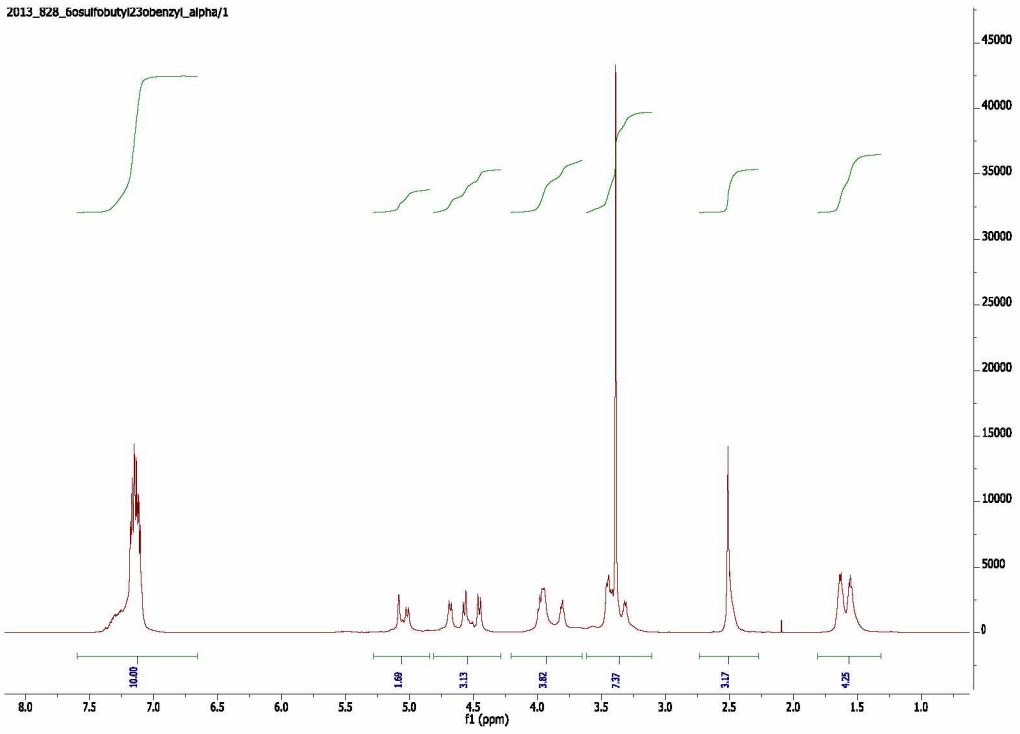

Figure A3. ^{1}H NMR spectrum of 5a in dmso-d_6. Solvent dmso-d_6 resonance overlaps CH_2 signal at 2.5 ppm. Water resonance overlaps signal at ~3.4 ppm.

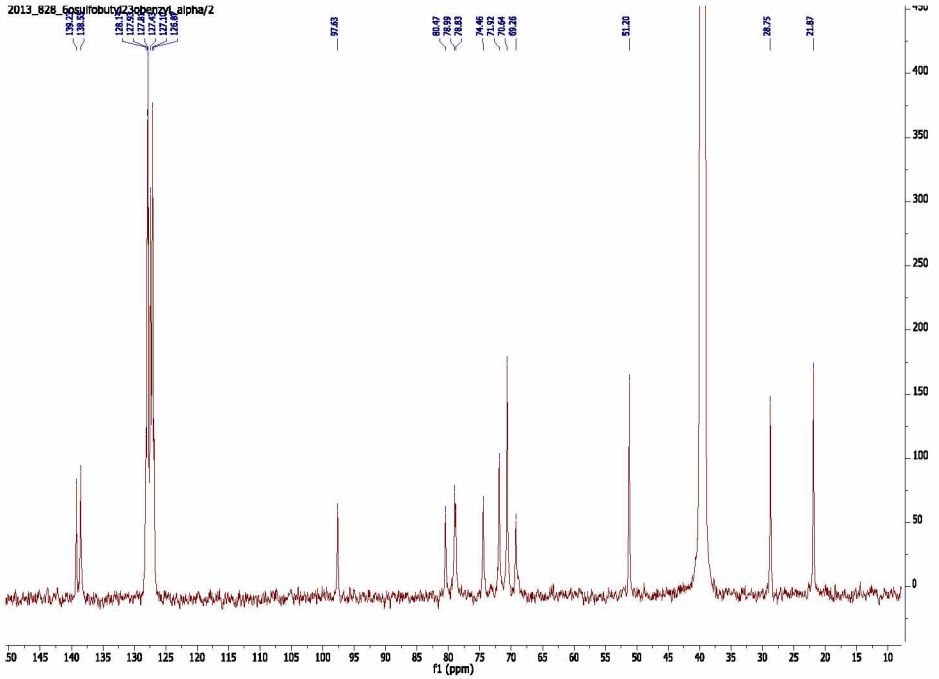

Figure A4. ^{13}C NMR spectrum of 5a in dmso-d_6. ^{13}C NMR resonance of solvent appears at 39 ppm.

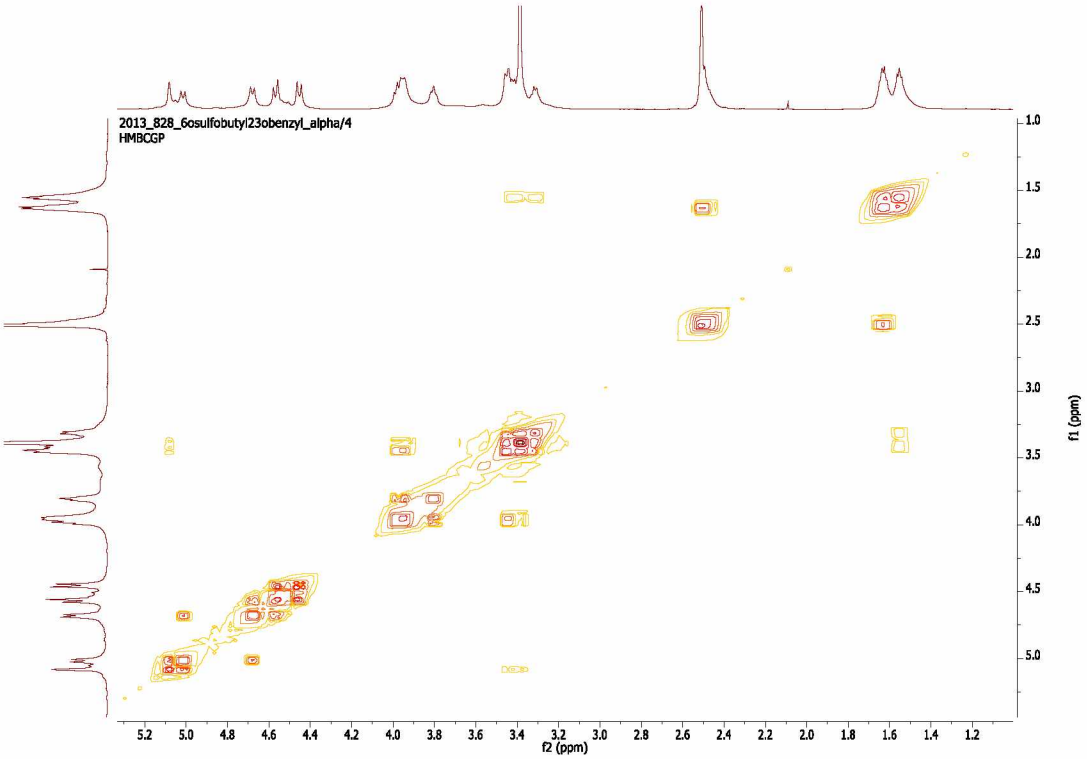

Figure A5. ^{1}H-^{1}H COSY spectrum of 5a in dmso-d_6.

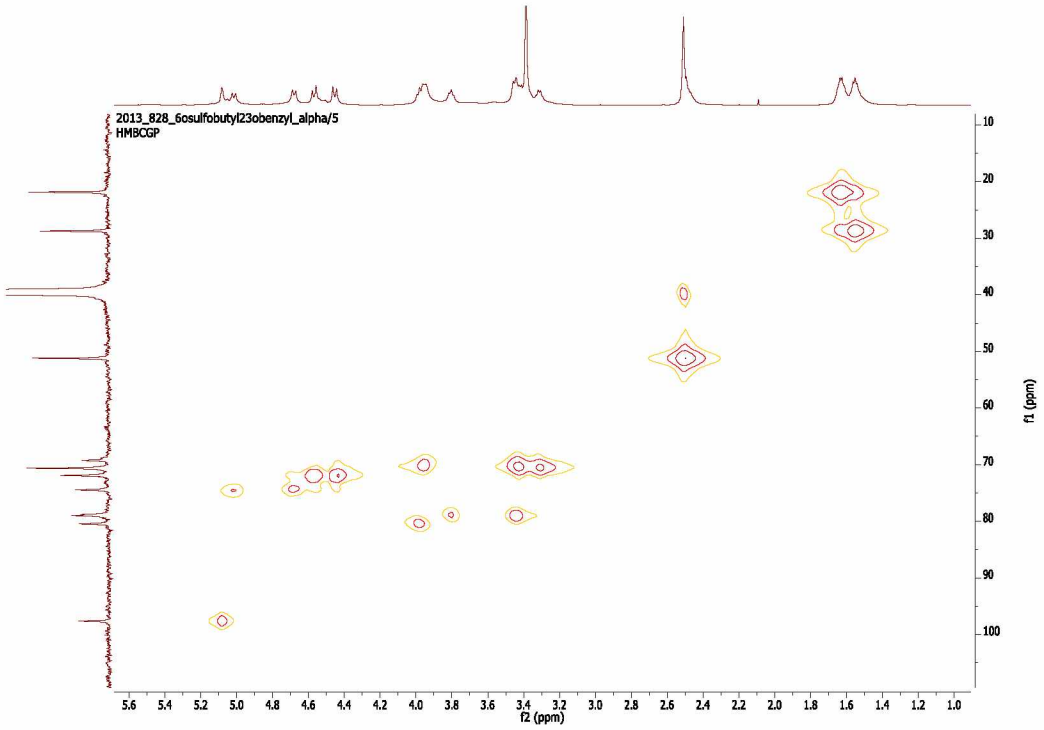

Figure A6. ^{1}H-^{13}C HMQC of 5a in dmso-d6 (expanded region).

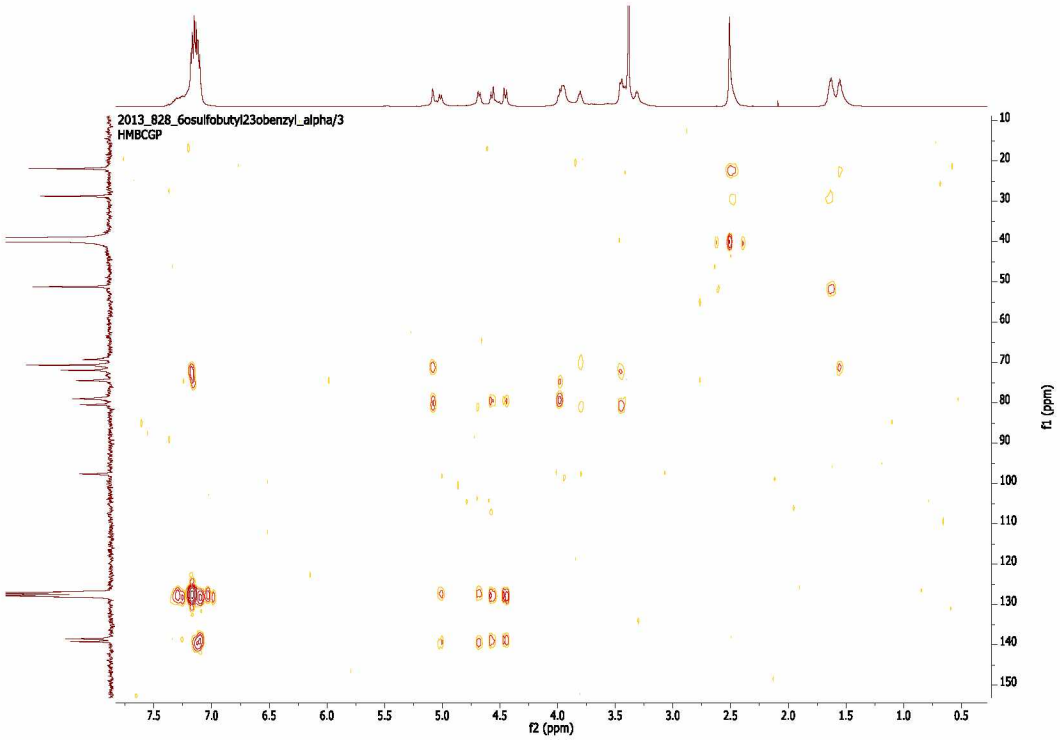

Figure A7. HMBC spectrum of 5a in dmso-d_6.

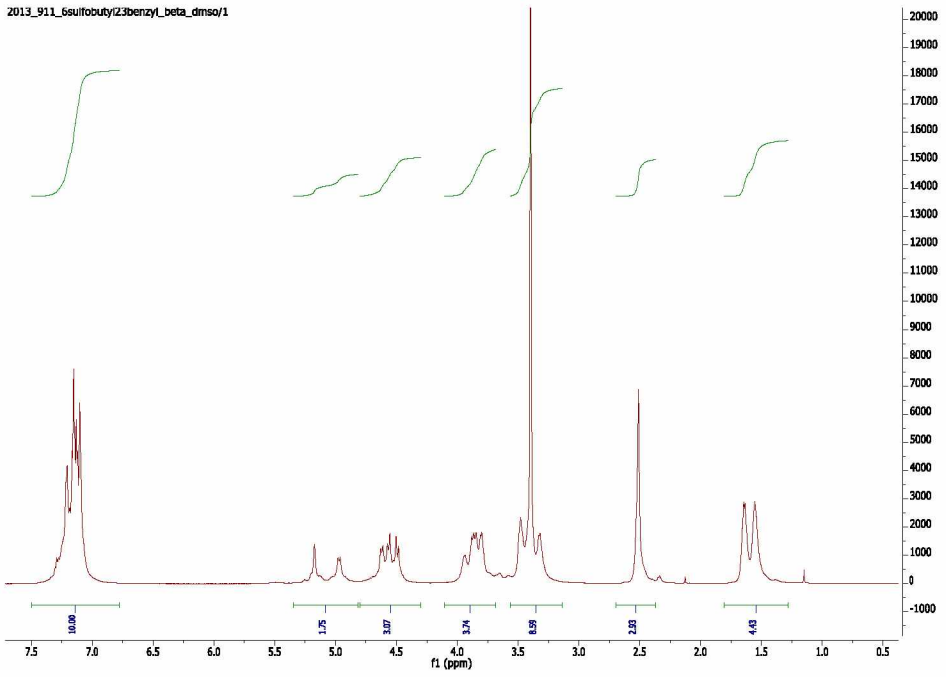

Figure A8. ^{1}H NMR spectrum of 5b in dmso-d_6. Solvent dmso-d_6 resonance overlaps CH_2 signal at 2.5 ppm. Water resonance overlaps signal at ~3.4 ppm.

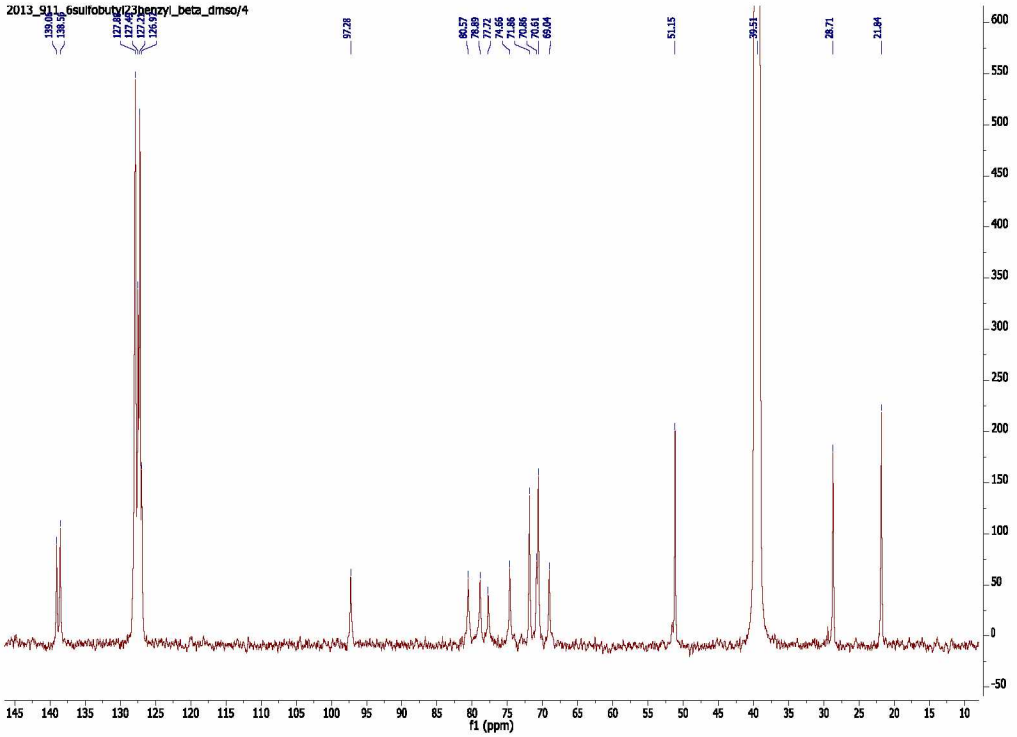

Figure A9. ^{13}C NMR spectrum of 5b in dmso-d_6. ^{13}C NMR resonance of solvent appears at 39 ppm.

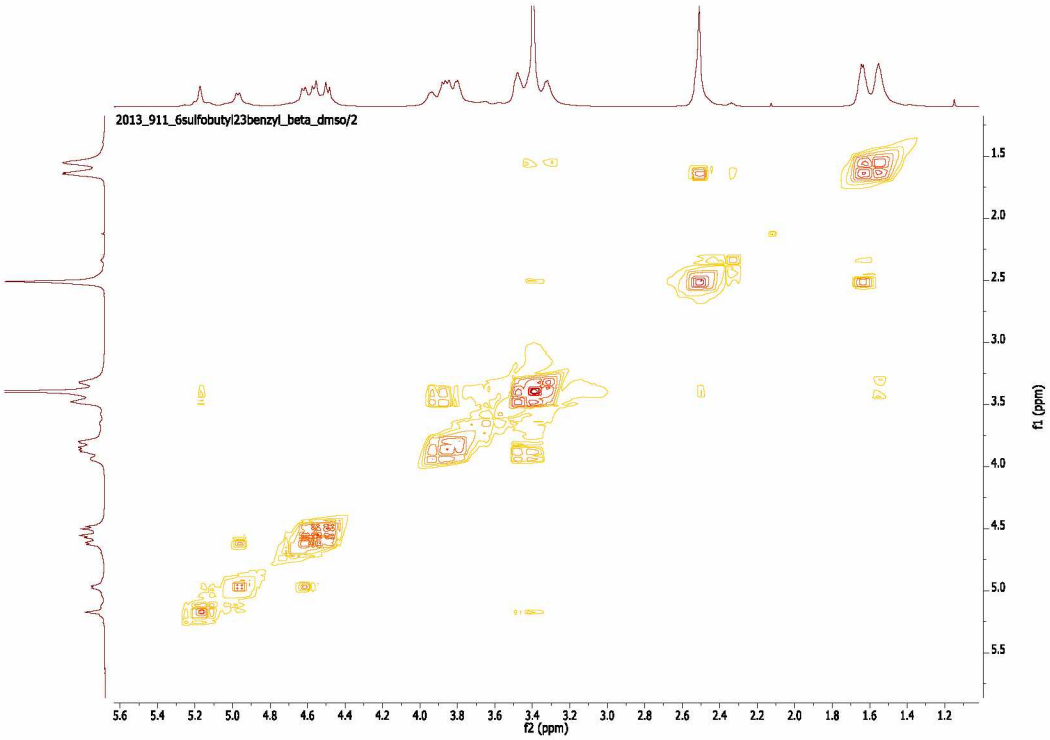

Figure A10. ^{1}H-^{1}H COSY spectrum of 5b in dmso-d6. .

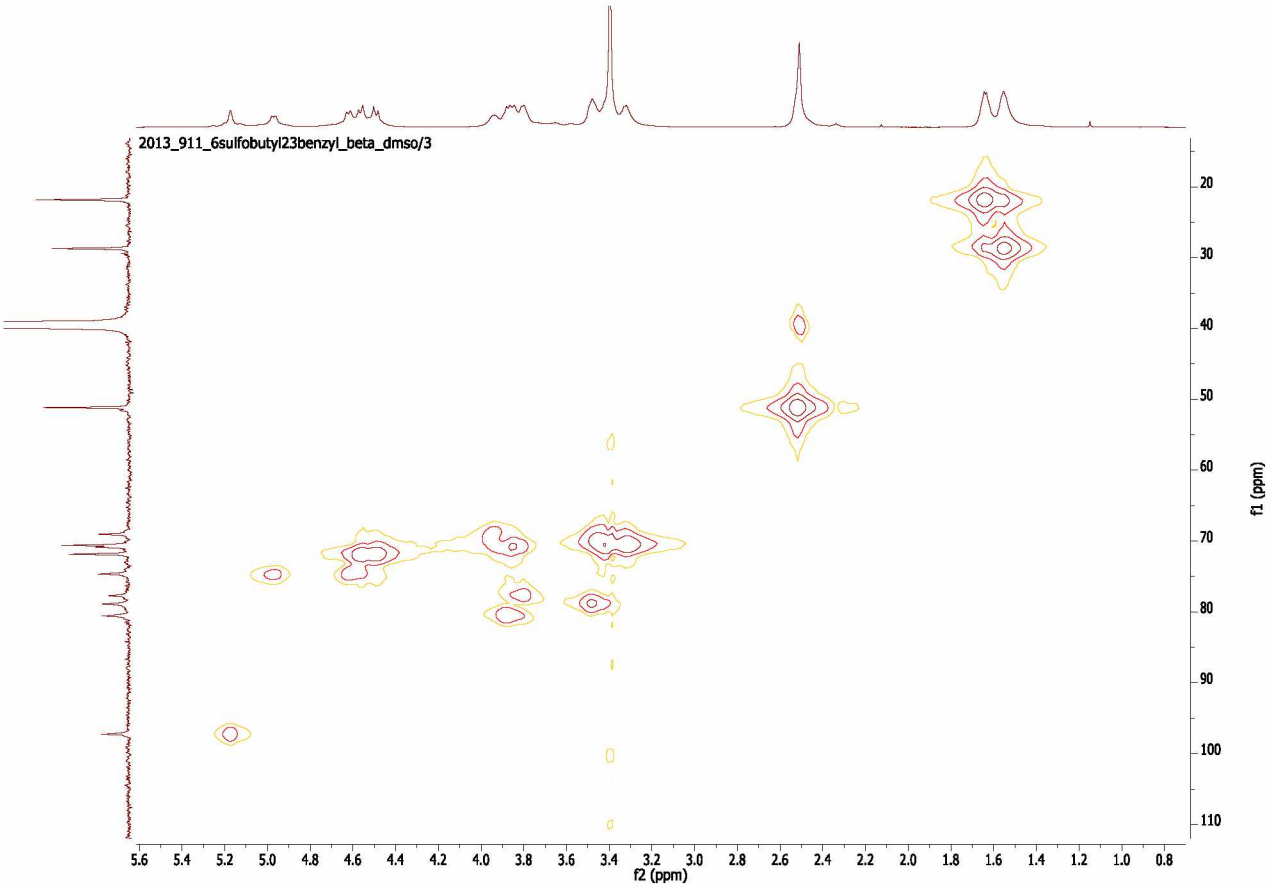

Figure A11. ^{1}H-^{13}C HMQC of 5b in dmso-d6 (expanded region).

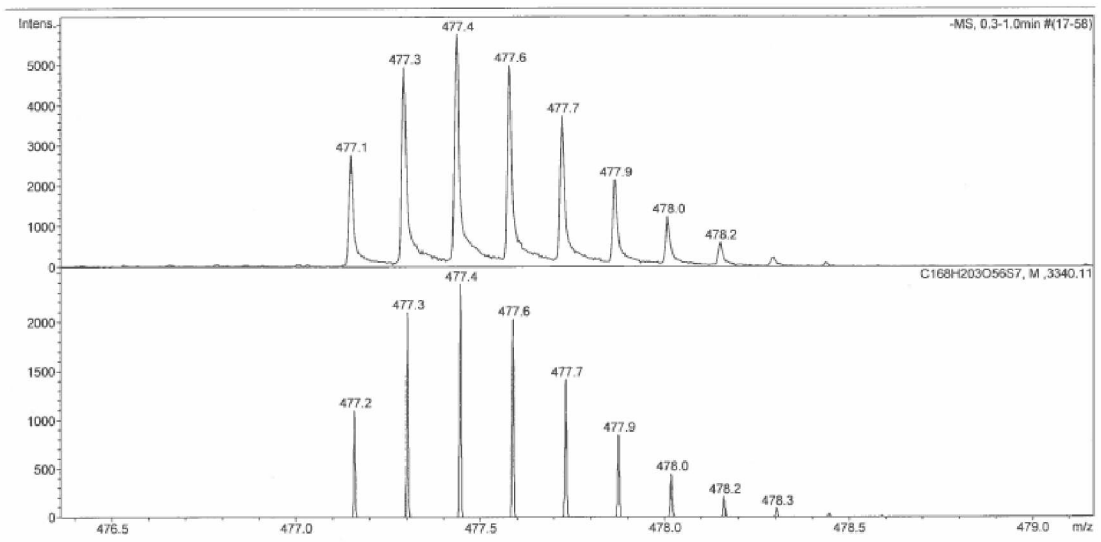

Figure A12. Mass spectrum of 5a. Sample was infused into MaXis QTOF MS for analysis in negative ion mode. Zoom-in spectrum and theoretical pattern are provided. Peaks correspond to isotopes abundances of M-6Na products.

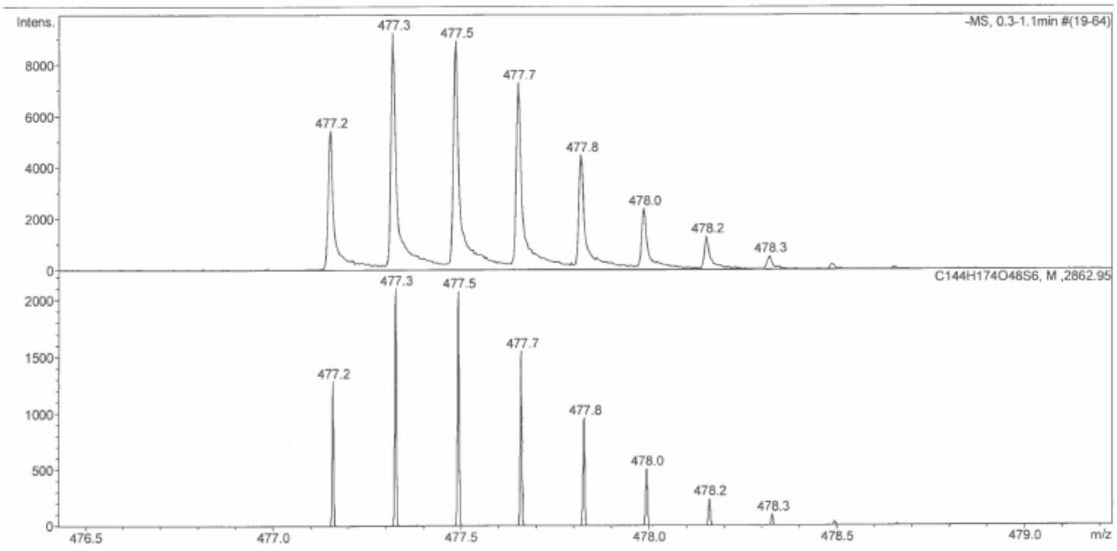

Figure A13. Mass spectrum of 5b. Sample was infused into MaXis QTOF MS for analysis in negative ion mode. Zoom-in spectrum and theoretical pattern are provided. Peaks correspond to isotopes abundances of M-7Na products.

Chapter 3. Solubilization of Hexafluorobenzene by the Micellar Aromatic Core formed from Aggregation of Amphiphilic (2,3-*O*-dibenzyl, 6-*O*-sulfobutyl) Cyclodextrins.[1]

3.1 Introduction

Surfactants composed of a single aliphatic hydrocarbon have been studied for over a century.[1] New systems of association colloids are in demand due to their roles in separation science, biochemical research, and green chemistry.[2] Surface active amphiphiles that contain renewable biological units in their structure have become more desirable in recent years. Cyclodextrins are glucose macrocycles that are well known for their encapsulation properties. [3] They are also fairly rigid structures with well characterized dimensions. These structures can be thought of as nanoscaffolds, upon which structural groups can be grafted to promote aggregation. Typically, native cyclodextrins are used to alter the properties of micellar solutions via inclusion complexation of the surfactant.[4] Cyclodextrins themselves, however, have been shown to be surface active if they are sufficiently derivatized to promote self-aggregation.[5] Amphiphilic cyclodextrins merge the supramolecular properties of macrocycles with the aggregation behavior of amphiphiles. Cyclodextrins with hydrophobic chains have demonstrated high water solubility and the ability to form micelles.[6,7] Nonionic cyclodextrin amphiphiles have demonstrated very low CMCs in the micromolar range, whereas anionic cyclodextrin amphiphiles have CMCs that are nearly two orders of magnitude higher.[8,9] Amphiphiles with multiple hydrophobic and anionic groups (*e.g.* gemini and oligomeric surfactants) have solution properties that are dictated by fixed intramolecular relationships between electrostatic and hydrophobic moieties. These molecules tend to have lower critical micelle concentrations (CMCs), closer hydrophobic

---

[1] James A. McKee, Thomas K. Green. Solubilization of Hexafluorobenzene by the Micellar Aromatic Core formed from Aggregation of Amphiphilic (2,3-*O*-dibenzyl-6-*O*-sulfobutyl) Cyclodextrins. *Journal of Physical Chemistry B*. 2016. 120, 4182-4194.

packing, and greater aqueous solubility than the equivalent conventional analog.[10,11] Double chained surfactants are known to preferentially form vesicles, unless electrostatic repulsions are reduced, where micelles are preferred.[12] The hydrophobicity of the micellar core can be approximated as a separate phase in aqueous solution. This approximation has been termed as a "pseudophase".[13] It is well known that the interior of micelles can solubilize and concentrate hydrophobic molecules in aqueous solution. Gemini surfactants are known to possess higher solubilization capacities of hydrocarbons than the corresponding single chain analogs. [14,15] It has been found that changes in structure of solubilizate changes the preferred location in the aggregate. Aromatic solubilizates (e.g. benzene, naphthalene, N, N-dimethylaniline) tend to adsorb near the palisade layer, while they accumulate in the micellar core at higher concentrations. Aliphatic analogs of aromatic molecules, like most alkanes, concentrate in the micellar core. [16-18]

Micelles with aromatic cores are unusual, but not unprecedented. Aromatic peptide amphiphiles, compounds in which the hydrophilic and hydrophobic components are polar amino acids and aromatic moieties (e.g. 9-fluorenylmethoxycarbonyl), respectively, have been used to form hydrogels, micelles, sheets, and other nanostructures based upon the complementary stacking of aromatic substituents. [19,20] The variety in the structures is also a function of the choice of the hydrophilic amino acid. Furthermore, aromatic substituents allow the aggregation of these short peptide (e.g. dipeptide) segments, reminiscent of amyloid plaque formation.[20]

A classical interior of a micelle is grease-like, the strength of interactions are determined from van der Waals stabilization. Aromatics, however, interact with each other not only through van der Waals interactions supplemented with π-orbital polarizability, but electrostatic stabilization that imparts directionality. Aggregations of aromatic molecules therefore promote a more

ordered system, often in a herringbone arrangement, than their alkyl counterparts.[21,22] Nonpolar (e.g. cyclohexane) and aromatic molecules with aliphatic substituents are preferentially sequestered in the core at all concentrations of solubilizate. Surfactants are known to aggregate in an aqueous system due to the entropically driven sequestration of nonpolar hydrophobic moieties away from polar molecules. The classical hydrophobic effect describes this process in which there is a net increase in disorder in the aqueous system via the dispersal of waters that would have been highly ordered if the solute hydrophobe were not to self-aggregate.[23] The agglomeration of hydrocarbons, typically aliphatic, is thereby a spontaneous event. Aromatic hydrocarbons, however, differ from alkanes in their polarizability, planarity, and their quadrupolar nature; these attributes dominate their interactions with other molecules.[21,24] Amphiphiles with aromatic functional groups were shown to form stable aggregates that possessed strong non-covalent interactions dominated by edge-face and face-face interactions.[25] These moieties introduce highly polarizable conjugated planar π systems for the purposes of aggregate stability, novel photophysics, and molecular structural engineering. [24-28]

Hexafluorobenzene (HFB) is an aromatic molecule in which quadrupolar interactions are complementary to those of benzene or benzyl moieties. The electrostatic isosurface of HFB illustrates regions of electron deficiencies near the center of the molecule; the six fluorines inductively remove electron density equally due to C_{6V} symmetry from the aromatic π system. Benzene has high electron density near the molecular center. Benzene and HFB form sandwich-like complexes with some alteration due the steric/dispersion interactions between the fluorines and the benzene hydrogens. The strong interaction between benzene and hexafluorobenzene, in the range of -15.5 to -23.4 kJ/mol, is function of their complementary quadrupolar moments (-29×10^{-40} C m^2 and $+32 \times 10^{-40}$ C m^2), proton/fluorine interactions, and dispersion forces.[21,24]

These interactions form the basis of many crystal structures, supramolecular synthons, and environments for reaction chemistry in both chemical, biochemical, and industrial milieu.[22,24,29-31]

The incompatibility of hydrocarbons and fluorocarbon systems, due to the enhanced hydrophobicity of the latter, results in few examples of hexafluorobenzene solubility in hydrocarbon micellar phases.[32] ^{19}F NMR data demonstrates that hexafluorobenzene has poor solubility in aqueous bile salts (sodium deoxycholate), even compared to mono-fluorinated aromatic species.[33] Polymeric surfactant aggregates (compartmentalized micelles) comprised of sequestered fluorocarbon and hydrocarbon interiors demonstrate selective fluorocarbon partitioning into only fluorinated parts of the micelle.[34-36] Amphiphilic block copolymers, amphiphiles formed via successive rounds of polymerization, that contained fluorine were able to solubilize hexafluorobenzene compared to their hydrocarbon analogues.[37] Coordination cages designed to sequester fluorinated compounds rely on aliphatic fluorocarbon self-aggregation; highly fluorinated aromatic compounds are not retained.[38] Encapsulation of highly fluorinated aromatics, however, should be possible in an aromatic hydrocarbon micelle interior due to the strength of arene-perfluoroarene interactions.[24]

We have synthesized hexakis (2,3-*O*-dibenzyl-6-*O*-sulfobutyl) cyclomaltohexaose (DBSBA) and heptakis (2,3-*O*-dibenzyl-6-*O*-sulfobutyl) cyclomaltoheptaose (DBSBB) previously (Figure 1);[39] they possess 12 and 14 benzyl groups each, respectively, in their hydrophobic regions that contribute to an aromatic micellar interior region when their concentrations are in excess of the CMC. DBSBA and DBSBB demonstrated a critical micelle concentration of approximately 90 μM as determined by pyrene fluorescence studies.[39]

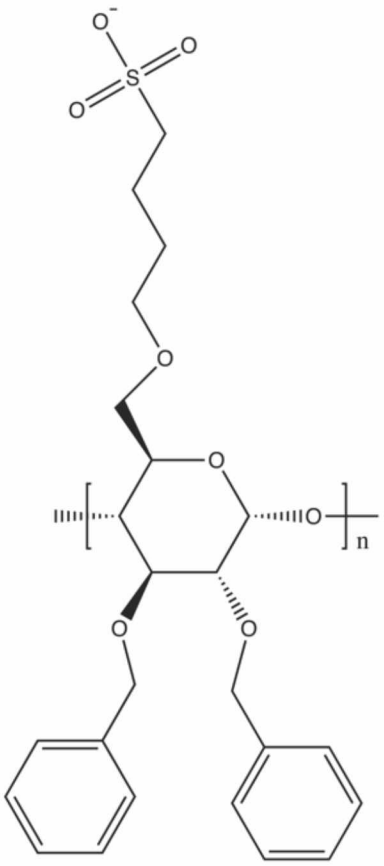

Figure 1. Structures of DBSBA and DBSBB. DBSBA is composed of 6 substituted residues of glucose (n = 6) while DBSBB is composed of 7 residues (n = 7)

^{19}F NMR can be used to probe molecular environments and it has advantages over ^{1}H NMR. The fluorine nucleus possesses high sensitivity to its local environment, a consequence of its natural abundance and gyromagnetic ratio. ^{19}F NMR has a wide chemical shift range for groups with various degrees of substituted fluorine, evidence of its sensitivity to changes in environment and chemical structure.[40] HFB was used as a solubilization probe because it is possesses a strong ^{19}F singlet of sufficient intensity to study changes in chemical shift and linewidth, should prefer the interior of the micelle, and has been used previously to investigate partially fluorinated polysoaps.[41] DBSBA and DBSBB are not composed of any fluorine atoms in their structures, which makes for facile analysis of the changes in chemical shift and linewidth with changes in

surfactant concentration. Potential interactions between HFB and the benzylated interiors of DBSBA and DBSBB were modeled on benzene-hexafluorobenzene interactions.[21,42] The inclusion of HFB into the DBSBA and DBSBB tori was presumed to be minimal due to poor interaction between alkyl protons in the cyclodextrin torus and aromatic fluorines. Aromatic molecules that contain both fluorocarbon and hydrocarbon moieties will only interact with the cyclodextrin cavity via the hydrocarbon end.[43,44]

The purpose of this paper is to determine the critical micelle concentrations of DBSBA and DBSBB by other accepted methods, compare these to previous results, and to determine their morphological and thermodynamic properties in aqueous solution. Differences between aromatic interiors of DBSBA and DBSBB (i.e. electrostatic, dispersion, and charge transfer interactions) and more common aliphatic micelle interiors might promote environments for solubilization and catalysis that have not previously been explored. We were interested in the exploration of arene-perfluoroarene interactions in the core of benzylated micelle. Hexafluorobenzene (HFB) was chosen as a molecular probe because of its hydrophobicity, lipophobicity, and the subsequent and unique preference for an aromatic micelle interior but not a hydrophobic cyclodextrin pocket. The system under consideration contains only the micelle interior, the bulk water phase, and the HFB. Relaxation and binding studies of the interactions between DBSBA/HFB and DBSBB/HFB using ^{19}F nuclear magnetic resonance (NMR) experiments can quantify the strength of interaction and the occurrence of aggregation, if any, between probe and aggregate.

3.2 Materials

Hexakis (2,3-*O*-dibenzyl-6-*O*-sulfobutyl) cyclomaltohexaose sodium salt (DBSBA) and heptakis (2,3-*O*-dibenzyl-6-*O*-sulfobutyl) cyclomaltoheptaose sodium salt (DBSBB) were synthesized as

previously described.[39] Hexafluorobenzene was purchased from Sigma Aldrich (St. Louis, MO). D_2O (99%) was purchased from Cambridge Isotope Laboratories, Inc. (Andover MA). All compounds were used as received without purification or modification. ASTM (American Society for Testing and Materials) Type I water (18.0 MΩ·cm resistivity) was used to prepare all aqueous solutions.

3.3 Characterization

3.3.1 NMR

All diffusion measurements were performed on a Bruker Advance 600 MHz BBO NMR spectrometer using Topspin 3.2 software. The temperature of the probe was determined to be 22.3 ± 0.1°C using the difference in chemical shift between the hydroxyl and methyl groups in methanol.[45] A ledbpgp2s pulse program using a stimulated echo and longitudinal eddy current delay, with bipolar sine shaped gradient pulses and two spoiling gradients. All spectra were recorded with 16 K time domain points in the t_2 dimension and 32 t_1 increments, 16 transients for each t_1 increment, and a relaxation delay of 3 seconds. A diffusion time (Δ) of 300 milliseconds and a gradient pulse length (δ) of 4 milliseconds were used. The gradient pulse strength (G) was varied in 32 linear steps in an interval from 2 to 95% of the maximum gradient (55 G/cm) to ensure at least 95% signal attenuation. The NMR samples used in calculation of diffusion coefficients were prepared with D_2O (99%). All ^{19}F NMR measurements were performed on a Bruker Advance 600 MHz BBO NMR spectrometer using Topspin 3.2 software. A standard ^{19}F pulse sequence with proton decoupling, zgfhigqn.2, was used with 128 scans, an acquisition time of 0.489 seconds, a spectral width of 134 kHz at a frequency of 564.658 MHz. 2 μL of hexafluorobenzene was added to 1 ml of DBSBA and DBSBB solutions varying between 0 - 20

mM in D_2O (99%). All solutions were allowed to equilibrate for 24 hours before analysis. All solutions were comprised of a single phase in D_2O, as determined by the presence of a single intense peak in the ^{19}F chemical shift range in all solutions and solvents. All NMR spectra of DBSBB were acquired in triplicate. All NMR spectra of DBSBA were acquired in duplicate. ^{19}F-^{1}H HOESY spectra were acquired using the hoesyfhqfqnrv pulse sequence (^{19}F observe with ^{1}H decoupling) using a 200 ms mixing time and recycle delay of 5 s.

3.3.2 Conductance Measurements

The specific conductance ($\mu S\ cm^{-1}$) of fifteen concentrations of each amphiphilic cyclodextrin was measured using a VWR sympHony Four Cell Conductivity Probe (cell constant = 0.9 cm^{-1}) to determine the critical micelle concentration of each anionic cyclodextrin amphiphile. Nominal concentrations ranging from 5 μM to 250 μM were prepared. The conductivity meter was rinsed after each measurement and calibrated periodically using a 100 $\mu S\ cm^{-1}$ standard. The critical micelle concentrations of the respective amphiphilic cyclodextrins were calculated where the slope of specific conductance versus concentration changed with respect to the value of the slope arising from the lowest concentrations in the assay. The degree of counterion association was calculated from the ratio of the slope before and after the CMC. Thermodynamic measurements were calculated using the previous method, but allowing solutions of varying concentrations to thermally equilibrate to the desired temperature. Temperatures ranged from 22 to 50°C, via thermostatically controlled Fisher Scientific™ Isotemp™ Digital-Control Water Bath Model 202, with accuracy of ± 0.1°C; solution conductivity measurements were immediately taken to prevent heat loss. Temperatures were recorded using a Vernier Labquest temperature probe. Krafft temperatures were determined by cooling clear aqueous solutions of DBSBA and DBSBB to 4 °C and slowly warmed via water bath to 50 °C.

3.3.3 Molecular Modeling

All theoretical calculations were performed using version 8.01 of HyperChem Professional software package.[24] All cyclodextrin derivatives were geometrically optimized in the presence of water molecules using an OPLS force field, with a convergence limit SCF of 10^{-5}, a gradient RMS of 10^{-2} kcal/A mol, using a Polak-Ribere algorithm.

3.3.4 Profile Likelihood: Calculation of Association Constants Between HFB Between DBSBA and DBSBB

^{19}F NMR titration data were fit using the Microsoft EXCEL® Solver workbook published online by Sanderson.[46] Both a 1:1 HFB:CD and 2:1 HFB:CD model were fit, where HFB is hexafluorobenzene (constant at 17.3 mM) and CD is either DBSBB or DBSBA (0 – 20 mM). Data was fit to the 1:1 model, which provided a poor fit, following by a fit to the 2:1 model. In the 2:1 HFB:CD treatment, optimum K_1 and K_2 were determined by global minimization of the sum of the least squares of the residuals (SSR) using an iterative process. The minimum SSR value was then used to determine the 95% confidence intervals for the binding constants using the Profile Likelihood method. Specially, the minimum SSR values were multiplied by a value: Constant = exp(χ^2(0.95, df=1)/n) where χ^2 is the value which defines the upper 5% of a χ^2 distribution with 1 degree of freedom (df) or 3.841. A Cutoff SSR was then calculated where: Cutoff SSR = minimum SSR x exp(3.841). This cutoff SSR was then targeted in the calculation to obtain the range of both K_1 and K_2 values that provide the 95% confidence interval.

3.4 Results and Discussion

3.4.1 Characterization of Aggregation

We previously synthesized DBSBB and determined that enantiomers of fluorescent CBI-serine were baseline resolved at a concentration of 100 μM using capillary electrophoresis.[39] A pyrene fluorescence assay revealed this critical micelle concentration (CMC) and a hydrophobic environment similar to methylene chloride / benzyl alcohol.[47] Pyrene fluorescence is an established method to measure the critical micelle concentration of surfactants. The change in the fluorescent fine structure of pyrene scales with local dipole moment; the hydrophobicity of the solvent surrounding the molecular probe is indicated by changes in fluorescent fines structure of pyrene.[48] The synthesis of DBSBA used the same procedure as DBSBB and produced similar results in the pyrene fluorescence assay (Table 1). These amphiphiles demonstrated properties of surfactants thereby warranting further study and characterization.

Table 1. Critical Micelle Concentrations of Amphiphilic Cyclodextrins (10^{-3} M)

Name	Pyrene fluorescence	DOSY/NMR	Conductivity	Degree of ionization (α)
DBSBA	0.09	0.10	0.11	0.80
DBSBB	0.10	0.10	0.08	0.81
SHβCD	0.10	0.11	--	--

Determination of CMC is based upon the different physical properties of an aqueous solution with surfactant above and below the CMC of the surfactant. The CMC is defined as the point in the physical property versus concentration relationship where the maximum change in gradient occurs.[49] Changes in the physical properties of the surfactant solution occur at or above the CMC

due to the formation of micelles.[50] Characterization of the DBSBA and DBSBB aggregates should reveal the morphology (i.e. shape and dimensions), the thermodynamics of aggregation, and relative hydrophobicity, with respect to the bulk aqueous phase, of the micellar core.

NMR spectroscopy is sensitive to molecular motion/diffusion coefficient due to the relationship between the rate of transverse relaxation and particle radius.[51] Diffusion ordered spectrometry (DOSY) is an application of NMR spectroscopy that separates chemical shifts in one dimension on the basis of diffusion coefficient in a second dimension. The diffusion coefficient (D) is a measure of the rate of mean square displacement of a particle, with units of m^2 $second^{-1}$. Macromolecular diffusion can be measured by NMR techniques.[52] Smaller species have a greater mean square displacement within a given period of time than larger species; smaller particles have larger diffusion coefficients. The aggregation behavior of DBSBA and DBSBB would be evident from determining the diffusion coefficient of the cyclodextrin amphiphiles for a series of different nominal concentrations. The concentration at which the diffusion coefficients begin to decrease is defined as the critical micelle concentration.[52] The hydrodynamic radius of the aggregate can be calculated from the diffusion coefficient using the Stokes-Einstein equation. Moreover, the ratio of monomer radius to the radius of the aggregate can provide insight into the shape of the aggregate.[53]

There are many thorough reviews on how diffusion coefficients are obtained using NMR spectroscopy, but any discussion of DOSY and calculation of diffusion coefficient begins with the Hahn spin echo experiment and the pulse field gradient (PFG). [54-56] Spin echoes are sensitive to translational motion when a constant magnetic gradient (G) in $Gauss*cm^{-1}$ is placed with respect to the z direction of the sample. The diffusion coefficient of each species is calculated

from fitting each of the observed attenuated intensities, per step of the pulse sequence, to Equation 1.

$$I = I_0 \exp\left[-\gamma^2 G^2 \delta^2 \left(\Delta - \frac{\delta}{3}\right) D\right] \qquad (1)$$

where I_0 and I are the intensities of the chemical shift before and after the experiment, γ is the magnetogyric ratio of the nucleus, G is the gradient along the sample, δ is the length of the pulse, Δ is the time allocated to the diffusion of the particle (the time between the pulses) and D is the diffusion coefficient in m^2 $second^{-1}$. The diffusion coefficient of DBSBA and DBSBB and its aggregate are taken directly from the diffusion coefficient of the anomeric protons (H-1, ~5.2 ppm) of the D-glucose units. Anomeric protons are near the center of mass of the macrocycle; a smaller diffusion coefficient associated with the anomeric protons implies a larger particle. The diffusion coefficients of DBSBA and DBSBB remain constant with respect to concentration until 100 μM, respectively, where the diffusion coefficient decreases as the concentration of DBSBA and DBSBB are increased. Figure 2 illustrates the change in the diffusion coefficient as function of concentration. These CMCs, tabulated in Table 1, are defined as the point where a physical property of the solution (the solute diffusion coefficient) begins to change as a function of concentration. This phenomenon continues until 1000 μM, where the diffusion coefficient remains approximately constant as concentration continues to increase, an indication of aggregate stabilization. Heptakis (6-O-sulfo-2, 3-hexanoyl) cyclomaltoheptaose (SHβCD), an anionic cyclodextrin amphiphile with a published CMC, was synthesized and used as means to determine the accuracy of our DOSY measurements.[57] Our results, included in Table 1, compared well to literature values.

The CMCs and the degree of ionization (α) of ionic surfactants are routinely probed using conductivity measurements to determine the concentration at which aggregation occurs.[58] The degree of ionization of the surfactant polar headgroups dictates the colloidal behavior of ionic micelles.[59] Measurement of conductivity as a function of concentration has demonstrated its utility in the calculation of critical micelle concentrations due to the formation of weak electrolytic micelles from a strong electrolytic monomer. The electrolytic nature of a surfactant

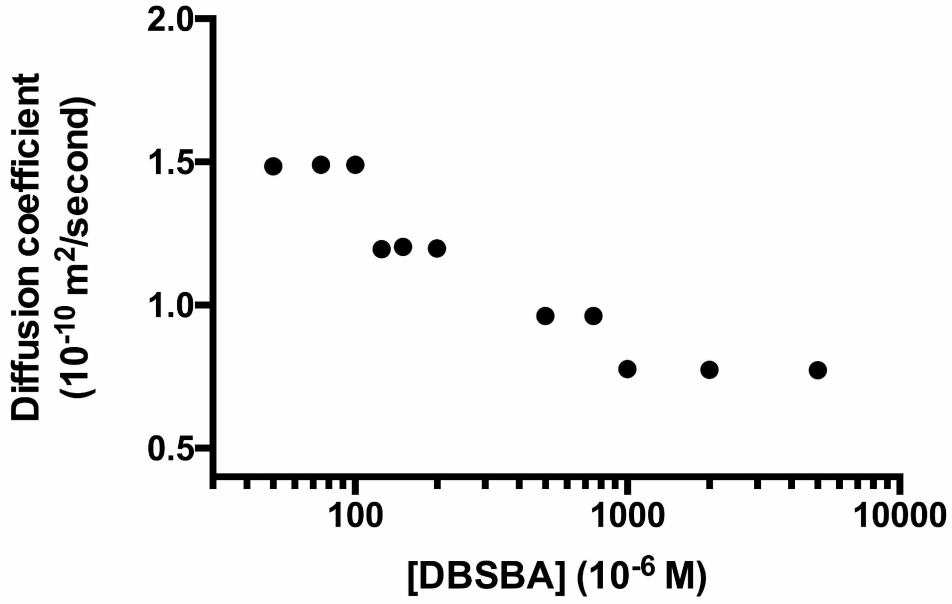

Figure 2. The observed diffusion coefficient, D_{obs}, as a function of DBSBA concentration as determined using diffusion ordered NMR spectroscopy (DOSY). The last concentration before a decrease in diffusion coefficient (m^2 second $^{-1}$) was taken as the critical micelle concentration (CMC).

solution changes upon aggregation; surfactant monomers are strong electrolytes where aggregated monomers are weaker electrolytes with a degree of ionization less than unity. The discontinuity in the slope of solution conductivity against concentration is a well-established

means of calculating the CMC of an ionic surfactant. The change in solution molar conductivity is due to the difference between aggregates and a hypothetical system of monomers in an unaggregated state; larger ionic aggregates retard conductivity as well as require the partitioning of counterions from bulk solution into the Stern layer to reduce Coulombic repulsions at the micellar surface.[58] Above the CMC, the decrease in slope indicates less than 100% counterion dissociation (a weaker electrolyte) with the cyclodextrin amphiphile. This change in electrolytic behavior is characteristic of the onset of micelle formation from charged species.[60] Figure 3 illustrates the relatively large change in CMC of DBSBA with change in temperature. DBSBB demonstrates a similar trend. All conductivity measurement data for DBSBA and DBSBB is included in the Appendix (Tables A1-A4).

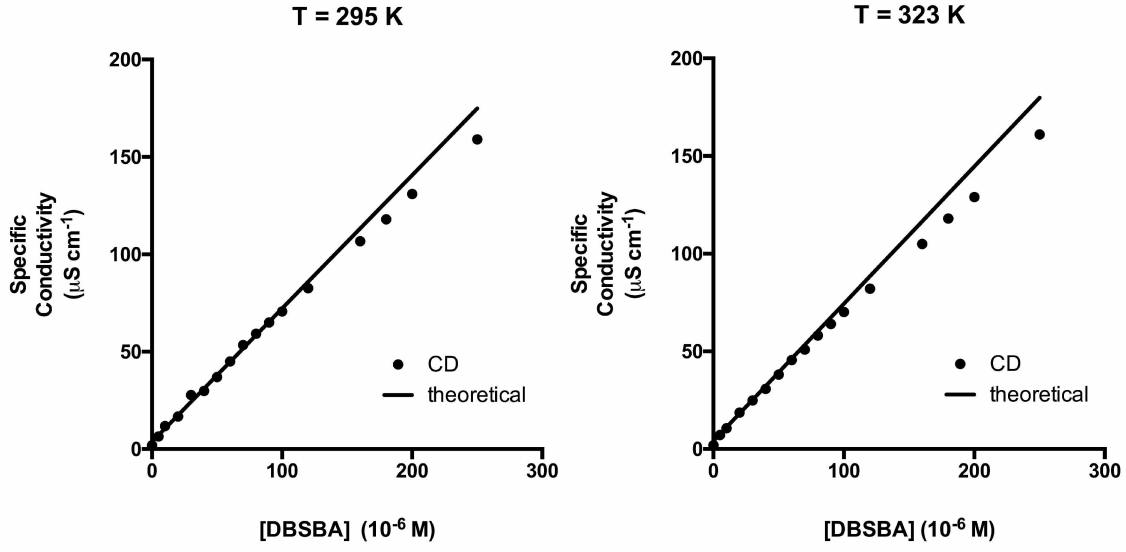

Figure 3. Plot of specific conductance vs. concentration of DBSBA for 295 and 323 K. The CMC was calculated at the point of discontinuity as indicated by the arrow. The degree of micellar counterion dissociation was calculated from the ratio of the slopes of the theoretical and experimental data.

A comparison of CMCs, taken at 22^{O}C, from each method (DOSY, pyrene fluorescence, and conductivity measurements) indicates a strong agreement of values regardless of method used. Table 1 illustrates the CMCs determined using pyrene fluorescence, DOSY, and conductivity measurements at 22°C. The CMC of SHBCD was calculated using surface tension measurements and was determined to be 0.11 mM.[8] This coherence of experimentally determined values based on the change in different solution physical properties allows the CMC of DBSBA and DBSBB to be estimated as 100 μM.

The preferred shape of the cyclodextrin amphiphile aggregate can be predicted using the molecular packing parameter approach.[61] The dimensions and volumes of DBSBA and DBSBB were predicted computationally using the HyperChem Professional 8.01 in which each structure was geometrically optimized using an OPLS (Optimized Potentials for Liquid Simulations) force field in a periodic box with approximately 2600 water solvent molecules.[24] The shape of an aggregate can be estimated by calculating a critical packing parameter (P_{cc}) as developed by Isrealachvili, Mitchell, and Ninham.[61]

$$P_{cc} = \frac{V_H}{a_o l_c} \qquad (2)$$

where V_H is the hydrophobic volume, l_c is the length of the hydrophobic chain, and a_o is surface area of the hydrophilic headgroup. This method has been used to calculate the critical packing parameter for dimeric and oligomeric surfactants based on geometric relationships.[10,62] We have adapted this method by using the dimensions of the macrocyclic amphiphiles DBSBA and DBSBB to calculate the packing parameter and predict aggregate shape and classification. The entire molecule, with the exception of the sulfonate moieties and sodium counterions, was taken

as the hydrophobic component. Per-O-alkylated cyclodextrins, with the exception of per-O-methylated, are practically insoluble in water and are considered lipophilic.[63] The V_H of DBSBA and DBSBB was taken as the van der Waals volume as computed using the QSAR module in HyperChem 8.01. l_c was taken as distance from the *para* hydrogen of the benzyl group to the alpha methylene carbon (proximal to sulfonate). The value of a_o was 59 $Å^2$,as determined from sodium dodecyl sulfonate monolayer data at an air/water interface.[64] These values can be found in Table 2. The value of the P_{CC} can be categorized into aggregates that form spherical micelles ($P_{CC} < 0.33$), cylindrical micelles ($0.33 < P_{CC} < 0.5$), curved bilayers ($0.5 < P_{CC} < 1.0$), planar bilayers ($P_{CC} = 1$), and inverted micelles ($P_{CC} > 1$).[61] Insertion of the values for V_H, l_c, and a_o into Equation 2 produces the value of the P_{CC}, 0.35, which corresponds to a near spherical shape for the aggregate, categorized as a micelle. The aggregation numbers, N_{agg}, of spherical DBSBA and DBSBB were estimated by dividing the volume of the theoretical micelle (using l_c as the radius) by the hydrophobic volume of the individual monomer.

The width of the probability distribution N_{agg} was calculated using the square root of the aggregation number.[45] The N_{agg}, found in Table 2, were calculated to be approximately 15 molecules of DBSBA and 12 molecules of DBSBB per micelle, respectively.

Table 2: Calculated Values for Packing Parameters (P_{CC})

Name	V_H ($Å^3$)	a_o ($Å^2$)	l_c (Å)	P_{CC}	N_{agg}
DBSBA	2252	354	18	0.35	15 ± 4
DBSBB	2628	413	18	0.35	12 ± 3

An estimate of the hydrodynamic radius of the observed aggregate in solution was calculated from diffusion coefficients derived from DOSY NMR data and the Stokes-Einstein equation.

$$D = \frac{k_B T}{6\pi\eta R_H} \qquad (3)$$

where k_b is the Boltzmann constant, T is the temperature in Kelvin, η is the viscosity of the solvent, and R_H is the hydrodynamic radius.[58] The hydrodynamic radius is the effective radius of a particle in solution that accounts for all of the waters of hydration that surround the particle. The hydrodynamic radii of the monomer and micelle were calculated by averaging the three limiting concentrations of the study; 50, 75 and 100 μM for monomeric radii while 1000, 2000, and 5000 μM were used for estimation of micellar dimensions (see Figure 1). Hydrodynamic radii were calculated to be 13.30 ± 0.02 Å for the monomer and 25.56 ± 0.06 Å for the micelle. The assumption of a spherical micelle seems reasonable (*i.e.* the monomer/aggregate ratio is nearly 2:1) given the computationally computed dimensions of the monomer (l_c = 18 Å) and the diameter of the water molecules (3 Å) that solvate the molecule. These experimentally determined values correlate well with the dimensions of the computational model, in Table 2, and the spherical shape suggested by the critical packing parameter calculations.

3.4.2 Thermodynamic Analysis of Micelle Formation in Aqueous Solution.

The standard Gibbs free energy (ΔG_m) for the transfer of 1 mol of amphiphilic cyclodextrin from the solution phase to the aggregation phase can be approximated by:[59]

$$\Delta G_m^\circ = (2 - \alpha) RT ln X_{CMC} \qquad (4)$$

where R is the ideal gas constant, T is the temperature, in Kelvin, and X_{CMC} is the mole fraction of the CMC. All thermodynamic calculations for micelle formation were taken from conductivity data. The enthalpies of micelle formation of DBSBA and DBSBB were calculated by determining how the CMC changed with temperature. A series of concentrations of DBSBA

and DBSBB were prepared as before and allowed to reach temperatures of 30, 40 and 50 °C in a thermostatically controlled bath. The CMCs of DBSBA and DBSBB were found to decrease with increasing temperature as shown in Figure 4.

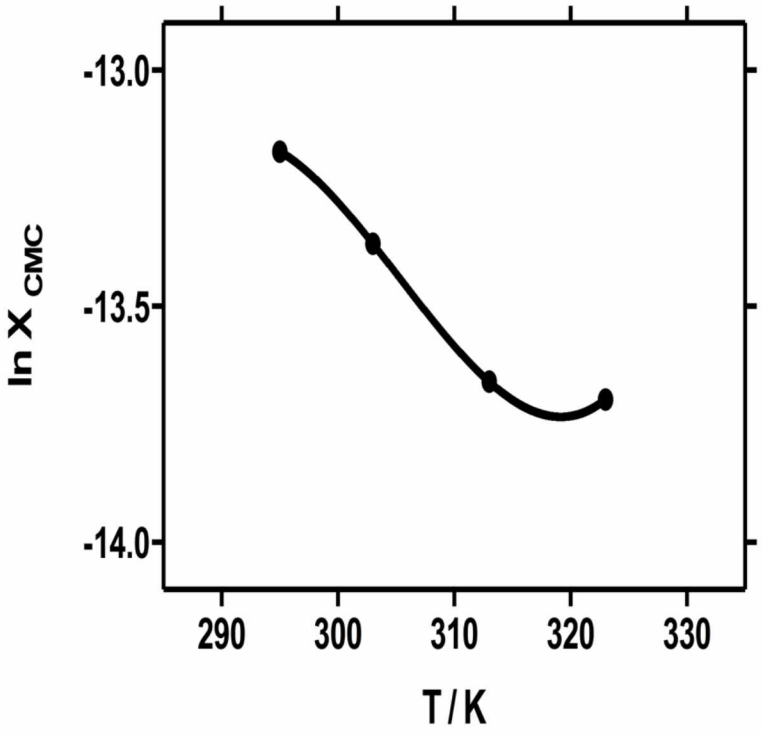

Figure 4. Relationship between natural logarithm of CMC (mole fraction) and temperature of solution from conductivity experiments of DBSBA solutions. Solid circles are data points while solid lines are lines of best fit using third degree polynomial (Equation 6) and regression analysis.

Enthalpies of micellization are often calculated using a modification of the Gibbs-Helmholtz equation by incorporating the relationship between CMC and Gibbs free energy in Equation 5. This equation, the van't Hoff approximation for micellization enthalpy, assumes that system

enthalpy is invariant with temperature and that the aggregation number of the micelle is large.[65,66]

$$\Delta H_m = -(2-\alpha)RT^2 \frac{d\ln[CMC]}{dT} \qquad (5)$$

The experimental observation of the dependence of CMC with temperature suggested the use of a correction (Equation 6) to account for the non-linear change in the CMC as a function of temperature. Our system (small aggregation numbers, evidence of temperature dependence) requires the fitting of the natural logarithm of the CMCs in mole fractions at given temperatures to the following third degree polynomial equation.[65,67]

$$\ln X_{CMC}(T) = a + bT + cT^2 + dT^3 \qquad (6)$$

where the coefficients (a, b, c, and d) were determined by least squares regression analysis. The enthalpy of micelle formation was calculated by differentiating Equation 6 with respect to temperature to generate Equation 7 and substituting in the temperatures for which we want to ascertain the respective enthalpies of micellization.

$$\Delta H_m = -(2-\alpha)RT^2\left(b + 2cT + 3dT^2\right) \qquad (7)$$

The values of the calculated enthalpies of micellization are plotted with respect to temperature in Figure 5. The entropies of micellization, as different temperatures, were calculated using Equation 8. A linear relationship of the changes in enthalpies and entropies with respect to temperature was found and plotted in Figure 5. The slope of this relationship yields the compensation temperature.[67] The values of the coefficients in Equation 6, the free energies,

enthalpies and entropies of micellization at all temperatures examined in this study are included in the Supporting Information (Tables S5, S6).

$$\Delta S_m = \frac{1}{T}\left(\Delta H_m - \Delta G_m\right) \qquad (8)$$

Examination of Figure 5 shows that the enthalpies and entropies of micellization for DBSBA and DBSBB exhibit a strong non-linear dependence on temperature while the Gibbs free energies of micellization are almost invariant by comparison. The large positive entropic component suggests that the process of micellization of DBSBA and DBSBB is entropically driven under the studied temperature regime with enthalpic contributions to micelle formation found at higher temperatures.

Water is not a passive medium; its molecules constantly cluster, re-organize and respond to perturbations of solute molecules.[23] It is clear that a full description of the DBSBA and DBSBB systems in terms of entropic changes is not sufficient to fully characterize the process of aggregation due to large positive enthalpies of micellization at lower temperatures. The peculiar nature of the relationship between the enthalpy of micellization in Figure 5 suggests a deviation from the predicted enthalpies (slightly positive or negative) that are associated with the classical hydrophobic effect. Figure 6 demonstrates the relationship between the enthalpic and entropic changes; the slope of this line is the compensation temperature. The phenomenon of the hydrophobic effect with respect to micellization has been well studied; the incompatibility of the nonpolar aliphatic hydrocarbons and solvent waters drives self-aggregation to reduce accessible hydrophobe surface area and increases the net entropy in the system. Reorganization of solvent molecules upon hydrophobic aggregation contributes to the small changes in enthalpy.[23,68,69]

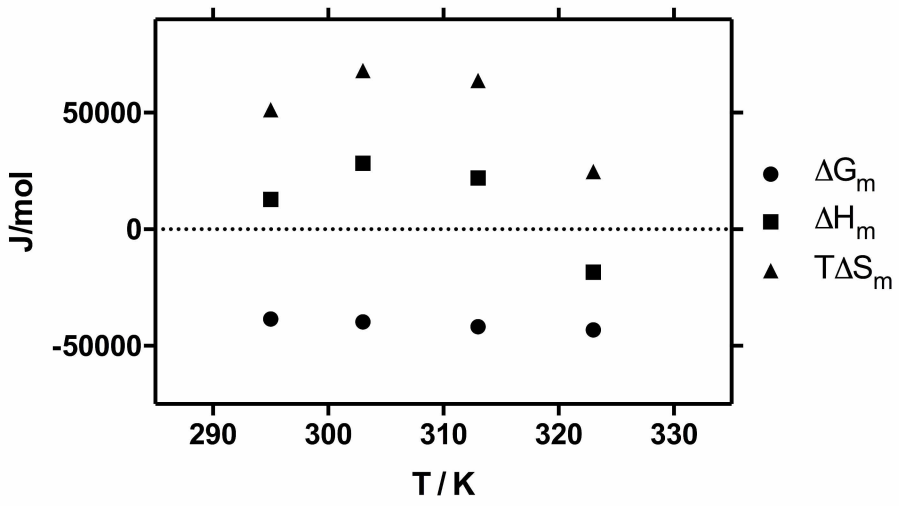

Figure 5. Plot of thermodynamic data with respect to temperature for DBSBA and with respect to temperature.

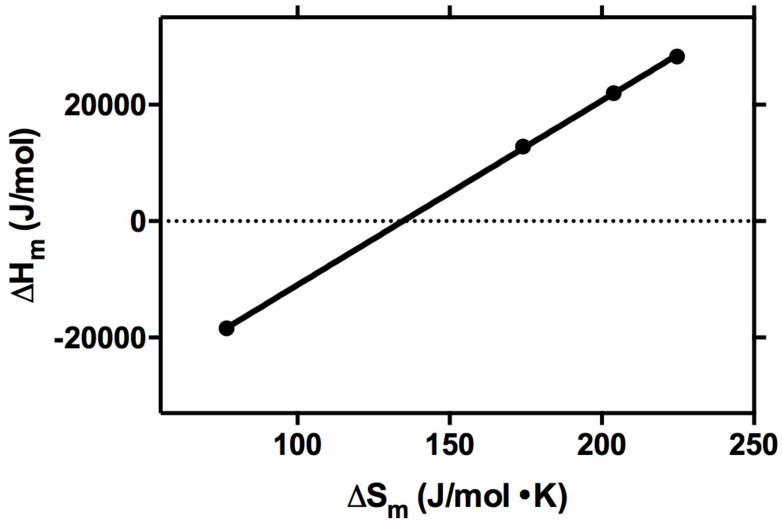

Figure 6. Plot of entropies of micellization against enthalpies of micellization for DBSBA. The compensation temperature was taken as the slope of the enthalpy/entropy compensation curves, which were calculated for DBSBA and DBSBB to be 317 K and 305 K respectively.

The large positive enthalpies of micellization for the lower temperatures found in this study, however, are not explained by the classical hydrophobic effect. This deviation may be a function of use of aliphatic hydrocarbons in theory of hydrophobic hydration, whereas the surfactants under examination, DBSBA and DBSBB, have 12 and 14 aromatic hydrocarbon substituents, respectively. Extrapolation of Equations 7 and 8 to higher temperatures, (i.e. > 73 °C) shows the process is completely enthalpy driven ($-\Delta H > T\Delta S$), however at lower temperatures, the opposite is true. This effect is often observed, that enthalpy dominates hydrophobic associations at high temperatures, while entropy is more important at low temperatures.[51] This phenomenon makes detailed interpretation of the mechanism challenging. The introduction of aromatic groups into the hydrophobic component of a surfactant changes the physical and chemical properties of aggregation due to differences between aliphatic and aromatic hydrocarbons.

There are substantial differences between the thermodynamics of the hydration of aliphatic and aromatic hydrocarbons. The hydration of benzene and its self-aggregation in water is a good illustration of these differences and the beginning of an explanation that accounts for the unusually large and positive enthalpies exhibited in this system. The Gibbs solvation free energy of a molecule ($\Delta G^{\bullet}$) is the process in which a solute is transferred from the gas phase into a liquid solvent.[70,71] This process is the sum of two opposing phenomena, the creation of a cavity in the solvent into which the molecule is placed (ΔG_c) and the van der Waals dispersion forces between the solute and the solvent (E_a). The former event opposes solvation while the latter interactions encourage it.

$$\Delta G^{\bullet} = E_a - T\Delta S_x = E_a + \Delta G_c \qquad (9)$$

The work associated with the creation of a cavity in aqueous solvent is entropic, ΔS_x, due to the reduction in volume available to solvent molecules.[72] Aliphatic hydrophobicity is a function of the large volume required for accommodating the solvent cage, the small size of water molecules with respect to the solute, the density and structure of the clustered waters around the molecule, and the weak interaction between alkanes and water.[73,74] The Gibbs free energy of the incorporation of aromatic hydrocarbons (e.g. benzene) from the gas phase into the aqueous phase (i.e. hydration) is spontaneous, -3.6 kJ/mol at 25 $^{\circ}$C, while the hydration of aliphatics are large, positive, and non-spontaneous.[75,76] The spontaneous aqueous solvation of benzene is due to the van der Waals interaction energies between benzene and water being larger in magnitude than the energies required for creation of the solvent cavity for benzene. The enthalpies associated with the hydration are large and negative, -29.6 kJ/mol [2,73], which suggests the dehydration process required for DBSBA and DBSBB micellization is an endothermic process of similar magnitude. The enthalpic contribution of the hydrophobic effect in larger aromatic hydrocarbons was found to be positive (endothermic) and scale with the size of the molecule.[77] The negative enthalpic contributions to micelle stability at the higher temperatures is attributed to the benzene/water model as well; increased thermal agitation of water molecules reduces the solubilization efficacy of hydration on benzene and allows the already favorable anisotropic quadrupolar interactions to increasingly dominate and promote self-aggregation.[72] An increase in temperature also reduces the hydration of the hydrophilic headgroup, favoring micelle formation, but also reduces the entropic component that promotes hydrophobic aggregation.[16] This compensation behavior makes for complex thermodynamic interpretation but examination of Figure 4 shows that the continued decrease in CMC with temperature seems attributable to

primarily entropic reasons below the compensation temperature and increasingly a function of enthalpy changes that favor micellization above it.

The aromatic contribution to the hydrophobic component of DBSBA and DBSBB are significant. The van der Waals surface area of the benzyl moieties in DBSBB contributes 1473 of the 3007 total square angstroms, or 49% of the hydrophobic component, as calculated using the QSAR module in HyperChem 8.01. A QSAR calculation of the solvent accessible surface area, with a probe radius of 1.4 Å finds that the benzyls comprise 73.9% of the surface area of the hydrophobic component. [24] Similar results are found for the aromatic contributions to the surface area of DBBSA. The benzyl aromatic substituents on DBSBA and DBSBB, located on the opposite end of the surfactant from the hydrophilic sulfonate headgroups, must be the hydrophobic anchor for the aggregation process. The complementary quadrupolar interactions between the benzyls should promote their sequestration due to stronger interactions between the benzyls, either edge-to-face (EF) or offset face-face (OFF) interactions, of approximately 10.4 kJ/mol, than weaker van der Waals interactions between aromatics and water (~ 2 kJ/mol). [21,24,78] The large positive entropic values are presumed to be a function of sequestration of 12 and 14 benzyl groups per macrocycle from aqueous solution, for DBSBA and DBSBB respectively, into the micellar interior, with concomitant release of free water molecules into solution.

3.4.3 Solubilization of Hexafluorobenzene in Solutions of DBSBA and DBSBB

There are many instrumental techniques that have been used to facilitate supramolecular studies.[79] UV/Vis spectroscopy, has often been used to monitor and correlate the changes in spectroscopic profile with system composition. This method would be a poor choice given the large number of benzyls in the interior of the micelles under observation. Chemical shifts and

linewidths in NMR spectroscopy are sensitive to molecular environment.[52] The gradual changes in these observables due to titration of designated guest (or host) have been used to study supramolecular systems.[80] ^{1}H NMR spectroscopy would be poor choice given the number of chemical shifts, their linewidths due to aggregation, and complexity of splitting patterns found in DBSBA and DBSBB spectra. The choice of ^{19}F NMR, however, provides many advantages over other supramolecular investigation techniques for our system of interest.

The intrinsic capacity of the micelle interior to solubilize the HFB, the aromatic core comprised of benzyl substituents, should be the major contribution to an association constant (K). The amount of HFB was kept constant (2 μL or 1.7 X 10^{-5} moles) as the concentrations of DBSBA and DBSBB were varied. The solution volume was kept constant at 1 mL (D_2O). The amount of HFB was chosen such that the HFB/D_2O/DBSBA and HFB/D_2O/DBSBB were one-phase systems in even the smallest concentration of 100 μM (CMC) of DBSBA and DBSBB used (i.e. single peak in the ^{19}F chemical shift range). It should be noted that the solubility limit of HFB in H_2O is only 0.42 μL HFB/mL H_2O.[81]Therefore, DBSBA and DBSBB increases the solubility of HFB approximately 5-fold at the minimum concentration required for the onset of micelle formation.

The relative changes in chemical shift of ^{19}F HFB resonances, with respect to the chemical shift of HFB in D_20 (δ = -163.2 ppm), were compared with the changes in transverse relaxation times of the ^{19}F nuclei as the concentrations of DBSBA and DBSBB were varied (Figure 7). An immediate observation of ^{19}F resonances in the HFB/DBSBA and HFB/DBSBB samples was the change in chemical shift and linewidth of HFB with increasing concentrations of DBSBA and DBSBB. An analysis of the change in linewidth of the ^{19}F chemical shifts with DBSBA and DBSBB micelle concentrations, with a subsequent calculation of apparent transverse relaxation

time (T_2^*) of fluorine nuclei in HFB, was performed to determine if aggregation was occurring in the micellar pseudophase. The linewidth of each ^{19}F peak was measured at half-height to determine how the T_2^* relaxation time changes with the concentration of DBSBA and DBSBB. The relationship between linewidth and the T_2^* relaxation time is shown in Equation 10.

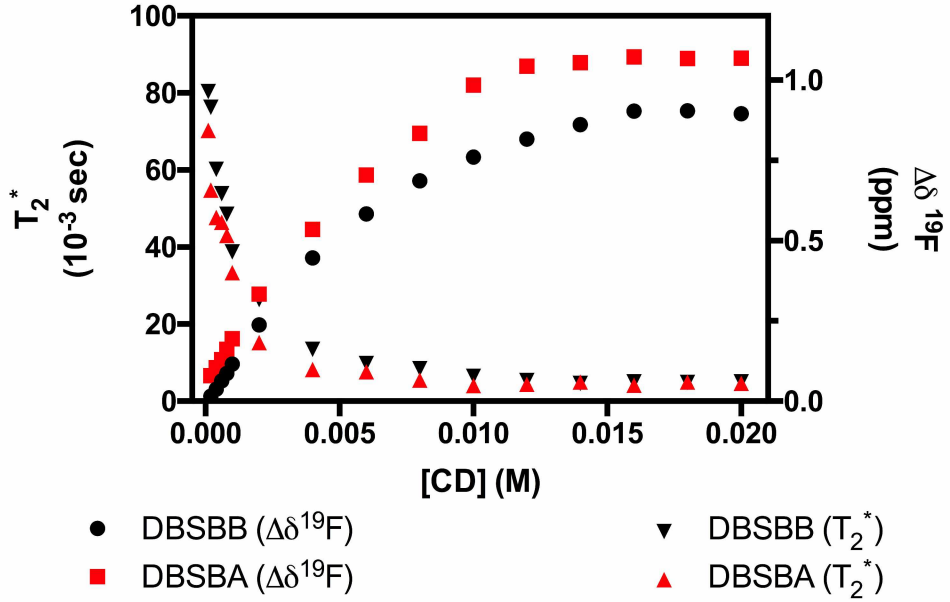

Figure 7. Change in T_2^* and ^{19}F chemical shift with changes in DBSBA and DBSBB concentrations. The progression toward smaller tranverse relaxation times with increasing concentrations means longer correlation time and subsequently larger aggregation volumes. Stabilization of T_2^* times implies stabilization of aggregation mass with the assumption of constant density. Progression toward increasing more positive chemical shifts in ^{19}F NMR indicates decreased shielding of ^{19}F nuclei.

$$\Delta\upsilon_{1/2} = \frac{1}{\pi T_2^*} \qquad (10)$$

The transverse relaxation rate (T_2) is the rate of relaxation of the spin vectors in the x-y (transverse) plane and is intimately tied to the size of the molecule as it tumbles through space. T_2^* is the apparent transverse relaxation time that has contributions from transverse relaxation time, T_2, and inhomogeneous broadening.[40] The time required for transverse relaxation decreases as the correlation time and molecular diameter increases. Figure 7 shows the decrease in T_2^* time (milliseconds) with increasing DBSBA and DBSBB concentration until T_2^* becomes nearly independent of concentration. The decrease then subsequent stabilization in T_2^* relaxation time with increasing concentration of DBSBA and DBSBB indicates that HFB micellar concentration reaches saturation. As HFB partitions into micelles, its motion is restricted from strong benzyl interactions. Equation 11 illustrates the relationship between correlation time and molecular volume, where r is the aggregate radius, k is Boltzmann's constant, T is temperature in K, V is aggregate volume, and η is the viscosity of the medium. HFB molecules therefore tumble as the micelle tumbles, decreasing T_2^* and increasing its correlation time. Molecular volume is proportional to molecular mass under the assumption of uniform density. An increase in aggregate diameter is represented by an increase in the correlation time. [82,83]

$$\tau_c = \frac{4\pi r^3}{3kT} = \frac{V\eta}{kT} \qquad (11)$$

The relative change in ^{19}F chemical shift with DBSBA and DBSBB concentration, with respect to HFB in D_2O, is shown in Figure 7 as well. This progression was observed to be toward a smaller (less negative) chemical shift in the ^{19}F spectrum which suggests the transition of HFB from a dipolar environment (D_2O) to quadrupolar one (micelle). The change in chemical shift toward more positive values indicates deshielding of fluorine nuclei, in opposition of the expected increase in shielding as hydrophobic hydrocarbon molecules partition into the more

non-polar environments of micelles. [84,85] The anisotropic magnetic fields generated by delocalized π electrons of DBSBA and DBSBB benzyls should deshield the ^{19}F nuclei of HFB due to the preferential parallel displaced configuration observed between benzene and HFB. Examination of Figure 7 also suggests that DBSBA and DBSBB have different affinities for HFB and that HFB experiences a slightly more non-polar environment in DBSBA than DBSBB. Figure 7 therefore exhibits the aggregation of HFB into the micellar interior using changes in ^{19}F nuclear shielding ($\Delta\delta^{19}F$) and transverse relaxation data (T_2^*).

The progressive deshielding of the HFB ^{19}F nuclei with increasing DBSBA and DBSBB concentration correlates well with the supposition of strong interactions between HFB and the aromatic micellar core. Quantification of these interactions can be accomplished by using Gibb's phase rule and the mass action model of micelle formation.[58,86] Micelles form via the association of a given number of surfactants under the conditions of equilibrium.

$$nS \rightleftharpoons M \qquad K_n \quad (12)$$

where K_n is the equilibrium constant for micelle formation, S is the surfactant monomer, and M are monodispersed micelles composed of n surfactants. We have chosen to model DBSBA and DBSBB as if these molecules have the capability to associate with guests independent of micelle aggregation. This approximation was done for the sake of model simplicity and the elucidation of the system with respect to the solubilizate (HFB). The stepwise equilibria (Equations 13-14) of the association between the host CD and HFB solubilizate are:

$$CD + HFB \rightleftharpoons CD(HFB) \qquad K_1 \quad (13)$$

$$CD(HFB) + HFB \rightleftharpoons CD(HFB)_2 \qquad K_2 \quad (14)$$

where $CD(HFB)_m$ denotes the cyclodextrin amphiphile associated with the m^{th} molecule of HFB solubilizate, K_m is the stepwise association constant between CD $(HFB)_m$ and monomer of solubilizate (HFB). The total number of components equals i +4 (solvent, monomer, micelle, solubilizate) and the number of phases under consideration is one (i.e. micellar phase). Using Gibb's phase rule, Equation 15, we can find the number of independent variables required to quantify the system under examination.

$$f = C + P - 2 \qquad (15)$$

where f is the number of degrees of freedom, C is the number of components and P is the number of phases. The i +1 equilibrium equations constrains the system and allows four degrees of freedom.[86] If we adhere to constant temperature and pressure conditions, there are two other intensive variables that can be selected to describe the system thermodynamically. If the total solubilizate (HFB) concentration is held constant such that only one phase is present, then the association between HFB and CD can be studied quantitatively by changing the ratio of CD to HFB. An illustration of this phenomenon occurs in Figure 8, where DBSBA is used as host CD. A similar relationship occurs between HFB and DBSBB, which is included in the supplementary information (SI).

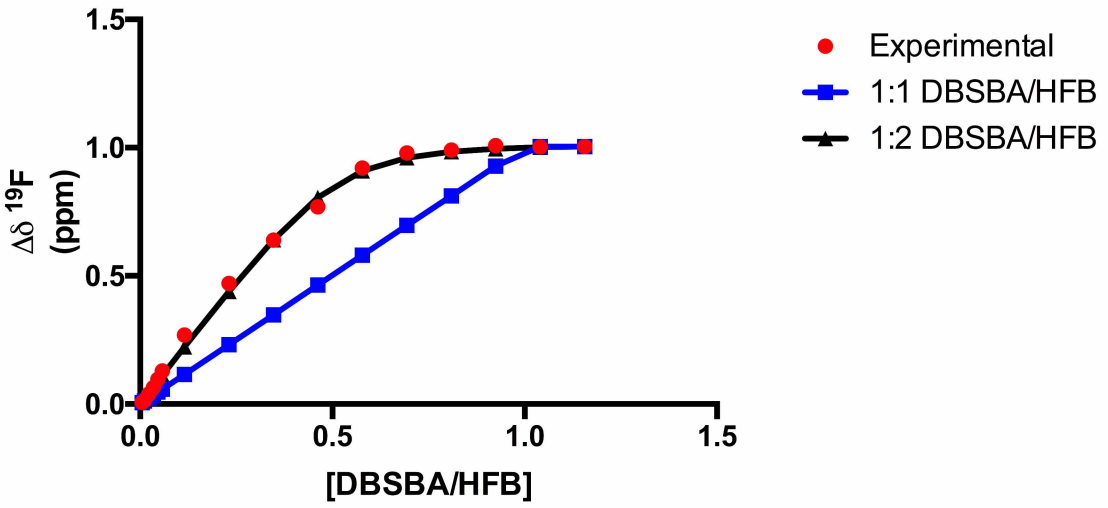

Figure 8. Comparison of 1:1 and 1:2 DBSBA/HFB models with experimental change in ^{19}F chemical shift of HFB. The concentration of HFB was constant in all samples (1.7 $X10^{-2}$ M).

The change in ^{19}F chemical shift ($\Delta\delta$) of HFB with respect to the ratio of DBSBA to HFB concentration (DBSBA/HFB) in Figure 8 illustrates the complex binding in this system. A good starting point an investigation into complexation stoichiometry is the assumption of a simple 1:1 model and subsequent analysis to accept or refute that assumption.[79] A 1:1 model (blue line) is an obvious poor fit for the data (red circles) although the boundary correlations with maximum and minimum chemical shift are good. The maximum change in chemical shift in this model occurs when the ratio of DBSBA/HFB is 1:1. The unaccounted area above the 1:1 region must therefore must belong to a DBSBA/HFB binding regime in excess of 1:1. Assumption of a 1:2 model (black line) provides a better fit to the data than the 1:1 model.[80]

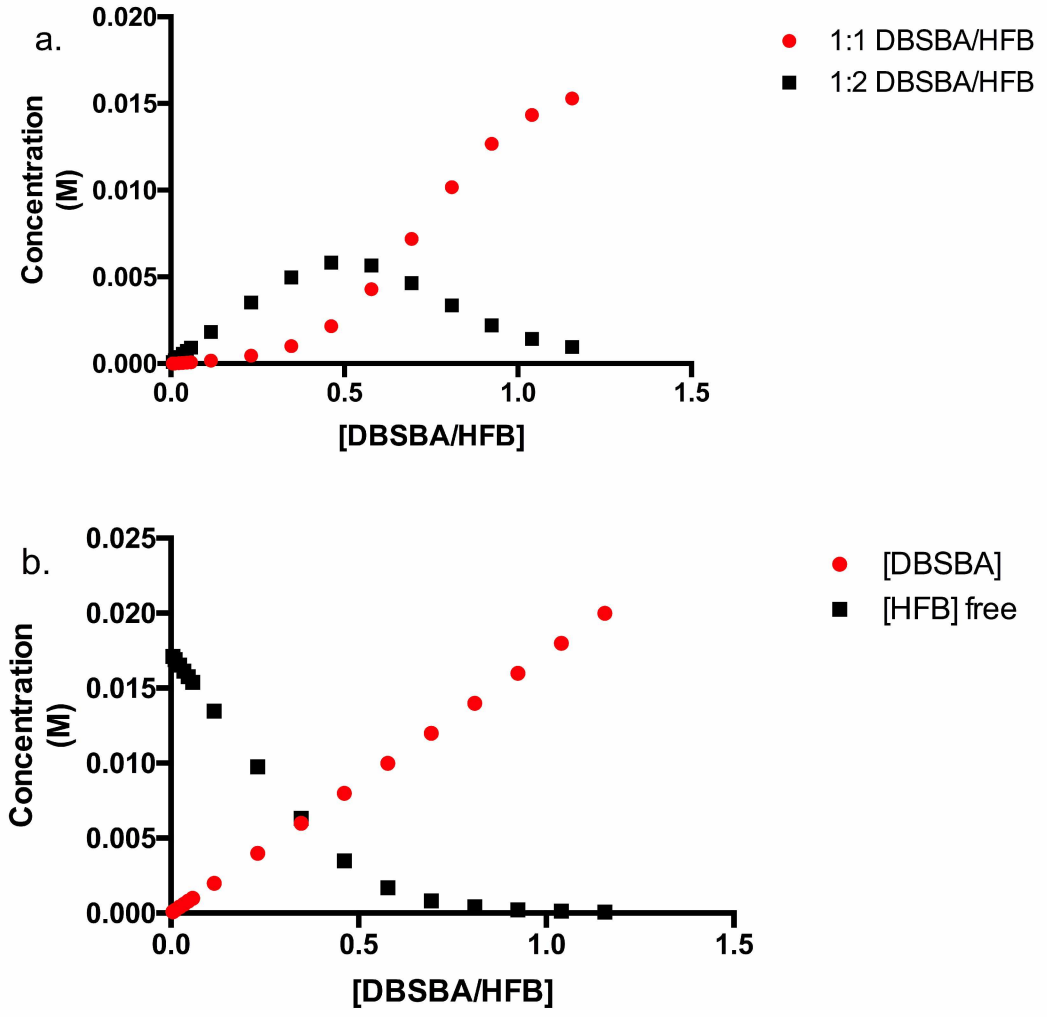

Figure 9 (a) The change in concentration of 1:1 HFB/DBSBA and 2:1 HFB/DBSBA complexes with changes in the ratio of nominal DBSBA to HFB concentrations. Association constants K_1 and K_2 were assumed to be 5 X 10^5 and 7 X 10^2 respectively (b) The reduction in concentration of free HFB with increasing concentration of DBSBA.

Figure 9 (a) demonstrates the deconvolution of the1:2 DBSBA/HFB assumption from Figure 8 into 1:1 and 1:2 binding regimes. The values for each binding regime was calculated by an iterative curve-fitting process using a Microsoft EXCEL® solver worksheet.[46] An assumed K_1 association constant of 5.0 X 10^5 was used; K_2 was subsequently calculated to be 7.3 X 10^2. The

maximum of 1:2 DBSBA/HFB complex occurs at 0.5 (or 1:2 DBSBA/HFB) while the maximum concentration of 1:1 DBSBA/HFB complex emerges at the 1:1 ratio of DBSBA to HFB free concentrations. The 1:2 complex dominates at lower DBSBA concentrations while it yields to a 1:1 complex at higher concentrations of DBSBA. The maximum ^{19}F chemical shift near the DBSBA/HFB ratio of 1.0 implies stoichiometric binding of HFB to DBSBA. The non-linear reduction of free HFB concentration with linear increase in DBSBA concentration (Figure 9 (b)) also suggests that more than 1 mole of HFB is being sequestered per mole of DBSBA.

The maximum calculated values of the equilibrium constants associated with the minimum RSS (residual sum of squares) for DBSBB gave a K_1 of 16700 and a K_2 of 511. Likewise, calculation of equilibrium constants for DBSBA generated a K_1 of 573000 and a K_2 of 775. A discussion of the intrinsic meaning of these calculated values begins with the appropriate error or confidence interval associated with these values, especially given the upper bound, the small change in RSS with large change in value of K.

The calculation of the appropriate confidence interval for the K_1 and K_2 is neither trivial nor straightforward. Micellar interactions with HFB solubilizate is a complex system; assumptions have been made to simplify the system (i.e. the summation of individual interactions of DBSBA with HFB does not differ significantly from micellar/HFB interactions and there are only two predominant equilibrium constants) and the error associated with our calculation must reflect these assumptions. A global analysis is more useful in systems with multiple and possibly cooperative binding.[80] The uncertainty estimation of our non-linear regression was performed using a grid search method. [80,87] We have chosen to use a Profile Likelihood Method in order to calculate our 95% confidence intervals for K_1, K_2 …K_n association constants using Chi-square

test. All valid combinations of K_1 and K_2 lie with the boundaries of the intervals. Figure 10 shows there is a relationship between K_1 and K_2, and that K_1 is large without an upper bound.

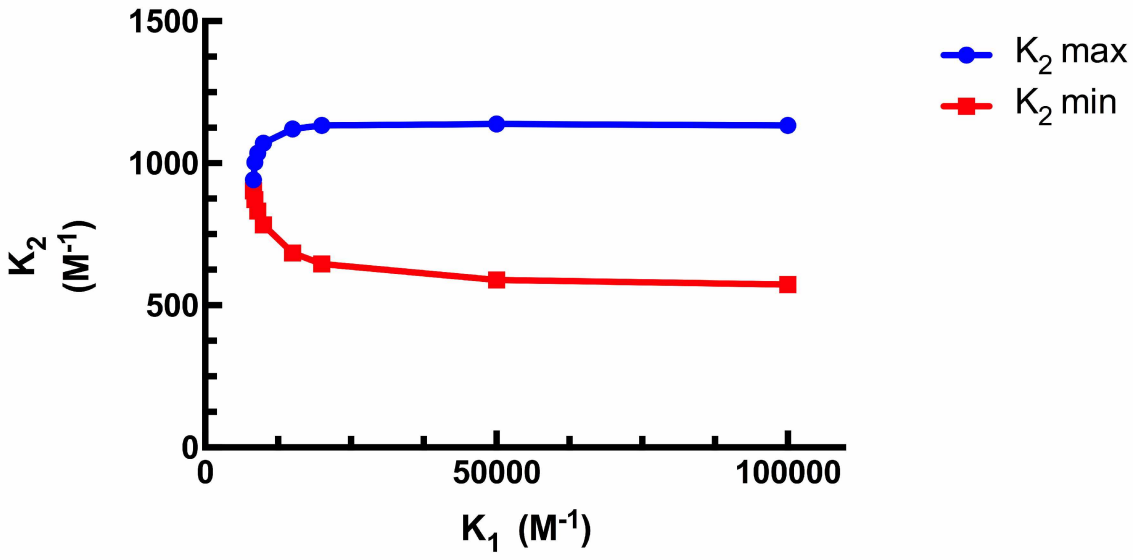

Figure 10. Likelihood profile for association constants of HFB with DBSBA. The lines with blue circles represent upper bound of 95% confidence interval, while lines with red squares demarcate lower bounds of values for association constants. The area of the graphs between the two boundaries represents the field of statistically valid values for K_1 and K_2.

The values, or range of values, of K_1 and K_2 for HFB association with DBSBA and DBSBB are included in Table 3.

Table 3. Calculated Values of K_1 and K_2 Using Profile Likelihood Method

Micelle	K_1 (M^{-1})	K_2 (M^{-1})
DBSBA	≥ 8300	570-1130
DBSBB	≥ 1100	350-1370

DBSBA and DBSBB both bind HFB strongly, but as the likelihood profiles of the association constants of HFB with DBSBA and DBSBB appear to differ, DBSBA binds HFB more strongly than DBSBB in K_1 and K_2. The calculated equilibrium constants for DBSBB are not significantly different, but K_1 and K_2 for DBSBA are. The calculated change in free energy due to HFB complexation, calculated from equilibrium constants in Table 3 and collected in the Supporting Information, fall within the ranges of benzene/hexafluorobenzene complexation. Origins of the differences between the affinities will require more extensive study. Our initial conjecture is that the DBSBA benzyl moieties are slightly closer together in space than in DBSBB. These structural differences could allow for a more cooperative (positive) effect in HFB/DBSBA interactions, hence stronger binding for both K_1 and K_2.

The suggestion of the unlimited nature of K_1 must be tempered with the limitation of the 1:2 model (i.e. likelihood of multiple simultaneous equilibria beyond 2 HFB guests per DBSBA host in micelle) and the inherent limitations of NMR titration studies. Nevertheless, our investigations can express that the interactions between HFB and the DBSBA micelle are a function of multiple equilibrium constants, at least quantified by K_1 and K_2, and that K_1 is much larger than K_2. The upper boundary values for K_1 were demarcated at 100,000 due to the limitations of the NMR titration method.[80]

3.4.4 The Effect of Change in Hydrophobic Substituent of Secondary Hydroxyl on Solubilization Behavior of HFB

It is well known that the structure of a molecule (or macromolecule) is intimately related to its function. Alteration of the chemical structure can have profound changes on its physical and chemical properties whether it be in interaction with itself or another chemical species. [60,61]An

illustration of the role of the benzylic substituents of DBSBB on HFB interaction/solubilization was performed by substitution with methyl and hexanoyl moieties. The structures of these amphiphilic cyclodextrins are pictured in Figure 11b (DMSBB) and 11c (SHBCD). The effect on solubilization of HFB with respect to increasing concentrations of the compounds featured in Figure 11 is illustrated in Figure 12.

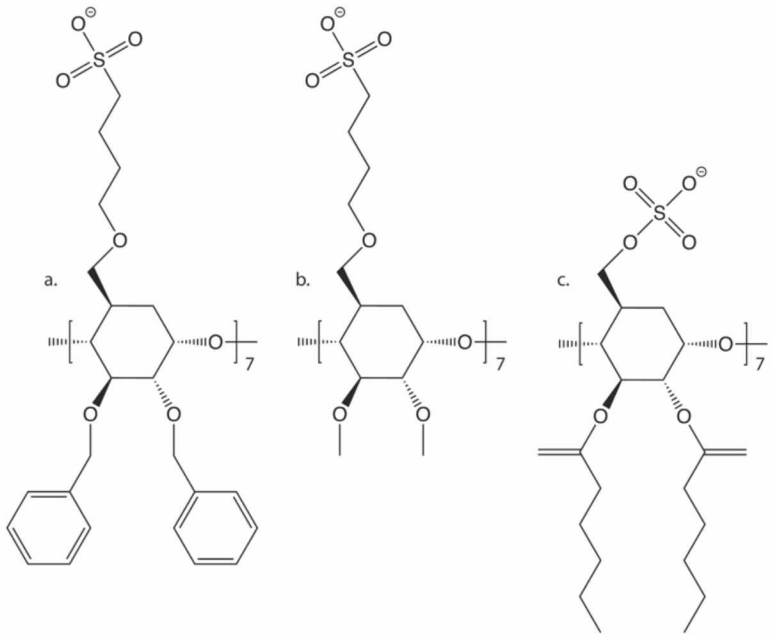

Figure 11. Structures of a) heptakis (2,3-*O*-dibenzyl, 6-*O*-sulfobutyl) cyclomaltoheptaose (DBSBB), b) heptakis (2,3-*O*-dimethyl, 6-*O*-sulfobutyl) cyclomaltoheptaose (DMSBB), and c) heptakis (2,3-*O*-dihexanoyl, 6-*O*-sulfato) cyclomaltoheptaose (SHBCD)

Figure 12 demonstrates the effect of the substitution of these hydrophobic moieties on the solubilization of HFB. The use of ^{19}F chemical shift measurements as a metric for hydrophobic environment (i.e. deshielding) clearly shows DBSBB providing the greatest ability to solubilize HFB. In contrast to the previously described interaction of DBSBB with HFB, the interaction of heptakis (2,3-*O*-dimethyl, 6-*O*-sulfobutyl) cyclomaltoheptaose (DMSBB) has a linear

relationship between increased deshielding of the fluorine nucleus (i.e. quadrupolar environment) and DMSBB concentration. DBSBM has demonstrated no evidence of micelle formation capability. An even greater alteration in physical relationship occurs between

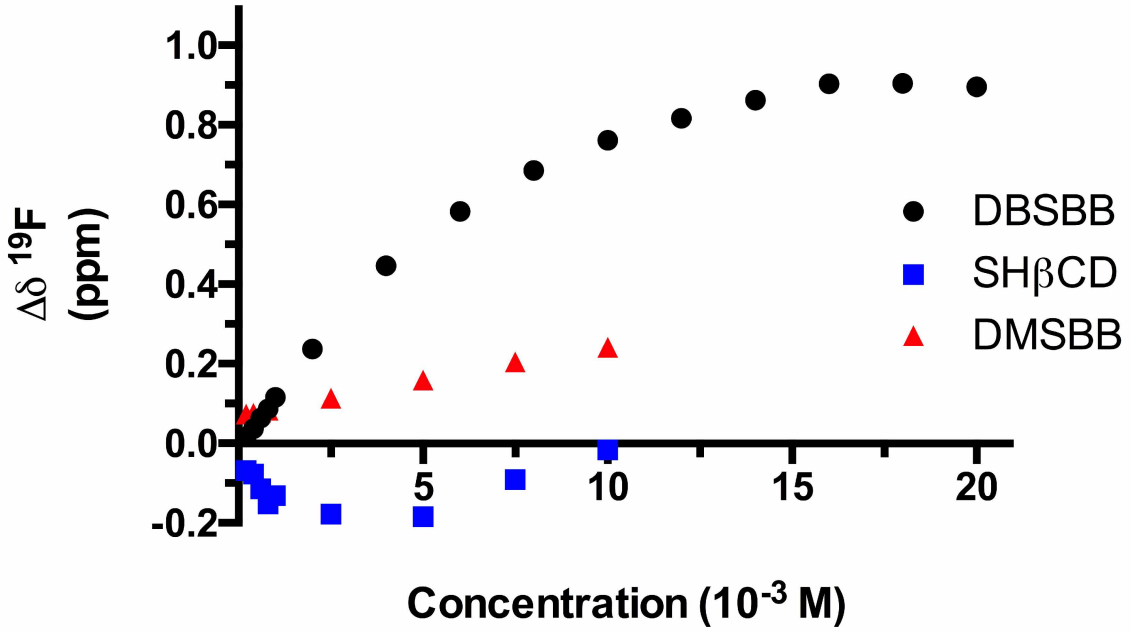

Figure 12. Comparison of change of substituents on β-CD with change in chemical shift due to HFB interaction. Positive values of Δδ indicate increased shielding (non-polar interactions) around HFB probe. Negative values of Δδ indicate decreased shielding (polar interactions). No change in chemical shift (Δδ = 0.0) is HFB in D_2O.

heptakis (2,3-*O*-dihexanoyl, 6-*O*-sulfato) cyclomaltoheptaose (SHBCD) and HFB. The inferred interaction between these two species from the ^{19}F chemical shift data in Figure 12 is that fluorine nuclei of HFB becomes initially more shielded with SHBCD concentration, then transitions through a critical point, then becomes progressively more deshielded as concentration of CD increases. Comparison between secondary rim substituents, benzyl and methyl, (DBSBB,

DBSBM) indicates that presence of benzyls facilitate sorption of HFB. The comparison of the solubility profile of HFB between the hydrophobic methyl, hexanoyl, and benzyl moieties is striking; $\pi-\pi$ interactions are clearly dominant with respect to solubilize HFB in Figure 12. The behavior of HFB with SHBCD is of even greater interest. Typical solubilization profiles of hydrophobic species in both single chained and polymeric surfactant aggregate systems illustrate increases in hydrophobe solubility with extension of hydrophobic chain. [15,58] In all concentrations of SHBCD with HFB, the fluorine nuclei are more shielded than in the absence of CD. Examination of the effect of secondary hydrophobic substitution illustrates the necessity of the benzyl moieties to not only anchor the formation of the micelle, but to solubilize HFB to any substantial extent. Finally, an HOESY 19F-1H experiment reveals a correlation between HFB and benzyl substituents on DBSBB but not with the cyclodextrin cavity. (Figure A10)

3.5 Conclusions

The CMCs of DBSBA and DBSBB have good agreement, approximately 90-100 μM, as determined by pyrene fluorescence, DOSY NMR, and conductivity measurement and analysis. The change in diffusion coefficient with concentration not only indicates aggregation, but an approximate doubling in hydrodynamic diameter that suggests a spherical aggregate or micelle. Molecular packing parameters calculated from the dimensions of DBSBA and DBSBB predicts a nearly spherical geometric shape with an estimated aggregation number of 15 and 12, respectively. Analysis of conductivity data with respect to concentration at different temperatures demonstrated decreasing CMC with increasing temperature. This data allowed for the calculation of thermodynamic micellization values; the aggregation of DBSBA and DBSBB is spontaneous, endothermic, and entropically favored at ambient temperatures. The large number of aromatic benzyl substituents on the surfactants appears to have a significant effect on the thermodynamics

of aggregation. The assessment of the near spherical geometry of the DBSBA and DBSBB micelles facilitates calculations and analysis with respect to both DBSBA/DBSBB aggregates and molecules that interact with them. Hexafluorobenzene (HFB) was used as a solubilization probe to test for the strength of arene-perfluoroarene interactions in the micelle interior. Reasonable conclusions are that HFB and DBSBA/DBSBB interactions are strong, HFB is concentrating in the aromatic micelle interior, and is a function of at least 2 non-equivalent association constants for DBSBA. Substitution of the aromatic benzyl groups for aliphatic substituents drastically decreases the solubility of HFB with respect to increasing amounts of amphiphilic cyclodextrin. This study demonstrates that hydrophobic and/or lipophobic molecules can potentially concentrate inside the DBSBA/DBSBB aggregate/micelle and that the aromatic micellar core is defining trait of the system. Future applications of DBSBA/DBSBB may include, but are not limited to, micellar catalysis and aqueous remediation involving aromatic or highly fluorinated aromatic chemicals, pesticides, or pharmaceuticals.

3.6 References

(1) Vincent, B. McBain and the Centenary of the Micelle. *Advances in Colloid and Interface Science* 2014, *203*, 51–54.

(2) Hiemenz, P.; Rajagopalan, R. *Principles of Colloid and Surface Chemistry*, 3rd ed.; CRC Press: New York, 1997.

(3) Szejtli, J. Introduction and General Overview of Cyclodextrin Chemistry. *Chemical. Reviews.* 1998, *98*, 1743–1754.

(4) Jiang, L.; Yan, Y.; Huang, J. Versatility of Cyclodextrins in Self-Assembly Systems of Amphiphiles. *Advances in Colloid and Interface Science* 2011, *169*, 13–25.

(5) Roux, M.; Perly, B.; Djedaïni-Pilard, F. Self-Assemblies of Amphiphilic Cyclodextrins. *European Biophysical Journal* 2007, *36*, 861–867.

(6) Auzély-Velty, R.; Djedaïni-Pilard, F.; Désert, S.; Perly, B.; Zemb, T. Micellization of Hydrophobically Modified Cyclodextrins. 1. Micellar Structure. *Langmuir* 2000, *16*, 3727–3734.

(7) Giacomelli, C.; Schmidt, V.; Putaux, J.-L.; Narumi, A.; Kakuchi, T.; Borsali, R. Aqueous Self-Assembly of Polystyrene Chains End-Functionalized with B-Cyclodextrin. *Biomacromolecules* 2009, *10*, 449–453.

(8) Dubes, A.; Bouchu, D.; Lamartine, R.; Parrot-Lopez, H. An Efficient Regio-Specific Synthetic Route to Multiply Substituted Acyl-Sulphated β-Cyclodextrins. *Tetrahedron Letters* 2001, *42*, 9147–9151.

(9) Lombardo, D.; Longo, A.; Darcy, R.; Mazzaglia, A. Structural Properties of Nonionic Cyclodextrin Colloids in Water. *Langmuir* 2004, *20*, 1057–1064.

(10) Zana, R. Dimeric and Oligomeric Surfactants. Behavior at Interfaces and in Aqueous Solution: a Review. *Advances in Colloid and Interface Science* 2002, *97*, 205–253.

(11) Rosen, M. J.; Tracy, D. J. Gemini Surfactants. *Journal of Surfactants and Detergents* 1998, *1*, 547–554.

(12) Nagarajan, R.; Ruckenstein, E. Aggregation of Amphiphiles as Micelles or Vesicles in Aqueous Media. *Journal of Colloid and Interface Science* 1979, *71*, 580–604.

(13) Berezin, I. V.; Martinek, K.; Yatsimirskii, A. K. Physicochemical Foundations of Micellar Catalysis. *Russian Chemical Reviews* 1973, *42*, 787–802.

(14) Dam, T.; Engberts, J. B. F. N.; Karthäuser, J.; Karaborni, S.; van Os, N. M. Synthesis, Surface Properties and Oil Solubilisation Capacity of Cationic Gemini Surfactants. *Colloids and Surfactants A* 1996, *118*, 41–49.

(15) Menger, F. M.; Keiper, J. S. Gemini Surfactants. *Angewandte Chemie International Edition in English.* 2000, *39*, 1906–1920.

(16) Myers, D. *Surfactant Science and Technology*, 3rd ed.; John Wiley & Sons: Hoboken, 2005.

(17) Eriksson, J.; Gillsberg, G. NMR-Studies of the Solubilization of Aromatic Compounds in Cetyltrimethylammonium Bromide Solution II. *Acta Chemica Scandanavia.* 1966, *20*, 2019–2027.

(18) Mukerjee, P.; Cardinal, J. R. Benzene Derivatives and Naphthalene Solubilized in Micelles. Polarity of Microenvironments, Location and Distribution in Micelles, and Correlation with Surface Activity in Hydrocarbon-Water Systems. *Journal of Physical Chemistry* 1978, *82*, 1620–1627.

(19) Zhao, X.; Pan, F.; Xu, H.; Yaseen, M.; Shan, H.; Hauser, C. A. E.; Zhang, S.; Lu, J. R. Molecular Self-Assembly and Applications of Designer Peptide Amphiphiles. *Chemical Society Reviews* 2010, *39*, 3480–3498.

(20) Fleming, S.; Ulijn, R. V. Design of Nanostructures Based on Aromatic Peptide Amphiphiles. *Chemical Society Reviews* 2014, *43*, 8150–8177.

(21) Hunter, C. A.; Lawson, K. R.; Perkins, J.; Urch, C. J. Aromatic Interactions. *Journal of Chemical Society, Perkin Transactions 2* 2001,5, 651–669.

(22) Dance, I. Π··· Π Interactions: Theory and Scope. In *Encyclopedia of Supramolecular Chemistry*; CRC Press, 2004; pp 1076-1092.

(23) Franks, F. *Water a Comprehensive Treatise: Volume 4: Aqueous Solutions of Amphiphiles and Macromolecules*; Plenum Press; New York, 1975.

(24) Salonen, L. M.; Ellermann, M.; Diederich, F. Aromatic Rings in Chemical and Biological Recognition: Energetics and Structures. *Angewandte Chemie International Edition in English.* 2011, *50*, 4808–4842.

(25) Whitten, D. G.; Chen, L.; Geiger, H. C.; Perlstein, J.; Song, X. Self-Assembly of Aromatic-Functionalized Amphiphiles: the Role and Consequences of Aromatic−Aromatic Noncovalent Interactions in Building Supramolecular Aggregates and Novel Assemblies. *Journal of Physical Chemistry B* 1998, *102*, 10098–10111.

(26) Geiger, H. C.; Perlstein, J.; Lachicotte, R. J.; Wyrozebski, K. Self-Assembly of Aromatic-Derivatized Amphiphiles: Phenyl, Biphenyl, and Terphenyl Fatty Acids and Phospholipids. *Langmuir* 1999,15, 5606–5616.

(27) Gu, W.; Gin, D. L. Aromatic Side Chain-Functionalized Long Chain Acid Salts: Structural Factors Influencing Their Lyotropic Liquid-Crystalline Behavior. *Langmuir* 2002, *18*, 7415–7427.

(28) Guo, W.; Fung, B. M.; Christian, S. D. NMR Study of Cyclodextrin Inclusion of Fluorocarbon Surfactants in Solution. *Langmuir* 1992, *8*, 446–451.

(29) Reichenbächer, K.; Süss, H. I.; Hulliger, J. Fluorine in Crystal Engineering—"the Little Atom That Could." *Chemical Society Reviews* 2005, *34*, 22–30.

(30) Lorenzo, S.; Lewis, G. R.; Dance, I. Supramolecular Potentials and Embraces for Fluorous Aromatic Molecules. *New Journal of Chemistry* 2000, *24*, 295–304.

(31) Reddy, L.; Nangia, A.; Lynch, V. M. Phenyl-Perfluorophenyl Synthon Mediated Cocrystallization of Carboxylic Acids and Amides. *Crystal Growth and Design* 2003, *4*, 89–94.

(32) Kirsch, P. *Modern Fluoroorganic Chemistry*, 2nd ed.; Wiley-VCH Verlag GmbH & Co. KGaA: Weinheim, Germany, 2013.

(33) Kolehmainen, E. Solubilization of Aromatics in Aqueous Bile Salts: II. Benzene and Some Substituted Benzenes in Sodium Deoxycholate and Cholate: ^{1}H and ^{19}F NMR Studies. *Journal of Colloid and Interface Science* 1989, *127*, 301–309.

(34) Moughton, A.; Hillmyer, M.; Lodge T. Multicompartment block polymer micelles. *Macromolecules* 2011, 45, 2-19.

(35) Lutz, J. F.; Laschewsky, A. Multicompartment Micelles: Has the Long-Standing Dream Become a Reality? *Macromolecular Chemistry and Physics.* 2005, *206*, 813–817.

(36) Marsat, J.-N.; Heydenreich, M.; Kleinpeter, E.; Berlepsch, von, H.; Böttcher, C.; Laschewsky, A. Self-Assembly Into Multicompartment Micelles and Selective Solubilization by Hydrophilic−Lipophilic−Fluorophilic Block Copolymers. *Macromolecules* 2011, *44*, 2092–2105.

(37) Matsumoto, K.; Kubota, M.; Matsuoka, H.; Yamaoka, H. Water-Soluble Fluorine-Containing Amphiphilic Block Copolymer: Synthesis and Aggregation Behavior in Aqueous Solution. *Macromolecules* 1999, *32*, 7122–7127.

(38) Takezawa, H.; Murase, T.; Resnati, G.; Metrangolo, P.; Fujita, M. Recognition of Polyfluorinated Compounds Through Self-Aggregation in a Cavity. *Journal of the American Chemical Society* 2014, *136*, 1786–1788.

(39) McKee, J. A.; Green, T. K. Synthesis of 2, 3-Dibenzyl-6-Sulfobutyl-α and β Cyclodextrins: New Chiral Surfactants for Capillary Electrophoresis. *Tetrahedron Letters* 2015, *56*, 4451–4454.

(40) Mirau, P. *A Practical Guide to Understanding the NMR of Polymers*, 1st ed.; John Wiley & Sons. Inc: Hoboken, NJ, 2005.

(41) Kotzev, A.; Laschewsky, A.; Adriaensens, P.; Gelan, J. Micellar Polymers with Hydrocarbon and Fluorocarbon Hydrophobic Chains. a Strategy to Multicompartment Micelles. *Macromolecules* 2002, *35*, 1091–1101.

(42) Waters, M. L. Aromatic Interactions in Model Systems. *Current Opinion in Chemical Biology* 2002, *6*, 736–741.

(43) Raju, R. K.; Hillier, I. H.; Burton, N. A.; Vincent, M. A.; Doudou, S.; Bryce, R. A. The Effects of Perfluorination on Carbohydrate–Π Interactions: Computational Studies of the Interaction of Benzene and Hexafluorobenzene with Fucose and Cyclodextrin. *Physical Chemistry Chemical Physics* 2010, *12*, 7959–7959.

(44) Ribeiro, J. P.; Bacchi, S.; Dell'Anna, G.; Morando, M.; Cañada, F. J.; Cozzi, F.; Jiménez-Barbero, J. A Combined NMR, Computational, and HPLC Study of the Inclusion of Aromatic and Fluoroaromatic Compounds in Cyclodextrins as a Model for Studying Carbohydrate–Aromatic Interactions. *European Journal of Organic Chemistry* 2008, 5891–5898.

(45) Van Geet, A. L. Calibration of Methanol Nuclear Magnetic Resonance Thermometer at Low Temperature. *Analytical Chemistry* 1970, *42*, 679–680.

(46) McDonnell, M. N.; Berry, N. M.; Cutting, M. A.; Keage, H. A.; Buckley, J. D.; Howe, P. R. C. Transcranial Doppler Ultrasound to Assess Cerebrovascular Reactivity: Reliability, Reproducibility and Effect of Posture. *Peer Journal* 2013, *1*, e65.

(47) Dong, D. C.; Winnik, M. A. The Py Scale of Solvent Polarities. *Canadian Journal of Chemistry* 1984, *62*, 2560–2565.

(48) Kalyanasundaram, K.; Thomas, J. K. Environmental Effects on Vibronic Band Intensities in Pyrene Monomer Fluorescence and Their Application in Studies of Micellar Systems. *Journal of the American Chemical Society* 1977, *99*, 2039–2044.

(49) Phillips, J. N. The Energetics of Micelle Formation. *Transactions of the Faraday Society* 1955, *51*, 561–569.

(50) Lopez-Diaz, D.; Velázquez, M. M. Variation of the Critical Micelle Concentration with Surfactant Structure: a Simple Method to Analyze the Role of Attractive–Repulsive Forces on Micellar Association. *Chemical Educator* 2007, *12*, 327–330.

(51) Jacobsen, N. *NMR Spectroscopy Explained*, 1st ed.; John Wiley & Sons, Inc.: Hoboken, NJ, 2007.

(52) Price, W. S. *NMR Studies of Translational Motion: Principles and Applications*; Cambridge University Press; New York, 2009.

(53) Basilio, N.; García-Río, L.; Martín-Pastor, M. NMR Evidence of Slow Monomer−Micelle Exchange in a Calixarene-Based Surfactant. *Journal of Physical Chemistry B* 2010, *114*, 4816–4820.

(54) Johnson, C. S. Diffusion Ordered Nuclear Magnetic Resonance Spectroscopy: Principles and Applications. *Progress in Nuclear Magnetic Resonance Spectroscopy* 1999, *34*, 203–256.

(55) Price, W. S. Pulsed-Field Gradient Nuclear Magnetic Resonance as a Tool for Studying Translational Diffusion: Part 1. Basic Theory. *Concepts in Magnetic Resonance* 1997, *9*, 299–336.

(56) Cohen, Y.; Avram, L.; Frish, L. Diffusion NMR Spectroscopy in Supramolecular and Combinatorial Chemistry: an Old Parameter? New Insights. *Angewandte Chemie International Edition* 2005, *44*, 520–554.

(57) Dubes, A.; Degobert, G.; Fessi, H.; Parrot-Lopez, H. Synthesis and Characterisation of Sulfated Amphiphilic α-, β- and γ-Cyclodextrins: Application to the Complexation of Acyclovir. *Carbohydrate Research* 2003, *338*, 2185–2193.

(58) Hunter, R. *Foundations of Colloid Science*, 2nd ed.; Oxford University Press: New York, 2001.

(59) Zana, R. Critical Micellization Concentration of Surfactants in Aqueous Solution and Free Energy of Micellization. *Langmuir* 1996, *12*, 1208–1211.

(60) Wennerstrom, H.; Evans, D. F. *The Colloidal Domain: Where Physics, Chemistry, and Biology Meet*, 1st ed.; Wiley-VCH.

(61) Israelachvili, J. N.; Mitchell, D. J.; Ninham, B. W. Theory of Self-Assembly of Hydrocarbon Amphiphiles Into Micelles and Bilayers. *Journal of Chemical Society, Faraday Transactions. 2* 1976, *72*, 1525–1568.

(62) Marques, E. F.; Regev, O.; Khan, A.; Lindman, B. Self-Organization of Double-Chained and Pseudodouble-Chained Surfactants: Counterion and Geometry Effects. *Advances in Colloid and Interface Science.* 2003, *100-102*, 83–104.

(63) Parker, D.; Kataky, R.; Kelly, P. M.; Palmer, S. Selectivity in the Binding and Detection of Charge Diffuse Ions. *Pure and Applied Chemistry* 1996, *68*, 1219-1223.

(64) Watry, M. R.; Richmond, G. L. Comparison of the Adsorption of Linear Alkanesulfonate and Linear Alkylbenzenesulfonate Surfactants at Liquid Interfaces. *Journal of the American Chemical Society* 2000, *122*, 875–883.

(65) Chen, L. J.; Lin, S. Y.; Huang, C. C. Effect of Hydrophobic Chain Length of Surfactants on Enthalpy-Entropy Compensation of Micellization. *Journal of Physical Chemistry* 1998, 102, 4350-4356.

(66) Chatterjee, A.; Moulik, S. P.; Sanyal, S. K.; Mishra, B. K.; Puri, P. M. Thermodynamics of Micelle Formation of Ionic Surfactants: a Critical Assessment for Sodium Dodecyl Sulfate, Cetyl Pyridinium Chloride and Dioctyl Sulfosuccinate (Na Salt) by Microcalorimetric, Conductometric, and Tensiometric Measurements. *Journal of Physical Chemistry B* 2001, *105*, 12823–12831.

(67) Jolicoeur, C.; Philip, P. R. Enthalpy-Entropy Compensation for Micellization and Other Hydrophobic Interactions in Aqueous Solutions. *Canadian Journal of Chemistry* 1974, *52*, 1834–1839.

(68) Southall, N. T.; Dill, K. A.; Haymet, A. A View of the Hydrophobic Effect. *Journal of Physical Chemistry B* 2002, *106*, 521–533.

(69) Fisicaro, E.; Compari, C.; Braibanti, A. Entropy/Enthalpy Compensation: Hydrophobic Effect, Micelles and Protein Complexes. *Physical Chemistry Chemical Physics* 2004, *6*, 4156–11.

(70) Ben-Naim, A. *Solvation Thermodynamics*; Springer Science+Business Media LLC: New York, NY, 1987.

(71) Graziano, G. Solvation Thermodynamics in a Van Der Waals Liquid. *Thermochimica Acta* 2003, *399* (1-2), 181–187.

(72) Graziano, G. Hydrophobicity of Benzene. *Biophysical Chemistry* 1999, *82*, 69–79.

(73) Graziano, G. Benzene Solubility in Water: a Reassessment. *Chemical Physical Letters* 2006, *429*, 114–118.

(74) Fisicaro, E.; Compari, C.; Duce, E.; Biemmi, M.; Peroni, M.; Braibanti, A. Thermodynamics of Micelle Formation in Water, Hydrophobic Processes and Surfactant Self-Assemblies. *Physical Chemistry Chemical Physics.* 2008, *10*, 3903.

(75) Lee, B. Solvent Reorganization Contribution to the Transfer Thermodynamics of Small Nonpolar Molecules. *Biopolymers* 1991, *31*, 993–1008.

(76) Graziano, G.; Lee, B. Hydration of Aromatic Hydrocarbons. *Journal of Physical. Chemistry B* 2001, *105*, 10367–10372.

(77) Solomonov, B. N.; Sedov, I. A. Quantitative Description of the Hydrophobic Effect: the Enthalpic Contribution. *Journal of Physical. Chemistry B* 2006, *110*, 9298–9303.

(78) Graziano, G. Aliphatics vs. Aromatics Hydration Thermodynamics. *Biophysical Chemistry* 2004, *110*, 249–258.

(79) Connors, K. A. *Binding Constants: the Measurement of Molecular Complex Stability*, 2nd ed.; John Wiley & Sons: New York, 1987.

(80) Thordarson, P. Determining Association Constants From Titration Experiments in Supramolecular Chemistry. *Chemical Society Reviews* 2011, *40*, 1305–1323.

(81) Freire, M. G.; Razzouk, A.; Mokbel, I.; Jose, J. Solubility of Hexafluorobenzene in Aqueous Salt Solutions From (280 to 340) K. *Journal of Chemical & Engineering Data* 2005, *50*, 237–242.

(82) Bloembergen, N.; Purcell, E. M.; Pound, R. V. Relaxation Effects in Nuclear Magnetic Resonance Absorption. *Physical Review* 1948, *73*, 679–712.

(83) Pochapsky, T.; Pochapsky, S. *NMR for Physical and Biological Scientists*, 1st ed.; Rogers, R., Scholl, S., Eds.; Garland Science. Taylor and Francis Group LLC: New York, 2007.

(84) Brey, W. S.; Brey, M. L. *Fluorine-19 NMR*; John Wiley & Sons, Ltd: Chichester, UK, 2007.

(85) Huc, I.; Oda, R. Gemini Surfactants: Studying Micellisation by ^{1}H and ^{19}F NMR Spectroscopy. *Chemical Communications* 1999, 2015–2016.

(86) Moroi, Y. *Micelles*, 1st ed.; Springer Science+Business Media LLC: New York, NY, 1992.

(87) Beechem, J. M. Global Analysis of Biochemical and Biophysical Data. *Methods in. Enzymology* 1992, *210*, 37–54.

Appendix

Table A1: DBSBA conductivity data.

[DBSBA] (μM)	295 K	302 K	313 K	323 K
0	1.1	1.1	1	1
5	5.8	5.8	4.7	6
10	10.1	9.4	7.9	9
20	15.3	14.1	14	15
30	20.8	21.3	22.3	20
40	29.9	30.1	32.3	30.8
50	32	32	32	31.1
60	40	39.8	39.7	38
70	45	44.1	43	42.3
80	49.1	50.5	49.2	47
90	55.4	56	52.5	52
100	60.3	59.8	59.3	57
120	72.4	71.8	70.3	66
140	80.8	80.5	79.6	77
160	89.8	91	89.9	85.6
180	99.6	102.1	98	97.3
200	111.4	112.8	109	109
250	132	132	131	126
Pre CMC				
m	0.5797	0.5999	0.6096	0.5836
b	3.3611	2.7215	1.8748	2.5206
Post CMC				
m	0.4675	0.4889	0.4915	0.4814
b	15.848	12.467	9.8585	9.0151

Table A2. DBSBB Conductivity data.

[DBSBB] (μM)	295 K	302 K	313 K	323 K
0	2	1	4	2
5	6.5	6.3	9.7	7.2
10	11.8	12.1	14	10.6
20	16.7	16.8	19.5	18.6
30	27.7	23.45	26.3	24.9
40	29.9	30.1	32.3	30.8
50	37	37.8	41.5	38.1
60	45	45.1	47.3	45.6
70	53.4	54.5	57	50.9
80	59.2	58.7	60.2	58.1
90	65	64.3	65.5	64
100	70.7	71.4	73.4	70.1
120	82.6	83.5	86	82
160	106.7	106.8	107	105
180	118	118	120	118
200	131	130.4	131.7	129
250	159	160	160	161
Pre CMC				
m	0.7011	0.7138	0.6999	0.7038
b	3.3291	2.5328	5.514	3.3096
Post CMC				
m	0.5912	0.5932	0.5866	0.6031
b	11.813	11.693	13.95	9.3594

Table A3. DBSBA CMC and degree of ionization (α) data as function of temperature

Temperature (K)	CMC (μM)	α
295	106 ± 2	0.81 ± 0.02
303	87 ± 2	0.81 ± 0.02
313	65 ± 2	0.82 ± 0.02
323	62 ± 1	0.83 ± 0.02

Table A4. DBSBB CMC and degree of ionization (α) data as function of temperature

Temperature (K)	CMC (μM)	α
295	92 ± 2	0.84 ± 0.01
303	80 ± 2	0.83 ± 0.01
313	73 ± 1	0.84 ± 0.01
323	63 ± 2	0.85 ± 0.01

Table A5. Coefficients from least squares regression of $\ln X_{CMC}$ temperature data

$$\ln x_{cmc}(T) = a + bT + cT^2 + dT^3$$

	DBSBA	DBSBB
a	-1577	-811.7
b	15.43	7.905
c	-0.0506	-0.02603
d	5.53×10^{-5}	2.85×10^{-5}
R^2	0.999	0.999

Table A6. Free energies, enthalpies, and entropies of micellization as calculated using Eq. 4 – 8.

$$\Delta H_m^\circ = -(2-\alpha)RT^2\left(b + 2cT + 3dT^2\right)$$

T (K)	DBSBA	DBSBB
	ΔG_m (J/mol)	ΔG_m (J/mol)
295	-38562.2	-37756.0
303	-39775.5	-39756.3
313	-41853.0	-41233.3
323	-43227.6	-41994.8
	ΔH_m (J/mol)	ΔH_m (J/mol)
295	12792.9	12209.8
303	28298.1	19545.2
313	21977.3	15334.3
323	-18436.5	-6603.5
	ΔS_m (J/mol)	ΔS_m (J/mol)
295	174.1	169.4
303	224.7	195.7
313	203.9	180.7
323	76.8	109.6
T_C	316.7	305.7

Table A7. Diffusion coefficients and hydrodynamic radii of DBSBB monomers and aggregates

Concentration (10^{-6} M)	D_{obs} (10^{-10} m^2 sec^{-1})	Hydrodynamic radius (Å)
50	1.191 ± 0.012	16.73± 0.17
75	1.191 ± 0.012	16.73± 0.17
100	1.190 ± 0.012	16.74 ±0.17
125	1.076 ± 0.011	18.52± 0.19
150	1.076 ± 0.011	18.52± 0.19
200	1.045 ± 0.010	19.06± 0.19
250	1.035 ± 0.010	19.25± 0.19
300	0.9634 ± 0.010	20.68± 0.21
500	0.9587 ± 0.010	20.78± 0.21
750	0.7773 ± 0.008	25.63± 0.26
1000	0.7759 ± 0.008	25.68 ±0.26
2000	0.7737 ± 0.008	25.75± 0.26
3000	0.6166 ± 0.006	32.31± 0.32
4000	0.6166 ± 0.006	32.31± 0.32
5000	0.6166 ± 0.006	32.31 ± 0.32

Table A8. Diffusion coefficients and hydrodynamic radii of DBSBA monomers and aggregates

Concentration (10^{-6} M)	D_{obs} (10^{-10} m^2 sec^{-1})	Hydrodynamic radius (Å)
50	1.485 ± 0.015	13.32 ± 0.13
75	1.489 ± 0.015	13.29 ± 0.13
100	1.489 ± 0.015	13.29 ± 0.13
125	1.333 ± 0.013	14.84 ± 0.15
150	1.203 ± 0.012	16.45 ± 0.16
200	1.198 ± 0.012	16.52 ± 0.17
500	0.9616 ± 0.010	20.58 ± 0.21
750	0.9616 ± 0.010	20.58 ± 0.21
1000	0.7762 ± 0.008	25.50 ± 0.26
2000	0.7738 ± 0.008	25.58 ± 0.26
5000	0.7727 ± 0.008	25.61 ± 0.26

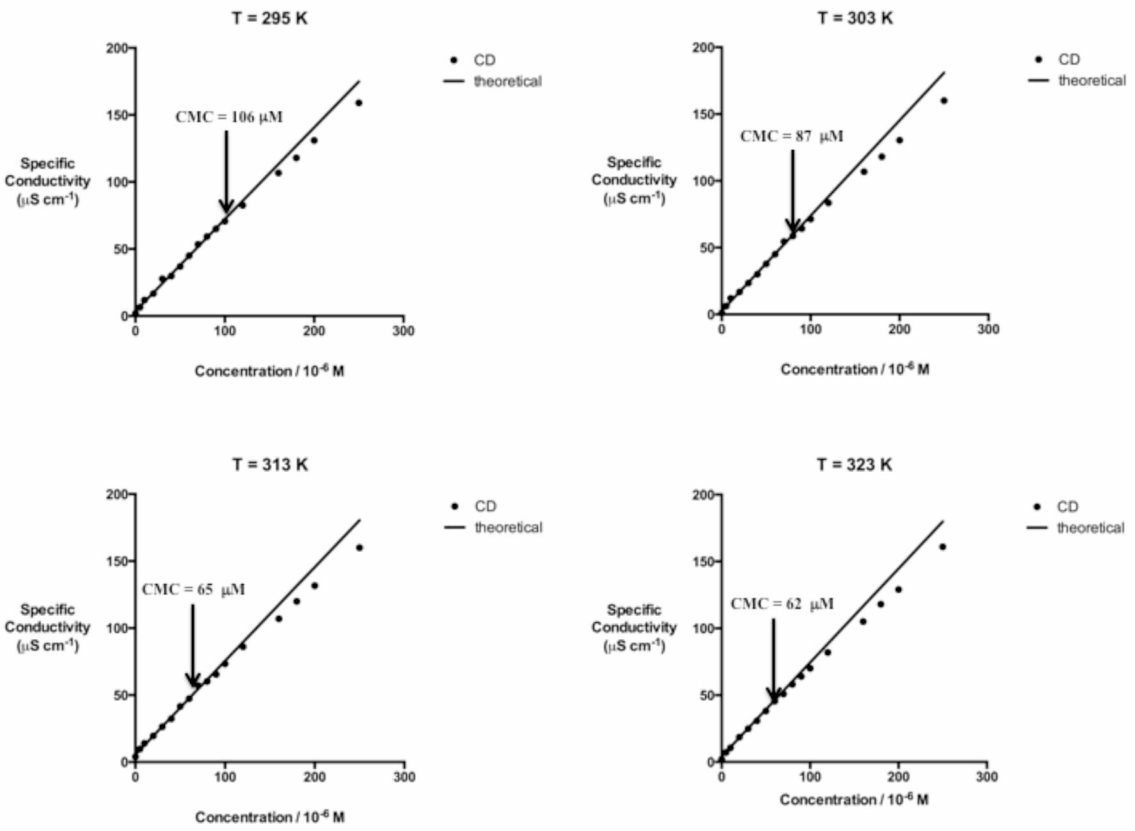

Figure A1. Plot of specific conductance vs. concentration of DBSBA for 295, 303, 313, and 323 K. The CMC was calculated at the point of discontinuity as indicated by the arrow. The degree of micellar counterion dissociation was calculated from the ratio of the slopes of the theoretical and experimental data.

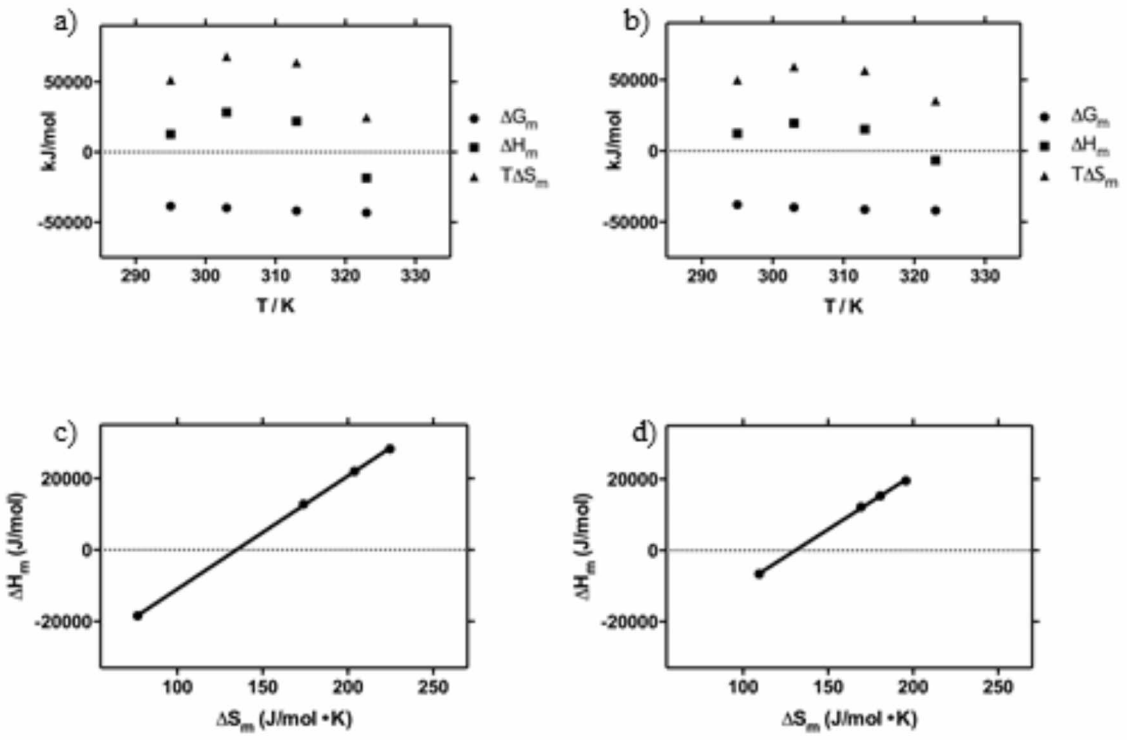

Figure A2. Plot of thermodynamic data with respect to temperature for (a) DBSBA and (b) DBSBB with respect to temperature. Plot of entropies of micellization against enthalpies of micellization for (c) DBSBA and (d) DBSBB. The compensation temperature was taken as the slope of the enthalpy/entropy compensation curves, which were calculated for DBSBA and DBSBB to be 317 K and 305 K, respectively.

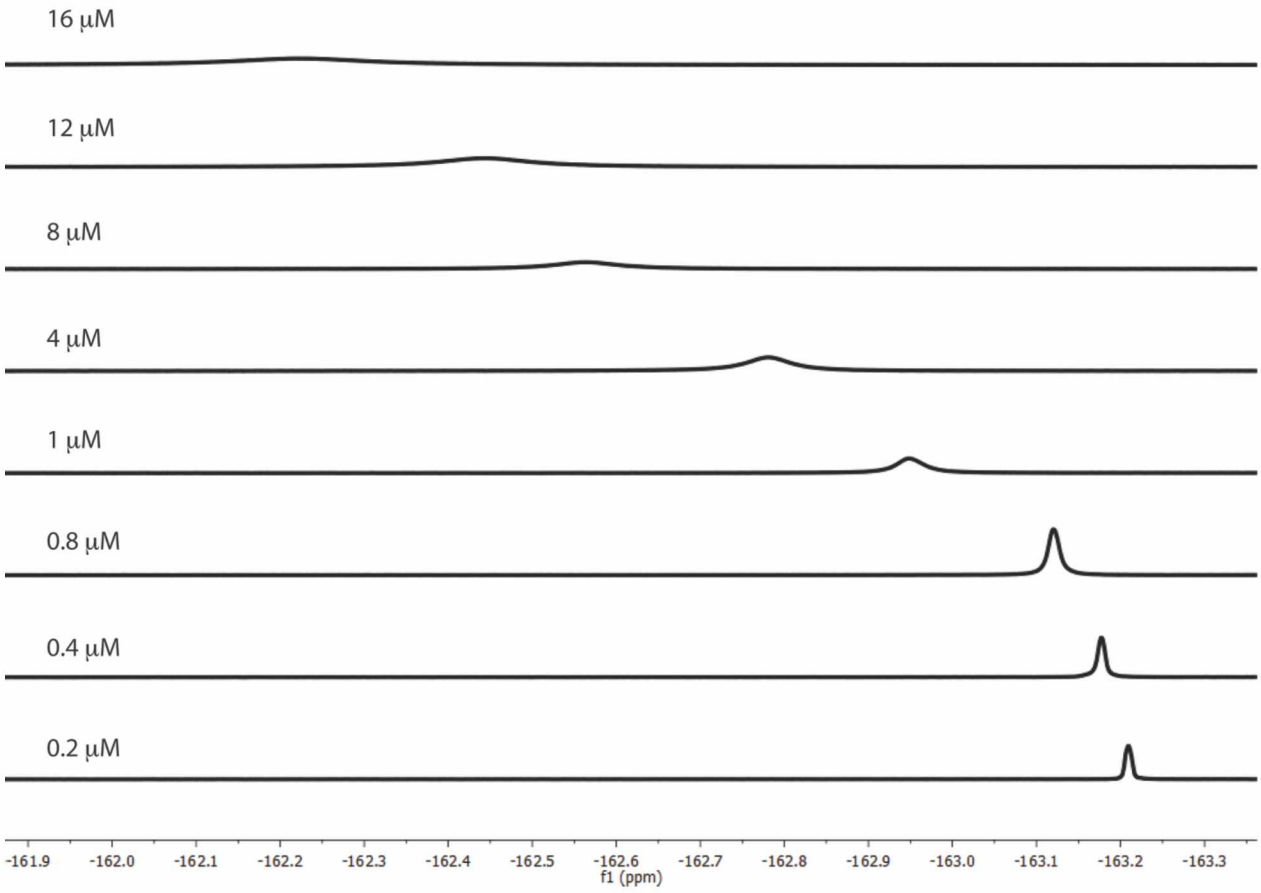

Figure A3. The effect of increasing concentrations of DBSBA solutions on the ^{19}F resonance linewidths of hexafluorobenzene. Linewidth broadening is due to smaller relaxation times (T_2) due to solubilization of hexafluorobenzene. Downfield shifts of ^{19}F resonances are due to the increased effects of shielding due to environment of micellar core.

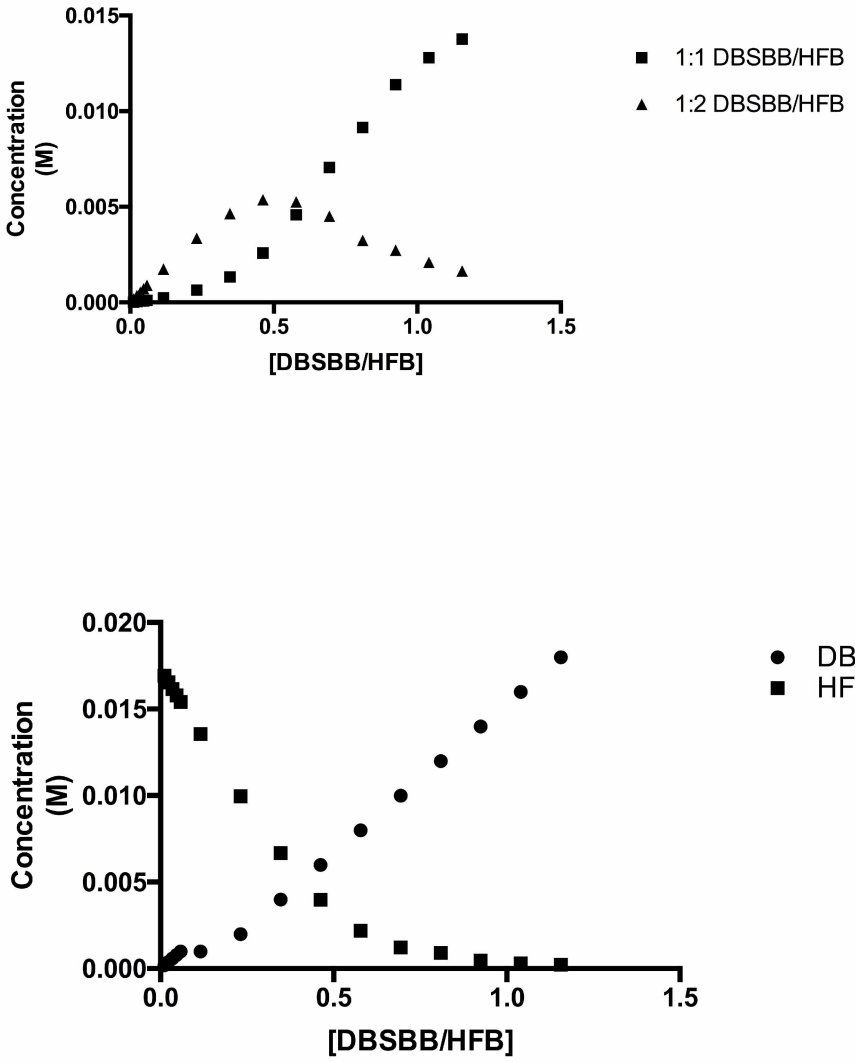

Figure A4. (a) The change in concentration of 1:1 HFB/DBSBB and 2:1 HFB/DBSBB complexes with changes in the ratio of nominal DBSBB to HFB concentrations. Association constants K_1 and K_2 were assumed to be 1.3 X 10^4 and 5 X 10^2 respectively (b) The reduction in concentration of free HFB with increasing concentration of DBSBB.

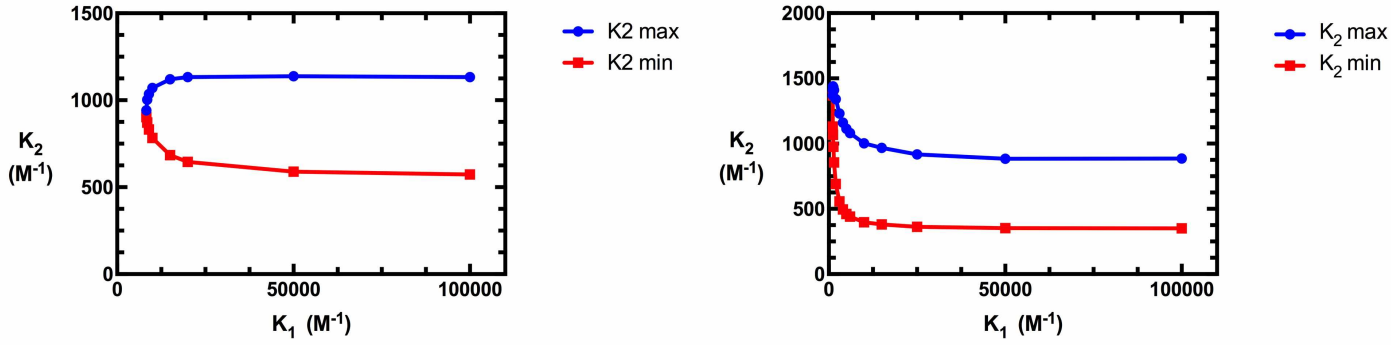

Figure A5. 95% confidence interval (profile likelihood method) for K_1 and K_2 for DBSBA and DBSBB.

Table A9. Calculation of free energy changes upon complexation with HFB.

Micelle (T = 290 K)	K_1 (M^{-1})	ΔG (kJ/mol)	K_2 (M^{-1})	ΔG (kJ/mol)
DBSBA	≥ 8300	≥- 21.8	570-1130	-15.4 - -17.0
DBSBB	≥ 1100	≥ -16.9	350-1370	-14.2 - -17.5

Table A10. Experimental δ19F chemical shift values of HFB/CD assay

[DBSBB] (mM)	δ ^{19}F	[DBSBA] (mM)	δ ^{19}F
0.2	-163.184	0.2	-163.161
0.4	-163.163	0.4	-163.152
0.6	-163.137	0.6	-163.129
0.8	-163.113	0.8	-163.115
1.0	-163.084	1	-163.095
2.0	-162.962	2	-163.055
4.0	-162.754	4	-162.897
6.0	-162.617	6	-162.715
8.0	-162.514	8	-162.502
10.0	-162.439	10	-162.365
12.0	-162.384	12	-162.269
14.0	-162.338	14	-162.173
16.0	-162.297	16	-162.145
18.0	-162.295	18	-162.165
20.0	-162.304	20	-162.132

The experimentally determined chemical shift (single phase) for hexafluorobenzene in D_2O was δ ^{19}F = -163.2

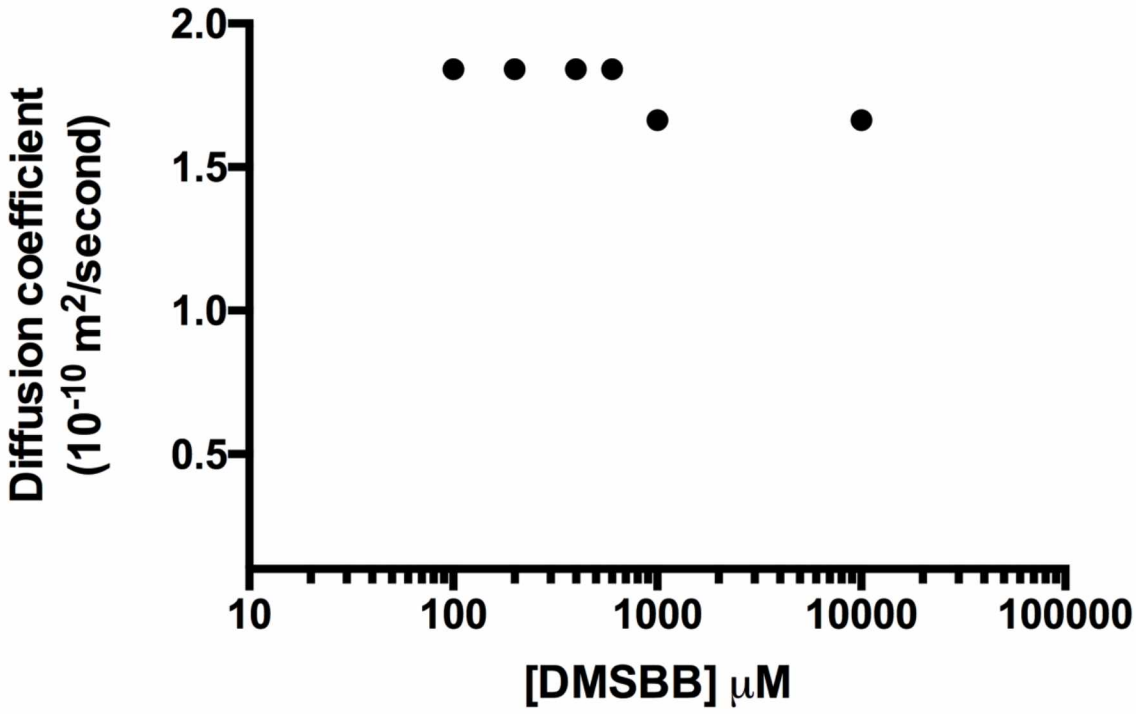

Figure A6. The observed diffusion coefficient, D_{obs}, as a function of DMSBM concentration. The consistency of the DMSBB diffusion coefficient, as determined by diffusion ordered NMR spectroscopy (DOSY) with respect to large concentration range is interpreted as an inability to form aggregates.

Profile Likelihood Method (PLM) for the treatment of ^{19}F NMR titration data of DBSBA and DBSBB.

Background

The Sanderson workbook, available online the website below, was used to determine binding constants for the HFB and DBSBA/DBSBB systems.

https://community.dur.ac.uk/j.m.sanderson/science/downloads.html

The workbook employs Microsoft Excel Solver and the following equilibrium for the Host and Guest for a 2:1 complex.

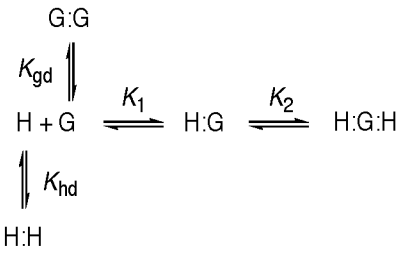

In the Sanderson treatment and in definitions in Reference 67, the Host concentration constant and the Guest concentration is varied. In our treatment, the [HFB] concentration is kept constant and therefore is the Host, with the Guest defined as DBSBA or DBSBB. Thus the 2:1 model (HHG) of Sanderson was employed. Also, in our treatment, dimer formation is not considered, i.e. both K_{gd} and $K_{hd} = 0$.

The following equations are used to calculate the 2:1 binding isotherm, with the calculations using DBSBA illustrated;

$$\Delta\boldsymbol{\delta}_{obs} = \left[\frac{\boldsymbol{K_1[G](\delta_{obs1} - \delta_{free}) + 2K_2[HG](\delta_{obs2} - \delta_{free}) + 2K_{hd}[H](\delta_{di} - \delta_{free'})}}{\boldsymbol{1 + K_1[G] + 2K_2[HG] + 2K_{hd}[H]}}\right] + \boldsymbol{\delta}_{free}$$

where relevant definitions are:

δ_{free} is the chemical shift of the free host in the titration; $^{19F}\delta$ of HFB in D_2O, set to a value of 0.

δ_{obs1} is the limiting complexation induced chemical shift change of the host in 1:1 complex; defined as the plateau of the $^{19F}\delta$ vs [CD] curve, with δ_{obs1} =1.09 for DBSBA.

δ_{obs2} is the limiting complexation induced chemical shift change of the host in 2:1 complex; defined as the plateau of the $^{19F}\delta$ vs [CD] curve, with δ_{obs2} =1.09 for DBSBA

$[H]_0$ and $[G]_0$ are the initial concentrations of the host and guest; $[H]_0 = [HFB]_0 = 0.0173$ M (constant) and $[G]_0 = [DBSBA]_0$ which varies from 0 to 0.020 M.

[H] and [G] are the concentrations of the free host and guest at equilibrium.

The concentrations of the complexes are calculated iteratively by solving the following equations (reproduced from the Sanderson workbook):

$$[\boldsymbol{HG}] = \frac{1+K_1\,([H]_0+[G]_0-3[H_2G]-2[H_2]-2[G_2])-\sqrt{\{1+K_1([H]_0+[G]_0-3[H_2G]-2[H_2]-2[G_2])\}^2-4K_1^2([G]_0-[H_2G]-2[G_2])([H]_0-2[H_2G]-2[H_2])}}{2K_1}$$

$$[\boldsymbol{H_2G}] = \frac{1+K_2\,([H]_0+2[G]_0-2[G]-[HG]-2[H_2])-4[G_2]\sqrt{\{1+K_2([H]_0+2[G]_0-2[G]-[HG]-2[H_2]-4[G_2])\}^2-8K_2^2([G]_0-[G]-2[G_2])([H]_0-[HG]-2[H_2])}}{4K_2}$$

The concentrations of free host and guest are calculated according to the concentration differences:

$$[H] = [H]_0 + [HG] + [HG_2] + 2[H_2]$$

$$[G] = [H]_0 + [HG] + 2[HG_2] + 2[G_2]$$

Illustration of Calculation.

To determine the optimized K_1 and K_2 binding constants for the [DBSBA] and [HFA] system, the spreadsheet was first optimized assuming a 1:1 system. The concentration of [HFB] was 0.0173 M. The [DBSBA] was entered directly under Conc. Guest on the spreadsheet. The Vol Guest, Vol Host, [G] stock are not used in the calculation, with numbers entered only as place holders (no dilution was performed). The results of the 1:1 iteration is shown on Figure 8. The resulting binding constant is on the order of $\sim 10^{10}$ and the fit is poor.

The 2:1 fit type was then conducted to give the results on Figure 8. A global minimum in ss residuals was obtained iteratively by imposing various constraints on K_1 and K_2 in the Solver parameters window under Tools. The global minimum ssr for DBSBA was 0.005338 with K_1 and K_2 for DBSBA of 570,000 and 770, respectively.

Once the minimum ssr was obtained, the ssr was multiplied by the constant = exp(χ^2(0.95, df=1/n) where n is the sample size and χ^2 is the value which defines the upper 5% of a χ^2 distribution with 1 degree of freedom, which is χ^2(0.95,df=1) = 3.841459. Thus the constant = exp(3.841459/n). Since n = 16 for DBSBA then constant = 1.271. Thus the cutoff ssr for DBSBA is (0.005338)x 1.271 = 0.006784.

The cutoff value ssr was then constrained in the Solver calculation with K_1 as constant value (*e.g.* 10000) and K_2 allowed to vary between a defined range (e.g. 300-900). See Figure 10 as an example. For a given value of K_1 there are two solutions for K_2, an upper and lower bound. These values then define the PLM curve (see Figure 10 in the manuscript)

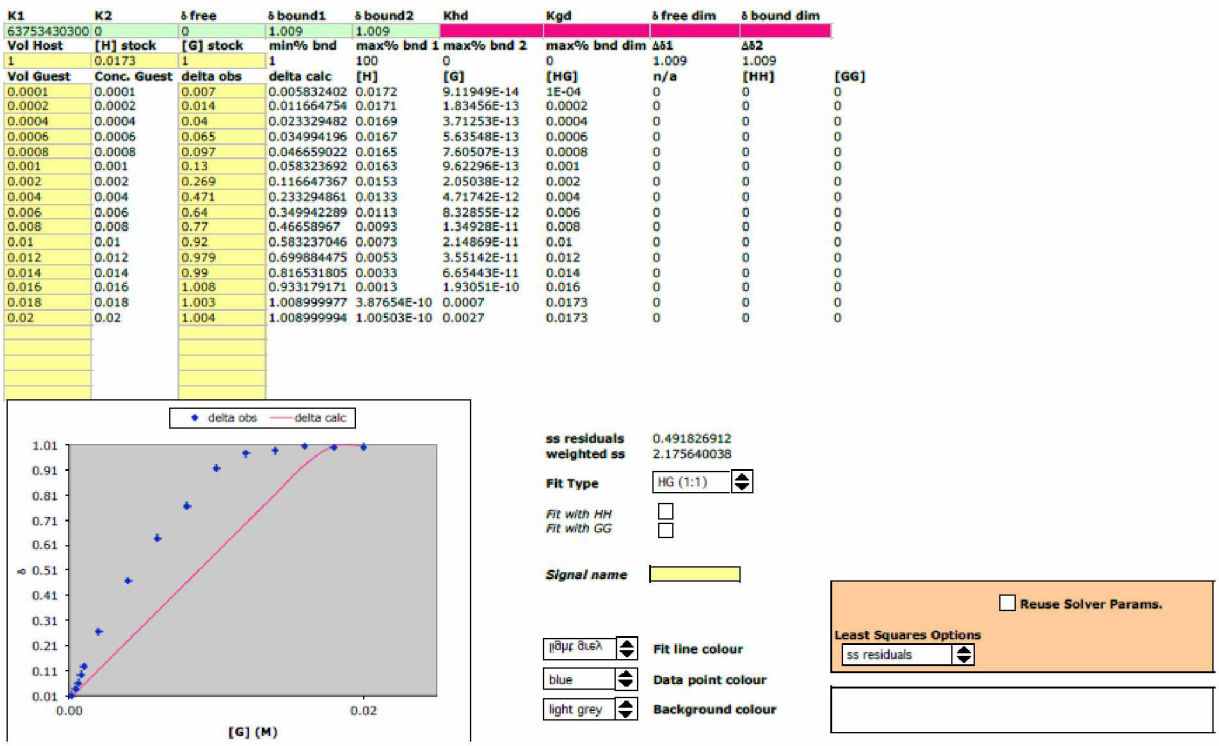

K1	K2	δ free	δ bound1	δ bound2	Khd	Kgd	δ free dim	δ bound dim	
63753430300	0	0	1.009	1.009					
Vol Host	[H] stock	[G] stock	min% bnd	max% bnd 1	max% bnd 2	max% bnd dim	Δδ1	Δδ2	
1	0.0173	1	1	100	0	0	1.009	1.009	
Vol Guest	Conc. Guest	delta obs	delta calc	[H]	[G]	[HG]	n/a	[HH]	[GG]
0.0001	0.0001	0.007	0.005832402	0.0172	9.11949E-14	1E-04	0	0	0
0.0002	0.0002	0.014	0.011664754	0.0171	1.83456E-13	0.0002	0	0	0
0.0004	0.0004	0.04	0.023329482	0.0169	3.71253E-13	0.0004	0	0	0
0.0006	0.0006	0.065	0.034994196	0.0167	5.63548E-13	0.0006	0	0	0
0.0008	0.0008	0.097	0.046659022	0.0165	7.60507E-13	0.0008	0	0	0
0.001	0.001	0.13	0.058323692	0.0163	9.62296E-13	0.001	0	0	0
0.002	0.002	0.269	0.116647367	0.0153	2.05038E-12	0.002	0	0	0
0.004	0.004	0.471	0.233294861	0.0133	4.71742E-12	0.004	0	0	0
0.006	0.006	0.64	0.349942289	0.0113	8.32855E-12	0.006	0	0	0
0.008	0.008	0.77	0.46658967	0.0093	1.34928E-11	0.008	0	0	0
0.01	0.01	0.92	0.583237046	0.0073	2.14869E-11	0.01	0	0	0
0.012	0.012	0.979	0.699884475	0.0053	3.55142E-11	0.012	0	0	0
0.014	0.014	0.99	0.816531805	0.0033	6.65443E-11	0.014	0	0	0
0.016	0.016	1.008	0.933179171	0.0013	1.93051E-10	0.016	0	0	0
0.018	0.018	1.003	1.008999977	3.87654E-10	0.0007	0.0173	0	0	0
0.02	0.02	1.004	1.008999994	1.00503E-10	0.0027	0.0173	0	0	0

Figure A7. Curve fitting of HFB:DBSBA titration using 1:1 complexation model.

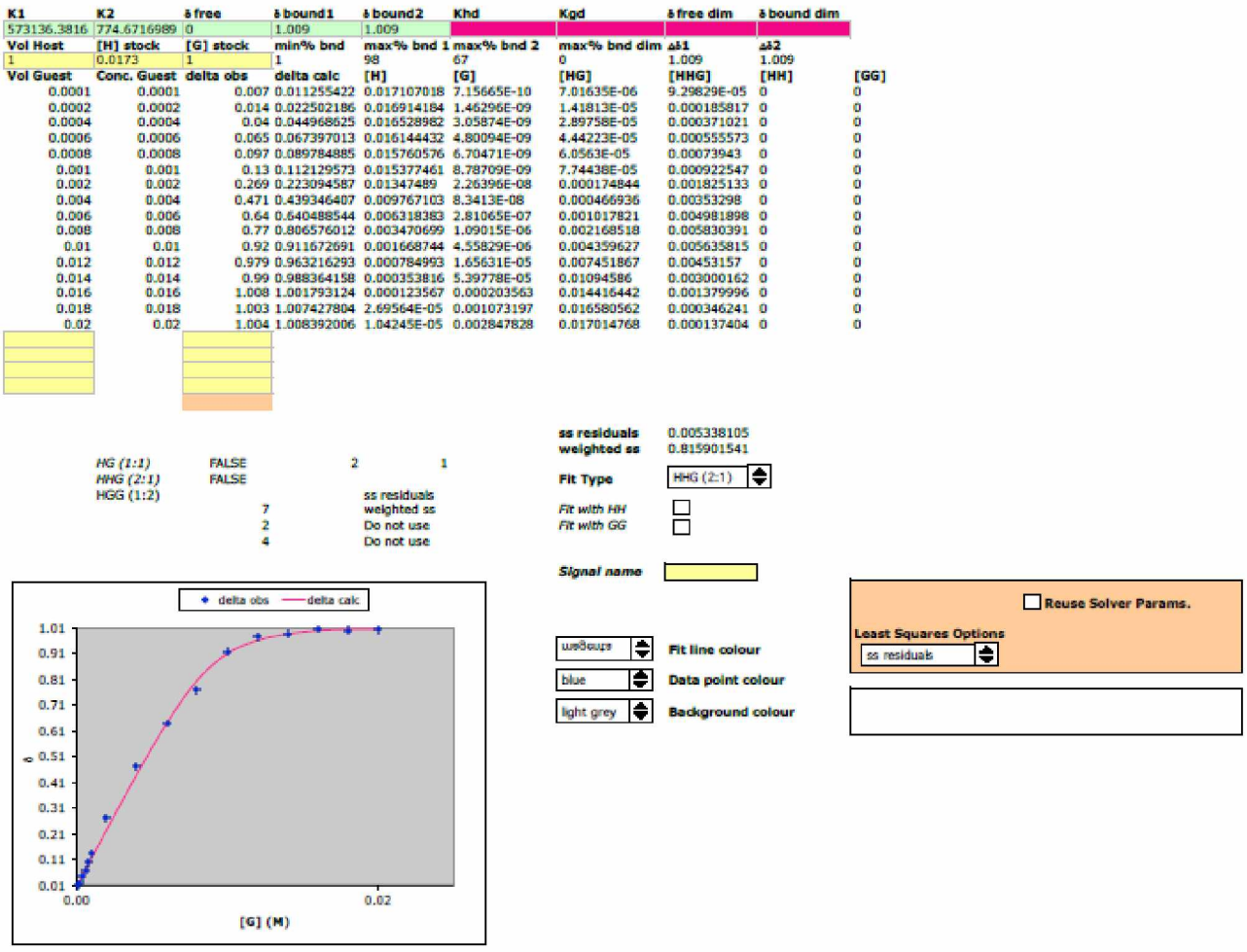

Figure A8. Curve fitting of HFB:DBSBA titration using 2:1 complexation model.

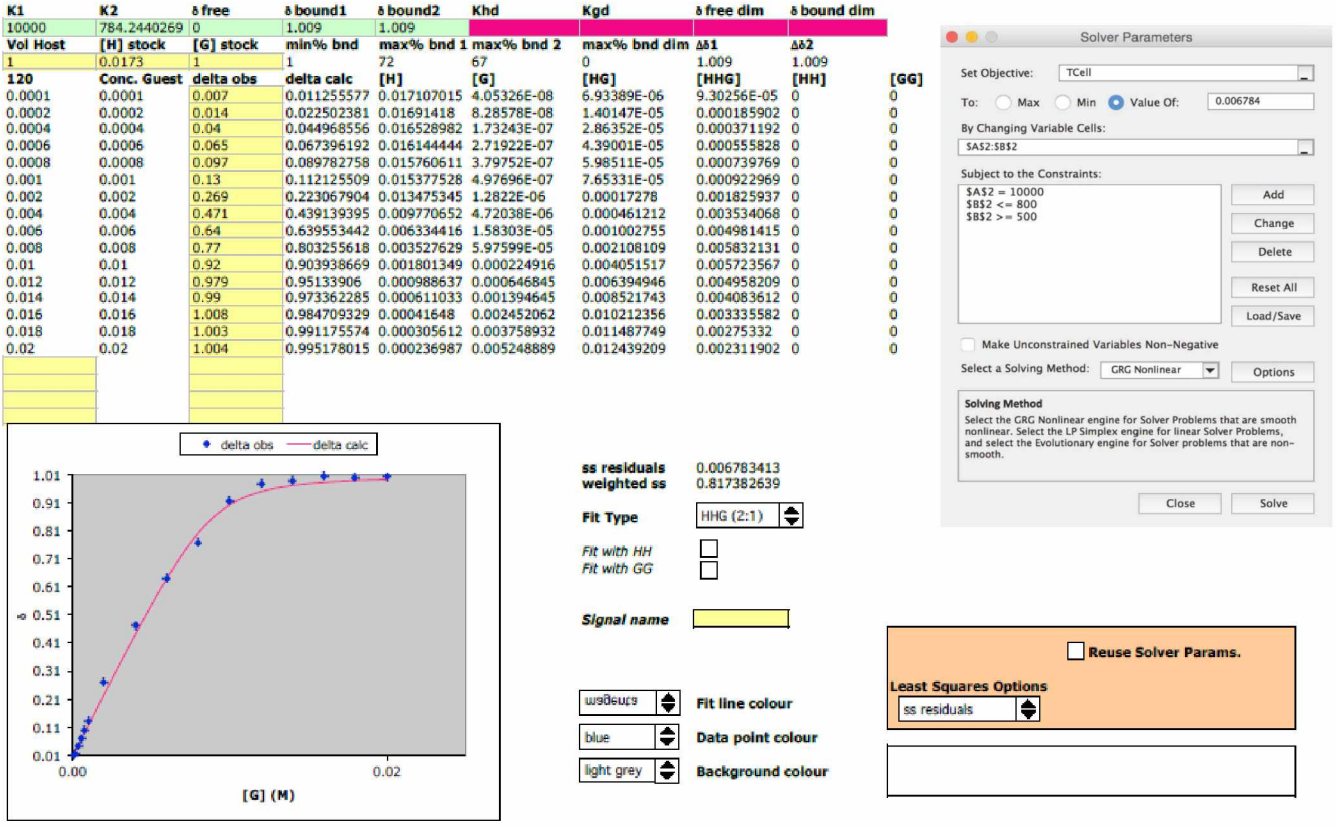

Figure A9. Curve fitting of HFB:DBSBA titration using 2:1 complexation model. The value of ss residuals was constrained to minimum of 0.005338 x constant where constant = exp(χ^2(0.95, df=1/n) where n is the sample size and χ^2 is the value which defines the upper 5% of a χ^2 distribution with 1 degree of freedom, which is χ^2(0.95,df=1) = 3.841459. Constant = exp(3.841459/16) = 1.27.

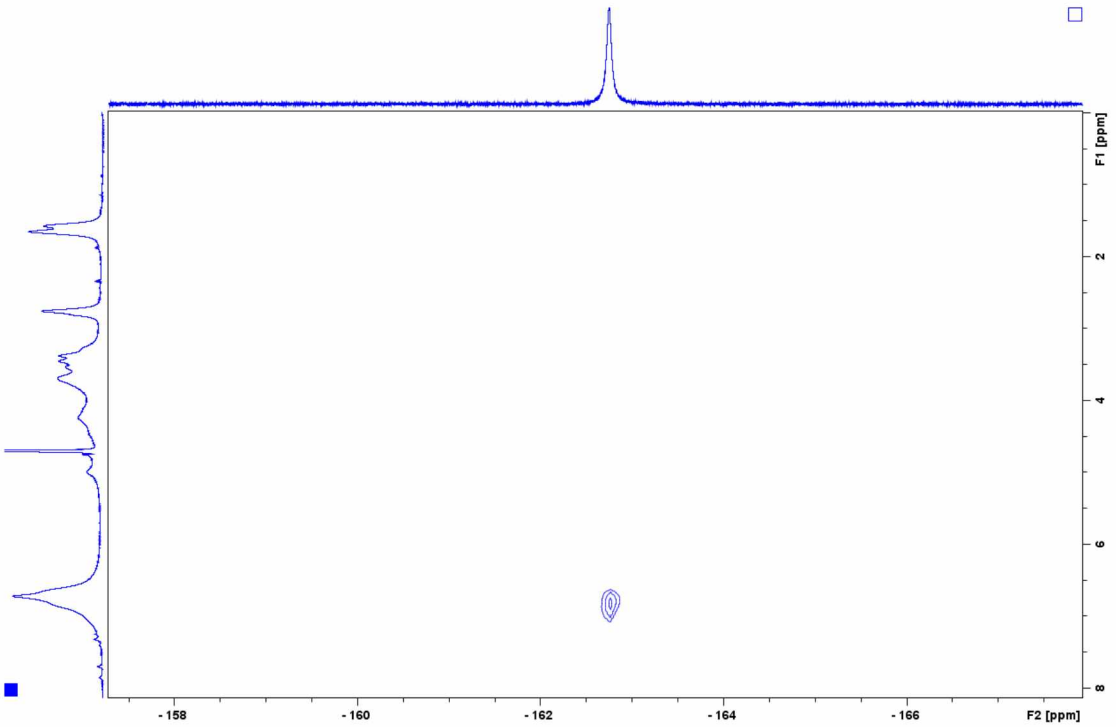

Figure A10. ^{19}F-^{1}H HOESY spectrum of 1:3 DBSBB:HFB mixture in D_2O. Recycle delay: 5 s, Mixing time: 200 ms.

Determination of Krafft Temperature.

The behavior of solvated amphiphilic molecules is a function of the solution temperature. The Krafft temperature is the temperature at which ionic surfactant solubility increases to the point at which micelle formation becomes possible. Solutions of DBSBA and DBSBB were examined over a temperature range between 0 and 50 °C where no precipitation was observed. The Krafft temperature is therefore considered to occur below 0 °C.

Chapter 4. Quantitative Physisorption of Heptakis (2,3-*O*-dibenzyl-6-*O*-sulfobutyl) Cyclomaltoheptaose on Polystyrene Nanoparticles by Emulsion Polymerization[1]

4.1 Introduction

Cyclodextrins (CDs) are macrocyclic oligosaccharides composed of glucosidic units using 1-4 α linkages. CDs are synthesized from starch using glucosyl transferases and have well defined structural and physical characteristics.[1] It is well known that CDs form inclusion complexes with hydrophobic molecules.[2-4] Chemical modification of CDs is well established in the literature; a common purpose of modification is to graft functional groups that perturb guest/host equilibrium complexation. CDs can also be modified to not only change their interactions with other molecules, but to interact with themselves; CDs with hydrophobic moieties have been shown to self-aggregate.[5-8] "Medusa-like" CDs possess long alkyl (or hydrophobic) substituents on the primary hydroxyl face while "skirt-shaped" CDs have these hydrophobic groups grafted to the secondary hydroxyls. Both of these amphiphilic CDs promote the formation of nanoparticles.[9,10] The hydrophobic anchors present the cyclodextrin hydroxyls, or modified polar substituent, at the surface of nanoparticles in aqueous solution. These cyclodextrins can also be thought of as nanoscaffolds due to their well-defined structures and the ability to derivatize its primary and secondary hydroxyls. They also possess a high degree of symmetry and two frames of different sizes on upper and lower rims.

Cyclodextrins, native and derivatized, have been previously used in emulsion polymerization recipes to stabilize emulsions[11], act as phase transfer agents[12], increase polymerization rates, and narrow particle size distributions (PSD)[13,14] even though they increase critical micelle

[1] James A. McKee, Thomas K. Green

concentration and surface tension while decreasing latex stability and PSD uniformity when they act in concert with surfactants.[15] Hydrophobic molecules favorably partition into the cyclodextrin interior when present in aqueous systems. Monomers used in emulsion polymerization recipes are typically sparingly soluble; increases in aqueous monomer concentration can accelerate polymerization rate and promote narrow particle size distributions. [13,14,16,17] CDs can solubilize agents that are too hydrophobic for fast homogeneous transfer to the growing polymer particles. CDs are effective for polymerizations of monomers that have different aqueous solubilities. Common techniques in which CDs are used as additives to influence the surface chemistry of polystyrene include click chemistry,[16,17] atom transfer radical polymerization (ATRP)[18] reversible addition-fragmentation transfer (RAFT),[19,20] and the formation of powder coat resins.[21] CDs have been included in polymers themselves, often as hydrogels, in which native or modified CDs act as hosts for drug delivery, polymerization loci, or a means of supramolecular stabilization of polymeric structure. [22-25] Surfactants (or other amphiphilic species) are typically required to stabilize colloidal suspensions; they illustrate a strong tendency to adsorb onto hydrophobic particle surfaces and in doing so, alleviate the interfacial tension between the hydrophobe and the aqueous medium. CDs conventionally are used to form stronger interactions with surfactants than the propensity of surfactants to self-aggregate; CD/surfactant complexes hinder aggregation and increase critical micelle concentrations.[15,26] Modified CDs that act as surfactants, not as additives, for use in emulsion polymerization have not been investigated in the literature to our knowledge.

We have found that heptakis (2,3-*O*-dibenzyl-6-*O*-sulfobutyl) cyclomaltoheptaose (DBSBB, Figure 1) forms micelles with a critical micelle concentration of ~100 μM. [27,28] The purpose of this research is to use batch emulsion polymerization as a means to place substituents,

grafted to the primary rim of cyclodextrins (DBSBB), on the surface of polystyrene (PS) with a nearly monodispersed particle sized distribution. We postulated that strong π-π interactions between benzyl substituents and the aromatic rings of polystyrene should provide a strong anchor for these nanoscaffolds to adhere to the nanoparticle surface without the complexities of chemical modification. Moreover, the ability to modify the primary face of the cyclodextrin with ionic or non-ionic functional groups would allow the future tailoring of the polystyrene surface for desired properties. The sulfonates moieties were chosen to produce anionic surfactants that are robust with respect to pH and ease of synthesis.

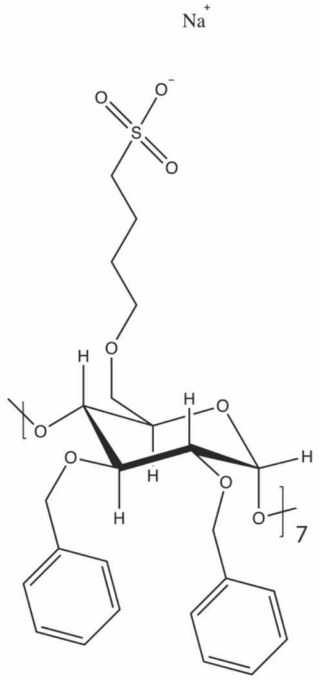

Figure 1. Structure of heptakis (2,3-*O*-dibenzyl-6-*O*-sulfobutyl) cyclomaltoheptaose sodium salt (DBSBB).

We report here the emulsion polymerization of styrene in the presence of DBSBB as surfactant. The resulting DBSBB-PS nanoparticles were found to be monodisperse in the range of 70-100

nm, which depended on DBSBB concentration. More significantly, we found that DBSBB is quantitatively bound to the surface of the nanoparticle, consistent with strong π-π interactions between DBSBB and the polystyrene surface. Surface coverage of DBSBB on the DBSBB-PS nanoparticles increased with surfactant concentration as determined by conductivity. Surface sulfobutyl groups of DBSBB were observable by liquid-phase ^{1}H NMR spectroscopy.

4.2 Experimental

4.2.1. Materials. Sodium dodecyl sulfate, potassium persulfate, sodium bicarbonate were used as received. ASTM (American Society for Testing and Materials) Type I water (18.0 MΩ·cm resistivity) was deoxygenated via argon purge for all solution and latex preparations. 4-tert-butyl catechol, a free radical inhibitor, was removed from styrene by washing with aqueous NaOH. The styrene was dried with anhydrous magnesium sulfate, and purified using column chromatography. Divinylbenzene (80%) was purified in the same manner. Styrene and divinylbenzene were stored under argon at -20°C until use.

4.2.2. Emulsion Polymerization. Batch emulsion polymerizations were performed in a three-neck round bottom flask under argon atmosphere using a magnetic stirrer at 1100 rpm. All aqueous solutions were prepared with Milli-Q water that was purged with argon bubbler for at least 90 minutes. Additions were allowed to dissolve before the next addition was made. Sodium bicarbonate was added as a buffering agent. The styrene/divinylbenzene was mixed and purged with argon for 20 minutes before addition. Potassium persulfate initiator was added last and allowed to stir for 20 minutes at 1100 rpm. The vessel was placed in a thermostated bath and allowed to come to 80°C during a two hour period. The reaction was heated for 8 hours to ensure completion, allowed to cool, and then filtered through glass wool.[29] Latex was diluted 100 times (v/v) and ultrafiltered until the filtrate had a conductivity of < 5 μS/cm. The recipes for each

latex are summarized in Table 1. All latexes used 10 mL H_2O, 5 mg of sodium bicarbonate, 10 mg of potassium persulfate, 1.8 g of styrene and 0.2 g of divinylbenzene. The naming convention of the sample arises from the multiplicative factor of the surfactant CMC used in the recipe (*e.g.* CD_25X recipe used 2.5 mM of DBSBB or 25 times the CMC of 100 μM).

Table 1. Emulsion Polymerization Recipe for DBSBB and SDS.

Name	Mass emulsifier (mg)	Mass H_2O (g)
CD_5X	17.5	10.0
CD_10X	35.0	10.0
CD_15X	52.5	10.0
CD_20X	70.0	10.0
CD_25X	87.5	10.0
SDS_10X	288.4	10.0
SDS_20X	576.7	10.0

After reaction, the suspension was passed through glass wool. Removal of low molecular salts was then accomplished by ultrafiltration in a 400 mL Amicon ultrafiltration cell with a 1000 MWCO RC (regenerated cellulose) membrane at 60 psi N_2 pressure until the filtrate was </5 μS/cm conductance. This membrane is sufficient for the SDS to pass through, but not DBSBB (MW = 3500 g/mol). In order to determine if any free DBSBB surfactant existed in the aqueous phase of the latex, the CD_25X latex samples were centrifuged in triplicate (10,000 rpm, 20 minutes) and the supernatants were then passed through a 100,000 MWCO polyethersulfone (PES) filter. The filtrate was collected, dried, dissolved in d_6-DMSO, and examined for free DBSBB using NMR spectroscopy. There was no evidence of the DBSBB

resonances in the filtrate during these investigations, indicative of quantitative physisorption of DBSBB by the polystyrene DBSBB-PS nanoparticles (Supporting Information).

4.2.3. Molecular Dynamics. All molecular dynamics (MD) calculations were performed using Desmond (Desmond Molecular Dynamics System, version 4.3, D.E. Shaw Research, New York, NY, 2015; Maestro 10.3.014, Schrodinger 2015-3). DBSBB structure was solvated in 74949 $Å^3$ box, 7065 atoms. 2216 molecules (DBSBB, 7 Na^+, and 2208 water molecules) using a TIP3P solvent model, minimized using a Berendsenn NPT simulation, using OPLS-2005 force field. Simulation time of 20 nanoseconds, with a recording interval energy of 1.2 ps and a trajectory of 4.8 was used. The simulation was performed with an NPT ensemble class, at 300.0 K (Nose-Hoover chain thermostat) and a pressure of 1.01325 bar (Barostat Martyna-Tobias-Klein) with 2.0 ps relaxation time. Equations of motions were integrated using RESPA integrator with a bonded time step of 2 femtoseconds (fs), while near and far bonded time steps of 2 and 6 fs, respectively. Coulombic interactions were subject to a short range cutoff of 9.0 Å. MD calculations were boosted using NVIDIA GeForce GTX 650Ti Boost graphic processing unit (GPU) on Centos 3.1 Linux platform.

4.2.4. Conductance Measurements. Surface charge densities were determined via conductivity titration. 20 μL aliquots of 1.4 mM NaOH were added to 1% (v/v) latex under argon. NaOH solutions were purged with argon and standardized using KHP. The polystyrene latex was cleaned using a modified procedure used by Vanderhoff.[30] The diluted latex was ultrafiltered, ion exchanged by addition of an equal volume of 1 mM HCl, stirred overnight, ultrafiltered again, then purged with argon. Conductivity of filtrate was < 5 μS/cm at each step before proceeding to ensure removal of solution anion. Conductivity measurements were performed using VWR sympHony Four Cell Conductivity Probe (cell constant = 0.9 cm^{-1}). All

conductivity titrations were performed in triplicate.

4.2.5. Scanning Electron Microscopy (SEM). SEM images were recorded on JEOL JXA-8539F Electron Microprobe with an accelerating voltage of 25.0 kV. Samples were ultrafiltered to remove excess salts, diluted 1000 X, then placed on a glass slide and allowed to dry. The average number diameter (D_n) was obtained by measuring the diameters of at least 100 particles in the SEM images and calculated using the following equation, where the n_i is number of particles with diameter of D_i:

$$D_n = \frac{\sum n_i D_i}{\sum n_i} \qquad (1)$$

4.2.6. Dynamic Light Scattering and Zeta Potential. Dynamic light scattering (DLS) was used to determine the particle size distribution and polydispersity of the polystyrene latexes. Particle size distribution (PSD) and zeta potential measurements were performed sequentially on a Brookhaven Zeta Plus 90 Zeta Potential Analyzer with a 35 mW red diode laser, 660 nm, 90 degree scattering angle. Ten measurements were performed and averaged. All latexes were diluted until consistent diameters were observed. All dilutions were made with 10^{-4} M NaCl using ASTM water, filtered through a 0.2 micrometer filter and placed into a triply rinsed cuvette. All sample measurements were performed at room temperature (22.0 ± 0.5°C).

4.2.7. NMR. All NMR experiments were performed on a Bruker Advance 600 MHz BBO NMR spectrometer using Topspin 3.2 software. The temperature of the probe was determined to be 22.3 ± 0.1 °C using the difference in chemical shift between the hydroxyl and methyl groups in methanol.[31] Latexes were diluted to 20 mg/mL using D_2O. An external standard (TSP) in a sealed capillary tube containing 1.5 mg in 2.18 mL of D_2O (4 mM) was

added to the NMR tube containing the latex. A noesygppr1d water suppression pulse sequence was used, with 2048 scans, 18K spectral width, dwell time of 28 μsec, and an acquisition time of 1.8 sec. Latex filtrate for SDS and DBSBB after centrifugation was dried then dissolved using d_6-DMSO or D_2O for NMR investigations using a zg30 pulse sequence, 64 scans, 12K spectral width, dwell time of 41.6 μsec, and an acquisition time of 2.7 seconds.

4.3 Results and Discussion

4.3.1. Hydrophilic – Lipophilic Balance (HLB) of DBSBB.

In this work, we examined the possibility of physically grafting heptakis (2,3-dibenzyl-6-O-sulfobutyl) cyclomaltoheptaose (DBSBB) surfactants onto crosslinked polystyrene using a batch emulsion polymerization technique. The batch polymerization technique allows a simple means of nanoparticle synthesis. DBSBB has been previously shown to form micelles with a CMC of 100 μM.[27] The emulsion polymerization technique uses micelles as the loci for polymerization in aqueous solvent, but not all amphiphiles are suitable for this purpose. The suitability of DBSBB as an emulsification agent was determined using experiment and theory. Ionic surfactants aid the process of emulsification through reduction of interfacial tension between the hydrophobe and the aqueous medium while stabilizing the dispersed colloids via repulsion of electric double layer forces and/or steric stabilization from entropic considerations.[32] Calculation of the hydrophilic-lipophilic balance (HLB) of DBSBB was performed to determine the suitability of the surfactant to stabilize an emulsion and thereby foster the formation of monodisperse polystyrene latex particles. Bancroft's rule states that the continuous phase of an emulsion will be the phase in which the emulsifier is preferentially soluble (*i.e.* hydrophilic surfactants produce oil-in-water (O/W) emulsions while hydrophobic (non-water soluble) tend to make water-in-oil (W/O) emulsions).[33] Surfactants with greater hydrophilic contributions in their structure promote O/W

emulsions while those that are less water soluble tend to stabilize W/O emulsions (circumstances permitting). The structural balance in surfactants between hydrophilic and hydrophobic components (HLB) was first quantified by Griffin.[34] It is a semi-empirical approach to classify surfactants, based on the hydrophilic and hydrophobic components in their molecular structure, by suitable potential application. HLB ranges are typically from 0 to 20; low HLB means hydrophobic surfactant while higher HLB represent a hydrophilic surfactant. Surfactants that fall within a HLB range of 8-18 are useful for stabilizing oil-in-water (O/W) emulsions, like those particle loci that are found in emulsion polymerization. The HLB of DBSBB was calculated from a method previously used by Abdelwahed *et al.* [35], itself a modification of Griffin[34], to calculate HLBs of amphiphilic β-cyclodextrins. (Equation 2)

$$HLB = \frac{MW_{hydrophilic}/MW_{CD}}{5} X\ 100 \qquad (2)$$

where $MW_{hydrophilic}$ is the molar mass of the hydrophilic components of DBSBB (i.e. the cyclodextrin torus and the sulfonates) and MW_{CD} is total molar mass of DBSBB. The HLB of DBSBB equates to a value of 10.0 which indicates that DBSBB has excellent detergent properties and a good candidate to support an oil/water emulsion.[35,36] Surfactants with an HLB in the range of 8-18 have been found to be sufficient for the stabilization of particle nuclei in the 1st stage of emulsion polymerization.

4.3.2. Calculation of Particle Diameter Using SEM and DLS methods. Characterization of latex particles using Scanning Electron Microscopy (SEM) provides the most direct information, through observation, about particle morphology and polydispersity. It is useful for data validation of other particle sizing techniques, although SEM particle dimensions tend to be smaller due to solvent removal required for preparation.[37] The diameters of 150 particles of

CD_25X were recorded from the (SEM) photograph in Figure 3a. The DBSBB-PS nanoparticles were calculated to have a mean diameter of 48.4 ±10.2 nm producing a polydispersity of 0.044, making it a nearly monodisperse latex. The polydispersity index (PDI) is a metric that illustrates the width of the particle size distribution.

$$PDI = \left(\frac{\sigma}{d}\right)^2 \qquad (3)$$

where σ is the standard deviation and d is the mean diameter of the particles. A PDI of less than 0.1 is considered monodisperse.

Dynamic light scattering (DLS), in contrast, produces particle dimension data that are larger than the actual size, the hydrodynamic diameter, due to the presence of aqueous solvation shells. Hydrodynamic particle data generated from DLS is a statistical distribution, rather than individual particles (SEM).[38] The z-average diameter (mean intensity hydrodynamic diameter) and the polydispersity index are calculated using DLS.[39]

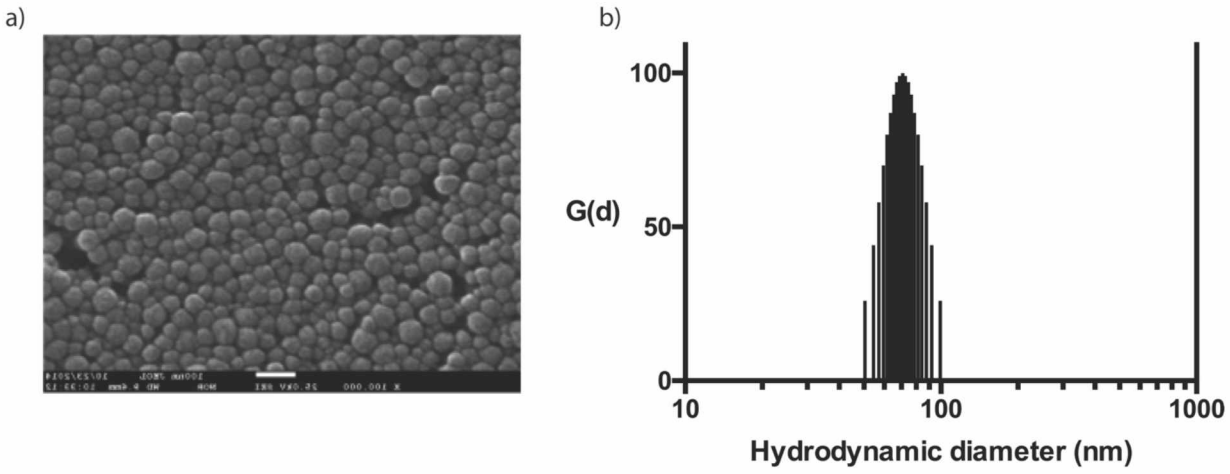

Figure 2. a) SEM of CD_25X (white bar represents 100 nm); b) The monomodal distribution of CD_25X hydrodynamic diameter.

Particle counting techniques produce a number size distribution where DLS calculates its particle size using an intensity size distribution. The nature of data acquisition in DLS produces an intensity size distribution, whereas counting and measuring of particles from SEM requires a number distribution. DLS particle size data was converted into a number size distribution and compared to SEM data (Table 2). Dynamic light scattering studies also found the CD_25X latex to be monodisperse and in the size regime of PS nanoparticles.[40] Particle size data for CD_25X latex is consistent in diameter and monodispersity, given the inherent benefits and flaws in the SEM and DLS techniques. The complementary nature of DLS and SEM methods illustrate that CD_25X latex is composed of nearly monodisperse latex spheres with particle diameter of approximately 70 nm.

Table 2. Comparison of SEM and DLS particle size distributions of CD_25X

Technique	Distribution	Diameter (nm)	Standard deviation	Standard error	PDI
SEM	number	48.4	10.2	0.84	0.044
DLS	number	63.7	7.9	1.88	0.015
DLS	intensity	70.8	8.5	1.80	0.043

4.3.3. Determination of Surface Charge Density. All electrostatically stabilized latex particles possess charged functional groups that are bound to the polystyrene. Surface charge density is difficult to measure directly; measurement of concentration of monovalent counterion in deionized latex is used instead.[41] The estimation of surface charge is a necessary part of latex characterization, quantified by the surface charge density. Under the governing assumption that the latex particles are spherical and uniform, the following formula can be used to calculate the

surface charge density of each latex at different concentrations of surfactant. The surface charge density (σ_0) is defined as:

$$\sigma_0 = \nu e N_s \qquad (4)$$

N_s is the number of charged sites per unit area, e is the electrostatic charge on each charged site (*e.g.* the charge of an electron), and ν is the charge magnitude. The specific surface area (SSA), the area to mass ratio, is the total surface area of 1 gram of polymer nanospheres.

$$SSA = \frac{\pi D^2}{\frac{\pi}{6} D^3 \rho} = \frac{6}{D\rho} \qquad (5)$$

where D is the diameter of the nanoparticle and σ is the density of polystyrene (1.055 g/cm^3).

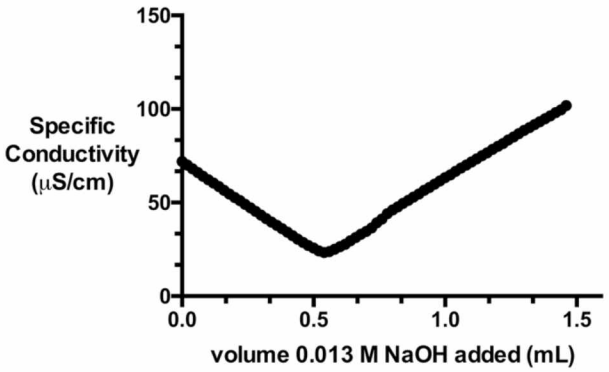

Figure 3. Conductivity titration curve for CD_25X. Illustration of only strong electrolytes present. Single nadir of curve occurs where all of strongly acidic sulfonate sites on latex have been neutralized by added base. Calculation of surface charge density of CD_25X is the function of number of moles of NaOH used to reach the nadir of the curve, mass of latex used in titration, and hydrodynamic radius of nanoparticle.

Conductivity titrations were performed on the all latexes to determine their surface charge density. The titration curve for the CD_25X (2.5 mM DBSBB) latex is shown in Figure 3. The equivalence point was taken to be the nadir of the titration curve. The knowledge of moles of base added plus the diameter of polystyrene nanoparticle allows surface charge density to be calculated.[42,43] The acidity of sulfonate groups (pKa ~ -2) dictates these groups are the sodium salts of a strong acid at circumneutral pH. The presence of the salts of strong acid are displayed in the conductivity titration curve from the lack of discontinuity past the equivalence point. The sulfur of the sulfonate group is directly attached to a carbon atom but the sulfate sulfur is attached via an oxygen bridge; the sulfate moiety is typically more susceptible to hydrolysis and subsequently converted to carboxyl from aqueous carbonate.

The area occupied per unit of charge, via conductivity titration, was calculated by determining the number of moles of charge per gram of polystyrene latex (dry weight). These values, divided by the specific surface area of the latex, allowed the area occupied by a single charge to be obtained. The CD has been shown to be a single isomer; every CD has 7 sulfonate anions.[27] The area of latex surface associated with a single CD can therefore be calculated by simply multiplying the single charge surface area by seven. The calculated surface charge density of CD_25X was determined to be 27.27 ± 1.24 $\mu S/cm^2$. A particle diameter of 70.8 nm from DLS measurements provides the surface area occupied by one DBSBB to be 408 ± 19 $Å^2$. This surface area is larger than that determined for the cross-sectional area of the DBSBB molecule of 235 $Å^2$ by molecular modeling (*vide infra*).

4.3.4. NMR of Latex of Particles.

4.3.4.1. Evidence of Surface Sulfobutyl Groups. NMR is spectroscopic technique that is sensitive to molecular motion because the rates of relaxation are highly dependent on the

environment of nuclei.[44] It is well known that polymer chains do not exhibit significant translational and rotational motion due to intermolecular forces below glass transition temperature and have faster rate of relaxation.[45,46] Liquid NMR experiments can be useful in the acquisition of quantitative information concerning the physical state of DBSBB-PS nanoparticles.[47,48] Changes in linewidth and signal broadening, due to changes in relaxation time upon immobilization to larger polymeric structures, have been shown to be indicative of both the immotile and more dynamic domains of a given macromolecule. Enhanced signal broadening of one fragment while the signals of another fragment remain relatively unchanged, with respect to the free molecule, indicate the former section has restricted mobility while the latter possesses a higher degree of molecular motion. In this way, NMR is a valuable tool for the assignment of grafting loci with a molecule and confirmation of modifications. Quantification of grafting density of ligands upon nanoparticle surfaces can be obtained from the integration of ^{1}H nuclei, an internal standard, and knowledge of total surface area.[47]

Polymers are subject to many complex intra- and intermolecular interactions. The most prominent spin interactions between nuclei in polymers is dipolar coupling. Decreased molecular mobility leads to increasing line widths. In this slow motion limit, the observed resonances are very broad and undetectable without special probes. Conversely, chain segments that operate in the fast motion limit, that exhibit chain end dynamics, are easily observable by conventional NMR techniques.[49] Therefore, we could potentially observe the ends of chains that have different molecular motions than the points from which they originate, provided the anchor exhibits significantly slower motion than the chain (*i.e.* the chain is faster than the block). Figure 4 shows ^{1}H NMR spectra of DBSBB-PS prepared with DBSBB (CD_25X, upper spectrum) and DBSBB (lower spectrum) in D_2O. The hydrogens on the sulfobutyl groups are labeled H-1

through H-4. All of the proton assignments of DBSBB were performed from the analysis of ^{1}H, ^{13}C, COSY and HMQC NMR spectra in d_6-DMSO.[27] Resonances that were broader in D_2O, due to relaxation effects from aggregation, were sharper in d_6-DMSO and facilitated assignments. The H-1 protons (OCH_2) of the sulfobutyl group are diastereotopic and distinguishable due to their close proximity to the chiral D-glucose unit, and appear as two broad singlets. The ^{1}H NMR spectrum of CD_25X latex shows resonances attributed to H-1 through H-4, but the resonances of the CD torus are not visible. The H-1 protons of the sulfobutyl group in the latex sample also appear as diastereotopic, Furthermore, the H-2 protons of the sulfobutyl group in the latex appear as diastereotopic, which is not revealed in the solution spectrum of DBSBB. These two spectra, taken together, indicate that the CD torus motion must be restricted by physisorption to polystyrene, but the sulfobutyl group is not restricted and possesses solution-like NMR behavior. The sulfobutyl groups are thus on the surface of the latex particle and not imbedded in the polystyrene particle.

4.3.4.2. Quantitation of Surface Sulfobutyl Groups by NMR. An external standard (trimethylsilyl propanoic acid, TSP) in sealed capillary tube was added to CD_25X latex that had been diluted with D_2O. The use of an external standard allows for a nondestructive and accurate measurement of detectable proton resonance concentration in the latex sample. The concentration of these resonances was determined using Equation 6.

$$C_X = \frac{\frac{I_X}{N_X} C_{TSP}}{\frac{I_{TSP}}{N_{TSP}}} \left(\frac{V_{TSP}}{V_{sample}} \right) \qquad (6)$$

where C_X is the concentration (mol/L) of butyl groups, I_X is the integration value of butyl protons of interest, N_X is the number of protons of interest (*i.e.* butyl, 8) from integration, C_{TSP} is the

concentration of trimethylsilyl propionate (TSP) in the internal standard (mol/L), I_{TSP} is the integration value of the TSP and N_{TSP} is the number of protons assigned to TSP (*i.e.* 9). The ratio of the volume of the sample to the volume of the TSP insert equals 10.04. The sum of the integration values of H-1 through H-4 resonances in Figure 4 and the concentration of TSP in the standard (4 mM) were entered into Equation 4 to yield C_x (mol/L).

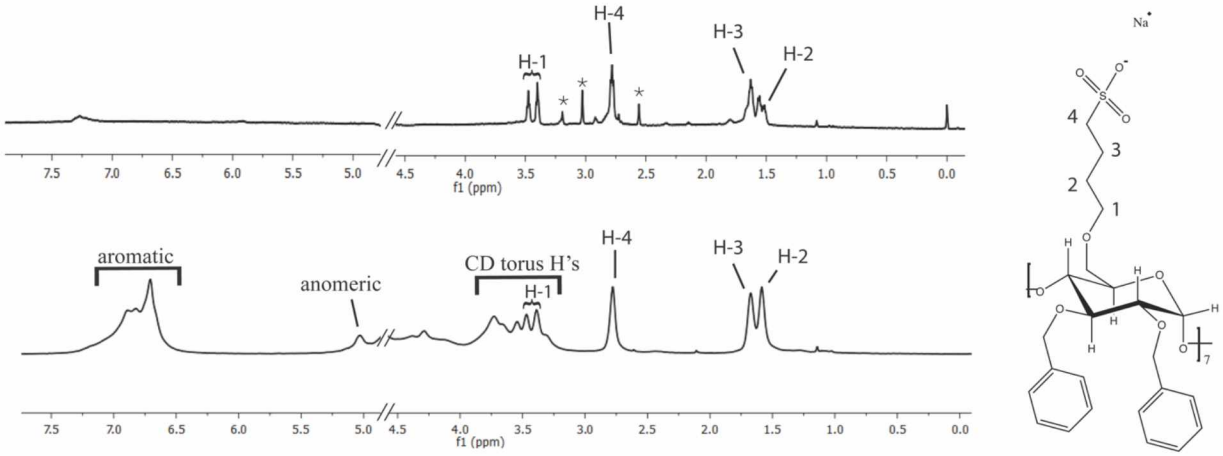

Figure 4. Comparison between ^{1}H NMR spectra of 10% dilution of CD_25X latex (v/v) (upper spectrum) and DBSBB (lower spectrum) in D_2O. Resonances marked with asterisks are unknown impurities.

The number of particles per liter of latex was calculated under the governing assumption that the latex particles are spherical, uniform, and smooth, by dividing the mass of the polymer (dry weight) per liter of latex by the mass of one DBSBB-PS nanoparticle.[50]

$$N_p = \frac{mass\ (g) latex\ per\ liter}{\frac{\pi}{6} D^3 \rho} \qquad (7)$$

where D is the hydrodynamic radius of the particle, obtained from DLS measurements, and σ is the density of polystyrene latex (1.055 g/cm^3). The mean surface area on the latex occupied by

one molecule of sorbent is a good metric for surface coverage and can be calculated by dividing the total number of moles of sorbent by the total surface area of the latex present in the sample of interest. One molecule of DBSBB therefore occupies 704 ± 18 $Å^2$ of surface area on the CD_25X latex sphere, given the moles of observed proton resonances, the number of sulfonated butyl chains (*i.e.* 7) per mole of DBSBB, and the total surface area of 70 nm latex spheres in the sample.

The calculation of surface charge density of the sulfonates of the sulfobutyl chains on the surface of the CD_25X latex particle allowed the calculation of the surface area per DBSBB to be determined. It is reasonable to assume that the number of surface-bound butyl groups should be approximately equal to the number of surface sulfonates, given they have a 1:1 stoichiometric relationship. Comparison between the areas required for one DBSBB on the surface of CD_25X as determined by conductive titration (408 ± 19 $Å^2$) and NMR integration (704 ± 18 $Å^2$) in Figure 5a finds they are in reasonable agreement given the fundamental differences in the analytical techniques. The qualitative observation of free butyl chains and absence of CD and aromatic resonances in the NMR spectra, and the reproducibility of the conductometric titration leads to the conclusion that DBSBB is adsorbed on the surface on CD_25X with existence of solvated sulfobutyl moieties projecting into solution.

4.3.5. Effect of Surfactant Concentration on Particle Size. Latex colloidal stability is a result of the balance between long range van der Waals attractions and much shorter ranged interparticle repulsions. Colloids with intrinsic surface charge are electrostatically stabilized against coagulation due to repulsive interactions that are greater than attractive van der Waals forces. The impact of these phenomena on colloidal dispersions is well known; electrostatically stabilized polystyrene latexes that possess greater surface charge densities and higher zeta

potentials demonstrate more colloidal stability against coagulation. [51,52] Ionized groups on the surface of particles dictate the charge density and the subsequent surface potential as a function of their presence, their concentration on the surface, and their degree of ionization. Charged particles are surrounded by an ionic corona; potential drops exponentially with distance from the particle. The zeta potential is the value of the potential on the periphery of the diffuse double layer; this measured potential can be used as a metric for the characterization of the electric double layer.[53] Calculation of surface charge density and measurement of zeta potentials provide not only measures of colloidal stability but an intuitive metric for the degree of ionic surfactant adsorption to latex particles. We determined the effect of the change in surfactant concentration on particle size, surface charge density, and zeta potential for several concentrations of DBSBB above the CMC. The amount of surfactant available for the stabilization of particle nuclei is an easily controllable parameter that affects the diameter of the latex.[36] To examine the surfactant concentration in particle size distribution and diameter, the amount of emulsifier (multiplicative factor of the critical micelle concentration) was varied while keeping all other reaction parameters constant. Table 3 illustrates the change in surface charge densities, zeta potentials, and particle diameter with the mass of DBSBB added in the recipe.

The comparison of the calculated surface charge density from conductivity titrations and the latex zeta potential with the hydrodynamic diameter of each DBSBB-PS nanoparticle in Table 3 illustrates the trends of increasing surface charge density and zeta potential of each latex particle with decreasing particle diameter. Surface charge densities from titration data often correlate only qualitatively with zeta potentials determined electrokinetically; surface charge densities are related to zeta potential but they are not synonymous. Their general correlation,

however, implies that the concentrations of ionized surface group are increasing as more DBSBB emulsifier is added to the recipe.

Table 3. Comparison of particle characteristics between DBSBB latexes and SDS latexes.

Name	Particle diameter (nm)	Surface charge density ($\mu S/cm^2$)	Zeta potential (mV)	Experimental Area per DBSBB ($Å^2$)	Theoretical Area per DBSBB ($Å^2$)
CD_5X	101.9 ± 0.6	2.97 ± 0.36	-38.9 ± 2.6	3714 ± 450	3707 ± 93
CD_10X	94.5 ± 0.5	7.11± 1.10	-42.0 ± 2.7	1506 ± 233	1999 ± 50
CD_15X	92 ± 1.3	12.0 ± 0.7	-43.7 ± 3.4	784 ± 48	1368 ± 34
CD_20X	73.2 ± 0.3	17.5 ± 4.6	-45.1 ± 2.6	668 ± 177	1290 ± 32
CD_25X	70.8 ± 0.5	27.3 ± 1.2	-50.0 ± 3.7	408 ± 19	1067 ± 27
SDS_10X	52.9 ± 1.2	1.66±0.15	-32.2 ± 1.6	-	-
SDS_20X	49.2 ± 0.4	7.71±0.40	-34.0 ± 3.0	-	-

Latex particles were also prepared using sodium dodecyl sulfate (SDS) as the surfactant. These studies were performed for the purpose of comparison to DBSBB prepared latex behavior. Examination of Table 3 shows that a doubling of SDS concentration (100 mM to 200 mM) in the recipe does not significantly change the latex particle diameter (- 7%) or its zeta potential (105 %). The surface charge density does increase, but given that an additional 288.4 mg (1 mmol) was added to the recipe, an increase in adsorbed surface charge could be expected. A doubling of the DBSBB concentration (1 mM to 2 mM), however does significantly affect the surface particle properties. The particle diameter decreases by 22.5%, surface charge density increases by 246%, and zeta potential by 107%. The large changes in surface properties between SDS and

DBSBB are dissimilar especially given the amounts (an additional 35 mg or 10^{-2} mmol) or much smaller concentrations required to achieve those changes.

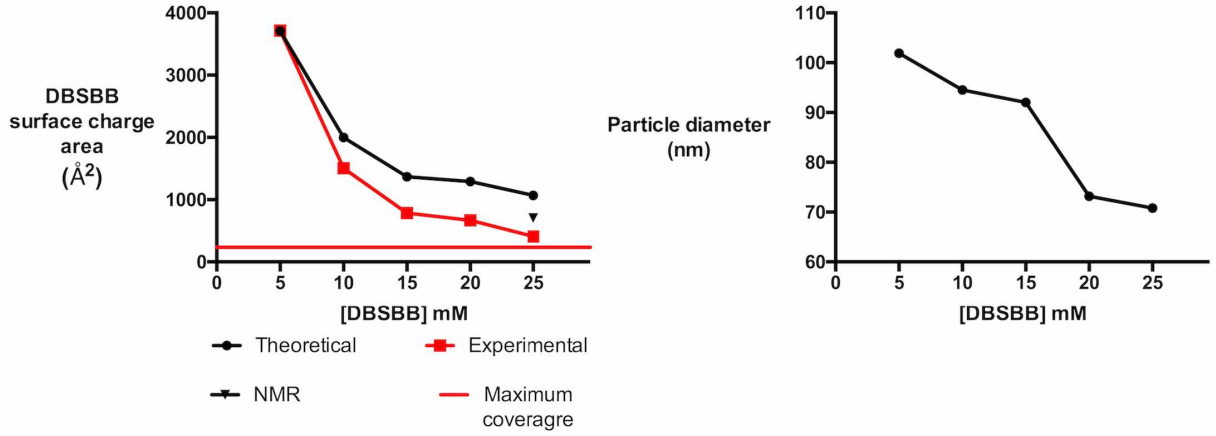

Figure 5a) The change in particle surface area associated with one DBSBB molecule as experimentally calculated from conductivity titration (red square) and its theoretical value (black circle) with increasing concentration of DBSBB in recipe. The particle surface area per DBSBB as determined from NMR titrations is included for CD_25X (black triangle). The red line is the cross sectional area of DBSBB, the theoretical maximum limit for surface coverage. b) The particle diameter with change in DBSBB recipe concentration.

The latex particle surface area occupied per DBSBB was plotted against the concentration of DBSBB in the polymerization recipe in Figure 5a. The latex particle surface area per DBSBB molecule was calculated using the number of DBSBB molecules in the recipe and the calculated total surface area of the latex in each sample. The experimentally determined area per DBSBB was derived from the surface charge density calculations while the theoretical value was calculated from the moles of DBSBB for a given recipe. Examination of Figure 5a illustrates that more DBSBB is adsorbing to the DBSBB-PS nanoparticle surface as more CD is added to the

recipe. A trend toward smaller surface areas allotted per DBSBB implies that total surface coverage of the latex by DBSBB is increasing. The theoretical surface area per DBSBB, the specific surface area (SSA) divided the number of DBSBB molecules, correlates well with the experimentally determined value. Additionally, the surface area per DBSBB molecule appears to asymptotically approach the theoretical minimum value of 235 Å (red line) associated with the cross-sectional area of DBSBB determined by MD simulation, suggesting that maximum coverage of the surface by DBSBB is approached with increasing DBSBB concentration in the recipe. Figure 5b demonstrates the decrease in hydrodynamic particle diameter with increasing CD. Consolidation of the information in Figures 6a and 6b elucidates that an increase in the concentration of DBSBB in the emulsion polymerization recipe results in a decrease in particle size while exhibiting an increase in DBSBB bound to the surface of the polystyrene nanoparticle.

4.3.6. Molecular Dynamics. The calculation of distance between sulfonates is not a static calculation but a dynamic one. The distance between sulfonate groups required for the calculation of the probable area occupied on the latex surface by one DBSBB (*i.e.* 7 sulfonates) should be based on the likely position of the sulfonates with respect to each other on the primary rim of the DBSBB. We chose to acquire this data through modelling the relative positions of the sulfobutyl arms with respect to each other using molecular dynamics. Molecular dynamics calculations were performed to obtain the mean diameter of the CD (*i.e.* the average distance between two sulfonates on opposite sides of the torus, a 1-4 configuration as seen in Figure 6a). The average diameter occupied by a single CD was calculated to be 17.3 Å, giving a cross-sectional area of 235 $Å^2$.

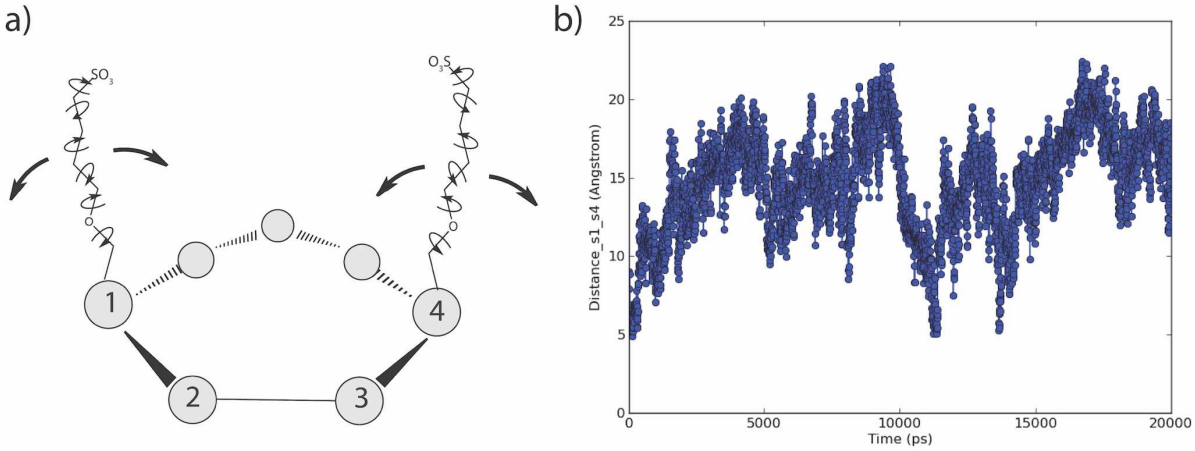

Figure 6a) Illustration of calculation of mean DBSBB diameter 1-4 glucose positioning. Intramolecular distances between sulfonates at 1-4 relationships were calculated using molecular dynamics (MD). The mean distance was calculated and used as the diameter. b) Variation of distance between intramolecular sulfonates with time. The mean distance, with subsequent ranges, were calculated from simulation over 20 nanosecond time interval.

4.3.7. Change in Number of Latex Particles with DBSBB Concentration. The relationship between DBSBB concentration and the subsequent number of latex particles was examined. Smith and Ewart investigated the kinetics of emulsion polymerization; increases in the surfactant concentration increased the number of polystyrene latex particles (N_p) at the expense of particle radius.[54] An increase in the concentration of surfactant also accelerates the rate of polymerization due to the larger number of micelles in solution. Smaller particle sizes correspond to larger numbers of particles while larger particle sizes correspond to smaller numbers of particles. The number of particles in solution, calculated from the particle size

distribution and the polymerization recipe, is dependent on the total concentration of surfactant in solution.[55]

$$N_p \propto [surfactant]^{0.6} \qquad (8)$$

A comparison between the calculated number of DBSBB-PS nanoparticles of each latex to the concentration of the DBSBB in the recipe should find a relationship approximating Equation 9, if the emulsion polymerization of styrene using DBSBB adheres to the Smith/Ewart kinetic theory. The logarithm of the molar concentration of cyclodextrin surfactant was plotted against the logarithm of the number of particles per liter of latex in Figure 7.

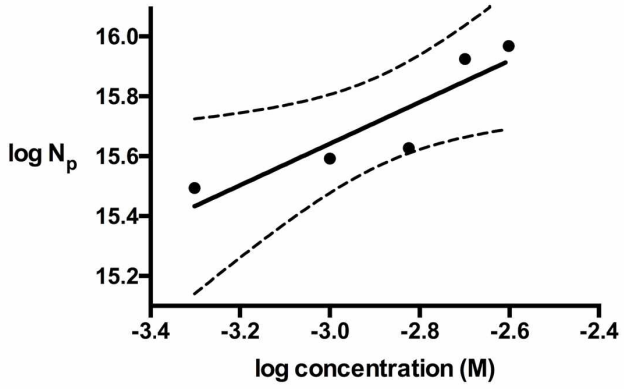

Figure 7. Log-log plot of surfactant concentration against number of latex particles in sample.

The slope of the log-log plot is 0.69 ± 0.19, is in general agreement with the predicted 0.6 predicted power dependence of surfactant concentration to the number of particles produced in emulsion polymerization theory. [55,56] The dashed lines are the 95% confidence interval. The positive slope is consistent with emulsion polymerization theory.[54] The deviation of the slope of the log-log plot in Figure 6 from a predicted 0.6 suggests that a degree of coagulative nucleation

occurred in addition to the micellar nucleation. Coagulative nucleation provides a more complex dependence of the number of particles on surfactant concentration, where the power dependence can range from 0.4 -1.2.[56]

4.4 Conclusion

The production of stable monodispersed DBSBB-PS nanoparticles was performed using batch emulsion polymerization and heptakis (2,3-dibenzyl-6-O-sulfobutyl) cyclomaltoheptaose (DBSBB) as a surfactant. The hydrodynamic diameters of these DBSBB-PS nanoparticles ranged from 70 to 100 nm. In each case, DBSBB quantitatively sorbed to the surface, possibly due to π-π interactions and/or entanglements with polystyrene polymer chains. The hydrophobic cavity of the cyclodextrin, however, is most likely occupied by styrene or polystyrene and unable to encapsulate other hydrophobic molecules. DBSBB was found to be clearly on the surface of the latex DBSBB-PS nanoparticles, as evidenced by ^{1}H NMR and corroborated by conductivity titrations. The ability to modify the primary face of the cyclodextrin with ionic or non-ionic functional groups could allow the tailoring of the polystyrene surface for desired properties. The solution-like behavior of the primary rim substituents on these cyclodextrin nanoscaffolds suggest new possible areas of research. Primary hydroxyls could be derivatized with carboxylated moieties, allowing for pH adjustment of surface charge and further addition of other substituents via esterification.

4.5 References

(1) Szejtli, J. Introduction and General Overview of Cyclodextrin Chemistry. *Chemical Reviews* 1998, *98*, 1743–1754.

(2) Rekharsky, M. V.; Inoue, Y. Complexation Thermodynamics of Cyclodextrins. *Chemical Reviews* 1998, *98*, 1875–1918.

(3) Connors, K. A. The Stability of Cyclodextrin Complexes in Solution. *Chemical Reviews* 1997, *97*, 1325–1358.

(4) Saenger, W. Cyclodextrin Inclusion Compounds in Research and Industry. *Angewandte Chemical International Edition in English,* 1980, *19*, 344–362.

(5) Lombardo, D.; Longo, A.; Darcy, R.; Mazzaglia, A. Structural Properties of Nonionic Cyclodextrin Colloids in Water. *Langmuir* 2004, *20*, 1057–1064.

(6) Auzély-Velty, R.; Djedaïni-Pilard, F.; Désert, S.; Perly, B.; Zemb, T. Micellization of Hydrophobically Modified Cyclodextrins. 1. Micellar Structure. *Langmuir* 2000, *16*, 3727–3734.

(7) Auzély-Velty, R.; Péan, C.; Djedaïni-Pilard, F.; Zemb, T.; Perly, B. Micellization of Hydrophobically Modified Cyclodextrins: 2. Inclusion of Guest Molecules. *Langmuir* 2001, *17*, 504–510.

(8) Mazzaglia, A.; Ravoo, B. J.; Darcy, R.; Gambadauro, P.; Mallamace, F. Aggregation in Water of Nonionic Amphiphilic Cyclodextrins with Short Hydrophobic Substituents. *Langmuir* 2002, *18*, 1945–1948.

(9) *Cyclodextrins and Their Complexes*, 1st ed.; Dodziuk, H., Ed.; WILEY-VCH Verlag GmbH & Co.: Heidelberg, Germany, 2006.

(10) Zerkoune, L.; Angelova, A.; Lesieur, S. Nano-Assemblies of Modified Cyclodextrins and Their Complexes with Guest Molecules: Incorporation in Nanostructured Membranes and Amphiphile Nanoarchitectonics Design. *Nanomaterials* 2014, *4*, 741–765.

(11) Xu, D.; Wang, M.; Ge, X.; Lam, M. H. W. Synthesis and Characterization of β-CD-Coated Polystyrene Microspheres by Γ-Ray Radiation Emulsion Polymerization. *Macromolecular Rapid Communications* 2012, *33*, 1945–1951.

(12) Leyrer, R. J.; Mächtle, W. Emulsion Polymerization of Hydrophobic Monomers Like Stearyl Acrylate with Cyclodextrin as a Phase Transfer Agent. *Macromolecular Chemistry and Physics.* 2000, *201*, 1235–1243.

(13) Hu, J.; Li, S. J.; Liu, B.L. Effects of β-Cyclodextrin on Emulsion Polymerization. *Journal of Polymer Materials* 2005, 22, 213-218..

(14) Hu, J.; Li, S.; Wang, D.; Liu, B. Influence of Cyclodextrin and Its Glucose Units on Polymerization of Styrene. *Polymer International.* 2004, *53*, 1003–1006.

(15) Saenger, W.; Muller-Fahrnow, A. Cyclodextrins Increase Surface Tension and Critical Micelle Concentrations of Detergent Solutions. *Angewandte Chemical International Edition in English.* 1988, *27*, 393–394.

(16) Li, N.; Binder, W. H. Click-Chemistry for Nanoparticle -Modification. *Journal of Materials Chemistry* 2011, *21*, 16717–16734.

(17) Fournier, D.; Hoogenboom, R.; Schubert, U. S. Clicking Polymers: a Straightforward Approach to Novel Macromolecular Architectures. *Chemical Society Reviews* 2007, *36*, 1369–1380.

(18) Min, K.; Gao, H.; Yoon, J. A.; Wu, W.; Kowalewski, T.; Matyjaszewski, K. One-Pot Synthesis of Hairy DBSBB-PS nanoparticles by Emulsion ATRP. *Macromolecules* 2009, *42*, 1597–1603.

(19) Apostolovic, B.; Quattrini, F.; Butté, A.; Storti, G.; Morbidelli, M. *Ab Initio* Emulsion Polymerization by RAFT (Reversible Addition–Fragmentation Chain Transfer) Through the Addition of Cyclodextrins. *Helvetica Chimica Acta* 2006, *89*, 1641–1659.

(20) Prescott, S. W.; Ballard, M. J.; Rizzardo, E.; Gilbert, R. G. RAFT in Emulsion Polymerization: What Makes It Different? *Australian Journal of Chemistry.* 2002, *55*, 415–424.

(21) Flosbach, C.; Herm, M.; Ritter, H.; Glöckner, P. Cyclodextrin-Assisted Polymerization—a New Way to Synthesize Powder Coat Resins. *Progress in Organic Coatings* 2003, *48*, 177–182.

(22) Koopmans, C.; Ritter, H. Formation of Physical Hydrogels via Host−Guest Interactions of B-Cyclodextrin Polymers and Copolymers Bearing Adamantyl Groups. *Macromolecules* 2008, *41*, 7418–7422.

(23) Kettel, M. J.; Dierkes, F.; Schaefer, K.; Moeller, M.; Pich, A. Aqueous Nanogels Modified with Cyclodextrin. *Polymer* 2011, *52*, 1917–1924.

(24) Moya-Ortega, M. D.; Alvarez-Lorenzo, C.; Concheiro, A.; Loftsson, T. Cyclodextrin-Based Nanogels for Pharmaceutical and Biomedical Applications. *International Journal of Pharmaceutics* 2012, *428*, 152–163.

(25) van de Manakker, F.; Vermonden, T.; van Nostrum, C. F.; Hennink, W. E. Cyclodextrin-Based Polymeric Materials: Synthesis, Properties, and Pharmaceutical/Biomedical Applications. *Biomacromolecules* 2009, *10*, 3157–3175.

(26) Palepu, R.; Reinsborough, V. C. Surfactant-Cyclodextrin Interactions by Conductance Measurements. *Canadian Journal of Chemistry* 1988, *66*, 325–328.

(27) McKee, J. A.; Green, T. K. Synthesis of 2,3-Dibenzyl-6-Sulfobutyl-α-and-β–Cyclodextrins: New Chiral Surfactants for Capillary Electrophoresis. *Tetrahedron Letters* 2015, *56*, 4451–4454.

(28) McKee, J. A.; Green, T. K. Solubilization of Hexafluorobenzene by the Micellar Aromatic Core Formed From Aggregation of Amphiphilic (2,3-O-Dibenzyl-6-O-Sulfobutyl) Cyclodextrins. *Journal of Physical Chemistry. B* 2016, *120*, 4182–4194.

(29) Jin, X.; Kang, H.; Liu, R.; Huang, Y. Controlled Radical Emulsion Polymerization of Polystyrene. *Colloid and Polymer Science* 2013, *291*, 2481–2485.

(30) Vanderhoff, J. W. Well-Characterized Monodisperse Polystyrene Latexes as Model Colloids. *Pure & Applied Chemistry* 1980, *52*, 1263–1273.

(31) Van Geet, A. L. Calibration of Methanol Nuclear Magnetic Resonance Thermometer at Low Temperature. *Analytical Chemistry* 1970, *42*, 679–680.

(32) Thickett, S. C.; Gilbert, R. G. Emulsion Polymerization: State of the Art in Kinetics and Mechanisms. *Polymer* 2007, *48*, 6965–6991.

(33) Bancroft, W. D. The Theory of Emulsification, I. *Journal of Physical Chemistry.* 1911, *16*, 177–233.

(34) Griffin, W. C. Classification of Surface-Active Agents by“ HLB.” *Journal of Cosmetic Science* 1949, *1*, 311–326.

(35) Abdelwahed, W.; Degobert, G.; Dubes, A.; Parrot-Lopez, H.; Fessi, H. Sulfated and Non-Sulfated Amphiphilic-Beta-Cyclodextrins: Impact of Their Structural Properties on the Physicochemical Properties of Nanoparticles. *International of Journal of Pharmaceutics* 2008, *351*, 289–295.

(36) Chern, C. S. *Principles and Applications of Emulsion Polymerization*, 1st ed.; John Wiley & Sons, Inc., Hoboken, 2008.

(37) Bootz, A.; Vogel, V.; Schubert, D.; Kreuter, J. Comparison of Scanning Electron Microscopy, Dynamic Light Scattering and Analytical Ultracentrifugation for the Sizing of Poly(Butyl Cyanoacrylate) DBSBB-PS nanoparticles. *European Journal of Pharmaceutics and Biopharmaceutics* 2004, *57*, 369–375.

(38) Perevyazko, I.; Vollrath, A.; Hornig, S.; Pavlov, G. M.; Schubert, U. S. Characterization of Poly(Methyl Methacrylate) DBSBB-PS nanoparticles Prepared by Nanoprecipitation Using Analytical Ultracentrifugation, Dynamic Light Scattering, and Scanning Electron Microscopy. *Journal of Polymer Science, Part A: Polymer Chemistry* 2010, *48*, 3924–3931.

(39) De Jaeger, N.; Demeyere, H.; Finsy, R.; Sneyers, R.; Vanderdeelen, J.; van der Meeren, P.; van Laethem, M. Particle Sizing by Photon Correlation Spectroscopy Part I: Monodisperse Latices: Influence of Scattering Angle and Concentration of Dispersed Material. *Particle & Particle Systems Characterization* 1991, *8*, 179–186.

(40) Tscharnuter, W. *Photon Correlation Spectroscopy in Particle Sizing*; Encyclopedia of Analytical Chemistry. John Wiley & Sons, Ltd: Chichester, UK, 2006.

(41) Roberts, J. M.; Linse, P.; Osteryoung, J. G. Voltammetric Studies of Counterion Diffusion in the Monodisperse Sulfonated Polystyrene Latex. *Langmuir* 1998, *14*, 204–213.

(42) Van den Hul, H. J.; Vanderhoff, J. W. Well-Characterized Monodisperse Latexes. *Journal of Colloid and Interface Science* 1968, *28*, 336–337.

(43) Stone-Masui, J.; Watillon, A. Characterization of Surface Charge on Polystyrene Latices. *Journal of Colloid and Interface Science* 1975, *52*, 479–503.

(44) Price, W. S. *NMR Studies of Translational Motion: Principles and Applications*; Cambridge University Press, New York, 2009.

(45) Brandrup, J.; Immergut, E. H. *Polymer Handbook, 3rd Edition*; John Wiley and Sons, New York, 1989.

(46) Ebewele, R. O. *Polymer Science and Technology*; CRC Press, New York, 2000.

(47) Garcia-Fuentes, M.; Torres, D.; Martín-Pastor, M.; Alonso, M. J. Application of NMR Spectroscopy to the Characterization of PEG-Stabilized Lipid DBSBB-PS nanoparticles. *Langmuir* 2004, *20*, 8839–8845.

(48) Lopez-Cebral, R.; Martín-Pastor, M.; Seijo, B.; Sanchez, A. Progress in the Characterization of Bio-Functionalized DBSBB-PS nanoparticles Using NMR Methods and Their Applications as MRI Contrast Agents. *Progress in Nuclear Magnetic Resonance Spectroscopy* 2014, *79*, 1–13.

(49) Kimmich, R.; Fatkullin, N. Polymer Chain Dynamics and NMR. *Advances in Polymer Science* 2004, 170, 1–113.

(50) Xu, X. J.; Goh, H. L.; Siow, K. S.; Gan, L. M. Synthesis of Polymerizable Anionic Surfactants and Their Emulsion Copolymerization with Styrene. *Langmuir* 2001, *17*, 6077–6085.

(51) Hiemenz, P.; Rajagopalan, R. *Principles of Colloid and Surface Chemistry*, 3rd ed.; CRC Press, New York, 1997.

(52) Hunter, R. *Zeta Potential in Colloid Science*, 3rd ed.; Academic Press, New York, 1988.

(53) Wennerstrom, H.; Evans, D. F. *The Colloidal Domain: Where Physics, Chemistry, and Biology Meet*, 2st ed.; Wiley-VCH, New York, 1999.

(54) Smith, W. V.; Ewart, R. H. Kinetics of Emulsion Polymerization. *Journal of Chemical Physics* 1948, *16* , 592.

(55) Odian, G. *Principles of Polymerization*, 4 ed.; John Wiley & Sons, Inc.: Hoboken, 2004.

(56) Feeney, P. J.; Napper, D. H.; Gilbert, R. G. Coagulative Nucleation and Particle Size Distributions in Emulsion Polymerization. *Macromolecules* 1984, *17*, 2520–2529.

Appendix.

Calculation of latex surface area occupied per butyl chain (^{1}H NMR)

$$C_X = \frac{\frac{I_X}{N_X} C_{TSP}}{\frac{I_{TSP}}{N_{TSP}}} (1/10.04)$$

Table A1: calculation of occupied surface area (Å^2) per DBSBB

Integration values of butyl resonances (Figure 5)	0.2463, 0.1492, 0.0958
Concentration of TSP (mol/L)	3.99×10^{-3}
Concentration of butyl groups (mol/L) in sample volume of 0.5 mL	2.199×10^{-4}
Number of butyl groups	6.621×10^{16}
Particle radius, from DLS measurement	3.54×10^{-8} meters
Surface area (SA) per particle	1.575×10^{-14} m^2
Volume per particle	1.858×10^{-22} m^3 or 1.858×10^{-16} cm^3
Density of polystyrene	1.055 grams/cm^3
Mass per particle =	1.911×10^{-16} grams
Mass of latex in 0.5 mL sample	8.29×10^{-4} grams
Number of particles in 0.5 mL sample	4.229×10^{12}
Total particle surface area	6.659×10^{-2} m2 or 6.659×10^{18} Å^2
SA occupied per butyl group = total particle surface area/ # butyl groups	100.6 Å^2/butyl group
Number of butyl groups per heptakis(2,3-O-dibenzyl, 6-O-sulfobutyl)cyclomaltoheptaose	7
Occupied surface area of latex particle per DBSBB	704.1 Å^2/ DBSBB

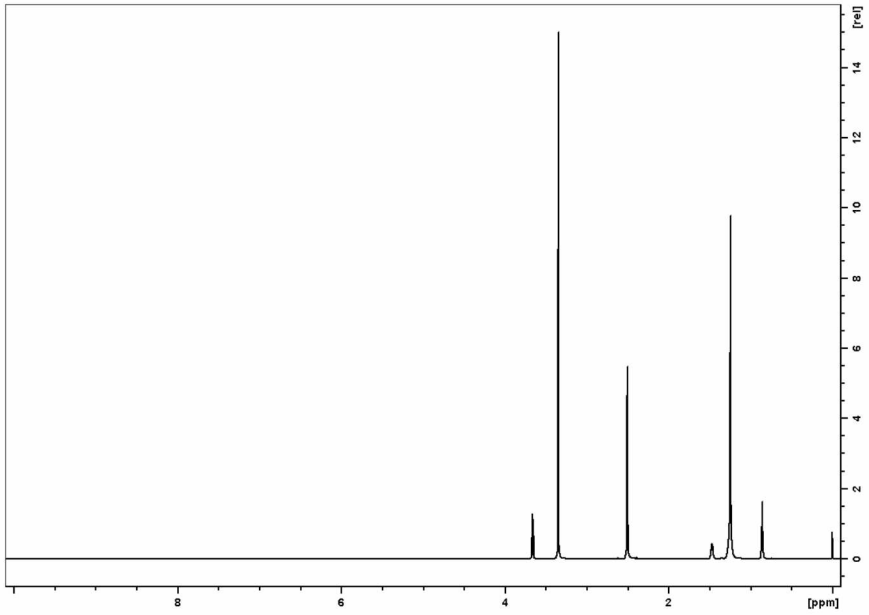

Figure A1. ^{1}H NMR spectra of SDS latex filtrate from 100000 MWCO filter (d_6-DMSO)

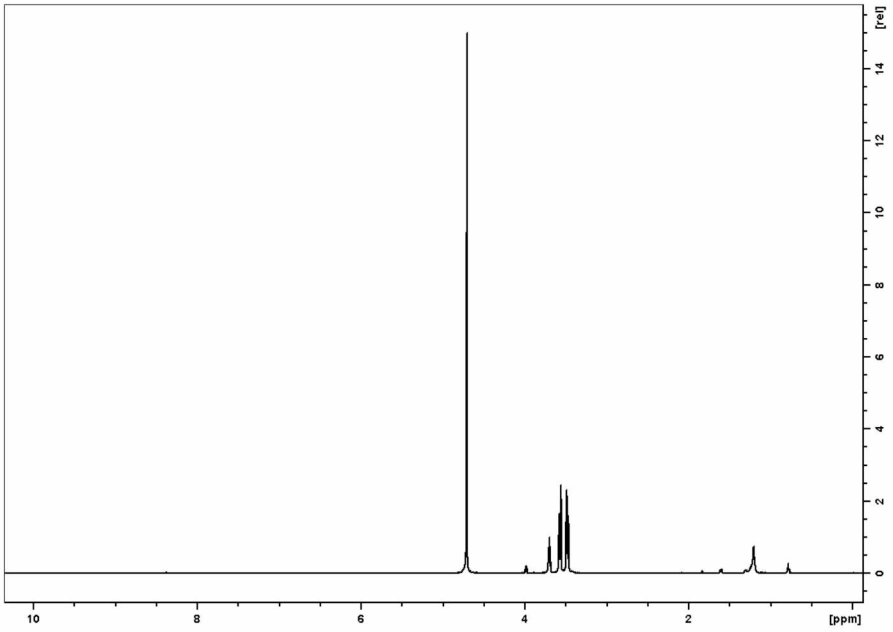

Figure A2. ^{1}H NMR spectra of DBSBB latex filtrate from 100000 MWCO filter (D_2O). Traces of cellulose acetate (filter) were observed but no DBSBB was detected.

Table A2: Molecular Dynamics data (units = Å)

	S1-S5	S3-S7	S2-S6	S5-S7	S1-S4	MEAN
MEAN	19.515	22.668	9.109	20.216	14.662	17.234
SD	3.060	2.398	2.533	2.097	3.299	2.677
MIN	7.842	14.039	4.559	10.612	4.901	8.390
MAX	26.675	28.354	18.780	25.083	22.426	24.263

Mean, SD, Min and Max refer to the arithmetic mean, standard deviation, minimum and maximum values, respectively for distances between sulfonates in the simulation. DBSBB has seven-fold symmetry; diameters used to calculate cross sectional areas were obtained using distances between sulfonates on the 1-4 and 1-5 glucose units.

Chapter 5. Summary and Future Work

5.1 Summary

The production of stable monodispersed polystyrene nanoparticles was performed using batch emulsion polymerization and used heptakis (2,3-*O*-dibenzyl-6-*O*-sulfobutyl) cyclomaltoheptaose (DBSBB) as a surfactant. The hydrodynamic diameters of these nanoparticles ranged from 70 to 100 nm. In each case, DBSBB quantitatively sorbed to the surface, possibly due to π-π interactions and/or entanglements with polystyrene polymer chains. The hydrophobic cavity of the cyclodextrin, however, is most likely occupied by styrene or polystyrene and unable to encapsulate other hydrophobic molecules.

The synthetic goals of producing single isomer amphiphilic cyclodextrins were successful. Hexakis (2,3-*O*-dibenzyl,6-*O*-sulfobutyl) cyclomaltohexaose (DBSBA) and heptakis (2,3-*O*-dibenzyl,6-*O*-sulfobutyl) cyclomaltoheptaose (DBSBB) were synthesized and characterized by ^{1}H, ^{13}C, ^{1}H-^{1}H COSY, and HMQC NMR spectroscopy and ESI-MS (Electrospray ionization mass spectrometry). There were several contributions made, in addition to the products themselves, that were of note. The perbenzylation of the secondary rim hydroxyls required the addition of *in situ* production of benzyl iodide (proposed theory) via the addition of tetrabutylammonium iodide salt. The addition of this reagent, used in non-stoichiometric amounts, was adapted from a procedure for the complete benzylation of sterically hindered glucose molecules.[1] The yields for heptakis 2,3-O-dibenzyl cyclomaltoheptaose increased from <5% to quantitative, the latter achieved with minimal cleanup. Sulfobutylation procedures of heptakis 2,3-*O*-benzyl cyclomaltoheptaose were also optimized. An initial successful procedure, using multiple steps including addition/removal of 18-crown-6 ether and ion-exchange columns, was simplified. The use of DMF (N, N-dimethylformamide) in place of THF (tetrahydrofuran) as

a solvent allowed solubilization of both product and reagent, as well as better promotion of nucleophilic substitution reactions. The addition of non-stoichiometric amounts of NaI (sodium iodide), and heat to the reaction mixture produce quantitative yields with minimal clean-up besides neutralization and ultrafiltration of the product (heptakis (2,3-*O*-benzyl,6-*O*-sulfobutyl) cyclomaltoheptaose). The alpha cyclodextrin derivative, hexakis (2,3-*O*-benzyl,6-*O*-sulfobutyl) cyclomaltohexaose, was synthesized using these modified procedures as well.

The procedures used to characterize the colloidal properties of these amphiphiles were straight forward; the analysis of the acquired data required more time and insight than anticipated. The quadrupolar nature of the hydrophobic anchors (*i.e.* the benzyl groups) illustrated the differences between aromatic and aliphatic molecules. Conductivity and temperature measurements found that CMC of both amphiphiles decreased with increasing temperature. The large enthalpic contribution of this phenomenon was ascribed to an adjustment of the classical hydrophobic effect; aromatic groups interact with water molecules via quadrupolar interactions. The solvent-solute interactions must be compensated before aggregation can commence.

The use of ^{19}F NMR to study the solubilization of hexafluorobenzene (HFB) by these colloids allowed an unencumbered study of the change in chemical shift with increasing amphiphile concentration. Calculation of binding interactions proved to be more complex than anticipated due to observable interaction between cyclodextrin and HFB that was not 1:1; most fitting equations and subsequent error analyses make this assumption. A curve fitting algorithm, executed by Microsoft EXCEL® solver was used to calculate binding interactions and populations of 1:1 and 2:1 complexes of CD:HFB species. A profile likelihood method (PLM), a derivative of χ-squared distribution and grid search methods, was used to calculate an error

space associated with K_1 and K_2, rather than an error range. This procedure was felt to be appropriate due to complex micelle/solubilizate interactions.

The production of polystyrene nanoparticles with benzylated cyclodextrins rooted on the surface was anticipated; the observation of sulfobutyl chains in solution phase ^{1}H NMR was not. The use of NMR in the investigation of polymers in the literature, without a solid phase probe, is not extensive. Slow relaxation of ^{1}H nuclei due to hindered molecular motion of the polystyrene lattice produces resonances that are too broad to be observable. The appearance of signals attributed to sulfobutyl moieties, but the deficiency of those signals assigned to the cyclodextrin torus and the benzyl groups suggested the latter is adsorbed to the particle, while the former has a higher degree of molecular motion. Also, the detection of diastereotopic resonances in the sulfobutyl chain not only corroborates this explanation, but suggests the extended pocket of the cyclodextrin could be chiral as well. The quantitative sorption of the amphiphilic cyclodextrins was an intriguing result; the benzyl anchors for the proposed nanoscaffolds seem to provide an alternative to covalent nanoparticle attachments of the cyclodextrin torus.

5.2 Future Research Proposals

The removal or remediation of heavy metals from waters is an interdisciplinary challenge. Heavy metals, unlike organic matter, cannot be degraded by microorganism, they can only be concentrated. Mobility of heavy metals scales with its bioavailability; greater mobility means greater ability for absorption. The cationic forms of heavy metals are generally most toxic. Heavy metals adsorbed by ion-exchange are physisorbed (general/non-specific) while metals captured or complexed by chelating groups, typically anionic, is chemisorption. Other parameters include pH, ionic strength and/or presence of non-toxic cations (Na^+, Mg^{2+}, Ca^{2+}),

the concentration of metal and mass of the absorbent. The chemical nature of the ligand has profound implications in coordination process with trace metals. Macrocyclic ligands can bind metal cations more strongly than their open chain chelating analogues. Adsorption is surface based process; it requires interaction between species of interest and surface of material. It is recognized as an efficient method of treatment process due to simplicity, feasibility. The primary research goals of this work were to synthesize an amphiphilic cyclodextrin surfactant, characterize its physical properties, and use that surfactant to promote the self-assembly of surface bound cyclodextrin nanoparticles that can be used for future trace metal remediation. DBSBB was found to be clearly on the surface of the latex nanoparticles, as evidenced by ^{1}H NMR and corroborated by conductivity titrations. The ability to modify the primary face of the cyclodextrin with ionic or non-ionic functional groups could allow the tailoring of the polystyrene surface for desired properties. The solution-like behavior of the primary rim substituents on these cyclodextrin nanoscaffolds suggest new possible areas of research. Primary hydroxyls could be derivatized with carboxylated moieties, allowing for pH adjustment of surface charge and further addition of other substituents via esterification.

Many challenges and questions remain. Sulfobutyl moieties are poor ligands for trace metals. These groups were used to facilitate characterization of the polystyrene surface, are well known polar head groups for surfactants, and due to ease of synthesis.[2-5] The presence of these amphiphilic cyclodextrins on the polystyrene has been demonstrated. The next avenues of research should be synthetic investigations into the addition of different functional groups that have been established to coordinate strongly to trace metals, quantitative determination of the extent of binding, and a means to immobilize the polystyrene latex onto a support polymer or resin.

Table 1: Functional groups in biomolecules responsible for trace metal binding

Functional group	Structure (protonated form)	pKa	Biomolecule/sorbent example
Hydroxyl		9.5-13	polysaccharide
Thiol	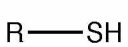	8.3 -10.8	cysteine
Amine (primary)	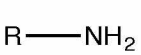	8-11	Amino acids (Lysine, Arginine) Chitosan
Carboxyl	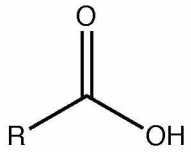	1.7-4.7	Amino acids (Aspartic, glutamic acids) Alginate
Amide	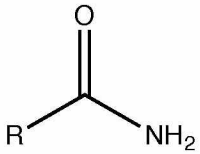	15.1	Asparagine, Glutamine
Sulfonate	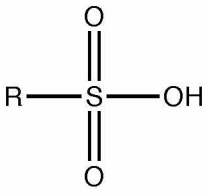	1.3	Heparin
Phosphonate	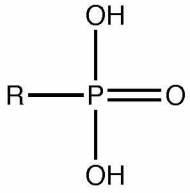	0.9-2.1 6.1-6.8	Phytic acid

The naturally occurring moieties that coordinate with metal ions in biomolecules can serve as starting points for synthetic design. Table 1 shows that the important chemical groups are hydroxyl, carboxyl, sulfonate, amine, amide, imidazole, phosphonate, and phosphonate esters. Oxygen, nitrogen, and sulfur donor atoms are present in active sites of metal dependent enzymes. Oxygen has been shown to be the least discriminating between metals; sulfur is the most discriminating. These trends are highly correlated with electronegativity of the atom (*i.e.* oxygen is more electronegative than sulfur).[6] Moreover, literature sources exist for adaptation of these functional groups to cyclodextrin hydroxyls.[7-11] Derivatization of these functional groups onto cyclodextrins should not only promote complexation of trace metal, but should improve binding affinity due to increased thermodynamic stability due to macroscopic effect.

5.2.1 Future Synthetic Pathways

Figure 1 illustrate several suggested synthetic goals, all of which extend from the 2,3-*O*-benzyl derivatized cyclodextrin. Substitution of the primary hydroxyl is typically the most facile of the cyclodextrin hydroxyls and the benzyls are required for strong physisorption to polystyrene. A possible replacement for benzylation may be the substitution of benzyl bromide for pentafluorobenzyl bromide. The addition of pentafluorobenzyl groups on the secondary rim may yield two interesting physical phenomena. The interaction between the pentafluorobenzyls and the polystyrene should be even stronger than the polystyrene/benzyl π-π interactions.[12] Additionally, micellization may occur at a lower critical micelle concentration (CMC), for a given temperature, due to the greater hydrophobicity and the strong complementary interactions between the pentafluorobenzyl groups. Investigation into the use of benzylated and perfluorobenzylated CD amphiphiles in the same aqueous system should be performed;

synergistic interactions between these CDs in the same micelle may prove to form more permanent colloidal particles than typical aggregates.

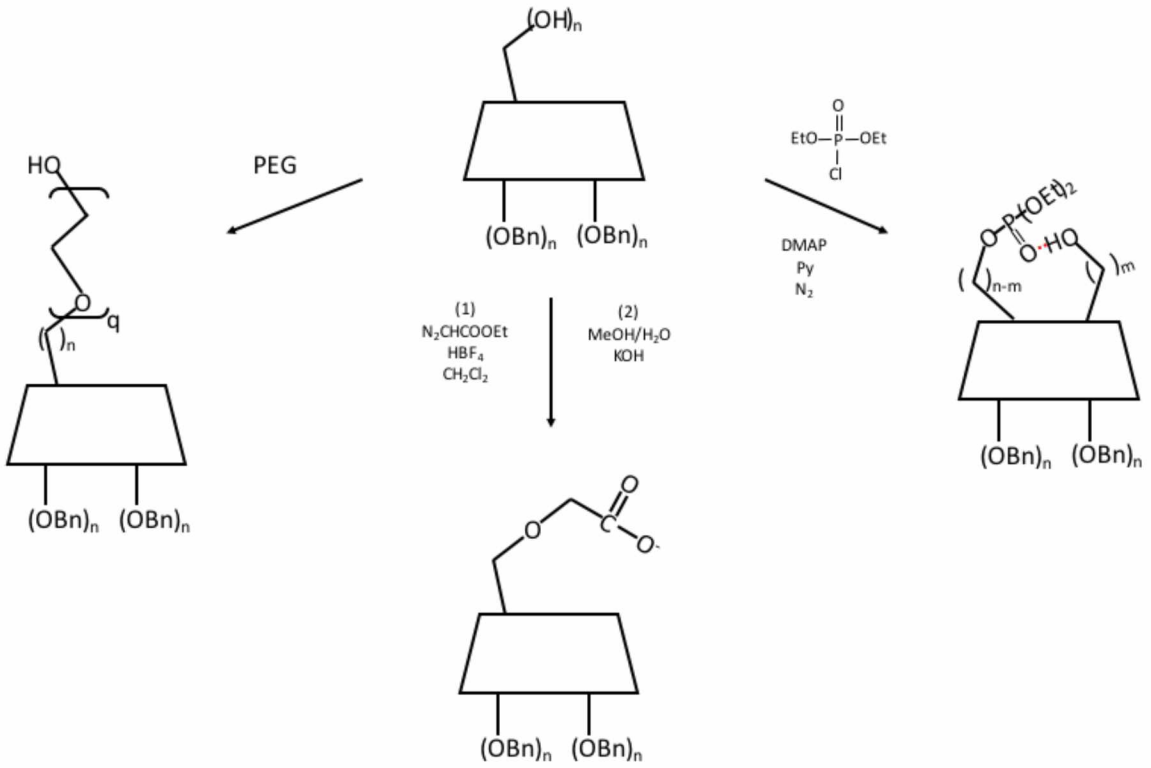

Figure 1. Reaction scheme for future syntheses of amphiphilic cyclodextrins

5.2.2 Synthesis of Hexakis (2,3-*O*-dibenzyl-6-*O*-carboxylmethyl) cyclomaltohexaose

It is well known that carboxyl groups coordinate with trace metals.[13] Carboxymethyl cyclodextrins have been shown to be a remediation strategy for cadmium, copper, lead cations as well as other toxic aqueous species.[14-17] The syntheses can be accomplished using the scheme described above, where ethyl diazoacetate is reacted with the free primary hydroxyl groups of deprotected α-cyclodextrin above, according to the procedure of Kraus.[9] The complete carboxymethylation of the primary rim should be achievable with minimal workup, as seen in Figure 2.

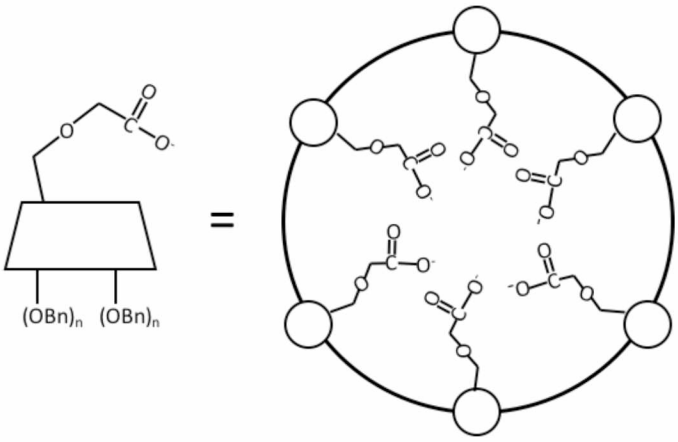

Figure 2. Representation (side, above) of hexakis (2,3-*O*-dibenzyl-6-*O*-carboxylmethyl) cyclomaltohexaose

5.2.3 Synthesis of Primary Diethylphosphonated Cyclodextrins

An inherent benefit of using scaffolds in chemical reactions is to fix the reagents in space and thereby allow the reaction to occur in a more controlled manner than in solution.[18] Scaffolds promote chemistry of interest because they contain a wide range of functional groups with known distances to each other. Alexandratos and Zhu have developed a series of polystyrene-based polyol scaffolds upon which are fixed ion selective phosphate groups.[19] The selectivity of these phosphate groups can be modified due to a proximal hydrogen bond donor. They propose that the electron density of phosphonyl oxygen is increased due to hydrogen bonding therefore "activating" the phosphonyl group with respect to metal affinity.

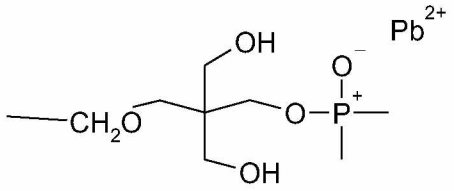

Figure 3: Activation of phosphonyl group by proximal hydrogen bond donor.[19]

Poly (vinylbenzyl chloride) was loosely crosslinked with divinylbenzene to produce a polymer support/bead size of 250-425 μm. Syntheses of specific polyols depended upon reagent and were phosphorylated with diethyl chlorophosphate in pyridine. Investigation of the position of the hydrogen bond donor revealed that the distance of the hydroxyl from the phosphonyl oxygen altered its polarizability and subsequent affinity for ions with a range of "softness". The degree of polarizability was assigned with respect to the Misono softness parameter σ.[20] Batch equilibrium experiments were performed using nitrate solutions of Pb^{2+}, Cd^{2+}, Cu^{2+}, Ni^{2+}, and Zn^{2+}. The affinities of the ions under consideration were quantified with respect to each polymer. Comparison of ionic affinities with respect to each polymer produced the general trend of $Pb^{2+} > Cd^{2+} > Cu^{2+} > Ni^{2+} > Zn^{2+}$[19]. The affinity of the ions for each polymer therefore resembles their relative ionic polarizability. A change in the distance and number of hydroxyls in close proximity to phosphonyl oxygen can alter the electron density and polarizability around the lone pairs of the P=O oxygen. The interactions between the phosphonyl group and the metal are influenced by this change in electron density.[20]

Phosphate moieties bound to polyols have variable distances between the hydrogen bond donating hydroxyl and the acceptor phosphate oxygen due to flexibility in the polyol and the crosslinking structure. A cyclodextrin possesses a rigid scaffold upon which a diethyl phosphate moiety can be attached. The attachment of phosphate onto the primary hydroxyl of a cyclodextrin allows for hydrogen bond formation between the phosphonyl oxygen and adjacent primary hydroxyl hydrogen and thus increases the knowledge of the specific structure, the distance between the donor/ acceptor and the predictability of the interaction.

Alexandratos and colleagues designed a series of polymer supported reagents that were shown to selectively complex toxic metal cations (Pb^{2+}, Cd^{2+}, Cu^{2+}, Ni^{2+}, Zn^{2+}) by tuning the polarizability

of the immobilized ligand.[19] While these metal cations have the same charge, they differ in their polarizability due to changes in their ionic radius. The Misono parameter, σ, is a quantitative measure of the polarizability of a metal cation.[21]

$$\sigma = \frac{10 I_Z R}{I_{Z+1}\sqrt{Z}} \qquad (1)$$

where Iz is the ionic potential of a metal with oxidation number, Z, and R is the ionic radius. This parameter,σ, can be used to classify the polarizability of metal cations as 'hard', 'borderline' or 'soft. [22,23] 'Soft' metal cations tend to be larger ions, are considered more polarizable and tend to interact more strongly with 'softer' Lewis bases. Conversely, 'hard' cations tend to be smaller ions and less polarizable. This 'hard'/'soft' acid base principle (HSAB) is useful in utilizing differences in polarizability to predict metal ligand binding.[24]

Figure 4 shows that a proximal hydrogen bond donor can affect the polarizability of a phosphonyl group. The 'hard' phosphonyl oxygen increases in polarizability, or increases the softness, as a ligand and thereby increases its affinity for heavy metals or transition metals. Alexandratos and Xhu found that the selectivity of these ligands for the metal cations under study depended strongly on the softness, which in turn depended on the location of the proximal hydroxyl. Depending upon the number of proximal hydroxyls and the number of carbons in the hydroxylated moiety, the positional and spatial relationship of the auxiliary hydroxyl promoted the difference in the binding affinity due to additions in the electron density on the phosphonyl oxygen. [19,25] ^{31}P NMR studies found that deshielding at the phosphorus was due to increased p donation from intramolecular hydrogen bonding between phosphonyl oxygen and hydroxyl.[26] The deshielding ^{17}O NMR studies found that these metals were not chelating to the hydroxyl.[27]

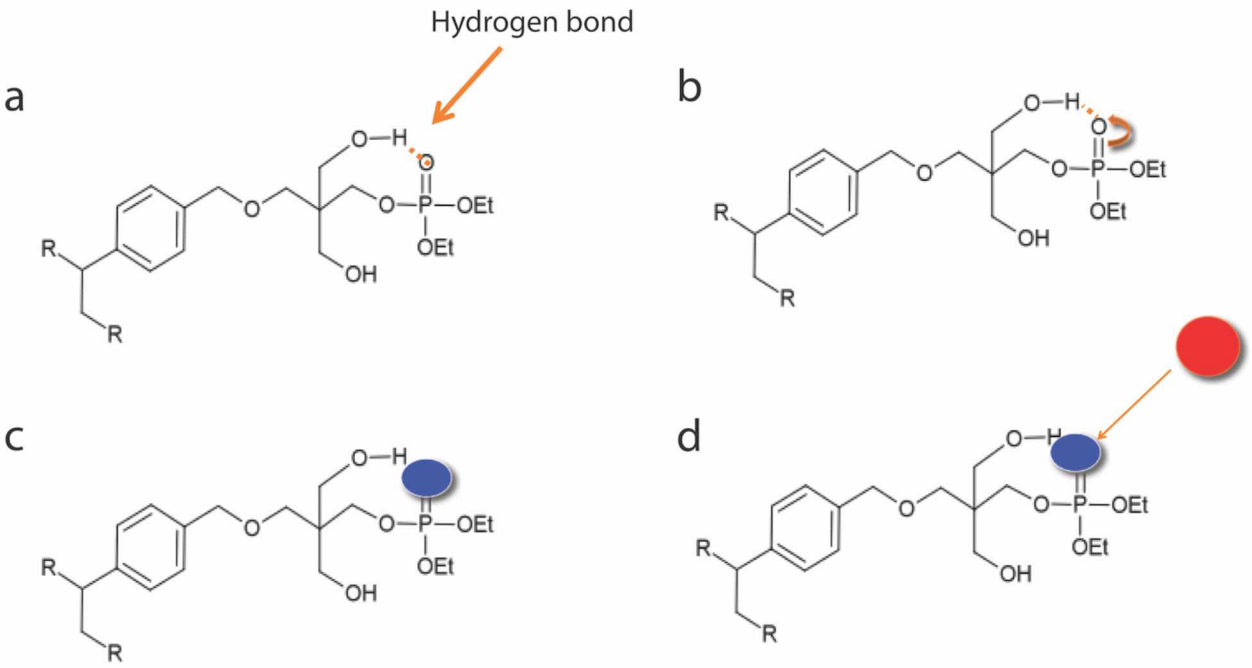

Figure 4. Increase in polarizability of phosphonyl oxygen due to proximal hydroxyl. A. Hydrogen bond forms between phosphonyl oxygen and hydrogen of hydroxyl. B. Hydrogen bond formation results in increased nucleophilicity of phosphonyl oxygen with subsequent shift in electron density from p orbitals. C. Electron density of phosphonyl oxygen changes and becomes more polarizable. D. Softer (more polarizable) oxygen attracts softer transition or heavy metal.

Synthesis shown in Figure 5, can be accomplished using a modification of the synthetic scheme of Lopez and Bols.[28] The phosphorylated derivatives are produced from reaction of the primary hydroxyl with chlorodiethylphosphate and 4-dimethylaminopyridine (DMAP) in pyridine.[29] A reduction in the number of equivalents of DIBAL while the remainder of the reaction progresses in a similar manner produces monophosphorylated cyclodextrins.[29] Confirmation of addition of phosphate moiety to cyclodextrin can performed by ^{31}P NMR analysis.

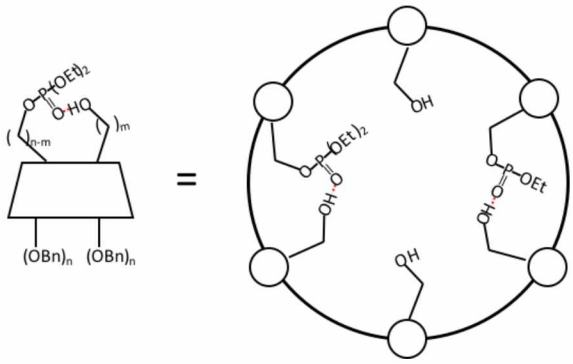

Figure 5. Representation (side, above) of diethylphosphonate interaction with unsubstituted primary hydroxyl.

The ability of these diethylphophonyl substituted cyclodextrins to selectively bind to divalent metals cations in aqueous buffers can be determined by inverse capillary electrophoresis methods. Metals could include the divalent transition metals of Pb^{2+}, Cd^{2+}, Cu^{2+}, Ni^{2+}, and Zn^{2+}. Mercury, arsenic, and other toxic metal species may be studied as well. These metals encompass a range of polarizabilities, as indicated by the Misono softness parameter, σ, which is a measure of the ion's ability to form a π bond. Selectivity will be determined by the slope of the binding constant vs. σ plot, where increasing slope indicates increasing selectivity.[19] Structural aspects to consider include (1) the size of the cyclodextrins macrocycle (α or β), (2) the degree of phosphorylation (3) and the proximity of the auxiliary OH ligand to the phosphonyl group. The proximity of the OH ligand can be varied by derivatization of the remaining primary hydroxyl groups to form respectively 2-hydroxyethyl and 3-hydroxypropyl groups on the primary positions as shown below.[30]

5.2.4. Synthesis of 2-hydroxyethyl and 3-hydroxyethyl Derivatives. Alexandratos and Zhu propose a change in the electronic environment around the phosphate can alter its polarizability and thereby its affinity for different ions. Phosphate moieties bound to different polyol

structures in which the hydrogen donor hydroxyls are bound to chains of different lengths accomplish this change in electronic environment.[19]

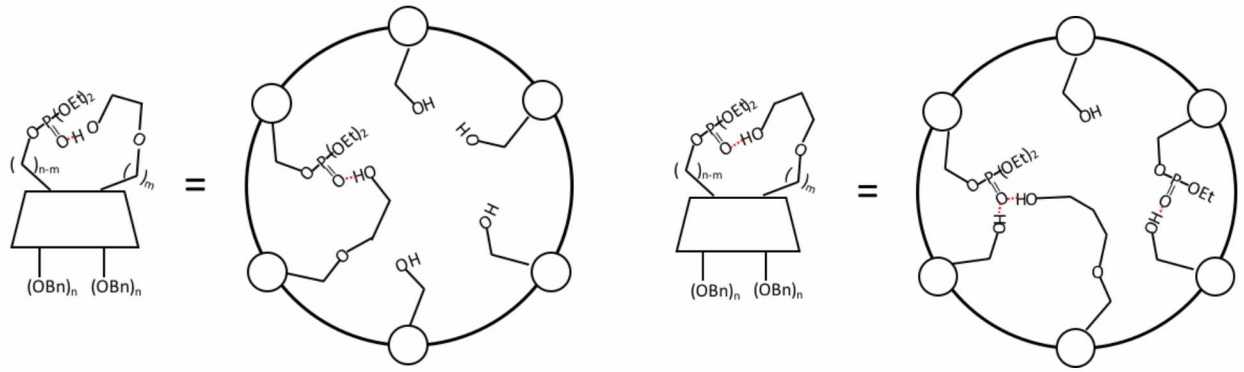

Figure 6. a) (left). Representation (side, above) of diethylphosphonate interaction with 2-hydroethyl derivative. b) (right). Representation (side, above) of diethylphosphonate interactions with 3-hydroethyl derivative and primary alcohol (separately)

The unreacted primary hydroxyl groups of the phosphorylated described above can be reacted to form 2-hydroxyethyl and 3-hydroxypropyl groups, where the free hydroxyl group is spaced further away from the primary face of the cyclodextrin (Figure 6). The increase in chain length with respect to the unsubstituted primary hydroxyl produces a different microenvironment in the vicinity of the phosphonyl oxygen, and alters it's binding with the metal ion. Hydroxyalkyl CDs are produced by reacting the CD under base using the appropriate chlorohydroxyalkane.

5.3 Batch Equilibrium Studies

Batch equilibrium studies can be performed with dilute solutions on polystyrene-supported CD derivatives and 10^{-4} M nitrate solutions of Pb^{2+}, Cd^{2+}, Cu^{2+}, Ni^{2+}, and Zn^{2+}. Analyses of the binding studies could be performed using the concentrations of free metal cations acquired by ICP-AES. Examination of the metal bound phosphonyl complex due to system pH alteration can

be examined. The concentration of metal bound complexes changes with pH. A recovery method that incorporates a change in pH with a resulting decomplexation from the phosphonyl group can be examined, as an increase in proton concentration should result in release of the metal cation. The ability of metal recovery from bound cyclodextrins should be investigated.

5.3.1 Trace Metal / Cyclodextrin Nanoparticle Complexation Studies

A quantitative measure of affinity between the phosphorylated and carboxylated cyclodextrins nanoparticles and the selected metal ions can be determined using capillary electrophoresis (CE) via indirect detection of the metal analyte.[31] Solutions of selected metal ions and cyclodextrin structures under investigation can be introduced into the CE capillary. A calculation of stability constants, a quantitative measure of binding affinity, requires knowledge of either the concentration of the host cyclodextrin, the metal guest, and/or the cyclodextrin-metal complex.[31] The stability constant (β_n) of the ML_n^+ complex can be calculated from the mass law expression:

$$M^+ + nL \quad ML_n^+ \qquad (2)$$

where β_n is the ratio between the concentrations of the free metal cation, the free ligands, and the ML_n^+ complex.

$$\beta_n = \frac{[ML_n^+]}{[M^+][L]^n} \qquad (3)$$

These equations can be simplified to Equation 3 when formation of higher complexes are suppressed by lower excesses of ligand:

$$\frac{1}{\mu_{eff}} = \frac{1}{\mu_M}(1 + \beta_+[\Lambda]) \qquad (4)$$

where L is the conductivity of the electrolyte, μ_M is the ionic mobility of the free metal cation, and [Λ] is the concentration of ligand, in this case the cyclodextrin. The conditional stability constant of the metal-ligand complex can then be calculated graphically from dependence of the reciprocal effective mobility ($1/\mu_{eff}$) of the metal on the ligand concentration. The effective mobility (μ_{eff}) of the cation can be calculated from a knowledge of total length of capillary (I_{tot}), the length to the detector (I_{det}), the applied voltage (V), the migration time of the metal cation (t_m) and the migration time of the electroosmotic flow (t_0).[31]

$$\mu_{eff} = \frac{I_{tot} I_{det}}{V}\left(\frac{1}{t_m} - \frac{1}{t_0}\right) \qquad (5)$$

The quantitative determination of metal/phosphorylated CD binding interactions could thus be calculated using inverse detection capillary electrophoresis. An inverse detection method can be used to quantify the concentration of the free metal ion in solution. An assumption of a 1:1 binding model of metal: phosphate allows for the calculation of binding constant β_n because all of the metal is either free or bound. The addition of electron density to the metal cation from the phosphate moiety should reduce the effective positive charge of the cation and therefore change its migration time.

5.4 Computational Studies

The aim of a future computational study will be to expand a previous study, shown in Figure 7, that examined the effect of changes in partial atomic charge (phosphonyl oxygen, phosphorus), phosphonyl bond length with changes in the number of hydrogen bonds and size of intramolecular hydrogen bond

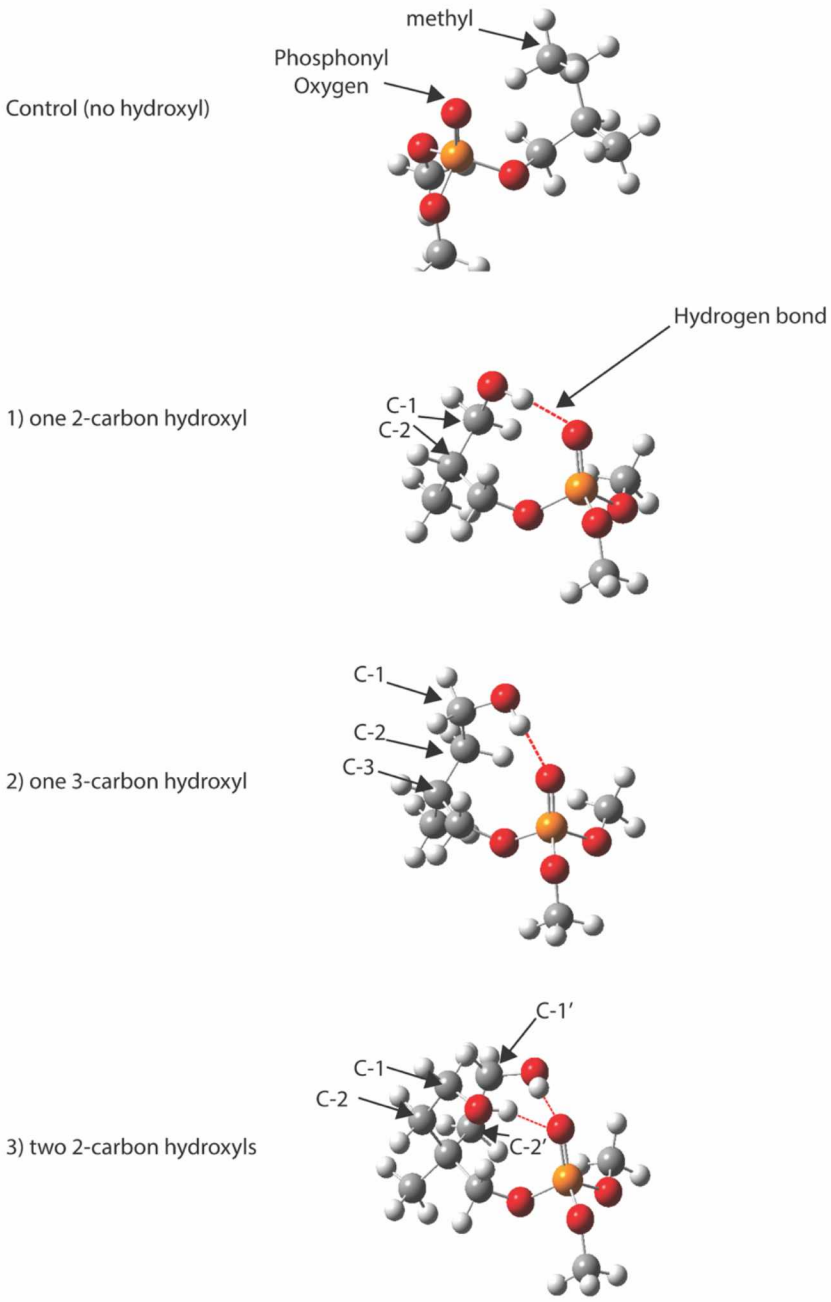

Figure 7. Illustration of Structures 1, 2, and 3. The nature of intramolecular hydrogen bonding in Structures 1, 2, and 3 affects electron density on their phosphonyl oxygen.[1]

[1] Unpublished work

ring formation. The structures in the previous study were modified from the literature in order to decrease computational time.[19]

Polymer supported ligands have been truncated to a methyl group in order to decrease the number of atoms but not sacrifice functionality. A future goal of this line of research is to investigate the affinity of phosphorylated cyclodextrins with transition metals in aqueous solution. The placement of phosphonyl groups in proximity to an auxiliary hydroxyl group has been hypothesized to increase the electron density on the phosphonyl oxygen through hydrogen bond interaction.[32] The role of ring strain is examined with respect to change in the aforementioned partial atomic charges and distances by inserting of additional carbon into the structures under examination. Batch transition metal affinity experiments have been conducted by Alexandratos and Xhu with structures similar to those under examination. The purpose of these batch equilibrium studies was to relate the design of polymer supported ion selective ligands to interaction with transition metal ions. The results of those experiments indicated that structures with two hydrogen bond donors in proximity to a phosphonyl bound transition metals ions with greater affinity than if one hydrogen bond donor were present.

A computational study into the change in electronic environment of the phosphonyl with hydrogen bond interactions using several methods and levels of theory would help to increase mechanistic understanding of this structure- affinity relationship. An increase in the partial atomic charge on the phosphonyl oxygen should occur in the presence of a hydrogen bond donor. The presence of a second hydroxyl should increase this effect. The decrease in ring strain from the addition of another carbon to the ring formed from the intramolecular hydrogen bond should lessen any deformation of the hydrogen bond and therefore promote a stronger interaction.

Calculations were performed the PM3 semiempirical method using the HyperChem software package and Gaussian 09 Revision A1 with B3LYP/6-31++ G ** (d,p) and B3LYP/6-31 G model chemistry.[33,34] All structures in Figure 7 were geometrically optimized using the "ultrafine" option in Gaussian 09 and 0.001kcal/Å mol in HyperChem. Partial atomic charges were computed using a Mulliken population analysis with respective methods and levels of theory. An examination of the intramolecular hydrogen bond interaction was undertaken using three structures in which the number of carbons in the ring formed by the hydrogen bond was increased by one and the number of available hydrogen bond donor hydroxyls were varied. The B3LYP/ 6-31++G** (d,p) level of theory contains polarization functions and diffuse functions that have been shown to simulate hydrogen bond interaction and phosphonyl chemistry. [35,36] The purpose of this experimental design was to determine the role of ring strain and number of hydrogen bond donors on the change in electron density versus control. The control structure is identical to Structure 1 with the exception of a methyl group in place of the hydroxyl in order to examine the partial atomic charges on the phosphorus and the oxygen of the phosphonyl and the length of the phosphonyl bond without the influence of intramolecular hydrogen bond donation.

Tables A1-A3 (See Appendix) illustrate the partial atomic charge on phosphonyl O and P atoms and the change in phosphonyl length, when compared with the control structure over several methods (PM3 and the B3LYP functional) and levels of theory. All changes in partial charge of the oxygen of the phosphonyl are with respect to the control structure. A proximal hydrogen bond donor seems to increase the negative atomic partial charge on oxygen and decrease the partial positive charge on phosphorus. The inclusion of a second hydrogen bond donor increases these effects. Increase in the length of the phosphonyl bond with respect to control would indicate a decrease in electron density between the oxygen and the phosphorus of the

phosphonyl. Figure 8 illustrates this trend with the change in phosphonyl oxygen partial atomic charge as a function of structure, method, and level of theory used in the computation. The results obtained from the highest level of theory, B3LYP 6-31++G**, would be most accurate due to inclusion of polarization and diffuse functions. Lower levels of theory, however, also exhibit the same trend toward greater polarization with inclusion of second hydroxyl The role of extension of carbon skeleton is inconclusive in lower levels of theory but seems to decrease the change of partial atomic charges with respect to control. The hydrogen bond donor/acceptor distance indicates that a strong hydrogen bond occurs.

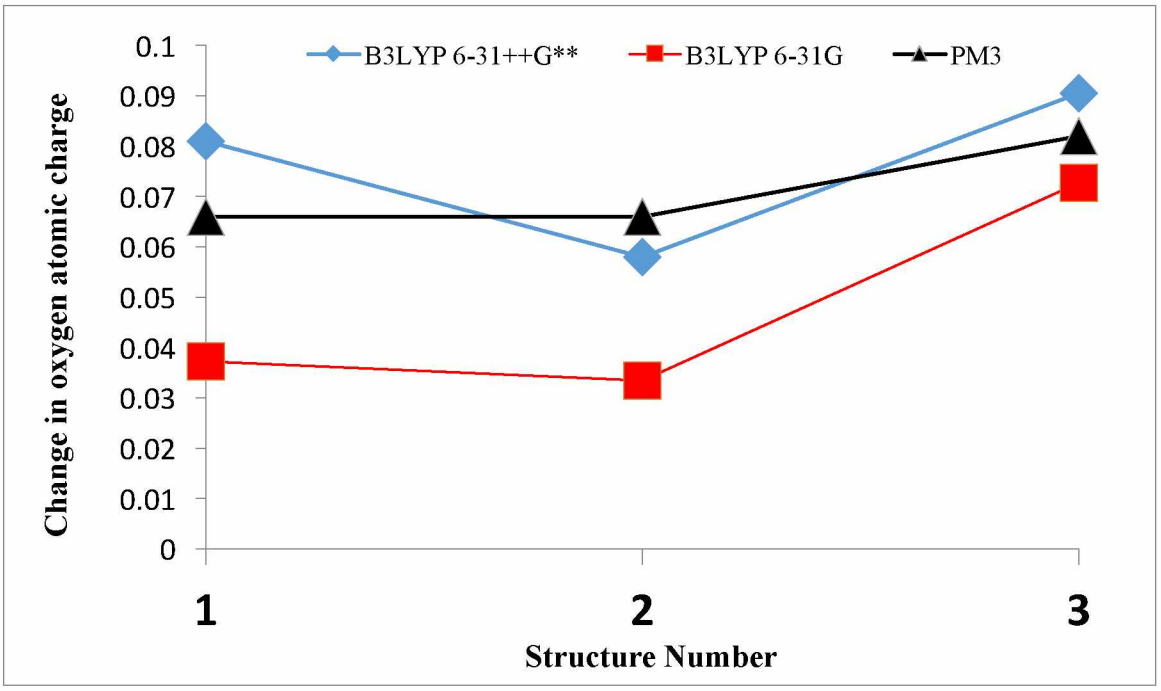

Figure 8. Changes in partial atomic charge on phosphonyl oxygen with structures 1-3 and different methods and levels of theory. Each structure exhibits at least one intramolecular hydrogen bond and demonstrates a corresponding increase in partial atomic charge on the phosphonyl oxygen. Structure 3, which has two intramolecular hydrogen bonds, has the best agreement between theories and the most additional partial charge.

The lack of change in the distances with respect to structure in lower levels of theory but an observed decrease in partial atomic charges on oxygen with an additional carbon using the more accurate B3LYP/6-31++G** indicates that ring strain in the molecule may assist the hydrogen bond interaction. The negative partial atomic charge of oxygen increased and the partial positive atomic charge on phosphorus decreases as the phosphonyl oxygen participated as a hydrogen bond acceptor. Inclusion of a second hydrogen bond donor increased these effects. This trend was demonstrated using both the B3LYP functional and the PM3 semiempirical method. An increase in the level of theory from 6-31 G to 6-31++G** to include the polarization of the hydrogen and oxygen atoms in hydrogen bonding exhibited this trend as well but indicates an increase in partial atomic charges may be assisted by ring strain. These findings correlate well with those experiments performed by Alexandratos; proximal hydrogen bonding increases electron density of the phosphonyl oxygen, thereby making it a softer ligand.

5.5 Immobilization of CD Nanospheres onto Silica via Epoxide Formation

An important attribute of nanoparticles is the large surface area provided for a given mass. An inherent problem, however, is the decrease in void volume when these particles are packed into a chromatography column and the substantial buildup of pressure if applied. Moreover, the suspended latex is difficult to collect if required because of its particle dimensions. The high solubility of cyclodextrins prevents their direct use for separation and purification; immobilization onto solid supports is possible via polymerization.[37] The high surface area and porosity of cyclodextrin-polymers enables the rapid sequestration of toxic aqueous species. These water-insoluble polymers have been used for detoxification, removal of heavy metal ions, organic contaminants, and other toxins.[38] The most straightforward and common means of crosslinking cyclodextrins is the use of epichlorohydrin as a cross-linker agent.[39]

Epichlorohydrin/cyclodextrin polymers are produced via a single step condensation by reacting the cyclodextrin in alkaline aqueous conditions.[40]

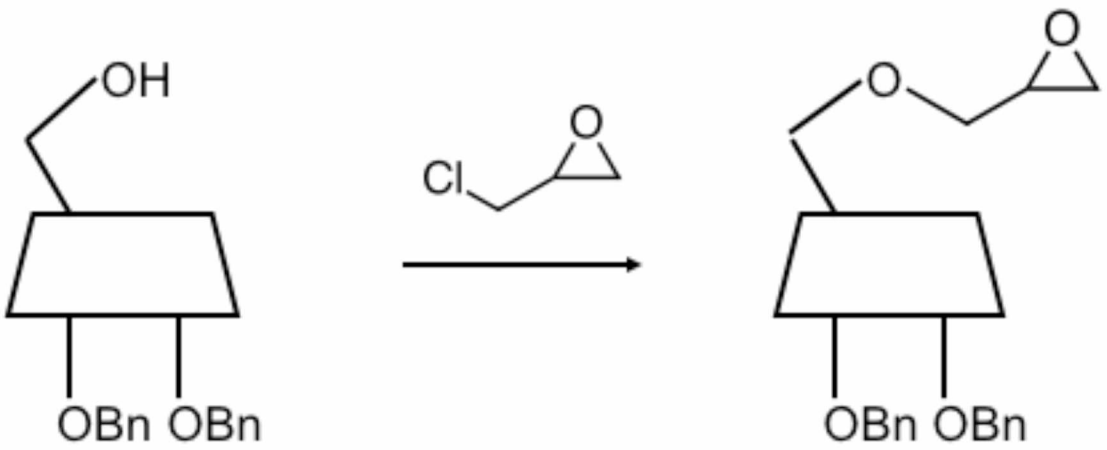

Figure 9. Synthesis of epoxide containing cyclodextrin using epichlorohydrin reagent.

Immobilization of the polystyrene nanoparticle should be realized via the addition of the product in Figure 9 to an emulsion polymerization recipe. Resins or polymer supports with nucleophilic functional groups can open the epoxide under alkaline conditions via nucleophilic substitution (SN_2).[40] The resulting covalent bond is resistant to the acidic conditions required for removal of coordinated heavy metals and subsequent recharge of ion exchange column properties.

5.6 References

(1) Czernecki, S.; Georgoulis, C.; Provelenghiou, C. Nouvelle Methode De Benzylation D'hydroxyles Glucidiques Encombres. *Tetrahedron Letters* 1976, *17* (39), 3535–3536.

(2) Vanderhoff, J. W. Well-Characterized Monodisperse Polystyrene Latexes as Model Colloids. *Pure and Applied Chemistry* 1980, *52*, 1263–1273.

(3) Sinton, S. Aggregation and Interfacial Properties of an Isomerically Pure Alkylaryl Sulfonate. *Journal of Colloid and Interface Science* 1987, *120* (2), 358–369.

(4) Kirschner, D.; Green, T. K. Nonaqueous Synthesis of a Selectively Modified, Highly Anionic Sulfopropyl Ether Derivative of Cyclomaltoheptaose (B-Cyclodextrin) in the Presence of 18-Crown-6. *Carbohydrate Research* 2005, *340* (11), 1773–1779.

(5) McKee, J. A.; Green, T. K. Synthesis of 2, 3-Dibenzyl-6-Sulfobutyl-α and β Cyclodextrins: New Chiral Surfactants for Capillary Electrophoresis. *Tetrahedron Letters* 2015, *56* (30), 4451–4454.

(6) Vandenbossche, M.; Jimenez, M.; Casetta, M.; Traisnel, M. Remediation of Heavy Metals by Biomolecules: a Review. *Critical Reviews in Environmental Science and Technology* 2015, *45* (15), 1644–1704.

(7) Croft, A. P.; Bartsch, R. A. Synthesis of Chemically Modified Cyclodextrins. *Tetrahedron* 1983, *39* (9), 1417–1474.

(8) Hanessian, S.; Benalil, A.; Laferriere, C. The Synthesis of Functionalized Cyclodextrins as Scaffolds and Templates for Molecular Diversity, Catalysis, and Inclusion Phenomena. *The Journal of Organic ...* 1995, *60* (15), 4786–4797.

(9) Kraus, T.; Buděšínský, M.; Závada, J. A Simple Synthesis of Hexakis (6-O-Carboxymethyl-2, 3-Di-O-Methyl) Cyclomaltohexaose and Heptakis (6-O-Carboxymethyl-2, 3-Di-O-Methyl) Cyclomaltoheptaose. *Carbohydrate Research* 1997, *304* (1), 81–84.

(10) Ashton, P. R.; Koniger, R.; Stoddart, J. Amino Acid Derivatives of B-Cyclodextrin. *J. Org. Chem.* 1996, *61*, 903–908.

(11) Szente, L.; Szejtli, J. Highly Soluble Cyclodextrin Derivatives: Chemistry, Properties, and Trends in Development. *Advanced Drug Delivery Reviews* 1999, *36* (1), 17–28.

(12) Hunter, C. A.; Lawson, K. R.; Perkins, J.; Urch, C. J. Aromatic Interactions. *J. Chem. Soc., Perkin Trans. 2* 2001, No. 5, 651–669.

(13) Belciug, M. P.; Modro, A. M.; Modro, T. A.; Wessels, P. L. Metal Ion Complexation by the Phosphoryl and the Carbonyl Groups Probed by 17O NMR Spectroscopy. *J. Phys. Org. Chem.* 1995, *8* (9), 605–609.

(14) Hoffman, D. R.; Anderson, P. P.; Schubert, C. M.; Gault, M. B.; Blanford, W. J.; Sandrin, T. R. Carboxymethyl-B-Cyclodextrin Mitigates Toxicity of Cadmium, Cobalt, and Copper During Naphthalene Biodegradation. *Bioresource Technology* 2010, *101* (8), 2672–2677.

(15) Badruddoza, A. Z. M.; Tay, A. S. H.; Tan, P. Y.; Hidajat, K.; Uddin, M. S. Carboxymethyl-B-Cyclodextrin Conjugated Magnetic Nanoparticles as Nano-Adsorbents for Removal of Copper Ions: Synthesis and Adsorption Studies. *Journal of Hazardous Materials* 2011, *185* (2-3), 1177–1186.

(16) Skold, M. E.; Thyne, G. D.; Drexler, J. W.; McCray, J. E. Determining Conditional Stability Constants for Pb Complexation by Carboxymethyl-B-Cyclodextrin (CMCD). *Journal of Contaminant Hydrology* 2007, *93* (1-4), 203–215.

(17) Skold, M. E.; Thyne, G. D.; Drexler, J. W.; McCray, J. E. Solubility Enhancement of Seven Metal Contaminants Using Carboxymethyl-B-Cyclodextrin (CMCD). *Journal of Contaminant Hydrology* 2009, *107* (3-4), 108–113.

(18) Crick, D. W.; Alexandratos, S. D. Polymer-Supported Reagents: Application to Separation Science. *Ind. Eng. Chem. Res.* 1996, *35* (3), 635–644.

(19) Alexandratos, S. D.; Zhu, X. Bifunctional Coordinating Polymers: Auxiliary Groups as a Means of Tuning the Ionic Affinity of Immobilized Phosphate Ligands. *Macromolecules* 2005, *38* (14), 5981–5986.

(20) Alexandratos, S. D.; Zhu, X. Polyols as Scaffolds in the Development of Ion-Selective Polymer-Supported Reagents: the Effect of Auxiliary Groups on the Mechanism of Metal Ion Complexation. *Inorg. Chem.* 2008, *47* (7), 2831–2836.

(21) Misono, M.; Ochiai, E.; Saito, Y.; Yoneda, Y. A New Dual Parameter Scale for the Strength of Lewis Acids and Bases with the Evaluation of Their Softness. *Journal of Inorganic and Nuclear Chemistry* 1967, *29* (11), 2685–2691.

(22) Pearson, R. G. Hard and Soft Acids and Bases, HSAB, Part II: Underlying Theories. *J. Chem. Educ.* 1968.

(23) Parr, R. G.; Pearson, R. G. Absolute Hardness: Companion Parameter to Absolute Electronegativity. *Journal of the American Chemical Society* 1983, *105* (26), 7512–7516.

(24) Beauvais, R. A.; Alexandratos, S. D. Polymer-Supported Reagents for the Selective Complexation of Metal Ions: an Overview. *Reactive and Functional Polymers* 1998, *36* (2), 113–123.

(25) Alexandratos, S. D. New Polymer-Supported Ion-Complexing Agents: Design, Preparation and Metal Ion Affinities of Immobilized Ligands. *Journal of Hazardous Materials* 2007, *139* (3), 467–470.

(26) Genov, D. G.; Tebby, J. C. … Analysis of (2-Substituted-Alkyl) Phosphoryl Compounds. 1. NMR Spectroscopic Studies of Dialkyl (2-Hydroxyalkyl) Phosphonates and Their Carboxylic Esters. *J. Org. Chem.* 1996, *61* (7), 2454–2459.

(27) Modro, A. M.; Modro, T. A.; Wessels, P. L. Metal-Ion Complexation by the Phosphoryl and the Carbonyl Groups Probed by O-17 NMR-Spectroscopy. *J. Phys. Org. Chem.* 1995, *8* (9), 605–609.

(28) López, Ó.; Bols, M. Effective Synthesis of Negatively Charged Cyclodextrins. Selective Access to Phosphate Cyclodextrins. *Tetrahedron* 2008, *64* (32), 7587–7593.

(29) Wang, W.; Pearce, A. J.; Zhang, Y.; Sinaÿ, P. Diisobutylaluminium-Promoted Regioselective De-O-Methylation of Cyclodextrins: an Expeditious Entry to Selectively Modified Cyclodextrins. *Tetrahedron: Asymmetry* 2001, *12* (3), 517–523.

(30) Irie, T.; Fukunaga, K.; Yoshida, A.; Uekama, K.; Fales, H. M.; Pitha, J. Amorphous Water-Soluble Cyclodextrin Derivatives: 2-Hydroxyethyl, 3-Hydroxypropyl, 2-Hydroxyisobutyl, and Carboxamidomethyl Derivatives of B-Cyclodextrin. *Pharm Res* 1988, *5* (11), 713–717.

(31) Muzikář, M.; Havel, J.; Macka, M. Capillary Electrophoretic Study of Interactions of Metal Ions with Crown Ethers, a Sulfated B-Cyclodextrin, and Zwitterionic Buffers Present as Additives in the Background Electrolyte. *Electrophoresis* 2002, *23* (12), 1796–1802.

(32) Alexandratos, S. D.; Zhu, X. Immobilized Tris(Hydroxymethyl)Aminomethane as a Scaffold for Ion-Selective Ligands: the Auxiliary Group Effect on Metal Ion Binding at the Phosphate Ligand. *Inorg. Chem.* 2007, *46* (6), 2139–2147.

(33) Frisch, M. J.; Trucks, G. W.; Schlegel, H. B.; Scuseria, G. E.; Robb, M. A.; Cheeseman, J. R.; Scalmani, G.; Barone, V.; Mennucci, B.; Petersson, G. A.; *et al.* Gaussian, Inc., Wallingford CT, 2009.

(34) Hypercube, Inc. HyperChem(TM) Professional 8.01. 8 ed. Hypercube, Inc., 1115 NW 4th Street, Gainesville, Florida 32601, USA: Gainesville, FL.

(35) Bermudez, V. M. Computational Study of Environmental Effects in the Adsorption of DMMP, Sarin, and VX on Γ-Al 2O 3: Photolysis and Surface Hydroxylation. *J. Phys. Chem. C* 2009, *113* (5), 1917–1930.

(36) Wang, J.; Gu, J.; Leszczynski, J. Theoretical Modeling Study for the Phosphonylation Mechanisms of the Catalytic Triad of Acetylcholinesterase by Sarin. *J. Phys. Chem. B* 2008, *112*, 3485–3494.

(37) Liu, H. *et al.* Adsorption mechanism based screening of cyclodextrin polymers for adsorption and separation of pesticides from water. *Water Research* 2011, *45*, 3499 – 3511.

(38) Alsbaiee, A. *et al.* Rapid removal of organic micropollutants from water by a porous β-cyclodextrin polymer. *Nature* 2016, 529, 190 -194.

(39) Morin-Crini, N; Crini, G. Environmental applications of water-insoluble b-cyclodextin-epichlorohydrin polymers. *Progress in Polymer Science.* 2013, 38, 344-368.

(40) Gidwani, B.; Vyas, A. Synthesis, characterization and application of Epichlorohydrin-b-cyclodextrin polymer. *Colloids and Surfaces B:Biointerfaces.* 2014, 114, 130-137.

Appendix.

Table A1: Atomic charges/distances for structures 1-3 as computed using the semiempirical PM3 method

(partial atomic units in Mullikans, lengths in Angstroms)

	Control	Structure 1	Structure 2	Structure 3
Phosphonyl P	2.168	2.162	2.165	2.164
Phosphonyl O	-0.806	-0.872	-0.872	-0.888
Hydroxyl O1	-0.179 (methyl C)	-0.356	-0.358	-0.359
Hydroxyl H1	0.109 (methyl H)	0.239	0.239	0.240
Hydroxyl O2				-0.371
Hydroxyl H2				0.232
Phosphonyl length	1.44824	1.46191	1.46034	1.47848
H bond length 1		1.82774	1.81753	1.8435
H bond length 2				1.82584

Table A2: Atomic charges/distances for structures 1-3 as computed using B3LYP method and 6-31G level of theory

(partial atomic units in Mullikans, lengths in Angstroms)

	Control	Structure 1	Structure2	Structure3
Phosphonyl P	1.5071	1.5288	1.5255	1.548
Phosphonyl O	-0.6323	-0.6696	-0.6658	-0.705
Hydroxyl O1	-0.413681 (methyl C)	-0.645318	-0.649349	-0.643072
Hydroxyl H1	0.157265 (methyl H)	0.414184	0.409470	0.416893
Hydroxyl O2				-0.651111
Hydroxyl H2				0.415718
Phosphonyl length	1.582	1.587	1.592	1.598
Hbond length 1		1.852	1.866	1.851
H bond length 2				1.901

Table A3: Atomic charges/distances for structures 1-3 as computed using B3LYP method and 6-31++G** level of theory

(partial atomic units in Mullikans, lengths in Angstroms)

	Control	Structure 1	Structure2	Structure3
Phosphonyl P	2.264	2.1718	2.2146	2.0669
Phosphonyl O	-0.751	-0.83199	-0.8089	-0.8415
Hydroxyl O1	-0.577172 (methyl C)	-0.505669	-0.429830	-0.491675
Hydroxyl H1	0.176830 (methyl H)	0.440181	-0.497245	0.453396
Hydroxyl O2				-0.448402
Hydroxyl H2				0.416571
Phosphonyl length	1.48	1.486	1.487	1.494
H bond length 1		1.927	1.926	1.907
H bond length 2				2.053